arXiv:0907.3449v2 [astro-ph.CO] 6 Oct 2009

Low-Resolution Spectroscopy of Gamma-ray Burst Optical Afterglows: Biases in the *Swift* Sample and Characterization of the Absorbers[1]

J. P. U. Fynbo[2,3], P. Jakobsson[3], J. X. Prochaska[4], D. Malesani[2], C. Ledoux[5], A. de Ugarte Postigo[5], M. Nardini[6], P. M. Vreeswijk[2,5], K. Wiersema[7], J. Hjorth[2], J. Sollerman[2,8], H.-W. Chen[9], C. C. Thöne[2,10], G. Björnsson[3], J. S. Bloom[11], A. Castro-Tirado[12], L. Christensen[13], A. De Cia[3], A. S. Fruchter[14], J. U. Gorosabel[12], J. F. Graham[14], A. O. Jaunsen[2], B. L. Jensen[2], D. A. Kann[15], C. Kouveliotou[16], A. Levan[17], J. Maund[2], N. Masetti[18], B. Milvang-Jensen[2], E. Palazzi[18], D. A. Perley[11], E. Pian[19], E. Rol[7], P. Schady[20], R. Starling[7], N. Tanvir[7], D. J. Watson[2], D. Xu[2], T. Augusteijn[21], F. Grundahl[22], J. Telting[21], P.-O. Quirion[22]

---

[2] Dark cosmology centre, Niels Bohr Institute, University of Copenhagen, Juliane Maries Vej 30, DK-2100 Copenhagen O

[3] Centre for Astrophysics and Cosmology, Science Institute, University of Iceland, Dunhagi 5, IS-107 Reykjavík, Iceland

[4] Department of Astronomy and Astrophysics, UCO/Lick Observatory; University of California, 1156 High Street, Santa Cruz, CA 95064

[5] European Southern Observatory, Alonso de Córdova 3107, Vitacura, Casilla 19001, Santiago 19, Chile

[6] SISSA - Via Beirut 2/4, I-34014 Trieste, Italy

[7] Department of Physics and Astronomy, University of Leicester, University Road, Leicester, LE1 7RH, UK

[8] Department of Astronomy, The Oskar Klein Centre, Stockholm University, 106 91 Stockholm, Sweden

[9] Department of Astronomy & Astrophysics and Kavli Institute for Cosmological Physics, University of Chicago, Chicago, IL, 60637, USA

[10] INAF - Osservatorio Astronomico di Brera, Via Bianchi 46 I-23806 Merate, Italy

[11] Department of Astronomy, University of California, Berkeley, CA 94720-3411, USA

[12] IAA-CSIC, PO Box 03004, E-18080 Granada, Spain

[13] European Southern Observatory, Karl-Schwarzschildstrasse 2, D-85748 Garching, Germany

[14] Space Telescope Science Institute, Department of Physics and Astronomy, Johns Hopkins University, 3700 San Martin Drive, Baltimore, MD 21218, USA

[15] Thüringer Landessternwarte Tautenburg, Sternwarte 5, D-07778 Tautenburg, Germany

[16] NASA Marshall Space Flight Center, Huntsville, Alabama 35805, USA

[17] Department of Physics, University of Warwick, Coventry CV4 7AL, UK

[18] INAF - Istituto di Astrofisica Spaziale e Fisica Cosmica di Bologna, via Gobetti 101, 40129 Bologna,Italy

[19] INAF-Trieste Astronomical Observatory, 34143 Trieste, Italy

[20] The UCL Mullard Space Science Laboratory, Holmbury St Mary, Dorking, Surrey RH5 6NT, UK

[21] Nordic Optical Telescope Apartado 474, 38700 Santa Cruz de La Palma, Santa Cruz de Tenerife, Spain

[21] Institute of Physics and Astronomy, University of Aarhus, Ny Munkegade, DK-8000 Aarhus C

ABSTRACT

We present a sample of 77 optical afterglows (OAs) of *Swift* detected gamma-ray bursts (GRB) for which spectroscopic follow-up observations have been secured. Our first objective is to measure the redshifts of the bursts. For the majority (90%) of the afterglows the redshifts have been determined from the spectra. We provide line-lists and equivalent widths (EWs) for all detected lines redward of Lyα covered by the spectra. In addition to the GRB absorption systems these lists include line strengths for a total of 33 intervening absorption systems. We discuss to what extent the current sample of *Swift* bursts with OA spectroscopy is a biased subsample of all *Swift* detected GRBs. For that purpose we define an X-ray selected statistical sample of *Swift* bursts with optimal conditions for ground-based follow up from the period March 2005 to September 2008; 146 bursts fulfill our sample criteria. We derive the redshift distribution for the statistical (X-ray selected) sample and conclude that less than 18% of *Swift* bursts can be at $z > 7$. We compare the high energy properties (e.g. γ-ray (15–350 keV) fluence and duration, X-ray flux and excess absorption) for three sub-samples of bursts in the statistical sample: *i)* bursts with redshifts measured from OA spectroscopy, *ii)* bursts with detected optical and/or near-IR afterglow, but no afterglow-based redshift, and *iii)* bursts with no detection of the OA. The bursts in group *i)* have slightly higher γ-ray fluences and higher X-ray fluxes and significantly less excess X-ray absorption than bursts in the other two groups. In addition, the fractions of dark bursts, defined as bursts with an optical to X-ray slope $\beta_{\rm OX} < 0.5$, is 14% in group *i)*, 38% in group *ii)* and $> 39\%$ in group *iii)*. For the full sample the dark burst fraction is constrained to be in the range 25%–42%. From this we conclude that the sample of GRBs with OA spectroscopy is not representative for all *Swift* bursts, most likely due to a bias against the most dusty sight-lines. This should be taken into account when determining, e.g., the redshift or metallicity distribution of GRBs and when using GRBs as a probe of star formation. Finally, we characterize GRB absorption systems as a class and compare them to QSO absorption systems, in particular the damped Lyα absorption (DLA) systems. On average GRB absorbers are characterized by significantly stronger EWs for H I as well as for both low and high ionization metal lines than what is seen in intervening QSO absorbers. However, the distribution of line strengths is very broad and several GRB absorbers have lines with EWs well within the range spanned by QSO-DLAs. Based on the 33 $z > 2$ bursts in the sample we place a 95% confidence upper limit of 7.5% on the mean escape fraction of ionizing photons from star-forming galaxies.

Subject headings: dust, extinction — galaxies: high-redshift — gamma rays: bursts

---

[1] Based on observations collected at the European Organisation for Astronomical Research in the Southern Hemi-

1. Introduction

The exploration of gamma-ray bursts (GRBs) has been among the most fascinating one in the last decade of astrophysical research. After the breakthrough in 1997, when X-ray and optical afterglows were discovered (Costa et al. 1997; van Paradijs et al. 1997), progress has been rapid. The connection between long-duration GRBs and star-forming galaxies has been empirically well established. There is an exclusive coincidence of long-duration GRBs with actively star-forming galaxies (e.g., Hogg & Fruchter 1999; Bloom et al. 2002; Fruchter et al. 2006), the majority of which show elevated specific star-formation rates (Christensen et al. 2004). In several cases long-duration GRBs have been directly associated with SNe (e.g., Hjorth et al. 2003; Stanek et al. 2003; Campana et al. 2006; Woosley & Bloom 2006). Only a decade after the first afterglow detection GRBs have allowed to probe the Universe to redshifts from almost 0 to larger than 8, representing larger look-back times than accessible with any other class of astrophysical objects (Jakobsson et al. 2006a; Tanvir et al. 2009; Salvaterra et al. 2009).

An important objective is to use GRBs as cosmological probes to study star formation primarily in the distant Universe. GRBs may be ideal probes as each burst pinpoints the location of a single massive star. Hence, GRBs may allow a census of where massive stars are formed throughout the observable Universe (e.g., Wijers et al. 1998). Through optical spectroscopy of the afterglows we can measure metallicities, molecular content and kinematical properties of the sight-lines to bursts within their hosts. After the bursts have faded away, imaging allows a detailed study of the host galaxies in emission, providing a census of the classes of galaxies contributing to the global star-formation density as a function of redshift. There are three main issues to consider in this context: observational bias, intrinsic bias, and the influence the GRBs and their afterglows may have on their environments. Concerning intrinsic bias it is believed that massive stars require a low metallicity to retain enough angular momentum to form a GRB (e.g., Hirschi et al. 2005; Woosley & Heger 2006) and the GRBs hence are biased tracers of star formation (e.g., Guetta & Piran 2007; Kistler et al. 2008). Nevertheless, to establish if the evidence supports a low metallicity bias it is necessary to first establish the importance and possible implications of observational bias, in particular as such a bias, if it exists, unavoidably will impact the measured distribution of metallicities for GRBs (see also Berger et al. 2007). Finally, concerning the issue of the impact of the GRBs and their afterglows on the gas along the line-of-sight it is now well established that UV pumping affects intervening gas in the hosts (Dessauges-Zavadsky et al. 2006; Vreeswijk et al. 2007; D'Elia et al. 2009a,b; Ledoux et al. 2009). It is also expected on theoretical grounds that GRB afterglows may

---

sphere, Chile, under programs 275.D-5022, 075.D-0270, 077.D-0661, 077.D-0805, 078.D-0416, 079.D-0429, 080.D-0526, 081.A-0135, 281.D-5002, and 081.A-0856. Also based on observations made with the Nordic Optical Telescope, operated on the island of La Palma jointly by Denmark, Finland, Iceland, Norway, and Sweden, in the Spanish Observatorio del Roque de los Muchachos of the Instituto de Astrofisica de Canarias. Some of the data obtained herein were obtained at the W.M. keck Observatory, which is operated as a scientific partnership among the California Institute of Technology, the University of California and the National Aeronautics and Space Adminisration. The Observatory was made possible by the generous financial support of the W.M. Keck foundation.

destroy dust in the near environment of the burst possibly out to as far as 100 pc from the GRB (Fruchter, Krolik & Rhoads 2001).

To address the issue of observational bias it is necessary to build a sample of GRBs for which the incompleteness is well understood and can be quantified. In this paper we present a spectroscopic sample of long-duration GRBs discovered by the *Swift* mission (Gehrels et al. 2004) for which follow-up optical spectroscopy has been secured. The purpose of the paper is twofold: *i)* to discuss the GRB absorbers as a class and compare this class of absorbers with QSO absorbers, and *ii)* to discuss to which extent our current sample of GRBs with measured redshifts from optical afterglow (OA) spectroscopy is a biased sub-sample of all GRBs. GRB absorbers have been compared with other classes of absorbers in several papers in the literature (e.g., Jensen et al. 2001; Savaglio et al. 2003, Jakobsson et al. 2006b, Fynbo et al. 2006b, Savaglio 2006; Prochaska et al. 2007a, 2008b; Fynbo et al. 2008a). However, most of these studies have been based on samples containing only few and/or predominantly optically bright afterglows. The issue of bias in the samples of GRBs with measured redshift has been discussed in the literature before (e.g., Bloom 2003; Fiore et al. 2007; Coward 2009). Fiore et al. discussed the importance of selection effects in the properties of the detection of the GRBs themselves, e.g. the sensitivity of the triggering detector as a function of energy. Coward argued that there is a learning curve at work in the following sense: over the years since the launch of *Swift* the mean time taken to acquire spectroscopic redshifts for a GRB afterglow has evolved to shorter times. He also finds a correlation between the mean time before a spectroscopic redshift is secured and the measured redshift suggesting that low redshift bursts were preferentially missed in the first years of *Swift* operation. We have been following the same follow-up strategy since the launch of *Swift*. Furthermore, for the present study we only include *Swift* bursts detected after March 2005 where *Swift* operations were well established. Hence, for the present study there should be no significant issue with a learning curve. Here we will rather try to infer to which extent the sample of bursts with follow-up optical spectroscopy could be biased against, e.g., dusty sight-lines.

The paper is organized in the following way: In Sect. 2 we define our sample and provide a list of the GRBs for which we present spectra in this paper. Sect. 3 describes our observations and data reduction. In Sect. 4.1 we present the redshift distribution of the statistical sample. In sect. 4.2 we discuss biases in the sample of bursts with optical afterglow spectroscopy. In Sect. 4.3 we discuss GRB absorbers as a class and compare them to QSO absorbers. In Sect. 4.5 we briefly discuss the intervening absorbers in the sample. Finally in Sect. 5 we offer our conclusions. In Appendices A and B we provide line-lists and plots of the spectra for the 77 optical GRB afterglows in our sample and provide notes on individual objects.

Throughout this paper we assume a flat cosmology with $\Omega_\Lambda = 0.70$, $\Omega_m = 0.30$, and a Hubble constant of $H_0 = 70$ km s^{-1} Mpc^{-1}.

2. The Sample

The aim of the sample selection is to construct a sample of long GRBs that is selected independent of the optical properties of the afterglows and at the same time has as high completeness in high quality optical follow-up as possible. We find that the optimal way to build such a sample is by including all *Swift* GRBs fulfilling the following criteria (Jakobsson et al. 2006a):

1. A *Swift* detected GRB with observed duration $T_{90} > 2$ s

   We wish to build a sample of long-duration GRBs known to be associated with massive stellar death. We could choose to make a stronger cut, e.g. $T_{90} > 5$ s, in order to avoid contamination from the long tail of the short-duration bursts. However, the number of bursts with $2 < T_{90} < 5$ s is so small that this would not make a significant difference for the statistical properties of the sample. Therefore we choose to keep the standard operational definition of long GRBs (Kouveliotou et al. 1993).

2. XRT afterglow position distributed within 12 hr

   With this criterion we secure that a precise afterglow position is available quickly which is crucial for efficient ground based follow-up. This criterion also excludes bursts close to the Moon.

3. Small foreground Galactic extinction: $A_{\rm V} < 0.5$ mag

   With this criterion we remove from the sample bursts with high Galactic extinction. These bursts are typically also located in very crowded fields. Removing these bursts from the sample does not introduce any bias on the intrinsic properties of the bursts.

4. Favorable declination: $-70^\circ < \delta < 70^\circ$

   For bursts close to the poles the probability to secure ground based follow-up is smaller and we therefore apply this declination cut to the sample.

5. Sun-to-field distance larger than 55°

   Bursts that are too close to the Sun cannot be observed from the ground for very long. With this criterion we will have at least one hour during night time to secure a spectrum within 24 hr after the burst.

About 50% of all *Swift* GRBs do not fulfill these criteria, primarily for two reasons: first *Swift* has to point close to the Sun a significant fraction of the time, and second the fraction of the sky with Galactic $A_{\rm V} > 0.5$ mag is about 34%. For bursts fulfilling the above criteria, we have attempted to detect optical and near-infrared afterglows and to measure their redshifts. Also, these bursts will have a high probability of being well observed by other follow-up teams.

3. Observations and Data Reduction

In this paper we include bursts in the time interval from March 2005 to September 2008. In this period, 146 bursts fulfilled our sample criteria (see Table A1). These we will refer to as the *statistical sample* in the following. For 69 of these we present spectroscopic observations in this paper. Most of the spectra have been obtained through our target-of-opportunity programs, but we also include a few spectra which we have obtained from the ESO and Gemini archives.

The spectra were obtained using one of the following instruments: *i)* the Nordic Optical Telescope (NOT) equipped with the Andalusian Faint Object Spectrograph and Camera (AlFOSC), *ii)* the ESO-VLT equipped with either one of the two FOcal Reducer and low dispersion Spectrographs (FORS1 and FORS2), or in rare cases the Ultraviolet and Visual Echelle Spectrograph (UVES), *iii)* one of the Gemini telescopes equipped with one of the Gemini Multi-Object Spectrographs (GMOS-N and GMOS-S), *iv)* the 3m Shane Telescope at Lick Observatory equipped with the dual-channel Kast spectrometer, *v)* the Keck telescope equipped with the Low Resolution Imaging Spectrograph (LRIS, Oke et al. 1995). In Table 1 we provide further details of each of the instrumental setups applied in this work.

The longslit spectra were reduced using standard methods for bias subtraction, flat-fielding and wavelength calibration. Most of the spectra have been flux calibrated using observations of spectrophotometric standard stars observed with the same setup as the afterglow spectra. For a few of the spectra no standard star spectra were secured and here we instead provide normalized spectra. Afterglows observed with UVES will be discussed in detail elsewhere (see, e.g., Fox et al. 2008; Ledoux et al. 2009), and for these bursts we here only show the spectra and provide equivalent width (EW) measurements of the Si II,1526 and/or C IV lines.

The spectra have been obtained under very diverse observing conditions (see Table 2). Given the transient nature of GRBs the afterglows often have to be observed at high airmass, with poor seeing, through clouds and/or with a large Moon phase. In a few cases we observed the afterglows in twilight.

The full list of spectroscopic targets is given in Table 2. In the table we also include 8 bursts that do not fulfill the sample criteria for which we also have secured spectra. In the following we refer to the bursts in Table 2 as the *spectroscopic sample.*

Table 1. Instrumental setups used for the spectroscopic data presented in this work. Resolutions are given for a 1 arcsec slit even though we some times used a slightly wider slit.

Telescope	Instrument	Grating	Resolution	Range [Å]
VLT	FORS1/2	300V	440	3400–9500
VLT	FORS1/2	1400V	2100	4600–5900
VLT	FORS1/2	1200R	2140	5800–7300
VLT	FORS1/2	600I	1500	6600–9400
VLT	UVES		45000	
Gemini-S/N	GMOS-S/N	R831	2200	5300–9000
		R400	965	5300–9000
		R150	315	4500–10000
		B600	844	3400–6000
Keck 1	LRIS	R300	540	3900–8000
		R400	1100	5800–9200
	HIRES		45000	
Shane-3m	Kast	600/7500	1000	3800–10000
		800/3460	1500	3800–7310
NOT	AlFOSC	G4	355	3600–9000

Table 2. The spectroscopic sample. We here list the burst names and details of the spectroscopic observations. The column Δt shows the time after trigger when the spectroscopic observation was started. $\mathrm{Mag}_{\mathrm{acq}}$ gives the approximate magnitude (typically in the R-band) of the afterglow in the acquisition image.

GRB	Instrument	Exptime (ks)	Airmass	Seeing (arcsec)	Δt (hr)	$\mathrm{Mag}_{\mathrm{acq}}$	Redshift	Ref
050319	AlFOSC	2.4	1.1	1.3	34.5	21.0	3.2425	(1)
050401	FORS2	11.6	1.1–1.7	0.7	14.7	23.3	2.8983	(2)
050408	GMOS-N	3.6				21.0	1.2356	(3)
050730	FORS2	1.8	1.2	1.5	4.1	17.8	3.9693	(4)
050801	LRIS	1.8	1.9	–	5.7	20.7	1.38	(5)
050802	AlFOSC	4.8	1.2	0.7	11.4	20.5	1.7102	(6)
050820A	UVES	12.1	2.1	1.0	0.5	16.0	2.6147	(7)
050824	FORS2	3.0	1.8	0.7	9.5	20.6	0.8278	(8)
050908	FORS1	3.6	1.1	0.6	1.6	20.5	3.3467	(9)
050922C	AlFOSC	2.4	0.9	1.3	1.0	16.5	2.1995	(1)
060115	FORS1	3.6	1.3–1.6	0.7	8.9	22.0	3.5328	(10)
060124	LRIS	1.0	1.6	1.0	16.1	19.5	2.3000	(11)
060206	AlFOSC	2.4	1.0	1.2	0.3	17.5	4.0559	(12)
060210	GMOS-N	3.0	1.1	–	1.2	20.6	3.9133	(13)
060502A	GMOS-N	3.6	1.6	–	5.2	21.2	1.5026	(14)
060512	FORS1	3.6	2.5	1.6	3.0	19.9	2.1	(15)
060526	FORS1	9.9	1.1–1.4	1.3	8.8	19.5	3.2213	(1)
060604	AlFOSC	1.2	1.7	1.0	10.0	21.5	$\lesssim 3$	(16)
060607A	UVES	12.0	1.9–1.0	1.0	0.1	14.7	3.0749	(17)
060614	FORS2	1.8	1.2	0.7	21.1	19.8	0.1257	(18)
060707	FORS2	5.4	1.0	1.1	34.4	22.4	3.4240	(1)
060708	FORS2	3.6	1.2	0.6	43.0	22.9	1.92	(19)
060714	FORS1	5.4	1.1	0.7	8.5	20.4	2.7108	(1)
060719	FORS2	2.4	1.1	2.2	50.0	24.5	$\lesssim 4.6$	(5)
060729	FORS2	5.4	2.0–2.6	1.5	13.2	17.5	0.5428	(20)
060807	FORS1	7.2	1.8	0.8	9.5	22.9	$\lesssim 3.4$	(21)
060908	GMOS-N	1.8	1.2	1.6	2.0	19.8	1.8836	(22)
060927	FORS1	5.4	1.2	1.5	12.5	24.0	5.4636	(23)
061007	FORS1	5.4	1.2–1.3	0.9	17.4	21.5	1.2622	(24)
061021	FORS1	1.8	1.9	0.8	16.5	20.5	0.3463	(25)
061110A	FORS1	5.4	1.4–1.8	0.8	15.0	22.0	0.7578	(26)
061110B	FORS1	3.6	1.3–1.5	0.7	2.5	22.5	3.4344	(27)

Table 2—Continued

GRB	Instrument	Exptime (ks)	Airmass	Seeing (arcsec)	Δt (hr)	Mag$_{\mathrm{acq}}$	Redshift	Ref
061121	LRIS	1.2	1.2	–	0.2	17.8	1.3145	(28)
070110	FORS2	5.4	1.5–1.9	1.0	17.6	20.8	2.3521	(29)
070129	FORS2	1.8	2.2	1.0	2.2	21.3	$\lesssim 3.4$	(1)
070306	FORS2	5.4	1.2–1.3	1.0	34.0	23.1	1.4965	(30)
070318	FORS1	1.8	1.6	0.7	16.7	20.2	0.8397	(31)
070419A	GMOS-N	2.4	1.2–1.3	–	0.8	20.4	0.9705	(5)
070506	FORS1	2.7	1.6–1.8	1.1	4.0	21.0	2.3090	(32)
070611	FORS2	3.6	1.1–1.2	1.0	7.7	21.0	2.0394	(33)
070721B	FORS2	5.4	1.2–1.5	1.2	21.6	24.3	3.6298	(34)
070802	FORS2	5.4	1.2	0.5	1.9	21.9	2.4541	(35)
071020	FORS2	0.6	2.0	1.0	2.0	20.4	2.1462	(36)
071025	HIRES	1.8	1.35	–	–	–	5.2	(1)
071031	FORS2	1.8	1.2	1.0	1.2	18.9	2.6918	(37)
071112C	FORS1	3.6	1.7	1.2	9.0	21.9	0.8227	(38)
071117	FORS1	5.4	1.4	0.9	9.0	23.0	1.3308	(39)
080210	FORS2	1.2	1.8–2.4	1.4	0.7	18.8	2.6419	(40)
080310	Kast	1.8	–	–	–	17.0	2.4274	(41)
080319B	FORS2	3.6	2.1–2.3	1.0	26.0	20.5	0.9382	(42)
080319C	GMOS-N	3.6	1.2	1.7	2.4	21.1	1.9492	(43)
080330	AlFOSC	1.8	1.8	1.5	0.8	17.6	1.5119	(44)
080413B	FORS1	0.6	1.5	0.5	0.8	19.3	1.1014	(45)
080520	FORS2	5.4	1.2	0.7	7.3	23.0	1.5457	(46)
080523	FORS2	5.4	1.8–2.0	1.0	10.9	23.	$\lesssim 3.0$	(47)
080603B	AlFOSC	2.0	1.3	1.0	2.0	17.5	2.6892	(48)
080604	GMOS-N	1.8	1.3	1.0	1.6	21.9	1.4171	(49)
080605	FORS2	0.6	1.4–1.9	0.9	1.7	20.4	1.6403	(50)
080607	LRIS	5.1	1.0	0.8	0.2	18.9	3.0368	(51)
080707	FORS1	2.4	2.1–2.5	2.2	1.1	19.6	1.2322	(52)
080710	GMOS-S	2.4	1.6	–	2.2	–	0.8454	(53)
080721	FORS1	1.2	1.5	1.7	10.2	20.0	2.5914	(54)
080804	UVES	4.7	2.1–2.5	0.9	0.8	19.0	2.2045	(55)
080805	FORS2	1.2	1.7	1.0	1.0	21.5	1.5042	(56)

Table 2—Continued

GRB	Instrument	Exptime (ks)	Airmass	Seeing (arcsec)	Δt (hr)	$\mathrm{Mag}_{\mathrm{acq}}$	Redshift	Ref
080810	AlFOSC	2.4	1.8	1.0	10.6	19.1	3.3604	(57)
080905B	FORS2	0.6	1.3	1.7	8.3	20.2	2.3739	(58)
080913	FORS2	1.8	1.0	1.1	2.0	24.2	6.7	(59)
080916A	FORS2	3.6	1.2	0.9	17.1	22.3	0.6887	(60)
080928	FORS2	1.8	1.6	1.1	15.5	20.4	1.6919	(61)
060904B[1]	FORS1	3.6	1.1–1.3	0.7	5.1	19.9	0.7029	(62)
060906[1]	FORS1	4.8	2.0	0.9	1.0	20.0	3.6856	(1)
060926[1]	FORS1	4.8	1.7–2.4	1.0	7.7	23.0	3.2086	(1)
070125[1]	FORS2	1.8	1.8	0.8	21.0	18.8	1.5471	(5)
070411[1]	FORS2	3.0	1.4–1.7	1.0	5.0	20.8	2.9538	(63)
070508[1]	FORS1	5.4	1.7	1.3	3.8	22.0	$\lesssim 3.0$	(64)
080411[1]	FORS1	0.6	2.3–2.6	1.1	2.4	17.5	1.0301	(65)
080413A[1]	UVES	2.7	1.2–1.6	0.7	3.7	19.0	2.4330	(66)

[1] Not part of the statistical sample

References. — (1) Jakobsson et al. (2006b); (2) Watson et al. (2006); (3) Foley et al. (2007); (4) D'Elia et al. (2005); (5) This work; (6) Fynbo et al. (2005); (7) Ledoux et al. (2005); (8) Sollerman et al. (2007); (9) Fugazza et al. (2005); (10) Piranomonte et al. (2006a); (11) (Prochaska et al. 2006a); (12) Fynbo et al. (2006b); (13) (Cucchiara et al. 2006a); (14) (Cucchiara et al. 2006b); (15) (Starling et al. 2006a); (16) Castro-Tirado et al. (2006); (17) Ledoux et al. (2006a); (18) Della Valle et al. (2006); (19) Jakobsson et al. (2006c); Oates et al. (2009); (20) Thöne et al. (2006a); (21) Piranomonte et al. (2006b); (22) (Rol et al. 2006); (23) (Ruiz-Velasco et al. 2007); (24) Jakobsson et al. (2006d); (25) Thöne et al. (2006b); (26) Thöne et al. (2006c); Fynbo et al. (2007); (27) Fynbo et al. (2006a); (28) (Bloom et al. 2006b); (29) Jaunsen et al. (2007b); (30) Jaunsen et al. (2008); (31) Jaunsen et al. (2007a); (32) Thöne et al. (2007b); (33) Thöne et al. (2007a); (34) Malesani et al. (2007); (35) Elíasdóttir et al. (2009); (36) Jakobsson et al. (2007c); (37) Ledoux et al. (2008); (38) Jakobsson et al. (2007d); (39) Jakobsson et al. (2007e); (40) Jakobsson et al. (2008a); (41) (Prochaska et al. 2008c); (42) Vreeswijk et al. (2008b); (43) (Wiersema et al. 2008a); (44) Guidorzi et al. (2009); (45) Vreeswijk et al. (2008c); (46) Jakobsson et al. (2008b);

(47) Fynbo et al. (2008b); (48) Fynbo et al. (2008c); (49) (Wiersema et al. 2008b); (50) Jakobsson et al. (2008c); (51) (Prochaska et al. 2009); (52) Fynbo et al. (2008d); (53) (Perley et al. 2008); (54) Starling et al. (2009); (55) Thöne et al. (2008d); (56) Jakobsson et al. (2008e); (57) de Ugarte Postigo et al. (2008); (58) Vreeswijk et al. (2008d); (59) Fynbo et al. (2008e); Greiner et al. (2009); (60) Fynbo et al. (2008f); (61) Vreeswijk et al. (2008e); (62) Fugazza et al. (2006); (63) Jakobsson et al. (2007a); (64) Jakobsson et al. (2007b); (65) Thöne et al. (2008b); (66) Thöne et al. (2008c);

4. Results

In Appendix A we provide notes on each burst in our spectroscopic sample. In Tables 5–72 in appendix B we provide linelists for all lines detected redward of Lyα both from the GRB absorbers and for intervening absorption systems. We provide measurements for all lines for which we can measure the EWs with a signal-to-noise ratio higher than 2. The EWs are measured in normalized spectra using an aperture given by 2 times the resolution full-width-at-half-maximum (for unresolved lines) or from where the profile reaches 1 on each side of the profile (for resolved or blended lines). The error bar includes the statistical noise and the error from the normalization. For the Lyα lines we do not provide EWs. Instead we in Table 4 provide the H I column densities derived from Voigt-profile fits to the Lyα lines. In cases where several lines are blended we provide the EWs for the full blend. In cases where three or more lines are blended we have drawn a dashed line around the blend in the tables to ease the reading. In Fig. 14 in the appendix we show 1- and 2-dimensional spectra of each of the 77 bursts listed in Table 2.

4.1. Redshift Distribution

Our first objective is to measure the true redshift distribution of *Swift* GRBs and in particular to constrain the fraction of *Swift* bursts that could be at very high redshifts (here $z > 6$–7). The error on the redshifts are typically a few permille.

As mentioned in Sect. 2, 146 *Swift* bursts fulfill our selection criteria for the statistical sample in Sect. 2. Table 73 in the appendix includes all 146 bursts and their redshift constraints. The optical and/or near-IR afterglow is detected for 108 of the bursts. This completeness of 74% is much higher than for pre-*Swift* samples where only about 30% of the bursts have detected optical/near-IR afterglows (e.g., Fynbo et al. 2001; Lazzati et al. 2002). For the full sample of all *Swift* bursts observed in the same period from March 2005 to September 2008, 198 out of 371 (53%) have detected optical/near-IR afterglows and this difference between the statistical sample and the full *Swift* sample illustrates the motivation for our sample criteria.

The redshift is determined from the OA for 72 bursts in the statistical sample (5 of these are photometric redshifts based on the detection of the Lyman-break or Lyα break in the spectral energy distribution of the afterglow). For an additional 12 the redshift is determined from the likely host galaxy. For 25 bursts an upper limit can be placed on the redshift through detection of the OA and hence establishing an upper limit to the position of the Lyman-limit or Lyα breaks. For the remaining 37 we have no constraints on the redshift from the OA or host galaxy (four of these are detected in the J, H and/or K-band, but these detection do not provide constraining, i.e. $z < 10$, redshift limits). For these bursts we follow Grupe et al. (2007) and assign a redshift upper limit to bursts with excess (over Galactic) X-ray absorbing column density above an equivalent H I column density of 2×10^{21} cm^{-2} (also taking uncertainty into account). Grupe et al. used an upper limit of $z = 2$, but we will be slightly more conservative and assign an upper limit of $z = 3.5$ to these bursts (corresponding to an upper limit on the intrinsic absorbing column of about 10^{23} cm^{-2} for Solar metallicity). 10 bursts fulfill this criterion at 90% confidence. We will return to the issue of X-ray absorption in Sect. 4.2 below. In Fig. 1 we show the resulting redshift distribution for the full sample of 146 bursts. Both the median and the mean of the measured redshifts is 2.2. The fraction of $z > 6$ bursts is constrained to be in the range 1–23% (2–34 out of 146) and the fraction of $z > 7$ bursts are less than about 18% (27 out of 146). Based on detections of likely host galaxies of dark bursts[2], Perley et al. (2009) constrain the fraction of $z > 7$ bursts further to $< 7\%$ at 90% confidence. A similar conclusion is reached from a study of a complete sample of GRB host galaxies (Hjorth et al. in preparation).

It has been argued that the redshift measurements of *Swift* GRBs show evidence for a "learning curve" in the sense that the mean time before a spectrum is secured is decreasing and that the mean redshift is also decreasing as a function of time since the launch of *Swift* (Coward 2009). In Fig. 2 we plot the magnitude of the afterglow at acquisition against the time of the burst and color code the points by redshift. The mean (median) times after burst at the start of integration are 9.7 (9.5) hr, 9.6 (8.5) hr, 10.4 (7.7) hr, and 5.3 (2.0) hr for 2005, 2006, 2007 and 2008 respectively. The corresponding median redshifts are 2.9, 2.7, 2.0, and 2.0. Hence, there does seem to be a tendency for the bursts to be spectroscopically observed earlier and for the median redshift to decrease. However, the effect is very small and the scatter is large. If we simply split the sample in two at the median time after trigger of 5 hr then we find mean redshifts and standard deviations for triggers before and after 5 hr are $< z >= 1.9$, $\sigma(z) = 1.2$ and $< z >= 2.5$, $\sigma(z) = 1.2$, respectively.

4.2. How Biased is the Optical Afterglow Spectroscopy Sample?

Whereas there is evidence that the QSO-DLAs drawn from samples of optically selected QSOs are fairly representative for the full underlying population (Ellison et al. 2001; Akerman et al. 2005; Ellison et al. 2008) this may well not be the case for the sample of GRB absorbers with OA spectroscopy. It was found soon after the discovery of OAs that some bursts are very faint in the optical (e.g., Groot et al. 1998). There is growing evidence that such bursts are mainly associated with dusty sight-lines (e.g., Levan et al. 2006; Watson et al. 2006; Berger et al. 2007; Jaunsen et al. 2008; Tanvir et al. 2008a; Elíasdóttir et al. 2009; Prochaska et al. 2009; Perley et al. 2009; Zheng, Deng & Wang 2009). Due to its high fraction of optical follow-up (and X-ray selection) our statistical sample is ideal to address this issue quantitatively.

In the following, we divide our statistical sample into three groups: *i)* bursts with redshifts measured from optical spectroscopy of the afterglow, *ii)* bursts with a detected OA, but no afterglow-based redshift measurement, and *iii)* bursts with no detection of the OA.

---

[2] Note that this work uses a somewhat different definition of dark bursts than the one we use in Sect. 4.2.3,

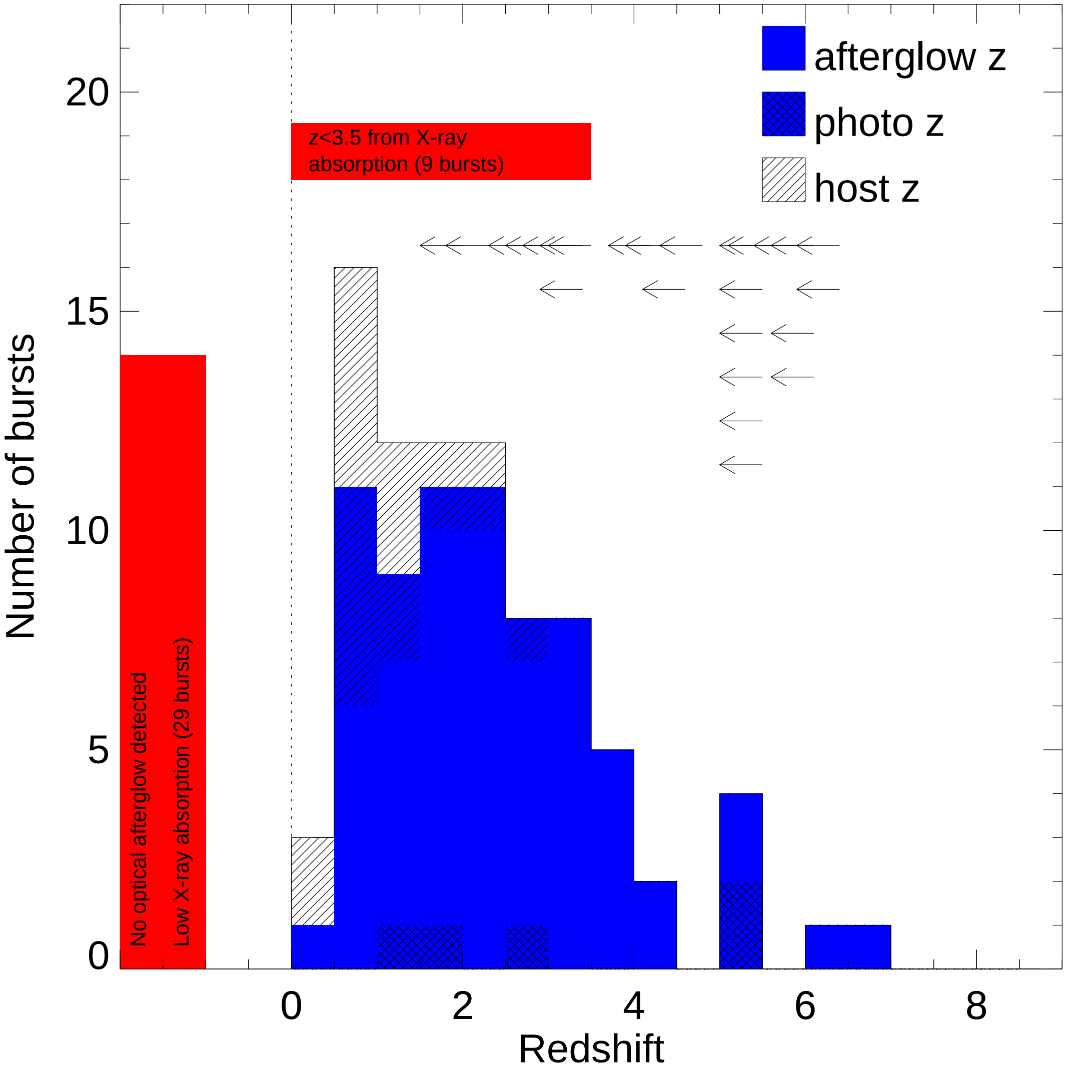

Fig. 1.— Redshift distribution of 146 *Swift* GRBs localized with the X-ray telescope and with low foreground extinction $A_{\rm V} < 0.5$. We indicate with different colors and shadings bursts depending on whether the redshift is based on afterglow spectroscopy, host emission lines (or both), or a photometric redshift based on the OA broadband colors. Bursts, for which only an upper limit on the redshift could be established from photometry of the OA, are indicated by arrows. The red histogram at the left indicates the 28 bursts with no OA detection, weak or absent X-ray absorption and no redshift measurement from the underlying host galaxy. For these bursts no redshift constraint could be inferred. The red block at the top indicates the 10 bursts for which the OA was not detected, but an upper limit of $z = 3.5$ could be placed based on excess X-ray absorption.

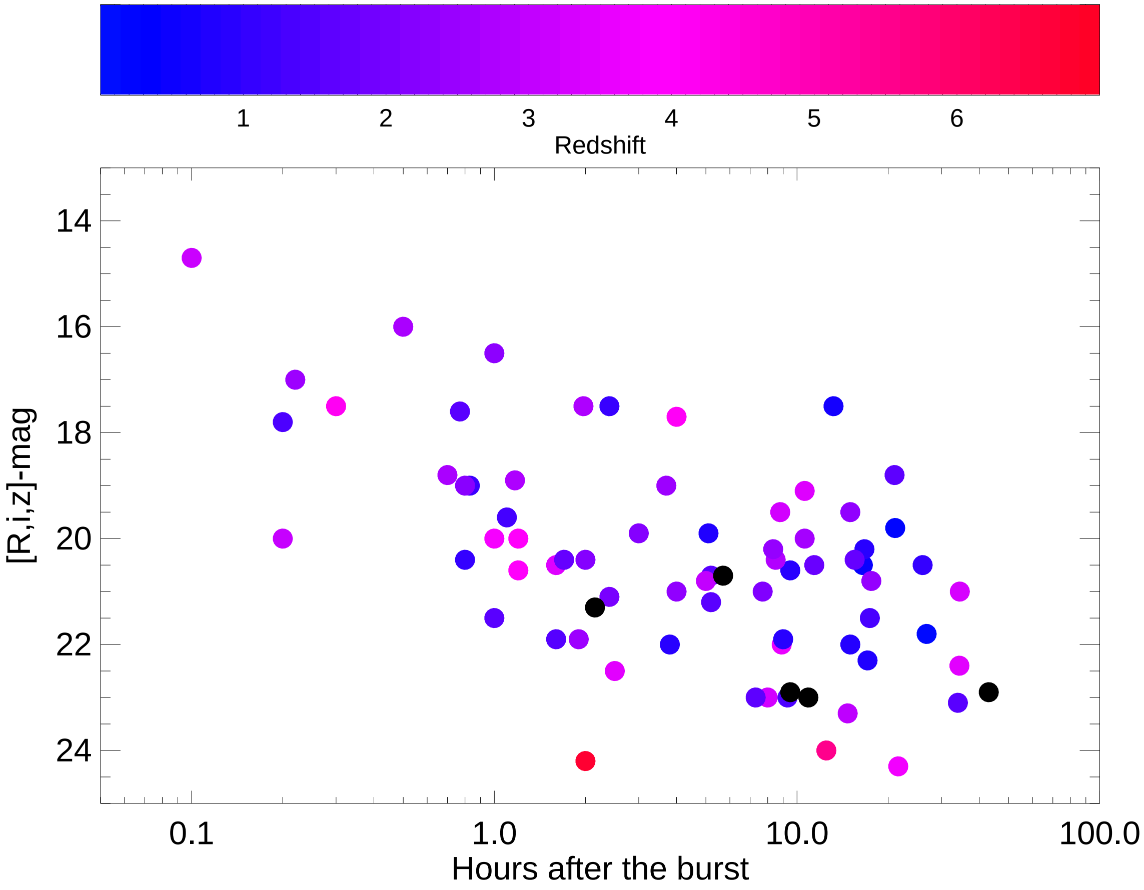

Fig. 2.— The R, i or z-band magnitude of the OAs in the acquisition image for the spectroscopy as a function of the time when the spectroscopic observations was started. The color bar in the top indicates the color code for the measured redshifts. Black points represents spectra for which we where not able to determine the redshift.

4.2.1. Distribution of the Sun Angle

As described in Sect. 2 we have defined our sample to only contain bursts with good conditions for optical/near-IR follow-up conditions. Nevertheless, it is clear that all the bursts in the statistical sample did not have equally good conditions for being observed from ground. In Fig. 3 we compare the Sun angle distribution for the three samples. The Sun angle is a good measure for how long a burst can be observed during night time from the ground. It is clear that bursts with no OA detections tends to be closer to the Sun and hence are more difficult to observe. This is one of the contributing reasons why these bursts do not have detected OAs.

4.2.2. Distributions of High-Energy Properties

In addition to the observational differences we are interested in revealing astrophysical differences between the bursts in the statistical sample. Essentially all long GRBs have an X-ray afterglow. In particular, in our statistical sample all bursts have available X-ray spectra from *Swift* (e.g., Evans et al. 2009). It is therefore interesting to compare the X-ray properties such as excess absorption and flux at fixed observed times for the the sample of GRBs with follow-up optical spectroscopy with those that do not. It has been found that the fluence of the prompt emission correlates with the flux of the X-ray afterglow at fixed rest-frame times (Nysewander, Fruchter & Peer 2009). We therefore compare both gamma-ray and X-ray properties of the three sub-samples. The results are shown in Fig. 4–7 (note that the number of bursts in each group is slightly different in the three plots as some of the measurements were unavailable for a few of the bursts). In Table 3 we provide the KS-test based probabilities that these three sub-samples are drawn from the same underlying distributions. It is clear that bursts in groups *ii)* and *iii)* have fainter afterglows and in particular more excess absorption than bursts in group *i)*. The most striking difference is the X-ray excess for which it is firmly excluded that groups *i)* and *iii)* are drawn from the same underlying distribution. A similar conclusion was reached by Schady et al. (2007a) based on a smaller sample.

4.2.3. Dark Bursts

We follow the definition of dark bursts advocated by Jakobsson et al. (2004), whereby dark bursts are defined as bursts with an optical to X-ray spectral slope $\beta_{\rm OX} < 0.5$. The fact that group *i)* is not representative for all bursts in the statistical sample is confirmed by the fraction of dark bursts in the three sub-samples (see Fig. 8). For 4 bursts in the sample it was not possible to calculate $\beta_{\rm OX}$ due to insufficient data (3 from group *ii)* and 1 from group *iii)*). In group *i)* the fraction of dark bursts is 14% (10/72), in group *ii)* it is 38% (12/32) and in group *iii)* the fraction has a lower limit of 39% (15/38). In the full statistical sample the fraction of dark bursts is constrained to be in the range 25–42%. Note that the $\beta_{\rm OX} < 0.5$ definition of dark bursts is conservative in the sense that a burst with an intrinsic $\beta_{\rm OX} = 1.25$ can suffer from ~ 6 mag extinction in the observed

R-band and still have an observed $\beta_{\rm OX} > 0.5$.

A contributing factor to the increasing "darkness" from groups *i)* to *iii)* could be a different fraction of bursts with cooling breaks between the optical and X-ray bands (Pedersen et al. 2006). However, the fact that GRBs in groups *ii)* and *iii*) have more excess absorption than bursts in group *i)* shows that dust extinction of the optical light most likely is the dominating factor for the higher dark burst fraction in groups *ii)* and *iii).* This is made clearer from Fig. 9 where we we plot $\beta_{\rm OX}$ against excess absorption for the full statistical sample. Bursts with $\beta_{\rm OX} < 0.5$ also have higher excess absorption than bursts with $\beta_{\rm OX} > 0.5$. The nine dark bursts in group *i)* are GRBs 050401, 050904, 060210, 070802, 080319C, 080605, 080607, 080805, and 080913. Two of these are dark due to high redshifts ($z > 6$) and the rest probably due to a combination of high column densities and high metallicities and hence high dust column densities.

4.3. GRB Absorption Systems Compared to QSO Absorption Systems

QSO absorption systems have been studied since the discovery of QSOs and for these systems a classification is well established (Weymann, Carswell & Smith 1981). Weymann et al. divided the QSO absorbers into four classes: A) associated broad absorption line systems, B) associated narrow line systems, C) intervening narrow metal line systems, and D) intervening Lyα forest systems. Classes C and D are further divided into subclasses such as Mg II absorbers, C IV absorbers, DLAs, sub-DLAs, etc. Clearly, these classes are not disjunct, i.e., DLAs are also Mg II and C IV absorbers, but the opposite is generally not true. The physical selection mechanism behind GRB absorption systems is fundamentally different from those of intervening QSO absorbers. Hence, the fact that GRB absorbers in many ways appear similar to mainly DLA absorbers provides interesting new information not only of the properties of the GRB host galaxies, but also about the physical origin of intervening QSO absorbers. Specifically, the fact that QSO-DLAs and GRB absorbers look so

Table 3. KS test probabilities that the bursts in group *ii)* (OA detected, but no OA based redshift) and group *iii)* (no OA detection) are drawn from the same distribution as group *i)* (bursts with OA based redshift measurement).

Property/group	*ii)*	*iii)*
0.3–10 keV flux 20000 s	6.1×10^{-2}	4.8×10^{-4}
X-ray excess abs	2.1×10^{-3}	7.0×10^{-7}
15-350 keV fluence	0.21	3.5×10^{-2}
15-350 peak flux	0.20	0.29
T_{90}	0.76	0.71

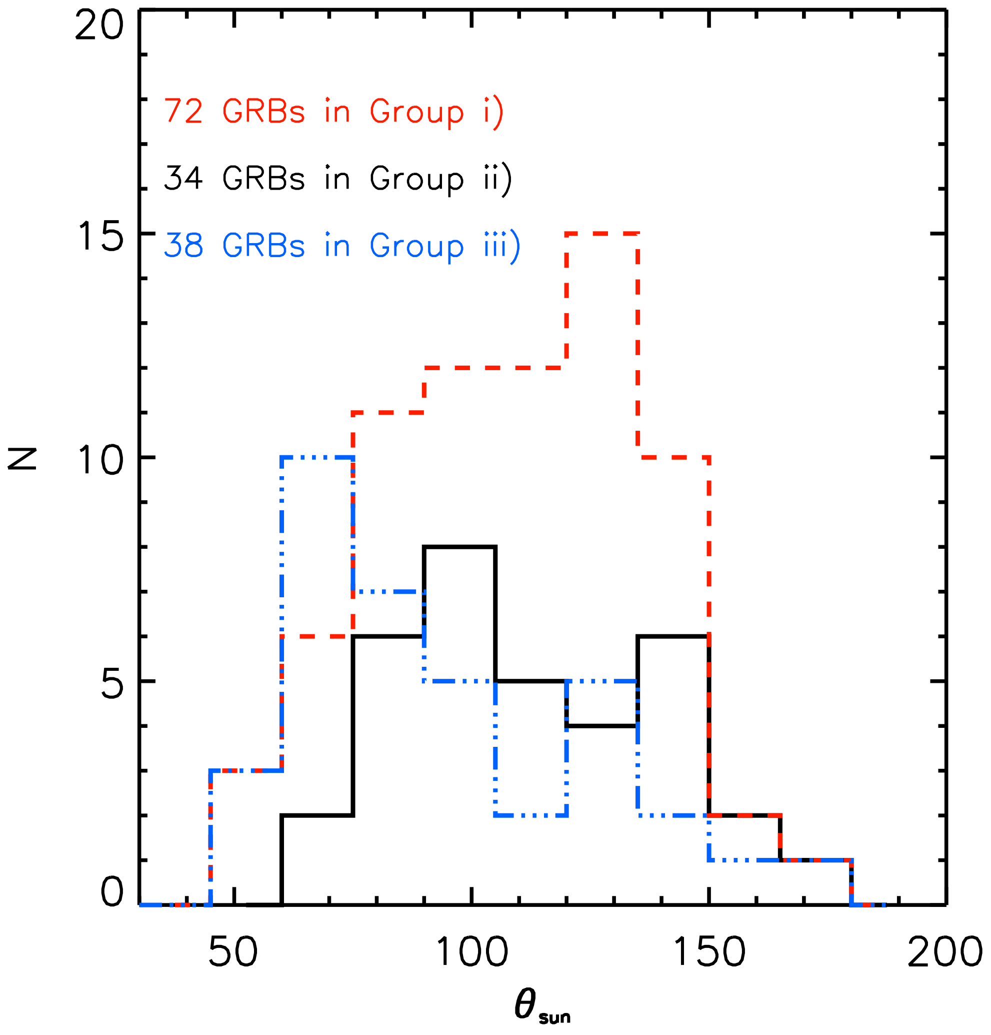

Fig. 3.— Sun angle distribution for members of the statistical sample.

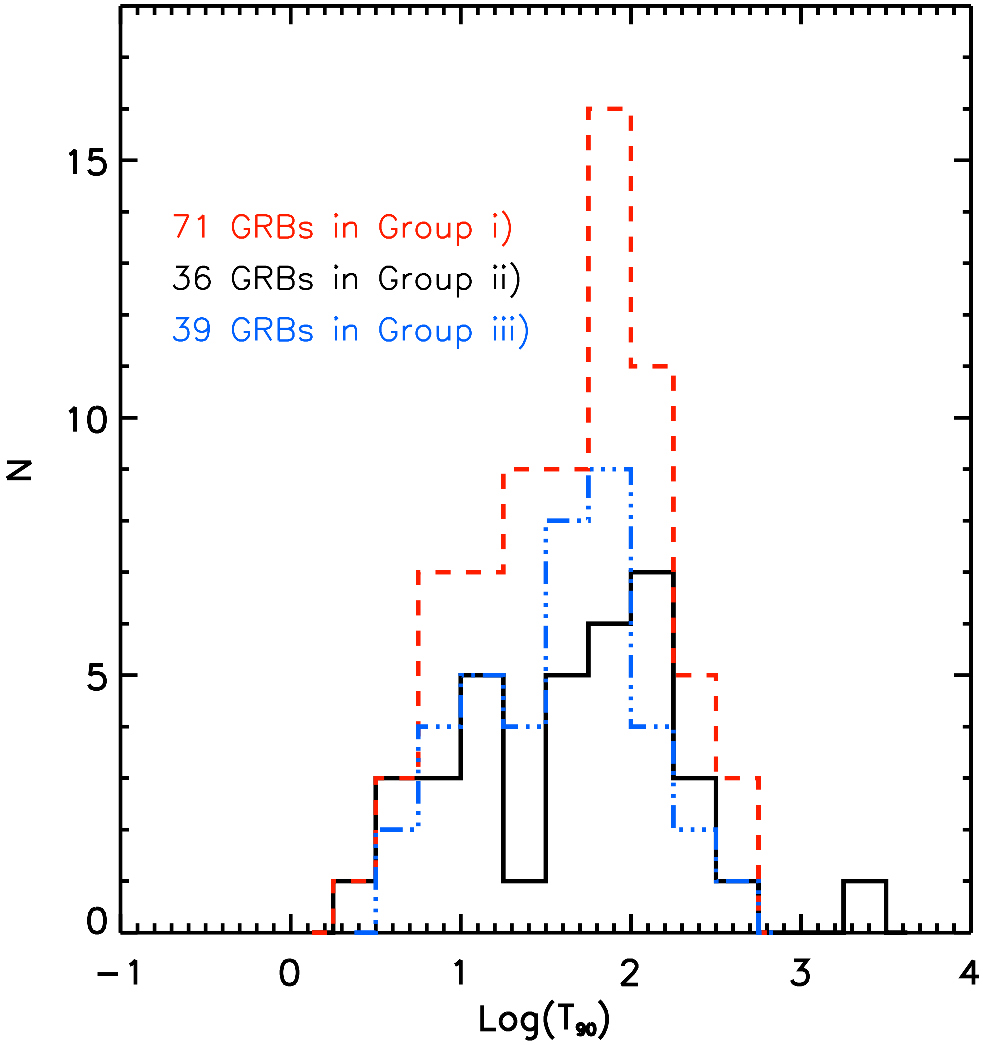

Fig. 4.— BAT T_{90} distribution for members of the statistical sample.

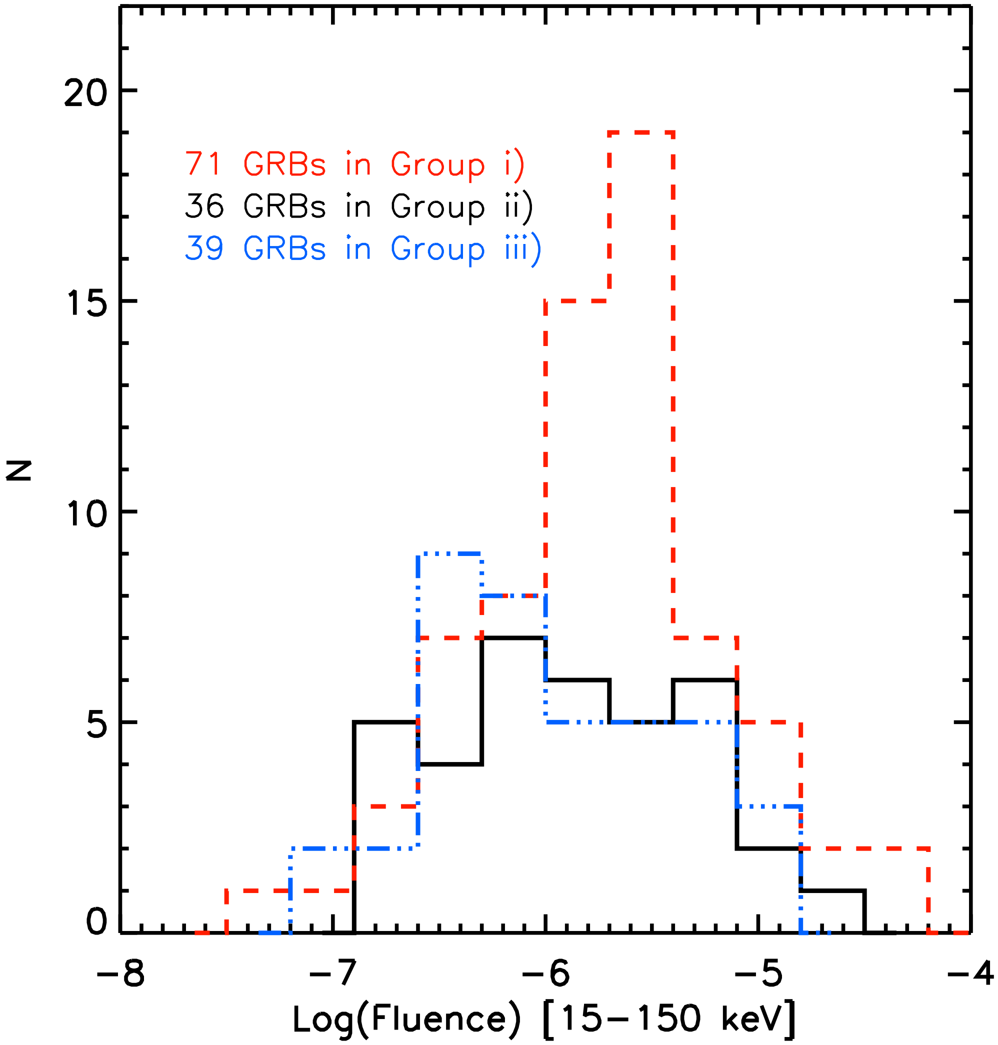

Fig. 5.— BAT Fluence distribution for members of the statistical sample.

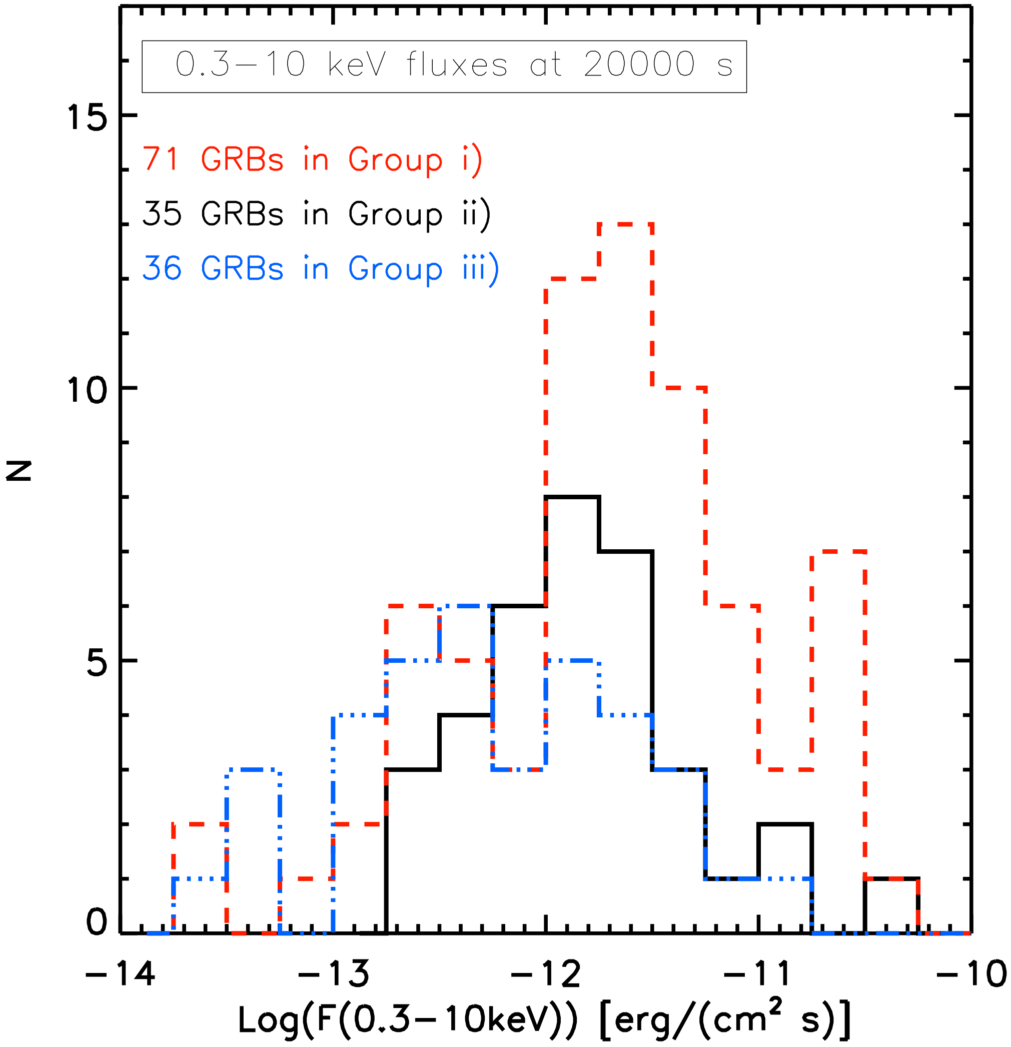

Fig. 6.— XRT flux distribution at 20000 s post burst for members of the statistical sample.

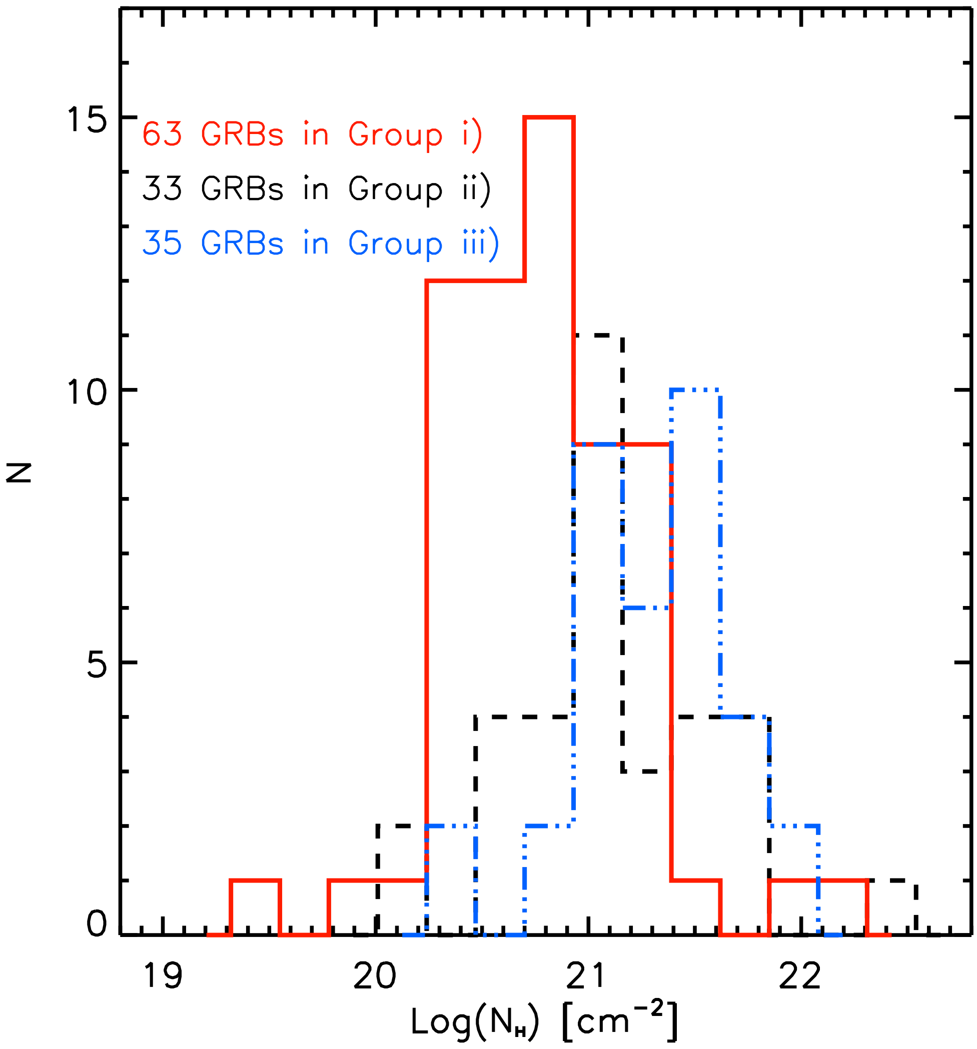

Fig. 7.— XRT excess absorption distribution (assuming $z = 0$) for members of the statistical sample.

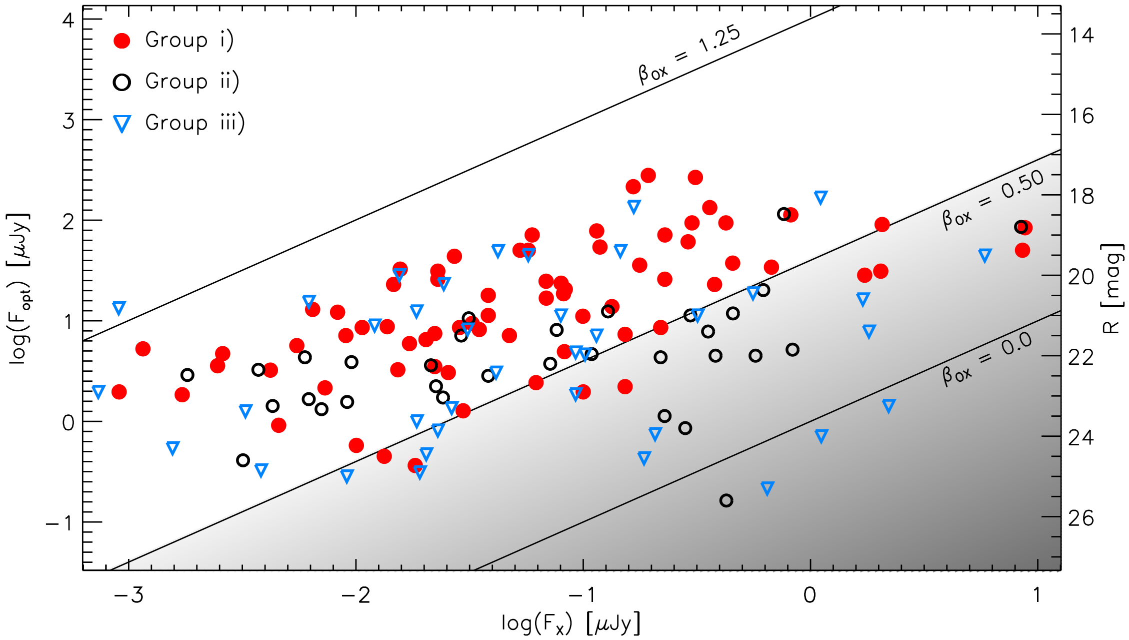

Fig. 8.— The dark burst diagram ($F_{\rm opt}$ vs. $F_{\rm X}$), first presented in Jakobsson et al. (2004)), for the statistical sample. GRB with $\beta_{\rm OX} < 0.5$ are defined as dark bursts. The $\beta_{\rm OX}$ values were calculated in an almost identical way as in Jakobsson et al. (2004). The only difference is that here we did not use 11 hr as a reference time. Rather, when possible, we selected measurements obtained a few hours after a burst to avoid the early stage of the X-ray canonical behavior. For low-z bursts we also avoided late-time measurements to prevent any host contamination in the OA flux.

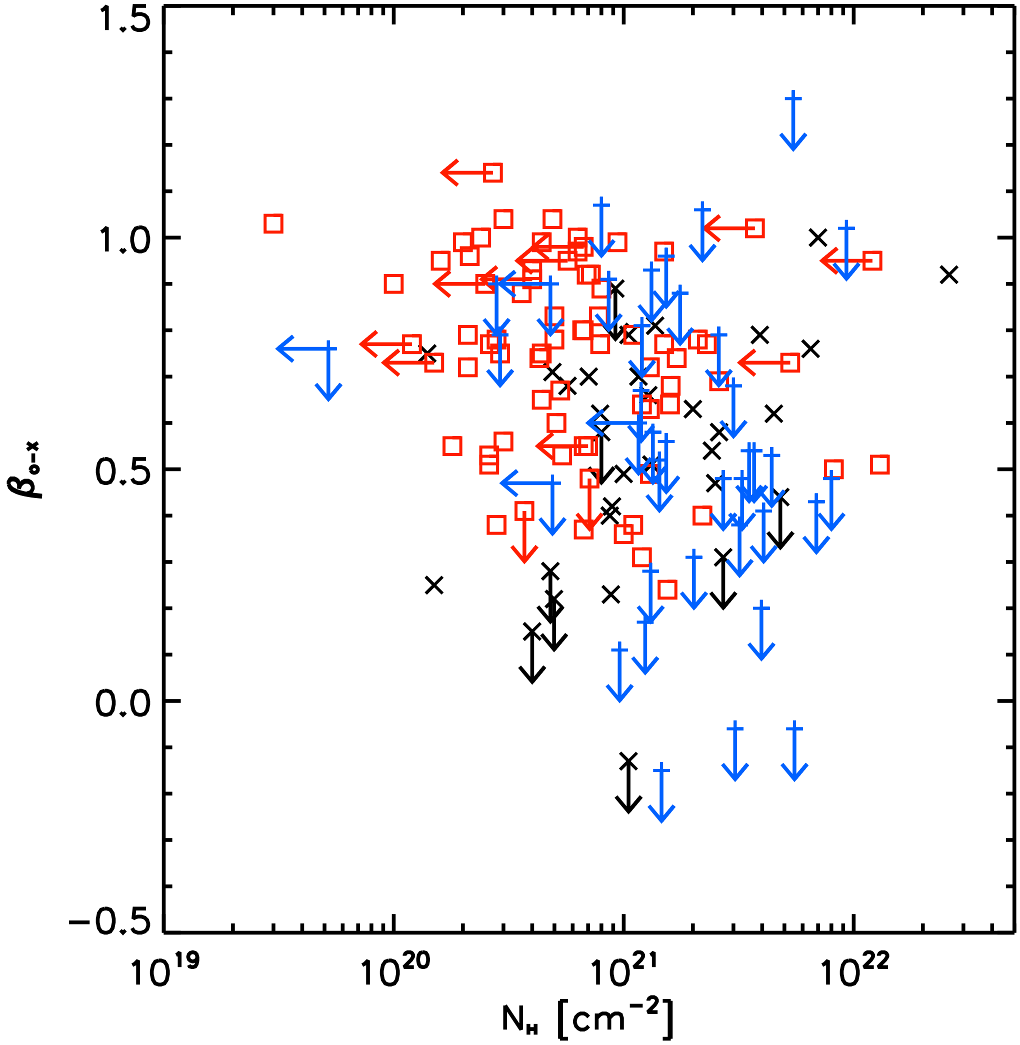

Fig. 9.— β_{OX} plotted against X-ray excess absorption (assuming $z = 0$). Dark bursts (defined by $\beta_{OX} < 0.5$) tend to have large X-ray excess absorption consistent with the interpretation that these bursts are obscured by dust.

similar strongly suggests that DLAs also originate from the interstellar medium of high-redshift galaxies.

Interestingly, GRB absorbers have overlapping properties not only with class C of Weymann et al., but also with their class B. There are even similarities between the afterglow spectrum of GRB 021004 and associated QSO absorbers from class A, namely both very high blueshifts and evidence for line-locking (Savaglio et al. 2002; Møller et al. 2002, but see also Chen et al. 2007b).

Using our large sample we will here try to characterize the GRB absorbers as a class in terms of their absorption line strengths. The low resolution of most of our data prevents us from comparing properties such as metallicities or kinematical structure.

4.3.1. Comparison of GRB- and QSO-DLA Absorption Systems

The issue of the distribution of H I column densities in *Swift* detected long-duration GRBs has already been addressed in Jakobsson et al. (2006b). Compared to that study we here provide 14 additional measurements. In addition we have improved measurements for some of the bursts in Table 3 of Jakobsson et al. (2006b), e.g., GRB 060607A and GRB 060124. The column densities for all 33 Lyα lines detected in our spectroscopic sample are listed in Table 4 and plotted in Fig. 10. The H I distribution covers five orders of magnitude from 10^{17} to $\lesssim 10^{23}$ cm^{-2}. Roughly 80% of the systems have measured H I column densities above 2×10^{20} cm^{-2}, which is the classical definition of a DLA system (e.g., Wolfe et al. 2005). There is evidence that the true distribution may extend to somewhat higher column densities, namely the fact that the three bursts with the highest column densities are dark bursts. The upper range of the distribution may also reflect the transition where the bulk of the hydrogen is in molecular form (Schaye 2001; Krumholz et al. 2009). We will return to this point in Sect. 4.2. The distribution of H I column densities for GRB absorbers has recently been successfully reproduced in a high resolution simulation of galaxy formation simulation (Pontzen et al. 2009).

Given that the majority if the bursts have column densities above 10^{20} cm^{-2} it is natural primarily to compare GRB absorbers with the QSO-DLAs.

Table 4. H I column densities from the spectroscopic sample

GRB	z	$\log(N_{\rm HI}/{\rm cm}^{-2})$
050319	3.240	20.90±0.20
050401	2.899	22.60±0.30
050730	3.968	22.10±0.10
050820A	2.612	21.10±0.10
050908	3.344	17.60±0.10
050922C	2.198	21.55±0.10
060115	3.533	21.50±0.10
060124	2.30	18.5 ± 0.5
060206	4.048	20.85±0.10
060210	3.913	21.55±0.15
060526	3.221	20.00±0.15
060607A	3.075	16.95±0.03
060707	3.425	21.00±0.20
060714	2.711	21.80±0.10
060906	3.686	21.85±0.10
060926	3.206	22.60±0.15
060927	5.464	22.50±0.15
061110B	3.433	22.35±0.10
070110	2.351	21.70±0.10
070411	2.954	19.30±0.30
070506	2.308	22.00±0.30
070611	2.041	21.30±0.20
070721B	3.628	21.50±0.20
070802	2.455	21.50±0.20
071020	2.145	<20.30
071031	2.692	22.15±0.05
080210	2.641	21.90±0.10
080310	2.427	18.70±0.10
080413A	2.433	21.85±0.15
080603B	2.690	21.85±0.05
080607	3.037	22.70±0.15
080721	2.591	21.60±0.10
080804	2.205	21.30±0.15

In Figs. 10,11, and 12 we compare the distributions of H I and metal-line strengths for QSO-DLAs and GRB absorbers in the spectroscopic sample (the histogram for QSO absorbers is renormalized to have the same number of systems as GRB absorbers with $\log N_{\rm HI} > 20.0$). In the two latter plots we only include GRB absorbers with $\log N_{\rm HI} > 20.0$ where we have comparison data from Sloan. We have used the original QSO-DLA sample from Noterdaeme et al. (2009) based on the SDSS-DR6 database of QSO spectra. These authors automatically searched for DLA lines, refining their Lyα fits whenever metal lines are detected redward of the Ly-alpha forest. We have selected all systems from their list with $\log N({\rm H\,I}) \geq 20$ and redshifts in the range $2.2 < z_{\rm abs} \leq 3.2$, located at least 5000 km s^{-1} from a background QSO with $R < 21$.

The EWS of two metal transition lines, namely, Si II λ1526 and C IV λ1549 (i.e., the blend of the 1548 and 1550 Å lines), were measured. These lines are strong so that they are detected in most cases and the risk of overestimating their EWs due to blending with unrelated absorption is minimal. For the measurements themselves, intervals of restframe widths 2 Å (3.5 Å) centered on the Si II λ1526 (C IV λ1549) were used. However, those systems where these metal lines lie inside the Lyα forest were not considered any further.

Among all EW measurements, only those satisfying the following two criteria were used: $\chi^2_{\rm r} < 1.5$ (where $\chi^2_{\rm r}$ is the reduced χ^2) and ${\rm err}_{\rm EW} < 0.3$ Å. These thresholds were determined from the distribution of data points in the χ^2_r vs. ${\rm err}_{\rm EW}$ plane in order to reject unreliable measurements. Among the remaining measurements, we provide 3σ upper limits when the S/N ratio is below 3.

Fig. 11-12 compare the rest-frame EWs of Si II and C IV for the GRB-DLAs and QSO-DLAs. We also show measurements of the strength of these interstellar lines from Lyman-break galaxies (LBGs) from Shapley et al. (2003). These measurements represent mean values of 4 composite spectra representing the quartiles of increasing Lyα EW from blue to red. Note that the C IV EWs for LBGs also contain a stellar contribution so they should be considered upper limits. For GRB-DLAs and QSO-DLAs, we plot these values against the N(H I) estimates which separate the GRB-DLAs from the majority of QSO-DLAs. In all of these comparisons, there is significant overlap between the QSO-DLA and GRB-DLA EW distributions but the GRB-DLA measurements extend to significantly higher EW values than what is seen in the much larger QSO-DLA sample. The large dataset presented here confirm the results of systematically larger Si II and CIV EWs in GRB-DLAs reported by Prochaska et al. (2008b). Similar results were found by Savaglio et al. (2004) in a comparison of Fe II, Si II and Mn II lines between GRB and QSO-DLA absorbers. The LBG measurements fall at the high end of the of GRB-DLA distribution. The LBG systems with the largest line strengths (both Si II and C IV) are those that have the strongest Lyα absorption. These systems also have the highest dust contents (Shapley et al. 2003; Noll et al. 2004).

To understand the difference between the GRB-DLA and QSO-DLA distributions it is natural to focus on the different ways the two absorber classes probe their host galaxies (see also Vreeswijk et al. 2004; Prochaska et al. 2007a; Fynbo et al. 2008a). GRB-DLAs probe the sight-line to the location of a massive star with a random orientation relative to the geometry of the galaxy (ignoring for now the issue of bias). QSO-DLAs probe H I cross-section selected random sight-lines through their host galaxies. The distribution of orientations of the host galaxy relative to the sight-line is not random, but weighted with the selection function. If the QSO-DLAs have a flattened geometry this will tend to produce a shorter sight-line through the host than for a random distribution of orientations. On the other hand, the GRB absorbers do not probe the full sight-line through their hosts, in particular for some systems located in the outskirts of their hosts towards us only a small fraction of the absorbing material will be probed. An additional piece of evidence is the distance between the location of the GRB and the bulk of the absorbing material which has been inferred for a few GRBs based on modeling of fine-structure line variability (Dessauges-Zavadsky et al. 2006; Vreeswijk et al. 2007; D'Elia et al. 2009a,b; Ledoux et al. 2009). These studies have found that the bulk of the absorbing material probed by the variable fine-structure lines are at distances of 50–100 pc, 1.7 kpc, 0.7–6 kpc, and 280 pc for the GRBs 020813, 060418, 080319B, and 080330 respectively. The nearly ubiquitous detection of strong Mg I absorption also indicates that a substantial quantity of neutral gas in GRB-DLAs is located at distances exceeding 100 pc (Prochaska, Chen & Bloom 2006b). Finally, also vibrationally extited H_2 lines have been used to infer a distance in the range 230–940 pc between GRB 080607 and the bulk of the absorbing material (Scheffer et al. 2009).

For strong and saturated lines like those presented in Figs. 11 and 12, the EW is weakly sensitive to the abundance of the ion. Instead, the EW values trace the kinematics of these ions along the sight-line. Prochaska et al. (2008b) have argued, based on comparisons of resonance and fine-structure transitions of SiII and FeII, that the large EWs in GRB-DLAs reflect motions in the "halos" of these galaxies, i.e. in gas at distances exceeding several kpc. The data presented here indicates that such motions are a generic property of gas in the galactic environment of GRBs. Of principal interest is whether these motions reflect gravitational dynamics (as argued by Prochaska et al. 2008b) or galactic-scale outflows driven by star-formation, AGN, etc. Independent of the mechanism, the fact that both the Si II and CIV histograms extend significantly beyond the range spanned by QSO-DLA (Figs 11 and 12) indicates the gas is either predominantly ionized or multi-phase. In other words, if C IV absorption was mainly produced in a roughly spherical, hot halo whereas the low-ionization lines where produced in a central, colder component then we would expect the C IV plot to be different than the Si II plot. Hence, C IV seems to probe the same volume as the low-ionization lines. The same conclusion has been reached by Prochaska et al. (2008b).

For QSO-DLAs the Si II 1526 line can be used as a proxy for metallicity through the relation $[M/H] = -0.92 + 1.41 \log(EW/Å)$ (Prochaska et al. 2008b). The underlying physical reason for this is believed to be a velocity width vs. metallicity relation (Ledoux et al. 2006b; Prochaska et al. 2008b). Roughly, a rest-frame EW of 1 Å corresponds to a metallicity of 0.1 Solar. We do not know yet if GRB absorbers follow this correlation, but there is some indication that they do (Prochaska et al. 2008b). The metallicities have been measured for GRBs 050401, 050730, 050820A, 050922C, 070802, 071031, 080310, 080413A and 080607 in our spectroscopic sample (Watson et al. 2006; Fox et al. 2008; Elíasdóttir et al. 2009; Prochaska et al. 2009; Ledoux et al. 2009), and these bursts seem to follow the correlation although possibly with a somewhat steeper slope.

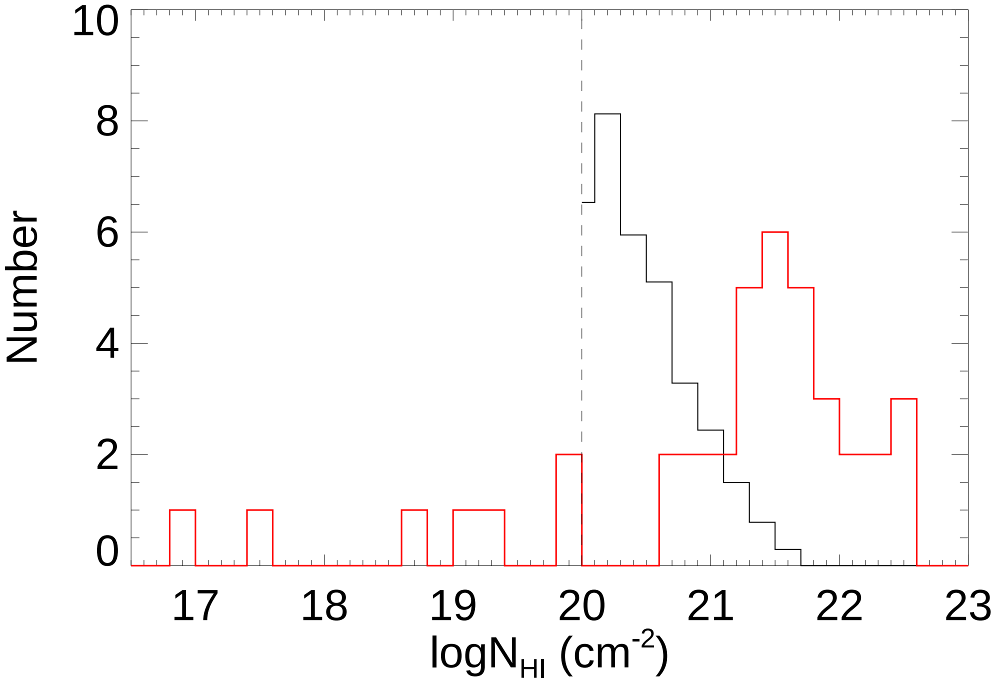

Fig. 10.— Distribution of H I column densities. Black: QSO-DLAs from the sample of Noterdaeme et al. (2009). Red: GRB absorbers from the spectroscopic sample. The numbers of QSO-DLAs have been renormalized to the same number of objects as the GRB absorbers.

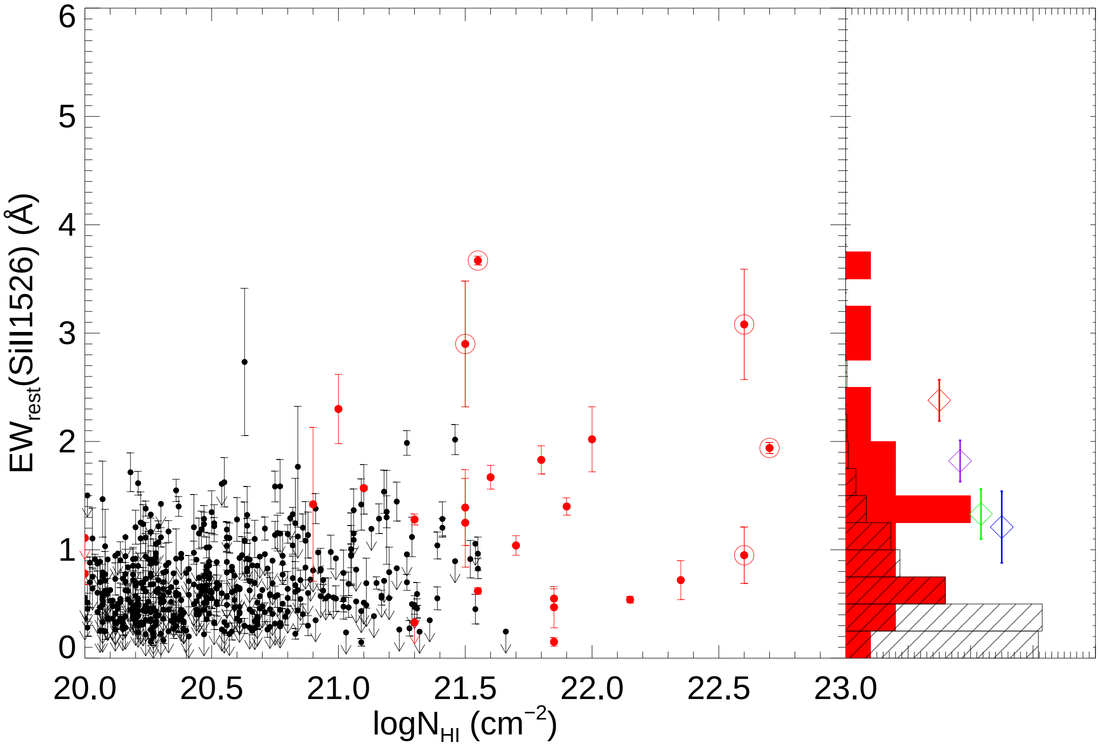

Fig. 11.— Black: QSO-DLAs measurements. Red: GRB absorbers from the spectroscopic sample with $\log N > 20$. Encircled points are dark bursts. The histograms are normalized to have the same area. Open diamonds: LBGs. The LBG points are displaced horizontally for visibility reasons. The LBG measurements represent mean values of 4 composite spectra representing the quartiles of increasing Lyα EW from blue to red.

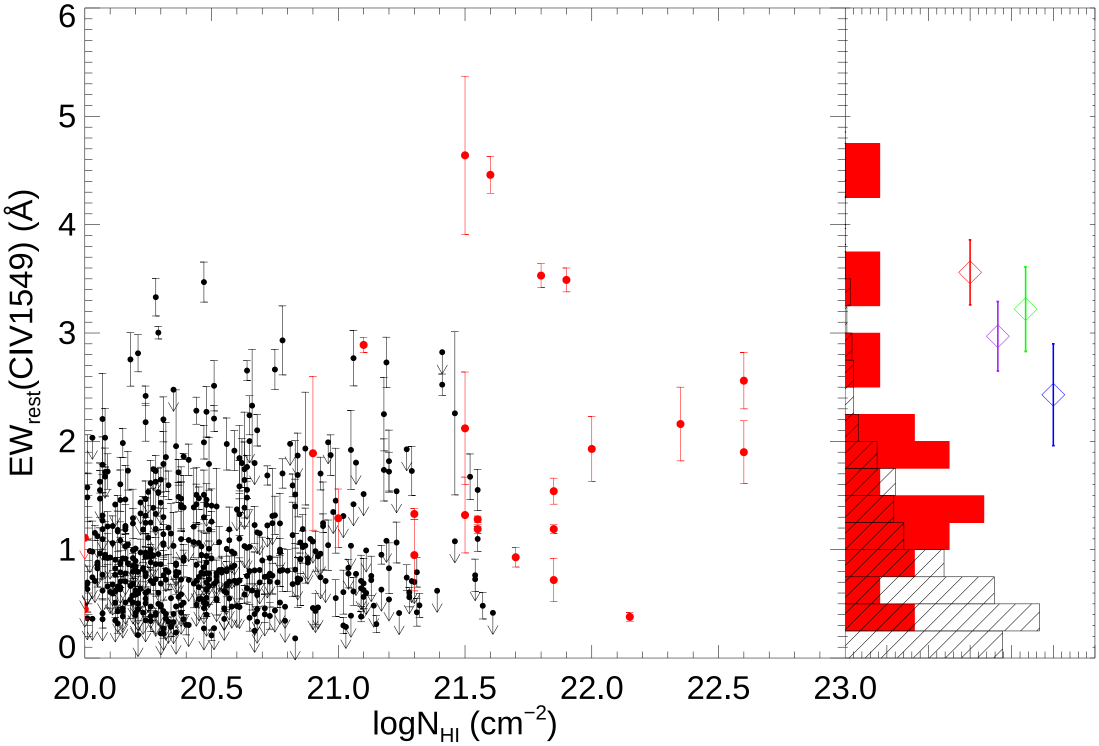

Fig. 12.— Black: QSO-DLAs measurements. Red: GRB absorbers from the spectroscopic sample with $\log N > 20$. The histograms are normalized to have the same area. Open diamonds: LBGs. The LBG points are displaced horizontally for visibility reasons. The LBG measurements represent mean values of 4 composite spectra representing the quartiles of increasing Lyα EW from blue to red.

As seen in Fig. 11, slightly more than half of the GRB absorbers have $\mathrm{EW_{rest}}$(Si II1526)>1 Å suggesting that about half of GRBs with afterglow spectroscopy at these redshifts have metallicity above 0.1 Solar. This is consistent with the metallicity distribution of GRB-DLAs based on direct estimates of N(H I) and a metal column density (e.g. Prochaska et al. 2007a). The true fraction could well be higher due to the bias against burst with high X-ray absorbing columns in the sample of GRBs with OA spectroscopy.

4.4. Implication for the Escape Fraction of Ionizing Photons in Star-Forming Galaxies at $z > 2$

An important utility of the spectroscopic sample of *Swift* GRBs in Table 3 is to constrain the escape fraction of ionizing photons $f_{\rm esc}$ in distant star-forming galaxies (Chen et al. 2007; Gnedin et al. 2008), which specifies the fraction of stellar-origin ionizing photons ($h\nu > 1$ Ryd) that escape from star-forming regions into the intergalactic medium (IGM). A traditional approach to obtain empirical constraints of $f_{\rm esc}$ is to search for high-energy photons detected at wavelengths below the Lyman limit transition of a distant galaxy. However, such measurements are subject to a number of systematic uncertainties that are difficult to quantify, including background subtraction, intrinsic spectral shape at ultraviolet wavelengths of star-forming galaxies, and line-of-sight variations of IGM Lyα absorption (see Chen et al. 2007 for a brief review).

Chen et al. (2007) introduced a new approach that determines $f_{\rm esc}$ in high-redshift star-forming galaxies based on the range of neutral hydrogen column density N(H I) found in the hosts of long-duration GRBs. The observed N(H I) in the host of each GRB from early-time afterglow spectra represents a measure of the integrated optical depth of Lyman limit photons along the line of sight away from the parent star-forming region where the progenitor resides. Considering the N(H I) distribution function of an ensemble of GRBs together therefore yields an estimate of the mean $f_{\rm esc}$ averaged over random lines of sight. Adopting a sample of 28 GRBs at $z \gtrsim 2$, Chen et al. (2007) found $\langle f_{\rm esc}\rangle = 0.02 \pm 0.02$ with a 95% c.l. upper limit $\langle f_{\rm esc}\rangle \leq 0.075$. Although the best-estimated $\langle f_{\rm esc}\rangle$ is among the lowest value reported for $z > 2$ star-forming galaxies, the subluminous nature of the majority of GRB host galaxies (e.g., Jakobsson et al. 2005; Chen et al. 2009) in combination with a steep faint-end slope of the distant galaxy population (e.g. Reddy et al. 2008) indicates that sub-$L*$ galaxies with $\langle f_{\rm esc}\rangle = 1 - 2$ % can already contribute a comparable amount of ionizing photons as QSOs to the ultraviolet background radiation at $z \sim 3$.

While the new approach of constraining $f_{\rm esc}$ based on the observed N(H I) distribution is not affected by the same systematic uncertainties that bias the $f_{\rm esc}$ measurements from the traditional method (see Chen et al. 2007 for related discussion), the accuracy of $\langle f_{\rm esc}\rangle$ depends on an unbiased sample of GRB hosts. Specifically, if some fraction of optically-thin sightlines are missed due to a lack of S/N in the afterglow spectra for identifying weak absorption features, then the estimated $\langle f_{\rm esc}\rangle$ would be biased toward a lower value. Chen et al. (2007) considered a sample of 28 GRBs at $z \gtrsim 2$ with available early-time afterglow spectra for constraining the N(H I), eight of which are

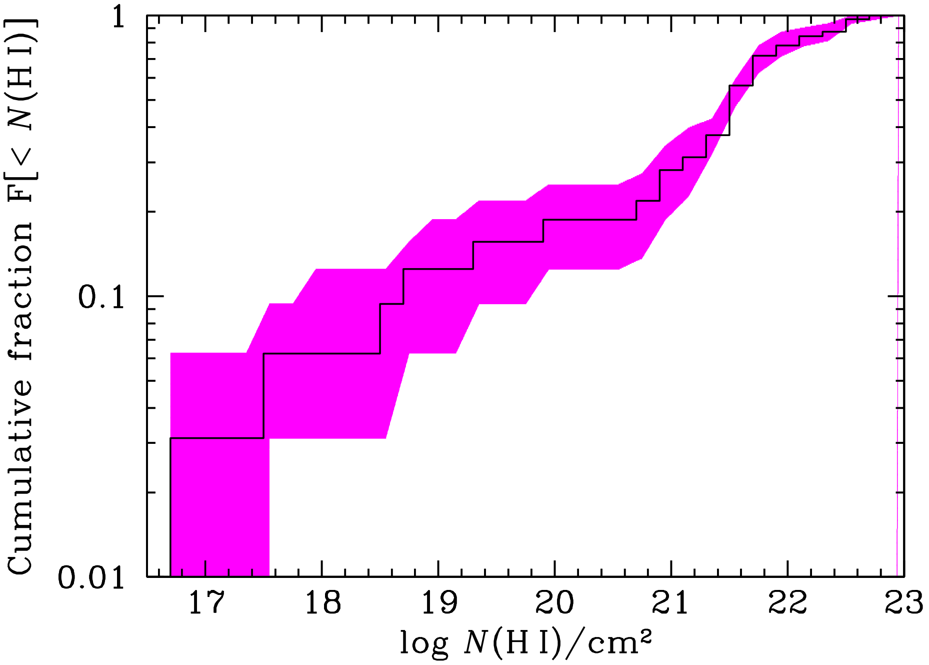

Fig. 13.— Cumulative distribution of neutral hydrogen column density $\mathcal{F}[< N(\mathrm{H\,I})]$ observed in the host galaxies of 32 long-duration GRBs discovered at $z \geq 2$ by *Swift* (solid histogram). The shaded area shows the 1-σ uncertainties evaluated using a bootstrap re-sampling method that accounts for both $N(\mathrm{H\,I})$ measurement uncertainties and sampling errors.

from the pre-*Swift* era when rapid localizations of the optical transients were challenging. It is not clear how significant the bias is due to missed optical transients.

The 33 GRBs discussed in this paper represent a uniform spectroscopic sample of *Swift* bursts with rapid localizations and allow us to obtain an accurate measurement of $\langle f_{\rm esc}\rangle$. Fig. 13 presents the cumulative N(H I) distribution, $\mathcal{F}[< N({\rm H\,I})]$ from the sample of 32 GRB host galaxies (excluding GRB 071020 due to the uncertain N(H I)), together with the 1-σ uncertainties determined based on a bootstrap re-sampling method (see Chen et al. 2007 for further illustrations). Adopting this sample of 32 GRBs at $z \gtrsim 2$, we find $\langle f_{\rm esc}\rangle = 0.02 \pm 0.02$ with a 95% c.l. upper limit $\langle f_{\rm esc}\rangle \leq 0.07$, in excellent agreement with the finding of Chen et al. We note that while the two samples are comparable in size, only roughly half of the new sample overlaps with those considered by Chen et al. In addition, including GRB 071020 and assuming a host N(H I) of log $N({\rm H\,I}) = 16.85$ (matching the lowest N(H I) found so far for a GRB host) would double the estimated value to $\langle f_{\rm esc}\rangle = 0.04$. Our new measurement confirms that the mean escape fraction of ionizing photons in distant star-forming galaxies is small.

4.5. Intervening Absorption Systems

The issue of intervening absorbers is interesting for two main reasons. The first is the puzzling result that there are more intervening Mg II absorbers along GRB sight-lines than along QSO sight-lines (Prochter et al. 2006; Vergani et al. 2009; Cucchiara et al. 2009). On the other hand there is no excess of C IV systems along GRB sightlines (Sudilovsky et al. 2007; Tejos et al. 2007). The other reason is that the search for galaxy counterparts of the absorbers is much easier along GRB sight-lines as the OA quickly fades away (Vreeswijk, Møller, & Fynbo 2003).

In our sample we detect several very strong intervening Mg II absorbers, i.e. 12 systems with EW> 2 Å. For a full statistical analysis of the excess we refer to Vergani et al. (in preparation).

We also detect a few strong intervening Lyα absorbers, e.g. along the sight-lines to GRB 050730, GRB 050908, and GRB 070721B (see also Schulze et al. and Milvang-Jensen et al. in preparation). In is interesting to note that the $z = 2.62$ sub-DLA towards GRB 050908 also has remarkably strong metal lines (e.g., a EW$_{\rm rest}$ of 2.2Å for the Si II,1526 line). Also, the $z = 3.09$ sub-DLA towards GRB 070721B has very strong lines (rest EW 1.7Å for the Si II,1526 line). QSO-DLAs with EW$_{\rm rest}$ larger than 1.5 Å for the Si II,1526 line are quite rare (see Prochaska et al. 2008b and Fig. 11 below). Unfortunately, our sample is too small to judge if the intervening Lyα absorbers towards GRB sight-lines are also statistically different from those along QSO sight-lines.

5. Conclusions

GRB afterglow spectroscopy provides a detailed analysis of the ISM of actively star-forming galaxies. In this work we have presented a large sample of GRBs detected by *Swift* for which primarily low-resolution spectroscopic observations have been secured. The majority ($\sim 80\%$) of the GRB host absorbers bear strong resemblance to high-column density QSO absorbers like DLAs and sub-DLAs. However, the GRB absorbers are characterized by a broader range of line strengths extending to significantly stronger lines (both for H I, Si II and C IV) than what is seen for high-column density QSO absorbers.

We find that the sample of GRBs for which optical spectroscopy is secured is a significantly biased subsample. In the statistical sample only about 50% have OA spectroscopy and this subsample have substantially smaller X-ray excess absorption and a substantially smaller fraction of dark bursts (by the Jakobsson et al. 2004 definition) than the other half of the sample.

The implication of this work is that the metallicity distribution we derive from optical afterglow spectroscopy likely is skewed towards low metallicities compared to the true underlying distribution (see also Ledoux et al. 2009). This is important to take into account, e.g., when establishing how well GRBs trace star formation and when inferring to which extent GRB progenitors may be restricted to massive stars with low metallicities.

This work also shows that if we can secure optical and/or nearIR spectroscopy for a much larger fraction of an X-ray selected sample it is likely that we will pick up sight-lines with significantly higher dust contents, molecular fractions, and higher metallicities. A similar conclusion was reached by Ledoux et al. (2009). Such studies will be ideal to study extinction curves and properties of star-forming regions, in particular at high redshifts. In the current sample dusty bursts like GRBs 070802, 080605, and 080607 were observed under fortunate conditions, i.e. very soon after the bursts and in good observing conditions. It is plausible that bursts for which the current search strategy and instrumentation cannot secure a redshift are similar to or even more dust obscured than these bursts.

Currently, most GRB error circles are only observed in optical bands. For further progress, systematic nearIR follow-up of an X-ray selected sample will be important. Such systematic nearIR follow-up is currently carried out by a few teams using, e.g., GROND, UKIRT and PAIRITEL (e.g. Greiner et al. 2009; Krühler et al. 2008; Tanvir et al. 2008a; Prochaska et al. 2009). For the spectroscopic follow-up, instruments like the newly commissioned X-shooter spectrograph that cover the full nearUV to nearIR range in a single shot (Kaper et al. 2009) will be important, but it is likely that we will have to wait for the advent of 30–40 m telescopes with similar instrumentation before we will reach a spectroscopic completeness of, e.g., 90%.

We thank our referee for a thorough and constructive report. JPUF thanks A. Shapley for helpful discussions. JPUF thanks the Centre for Astrophysics and Cosmology at the University of

Iceland for hospitality during the writing of most of this work. We thank the *Swift* team for carrying such a wonderful mission. The DARK centre is funded by the DNRF. PJ acknowledges support by a Marie Curie European Re-integration Grant within the 7th European Community Framework Program under contract number PERG03-GA-2008-226653, and a Grant of Excellence from the Icelandic Research Fund. H.-W.C. acknowledges support from NASA grant NNG 06GC36G and an NSF grant AST-0607510.

A. Notes on individual objects

A.1. GRB 050319 ($z = 3.2425$)

The data presented here have previously been published in Jakobsson et al. (2006b). The spectrum has a low signal-to-noise (SN) ratio, but due to the presence of the a strong Hydrogen Lyα line the redshift is secure.

A.2. GRB 050401 ($z = 2.8983$)

The data presented here have previously been published in Watson et al. (2006). This burst has one of the highest H I column densities measured along any sightline. The redshift is based on numerous metal lines including fine-structure lines. The spectrum also shows evidence for substantial SMC-type reddening and classifies as a dark burst by the definition of Jakobsson et al. (2004).

A.3. GRB 050408 ($z = 1.2356$)

The data presented here have previously been published in Foley et al. (2007). The redshift is based on numerous metal lines (including fine-structure lines).

A.4. GRB 050730 ($z = 3.9693$)

The data presented here have previously only been published in the GCN circulars (D'Elia et al. 2005). Spectra of this burst were also secured by Chen et al. (2005), Starling et al. (2005), D'Elia et al. (2007) and Ledoux et al. (2009). In the 2d spectrum we detect a foreground QSO ($z = 3.02$) at an impact parameter of 20 arcsec (153 kpc). This QSO is possibly associated with the $z = 3.022$ absorption system seen in the spectrum of GRB 050730.

A.5. GRB 050801 ($z = 1.38$)

The data presented here have not been published earlier. No standard star was observed and therefore no flux calibration has been attempted for this spectrum (the plotted spectrum is normalized to 1 in the continuum). We only detect a single unidentified line in the spectrum. The upper limit on the redshift based on the absence of a Lyα forest is about 2.3. Based on UVOT colors a photometric redshift of 1.38 has been determined for this burst (Oates et al. 2009).

A.6. GRB 050802 ($z = 1.7102$)

The data presented here have previously only been published in the GCN circulars (Fynbo et al. 2005). No standard star was observed and therefore no flux calibration has been attempted for this spectrum (the plotted spectrum is normalized to 1 in the continuum). The redshift is based on several weak metal lines. The upper limit on the redshift based on the absence of the Lyα forest is about 2.3.

A.7. GRB 050820A ($z = 2.6147$)

The UVES data for this burst are discussed in Ledoux et al. (2005) and Fox et al. (2008).

A.8. GRB 050824 ($z = 0.8278$)

GRB 050824 is an X-Ray Flash (XRF). The data presented here have previously been published in Sollerman et al. (2007). That work also established evidence for an associated SN and detected the host galaxy of the burst. Here the data have been re-reduced and reanalyzed and more lines have been identified. The redshift is based on both metal absorption lines and emission lines from the underlying host galaxy.

A.9. GRB 050908 ($z = 3.3467$)

The data presented here have previously only been published in the GCN circulars (Fugazza et al. 2005). The spectra will be discussed in more detail in Smette et al. (in preparation) where a H I column density of $\log N_{\rm HI} = 17.60 \pm 0.10$ is derived. This system is interesting due to its low H I column density and the detection of escaping ionizing radiation along its line-of-sight. Furthermore, there is an intervening sub-DLA at $z = 2.62$ with very strong metal lines.

A.10. GRB 050922C ($z = 2.1995$)

The data presented here have previously been published in Jakobsson et al. (2006b). For this burst high resolution spectra have been presented in Piranomonte et al. (2006b). The plotted spectrum is normalized.

A.11. GRB 060115 ($z = 3.5328$)

The data presented here have previously only been published in the GCN circulars (Piranomonte et al. 2006a). The redshift is based on both Lyα and fine-structure lines and is hence secure.

A.12. GRB 060124 ($z = 2.3000$)

The data presented here have previously only been published in the GCN circulars (Prochaska et al. 2006a). The GRB system is characterized by a low H I column density and the absence of low-ionization lines. A detailed discussion of the prompt emission and afterglow of this burst can be found in Romano et al. (2006).

A.13. GRB 060206 ($z = 4.0559$)

The data presented here have previously been published in Fynbo et al. (2006b) and Thöne et al. (2008a). Spectroscopic observations of this afterglow have also been published in Hao et al. (2007) who claimed variable absorption lines in the intervening system. This was subsequently falsified by Aoki et al. (2008) and Thöne et al. (2008a). There is tentative evidence for molecular absorption in this spectrum (Fynbo et al. 2006b, see also Prochaska et al. 2009). No standard star was observed at the night of the observation so we here show a normalized spectrum. The spectrum is strongly affected by fringing redwards of 7000 Å.

A.14. GRB 060210 ($z = 3.9122$)

The data presented here have previously only been published in the GCN circulars (Cucchiara et al. 2006a). We do not confirm their identification of an intervening system at $z = 1.47$. The burst has very strong low-ionization lines and classifies as a dark burst by the Jakobsson et al. (2004) definition. A detailed discussion of the prompt emission and afterglow of this burst can be found in Curran et al. (2007) who also infer substantial reddening based on broadband modeling of the afterglow.

A.15. GRB 060502A ($z = 1.5026$)

The data presented here have previously only been published in the GCN circulars (Cucchiara et al. 2006b). The redshift is based on a rich spectrum of low ionization (including fine-structure) absorption lines.

A.16. GRB 060512 ($z = 2.1$?)

GRB 060512 is an XRF. The data presented here have previously only been published in the GCN circulars (Starling et al. 2006a). For this burst there is uncertainty about the redshift in the GCN reports. An afterglow spectrum taken at the TNG indicates a redshift of around 2.1 (Starling et al. 2006b), which is supported by a spectral break detected by UVOT (De Pasquale & Cummings 2006; Oates et al. 2009) and which is supported by modeling of the broad band spectral energy distribution of the burst (Schady et al. 2007a). Bloom et al. (2006a) measure a redshift of 0.44 from a galaxy close to the afterglow position. This galaxy is offset by about 0.7 arcsec from the position of the afterglow. Based on a binning of the spectrum shown here we confirm the presence of a broad absorption line around 3750 Å consistent with a redshift of around 2.1 if interpreted as Lyα. This suggest that the $z = 0.44$ galaxy close to the line of sight is a foreground object. We do not detect significant metal lines in the afterglow spectrum.

A.17. GRB 060526 ($z = 3.2213$)

The data presented here have previously been published in Jakobsson et al. (2006b). Additional medium resolution spectra are discussed in Thöne et al. (2008e). The redshift is based on Lyα and metal absorption lines.

A.18. GRB 060604 ($z \lesssim 3$)

The data presented here have previously only been published in circulars (Castro-Tirado et al. 2006). In the spectrum we detect a single absorption line at 5219 Å. The origin of the line is unclear. The line appears too narrow to be Mg II at $z = 0.864$. A possibility is Al II at $z = 2.124$. This would be compatible with the tentative break detected by UVOT (Blustin & Page 2006). From the absence of the onset of the Lyα forest we infer an approximate upper limit on the redshift of $\sim$3. We do not confirm the tentative redshift of $z = 2.68$ proposed by Castro-Tirado et al. (2006).

A.19. GRB 060607A ($z = 3.0749$)

For this burst UVES spectra were obtained starting only about 7.5 minutes after the burst (Ledoux et al. 2006a). For a full analysis of the UVES data see Fox et al. (2008), Prochaska et al. (2008a), and Smette et al. (in preparation).

A.20. GRB 060614 ($z = 0.1257$)

The data presented here have previously been published in Della Valle et al. (2006). This is the lowest redshift burst in our spectroscopic sample. However, from the present spectrum no lines (either absorption or emission) are significantly detected. The upper limit on the redshift based on the absence of a Lyα forest is about 2.6. The redshift was later found to be $z = 0.1257$ based on emission lines from the underlying host galaxy (Della Valle et al. 2006). GRB 060614 is remarkable in being a long burst without an associated (bright) supernova (Fynbo et al. 2006c, Della Valle et al. 2006, Gal-Yam et al. 2006).

A.21. GRB 060707 ($z = 3.4240$)

The data presented here have previously been published in Jakobsson et al. (2006b). The burst is remarkable in having very strong metal lines while showing no sign of extinction.

A.22. GRB 060708 ($z = 1.92$)

The data presented here have previously only been published in the GCN circulars (Jakobsson et al. 2006c). The spectrum does not display any significant absorption or emission lines. An upper limit of $z \lesssim 2.8$ can be placed on the redshift of GRB 060708 from the lack of significant Lyα forest lines in the spectrum of the afterglow redwards of 4600 Å. Bluewards of 4600 Å there is very marginal evidence for broad absorption lines in the spectrum, but the spectrum is too noisy to establish a precise redshift. The *Swift* team has established a photometric redshift of 1.92 for this burst based on the UVOT imaging of the OA (Schady & Moretti 2006).

A.23. GRB 060714 ($z = 2.7108$)

The data presented here have previously been published in Jakobsson et al. (2006b). In the trough of the DLA line of the host absorption system Lyα emission is detected, presumably from the underlying host galaxy.

A.24. GRB 060719 ($z \lesssim 4.6$)

The data presented here have not been published earlier. This afterglow was extremely red with a R−K color of about 4.5 (Malesani et al. 2006) and the burst was considered a candidate high redshift burst. Our spectrum, taken with the 600I grating, shows a featureless continuum in the range 6800–9400 Å thereby placing an upper limit of ∼4.6 on the redshift. Hence, this is most likely a dust obscured burst.

A.25. GRB 060729 ($z = 0.5428$)

The data presented here have previously only been published in the GCN circulars (Thöne et al. 2006a). The broad undulations seen in the blue end of the spectrum are caused by systematic errors in the flux calibration due to the high airmass of the observation. All of the observed strong, spectral lines can be associated with a single absorption system. We associate the GRB redshift with this gas. The upper limit on the redshift based on the absence of a Lyα forest is about 2.1.

A.26. GRB 060807 ($z \lesssim 3.4$)

The data presented here have not been published elsewhere. We retrieved the data from the ESO archive. There is a single marginal line at 5200 Å in the spectrum. If due to Lyα the redshift of the burst is 3.28. From the absence of a spectral break we set a conservative upper limit of $z < 3.4$. For this burst there is evidence for emission lines in the X-ray spectrum (Butler 2006).

A.27. GRB 060904B ($z = 0.7029$)

The data presented here have previously only been published in the GCN circulars (Fugazza et al. 2006). The burst is not included in the statistical sample as it has too high foreground extinction ($A_V = 0.57$, Schlegel et al. 1998). The broad undulations seen in the spectrum are due to errors in the flux calibration. All of the observed strong, spectral lines can be associated with a single absorption system. We associate the GRB redshift with this gas. The upper limit on the redshift based on the absence of a Lyα forest is about 2.5.

A.28. GRB 060906 ($z = 3.6856$)

The data presented here have previously been published in Jakobsson et al. (2006b). The spectrum was obtained in twilight just before sun rise. We do not include this burst in the statistical sample due to its too high foreground extinction of $A_V = 0.54$ (Schlegel et al. 1998). The redshift is based on both Lyα and metal absorption lines.

A.29. GRB 060908 ($z = 1.8836$)

The data presented here have previously only been published in the GCN circulars (Rol et al. 2006). The redshift is based on a single C IV doublet and is confirmed by the detection of the Lyα line from the underlying host galaxy (Milvang-Jensen et al. in preparation). We hence do not confirm the tentative redshift of $z = 2.43$ reported by Rol et al. (2006). The redshift we infer is also consistent with the UVOT constraints (Morgan et al. 2006).

A.30. GRB 060926 ($z = 3.2086$)

The data presented here have previously been published in Piranomonte et al. (2006b). We do not include this burst in the statistical sample due to its too high foreground extinction of $A_V = 0.52$. In the trough of the DLA line of the host absorption system Lyα emission from the underlying host galaxy is detected. The H I column density is among the highest detected and there is evidence for substantial reddening.

A.31. GRB 060927 ($z = 5.4636$)

The data presented here have previously been published in Ruiz-Velasco et al. (2007). The precise redshift is based on a single low S/N Si II line. Based alone on the onset of the Lyα forest the redshift can be estimated to be in the range 5.5–5.6, the 2nd highest in the spectroscopic sample.

A.32. GRB 061007 ($z = 1.2622$)

The data presented here have previously only been published in circulars (Jakobsson et al. 2006d). This burst is one of the brightest in γ-rays observed by *Swift* and its afterglow was also very luminous both in the X-ray and optical bands (Schady et al. 2007b). The redshift is based on both metal absorption lines and emission lines from the underlying host galaxy.

A.33. GRB 061021 ($z = 0.3463$)

The data presented here have previously only been published in circulars (Thöne et al. 2006b). In the GCN circular no redshift measurement was reported. It was only after measuring the redshift from the underlying host galaxy (Hjorth et al. in preparation) that we identified Mg II absorption lines in the very blue end of the afterglow spectrum. This is the 2nd lowest redshift in our spectroscopic sample.

A.34. GRB 061110A ($z = 0.7578$)

The data presented here have previously only been published in circulars (Fynbo et al. 2007). The redshift is mainly based on emission lines from the underlying host galaxy. We also identify a broad absorption feature consistent with the Mg II doublet at the same redshift.

A.35. GRB 061110B ($z = 3.4344$)

The data presented here have previously only been published in circulars (Fynbo et al. 2006a). The redshift is based on both a very strong Lyα line and metal absorption lines, including fine structure lines.

A.36. GRB 061121 ($z = 1.3145$)

The data presented here have previously only been published in the GCN circulars (Bloom et al. 2006b). The redshift is based on a rich spectrum of low ionization (including fine-structure) absorption lines.

A.37. GRB 070110 ($z = 2.3521$)

The data presented here have previously only been published in circulars (Jaunsen et al. 2007b). In the trough of the DLA line of the host absorption system Lyα emission from the underlying host galaxy is detected.

A.38. GRB 070125 ($z = 1.5471$)

The data presented here have not previously been published. The redshift of the burst was determined from Gemini data (Cenko et al. 2008). The burst is peculiar in being very bright and having very weak absorption lines in its afterglow spectrum. For a typical fainter OA the redshift for such an absorption system would be very difficult to establish. The burst is not included in the statistical sample as the XRT position was distributed later than 12 hr after the burst. The upper limit on the redshift based on the absence of Lyα forest lines is about 2.3. The broad undulations in the blue end of the spectrum are due to systematics in the flux calibration.

A.39. GRB 070129 ($z \lesssim 3.4$)

The data presented here have not previously been published. A redshift could not be established as no significant lines are detected in the spectrum. We place a conservative upper limit of $z \lesssim 3.4$ from the upper limit on wavelength of the onset of the Lyα forest.

A.40. GRB 070306 ($z = 1.4965$)

The data presented here have previously been published in Jaunsen et al. (2008). The redshift is based on a single oxygen emission line. The identification with [OII] is secure as the doublet is resolved in a higher resolution spectrum (Jaunsen et al. 2008). The burst is remarkable in having a highly extinguished afterglow only detected in the K and H bands while being located in a blue host galaxy (Jaunsen et al. 2008).

A.41. GRB 070318 ($z = 0.8397$)

The data presented here have previously only been published in circulars (Jaunsen et al. 2007a). The afterglow spectrum displays a spectral break around 5000 Å (or about 2700 Å in the rest-frame), the nature of which is currently not understood. All of the observed strong, spectral lines can be associated with a single absorption system. We associate the GRB redshift with this gas. The upper limit on the redshift based on the absence of Lyα-frost features is about 2.1.

A.42. GRB 070411 ($z = 2.9538$)

The data presented here have previously only been published in circulars (Jakobsson et al. 2007a). The spectra were obtained with the two medium resolution gratings 1400V and 1200R. The burst is not included in our statistical sample as the foreground Galactic extinction is too high (A_V=0.76, Schlegel et al. 1998). The GRB absorption system has one of the lower H I column densities in our sample (see Table 4).

A.43. GRB 070419 ($z = 0.9705$)

The data presented here have not been published before. All of the observed strong, spectral lines can be associated with a single absorption system. We associate the GRB redshift with this gas.

A.44. GRB 070506 ($z = 2.3090$)

The data presented here have previously only been published in circulars (Thöne et al. 2007b). Redwards of 7000 Å the spectrum is strongly affected by fringing. The redshift is based on both Lyα and metal absorption lines.

A.45. GRB 070508 ($z \lesssim 3.0$)

The data presented here have previously only been published in circulars (Jakobsson et al. 2007b). No lines are detected in the spectrum and an upper limit of $z \lesssim 3$ is placed on the redshift from the upper limit on wavelength of the onset of the Lyα forest. The burst is not included in the statistical sample as the declination is too low (-78^o). The burst classifies as a dark burst by the definition of Jakobsson et al. (2004).

A.46. GRB 070611 ($z = 2.0394$)

The data presented here have previously only been published in circulars (Thöne et al. 2007a). The redshift is based on both Lyα and metal absorption lines. Also detected in the spectrum are two intervening Mg II systems.

A.47. GRB 070721B ($z = 3.6298$)

The data presented here have previously only been published in circulars (Malesani et al. 2007). A bright Lyα emitter is located 20 arcsec from the GRB position at the the same redshift as the GRB. A $z = 3.09$ intervening sub-DLA is detected in both the spectrum of the afterglow and in the spectrum of the neighbor Lyα emitter. A possible galaxy counterpart of the absorber is detected in emission 2 arcsec from the afterglow position. The spectrum will be discussed in more detail in Milvang-Jensen et al. (in preparation).

A.48. GRB 070802 ($z = 2.4541$)

The data presented here have previously been published in Elíasdóttir et al. (2009). The spectrum is remarkable is showing a strong 2175 Å dust extinction feature at the GRB redshift of $z = 2.45$ (see also Krühler et al. 2008). The burst classifies as a dark burst by the definition of Jakobsson et al. (2004). There are also two intervening Mg II systems in the spectrum, one of which is very strong.

A.49. GRB 071020 ($z = 2.1462$)

The data presented here have previously only been published in circulars (Jakobsson et al. 2007c). The spectrum will be discussed in more detail in Nardini et al. (in preparation). All of the observed strong, spectral lines can be associated with a single absorption system. We associate the GRB redshift with this gas.

The upper limit based on the absence of a Lyα forest is about 3.

A.50. GRB 071025 ($z = 5.2$?)

The data presented here have not previously been published. The data were obtained with the high resolution HIRES spectrograph. Weak, continuum flux is detected from the afterglow at wavelengths $\lambda > 7500$Å, but no emission is detected at shorter wavelengths. This flux 'decrement' may be associated with the IGM at $z \approx 5.2$ but could also be associated with a significant reddening of the afterglow. If one presumes the latter, the burst is still very likely to be at high redshift ($z > 2.5$) because a sharp decrement from dust is only expected at ultraviolet wavelengths. This redshift of $z \approx 5.2$ is consistent with the photometry which displays a break between the R and I bands (e.g. Rykoff et al. 2007). We do not show a figure of this spectrum.

A.51. GRB 071031 ($z = 2.6918$)

The data presented here have previously only been published in circulars (Ledoux et al. 2008). In addition to the 300V spectrum shown here spectra were secured with a range of higher resolution gratings and with the high-resolution UVES spectrograph (e.g., Fox et al. 2008). In the trough of the DLA line at the host redshift Lyα emission from the underlying host galaxy is detected. In the medium and high resolution spectra a large number of Fe II fine structure and metastable lines are detected.

A.52. GRB 071112C ($z = 0.8227$)

The data presented here have previously only been published in circulars (Jakobsson et al. 2007d). The redshift is based both on absorption lines from the GRB host system as well as emission lines from the underlying host galaxy.

A.53. GRB 071117 ($z = 1.3308$?)

The data presented here have previously only been published in circulars (Jakobsson et al. 2007e). The redshift is based on a single emission line at 8687 Å, which we interpret as O II at $z = 1.331$. The spectrum is affected by fringing redwards of about 7000 Å and the line is only seen after subtracting two of the individual exposures where the source has been offset along the slit from each other. Hence, we consider the significance of this redshift measurement to be marginal.

A.54. GRB 080210 ($z = 2.6419$)

The data presented here have previously only been published in circulars (Jakobsson et al. 2008a). The spectrum will be discussed in more detail in De Cia et al. (in preparation). There is evidence for substantial reddening. The redshift is based on both Lyα and metal absorption lines.

A.55. GRB 080310 ($z = 2.4274$)

This burst was observed both with the VLT/UVES spectrograph and the Kast spectrograph. Here we show the Kast spectrum previously published in Prochaska et al. (2008c). The GRB absorber is characterized by a low H I column density and several high ionization lines (see also Fox et al. 2008; Ledoux et al. 2009; De Cia et al. in preparation).

A.56. GRB 080319B ($z = 0.9382$)

This is the famous “naked eye burst” (Racusin et al. 2008; Woźniak et al. 2009; Bloom et al. 2009). The FORS2 spectrum presented here was obtained quite late, 26 hr after the burst. We retrieved the data from the ESO archive.

A.57. GRB 080319C ($z = 1.9492$)

The data presented here have previously only been published in circulars (Wiersema et al. 2008a). The data were obtained in poor conditions with cloud cover. The plotted spectrum is normalized. The redshift is based on the highest redshift metal line system in the spectrum. We also detect an intervening Mg II system. The upper limit on the redshift based on the absence of significant Lyα forest lines is about 2.7. The burst classifies as a dark burst by the Jakobsson et al. (2004) definition.

A.58. GRB 080330 ($z = 1.5119$)

GRB 080330 is an XRF. The data presented here have previously been published in Guidorzi et al. (2009). The burst was also observed with the VLT-UVES spectrograph (D'Elia et al. 2009b). All of the observed strong, spectral lines can be associated with a single absorption system. We associate the GRB redshift with this gas.

A.59. GRB 080411 ($z = 1.0301$)

The data presented here have previously only been published in circulars (Thöne et al. 2008b). The burst is not included in the statistical sample as it has too high foreground extinction ($\mathrm{A_V} = 0.54$, Schlegel et al. 1998). The burst is remarkable in having a bright X-ray afterglow visible for more than three weeks after the burst (Marshall et al. 2008). The OA spectrum has a fairly strong unidentified line at 4439Å.

A.60. GRB 080413A ($z = 2.4330$)

This burst was observed with VLT/UVES. The burst is not included in the statistical sample as it has too high foreground extinction ($\mathrm{A_V} = 0.52$, Schlegel et al. 1998).

A.61. GRB 080413B ($z = 1.1014$)

The data presented here have previously only been published in circulars (Vreeswijk et al. 2008c). Spectra were also secured in a number of higher resolution gratings. The broad undulations in the blue end of the spectrum are due to systematics in the flux calibration.

A.62. GRB 080520 ($z = 1.5457$)

The data presented here have previously only been published in circulars (Jakobsson et al. 2008b). The afterglow was very faint at the time of observation, but the redshift is based on both host emission lines and afterglow metal absorption lines and is hence secure.

A.63. GRB 080523 ($z \lesssim 3.0$)

The data presented here have previously only been published in circulars (Fynbo et al. 2008b). The afterglow was very faint at the time of observation and due to the lack of significant lines or breaks we can only place an upper limit of about 3.0 on the redshift.

A.64. GRB 080603B ($z = 2.6892$)

The data presented here have previously only been published in circulars (Fynbo et al. 2008c). The redshift is on both Lyα and metal (including fine-structure) absorption lines. We also detect an intervening Mg II system in the spectrum.

A.65. GRB 080604 ($z = 1.4171$)

The data presented here have previously only been published in circulars (Wiersema et al. 2008b). The plotted spectrum is normalized. All of the observed strong, spectral lines can be associated with a single absorption system. We associate the GRB redshift with this gas. The upper limit on the redshift is about 3.1 based on the absence of a Lyα forest in the spectrum.

A.66. GRB 080605 ($z = 1.6403$)

The data presented here have previously only been published in circulars (Jakobsson et al. 2008c). Spectra were also secured with a number of higher resolution gratings. This spectrum like the spectrum of GRB 070802 shows both C I absorption and evidence for the 2175 Å extinction feature. Spectroscopy of this afterglow will be further discussed in Xu et al. in preparation.

A.67. GRB 080607 ($z = 3.0368$)

The data presented here have previously been published in Prochaska et al. (2009). The spectrum is characterized by a very strong Lyα line and by the detection of both H_2 and CO molecular lines. The spectrum shows evidence for substantial reddening. Based on the broad band photometry there is also evidence for the presence of the 2175 Å extinction bump (Prochaska et al. 2009). The burst classifies as a dark burst by the Jakobsson et al. (2004) definition. In the figure of this spectrum we only show the R400 spectrum. For the blue grating spectrum covering Lyα we refer to Prochaska et al. (2009).

A.68. GRB 080707 ($z = 1.2322$)

The data presented here have previously only been published in circulars (Fynbo et al. 2008d). The spectrum was obtained under quite poor conditions with bad seeing and at high airmass. A spectrum was also secured with a higher resolution grating. All of the observed strong, spectral lines can be associated with a single absorption system. We associate the GRB redshift with this gas. The upper limit on the redshift is about 2.2 based on the absence of a Lyα forest.

A.69. GRB 080710 ($z = 0.8454$)

The data presented here have previously only been published in circulars (Perley et al. 2008). All of the observed strong, spectral lines can be associated with a single absorption system. The system also shows fine structure lines. We associate the GRB redshift with this gas. The plotted spectrum has been normalized.

A.70. GRB 080721 ($z = 2.5914$)

The data presented here have previously been published in Starling et al. (2009). Spectra were also secured with a number of higher resolution gratings. The spectrum is affected by fringing redwards of about 7000 Å. The redshift is on both Lyα and metal (including fine-structure) absorption lines.

A.71. GRB 080804 ($z = 2.2045$)

The data presented here have previously only been published in circulars (Thöne et al. 2008d). The spectrum was obtained with the high resolution UVES spectrograph.

A.72. GRB 080805 ($z = 1.5042$)

The data presented here have previously only been published in circulars (Jakobsson et al. 2008e). The strongest line in the spectrum is from a very strong intervening Mg II system. The proposed GRB redshift of 1.504 is based on a higher redshift weaker metal absorption line system. There is evidence for the presence of the 2175 Å extinction feature in the shape of the spectrum at the proposed GRB redshift. The burst classifies as a dark burst according the Jakobsson et al. (2004) definition.

A.73. GRB 080810 ($z = 3.3604$)

The data presented here have previously only been published in circulars (de Ugarte Postigo et al. 2008). A higher resolution spectrum was secured at the Keck telescope and this can be inspected in

Page et al. (2009). The host absorber is remarkable in having a relatively low H I column density. There is evidence for Lyα emission presumably from the underlying host galaxy.

A.74. GRB 080905B ($z = 2.3739$)

The data presented here have previously only been published in circulars (Vreeswijk et al. 2008d). The light form the afterglow is blended with light from another object on the slit. Spectra were also secured with a number of higher resolution gratings. The redshift is based on metal absorption lines including fine structure lines.

A.75. GRB 080913 ($z = 6.7$)

The data presented here have previously been published in Greiner et al. (2009). The redshift is based on the detection of the onset of the Gunn-Peterson trough at 9400 Å. No absorption or emission lines are detected in the spectrum. This is the most distant GRB for which the redshift has been determined in our spectroscopic sample. The burst classifies as a dark burst by the Jakobsson et al. (2004) definition.

A.76. GRB 080916A ($z = 0.6887$)

The data presented here have previously only been published in circulars (Fynbo et al. 2008f). The redshift is based on both absorption lines and emission lines from the underlying host galaxy.

A.77. GRB 080928 ($z = 1.6919$)

The data presented here have previously only been published in circulars (Vreeswijk et al. 2008e). This is another good example of a spectrum where the lines from the intervening absorber are significantly stronger than in the likely GRB absorber. The proposed GRB system is the highest redshift, but weaker, of two metal line systems detected in the spectrum. The upper limit on the redshift based on the absence of Lyα forest features is about 2.1.

B. Linelists and spectra of GRB afterglows

Table 5. GRB 050319 ($z = 3.2425$)

λ_{obs} [Å]	λ_{rest} [Å]	z	Feature	$\mathrm{EW}_{\mathrm{obs}}$ [Å]
5157.	1215.7		Lyα	
5348.2	1260.4	3.2425	Si II	8 ± 3
5530.5	1302.2	3.2425	O I	9 ± 3
	1304.4	3.2425	Si II	
5663.8	1334.5	3.2425	C II	9 ± 3
5913.2	1393.7	3.2425	Si IV	5 ± 3
5949.9	1402.7	3.2425	Si IV	9 ± 3
6472.8	1526.7	3.2425	Si II	6 ± 3
6578.9	1548.2	3.2425	C IV	8 ± 3
	1550.8	3.2425	C IV	

Table 6. GRB 050401 ($z = 2.8983$)

$\lambda_{\rm obs}$ [Å]	$\lambda_{\rm rest}$ [Å]	z	Feature	EW$_{\rm obs}$ [Å]
4739.	1215.7	2.8983	Lyα	
5074.4	1302.2	2.8983	O I	14±4
	1304.4	2.8983	Si II	
5180.0				6±3
5194.7				14±4
5205.0	1334.5	2.8983	C II	12±3
	1335.7	2.8983	C II*	
5422.2	1548.2	2.4982	C IV	14±2
5431.9	1550.8	2.4982	C IV	
5431.9	1393.8	2.8983	Si IV	
5842.6	1670.8	2.4982	Al II	8±2[1]
5900.0				5.5±1.6
5950.4	1526.7	2.8983	Si II	12±2
6036.5	1548.2	2.8983	C IV	10.0±1.0
6044.6	1550.8		C IV	
6273.9	1608.4	2.8983	Fe II	8.5±1.5
6510.9	1670.8	2.8983	Al II	7.0±1.4
6559.9				3.2±0.9
7049.0	1808.0	2.8983	Si II	3.2±0.7
7229.5	1854.7	2.8983	Al III	7.5±0.7
7262.0	1862.8	2.8983	Al III	7.5±0.8
7899.2	2026.1	2.8983	Zn II	5.7±0.8
	2026.5	2.8983	Mg I	
8020.8	2056.3	2.8983	Cr II	3.5±0.9
8042.2	2062.2	2.8983	Cr II	5.6±0.9
8042.2	2062.7	2.8983	Zn II	
8055.0	2066.2	2.8983	Cr II	3.0±0.9
8197.9	2344.2	2.4982	Fe II	3.7±0.8
8303.8	2374.5	2.4982	Fe II	2.3±1.0
8331.5	2382.8	2.4982	Fe II	7.4±0.7
8428.5	2411.3	2.4982	Fe II	3.8±1.1
8815.8	2260.8	2.8983	Fe II	3.7±0.9

Table 6—Continued

$\lambda_{\rm obs}$ [Å]	$\lambda_{\rm rest}$ [Å]	z	Feature	$\rm EW_{obs}$ [Å]
9023.8	2316.7	2.8983	Ni II**	5.4±0.9
9093.7	2600.2	2.4982	Fe II	9.2±0.8
9137.6	2344.2	2.8983	Fe II	5.5±0.7
9254.8	2374.5	2.8983	Fe II	6.2±1.0
9289.9	2382.8	2.8983	Fe II	6.2±1.0

[1] ikely blended with another line.

Table 7. GRB 050408 ($z = 1.2356$)

$\lambda_{\rm obs}$ [Å]	$\lambda_{\rm rest}$ [Å]	z	Feature	$\mathrm{EW}_{\rm obs}$ [Å]
		GMOS/R150		
4610.4	2056.25	1.2356	CrII	6.17 ± 1.51
	2062.2	1.2356	CrII	
	2062.7	1.2356	ZnII	
	2066.2	1.2356	CrII	
5241.4	2333.5	1.2356	FeII*	5.49 ± 0.77
	2338.7	1.2356	FeII*	
	2344.2	1.2356	FeII	
	2345.0	1.2356	FeII*	
	2349.0	1.2356	FeII*	
5310.0	2365.6	1.2356	FeII*	3.00 ± 0.67
	2374.5	1.2356	FeII	
5328.7	2381.5	1.2356	FeII*	4.22 ± 0.65
	2382.8	1.2356	FeII	
	2383.8	1.2356	FeII*	
	2389.4	1.2356	FeII*	
5782.9	2586.7	1.2356	FeII	3.55 ± 0.43
5812.7	2594.5	1.2356	MnII	7.83 ± 0.55
	2599.2	1.2356	FeII*	
	2600.2	1.2356	FeII	
	2606.5	1.2356	MnII	
	2607.9	1.2356	FeII*	
	2612.7	1.2356	FeII*	
6261.7	2796.4	1.2356	MgII	10.90 ± 0.66
	2803.5	1.2356	MgII	
6377.9	2853.0	1.2356	MgI	3.48 ± 0.39
7246.3	3240.0	1.2356	TiII*	2.24 ± 0.48
	3242.9	1.2356	TiII	
		GMOS/R831		

Table 7—Continued

$\lambda_{\rm obs}$ [Å]	$\lambda_{\rm rest}$ [Å]	z	Feature	EW$_{\rm obs}$ [Å]
6378.1	2853.0	1.2356	MgI	3.02 ± 0.29
6752.7	3021.5	1.2356	FeI	0.69 ± 0.19
6875.1	3073.9	1.2356	TiII	2.91 ± 0.30
7566.9	3384.7	1.2356	TiII	1.11 ± 0.21

Table 8. GRB 050730 ($z = 3.9693$)

$\lambda_{\rm obs}$ [Å]	$\lambda_{\rm rest}$ [Å]	z	Feature	$\rm EW_{obs}$ [Å]
4889.3	1215.7	3.022	Lyα	
5549.2	1215.7	3.5680	Lyα	
6040.	1215.7	3.9693	Lyα	
6230.6	1253.8	3.9693	S II	1.38±0.16
6261.9	1259.5	3.9693	S II	5.5±0.3
	1260.4	3.9693	Si II	
6291.1	1264.7	3.9693	Si II*	
6400.8	1402.7	3.5680	Si IV	0.65±0.13
6470.9	1302.2	3.9693	O I	7.1±0.2
6481.7	1304.4	3.9693	Si II	
6503.4	1309.3	3.9693	Si II*	
	2344.2	1.7728	Fe II	
6599.4	1334.5	3.9693	C II	3.0±0.2
	1549.5	3.25	C IV	
6632.3	1334.5	3.9693	C II	4.9±0.2
6720.9	1670.7	3.0222	Al II	0.99±0.11
6925.0	1393.7	3.9693	Si IV	7.1±0.2
6934.	1402.7	3.9693	Si IV	
6968.4	1402.7	3.9693	Si IV	4.6±0.2
	1526.7	3.5680	Si II	
6989.	1548.2	3.514	C IV	
6995.	1550.8	3.514	C IV	
7069.5	1548.2	3.5680	C IV	1.1±0.2
	1550.8	3.5680	C IV	
7110.1				1.2±0.2
7173.8	2586.7	1.7728	Fe II	4.2±0.2
7208.7	2600.2	1.7728	Fe II	
7348.9	1608.4	3.5680	Fe II	0.34±0.16
7694.1	1548.2	3.9693	C IV	1.1±0.2
7702.0	1550.8	3.9693	C IV	
7752.6	2796.3	1.7728	Mg II	7.1±0.3
7774.4	2803.5	1.7728	Mg II	
7990.7	1608.4	3.9693	Fe II	1.3±0.2

Table 8—Continued

$\lambda_{\rm obs}$ [Å]	$\lambda_{\rm rest}$ [Å]	z	Feature	$\rm EW_{obs}$ [Å]
8299.7	1670.7	3.9693	Al II	3.1±0.3
8415.0	2586.7	2.2533	Fe II	1.0±0.3
8457.8	2600.2	2.2533	Fe II	2.4±0.3
9097.6	2796.3	2.2533	Mg II	2.6±0.2
9121.7	2803.5	2.2533	Mg II	1.4±0.2

Table 9. GRB 050801

$\lambda_{\rm obs}$ [Å]	$\lambda_{\rm rest}$ [Å]	z	Feature	$\mathrm{EW_{obs}}$ [Å]
LRISb/B600				
LRISr/R600				
6040.7				2.32 ± 0.76

Table 10. GRB 050802 ($z = 1.7102$)

$\lambda_{\rm obs}$ [Å]	$\lambda_{\rm rest}$ [Å]	z	Feature	$\mathrm{EW_{obs}}$ [Å]
4199.4	1548.2	1.7102	C IV	7.4±1.5
4199.4	1550.8	1.7102	C IV	
6353.5	2344.2	1.7102	Fe II	7.1±0.9
6458.7	2382.8	1.7102	Fe II	7.3±0.9
7009.8	2586.7	1.7102	Fe II	5.0±1.1

Table 11. GRB 050820A ($z = 2.6147$)

$\lambda_{\rm obs}$ [Å]	$\lambda_{\rm rest}$ [Å]	z	Feature	$\mathrm{EW_{obs}}$ [Å]
5518.6	1526.7	2.6147	SiII	5.68 ± 0.05
5596.3	1548.2	2.6147	CIV	5.44 ± 0.04
5605.7	1550.8	2.6147	CIV	5.01 ± 0.05

Table 12. GRB 050824 ($z = 0.8278$)

$\lambda_{\rm obs}$ [Å]	$\lambda_{\rm rest}$ [Å]	z	Feature	$\mathrm{EW_{obs}}$ [Å]
4284.7	2344.2	0.8278	Fe II	1.8 ± 0.5
4337.9	2374.5	0.8278	Fe II	4.5 ± 0.8
4354.2	2382.8	0.8278	Fe II	
4728.6	2586.7	0.8278	Fe II	1.5 ± 0.4
5108.6	2796.3	0.8278	Mg II	1.7 ± 0.3
5124.5	2803.5	0.8278	Mg II	2.3 ± 0.3
6814.5	3727.7	0.8278	[O II]	emission
7074.4	3869.8	0.8278	[Ne III]	emission
7192.4	3934.8	0.8278	Ca II	3.0 ± 0.5
7752.9				1.2 ± 0.4
7938.4	4341.7	0.8278	Hγ	emission
8889.2	4862.7	0.8278	Hβ	emission
9067.6	4960.3	0.8278	[O III]	emission
9155.0	5008.2	0.8278	[O III]	emission

Table 13. GRB 050908 ($z = 3.3467$)

$\lambda_{\rm obs}$ [Å]	$\lambda_{\rm rest}$ [Å]	z	Feature	$\rm EW_{obs}$ [Å]
4402.7	1215.7	2.6208	Lyα	–
5280.6	1215.7	3.3467	Lyα	–
5527.8	1526.7	2.6208	Si II	8.1±0.2
5607.4	1548.2	2.6208	C IV	3.2±0.2
	1550.8	2.2613	C IV	
5627.8	1393.7	3.0383	Si IV	1.9±0.2
5664.9	1402.7	3.0383	Si IV	0.80±0.15
5683.8	1302.2	3.3467	O I	1.3±0.2
	1304.4	3.3467	Si II	
5695.0	1309.3	3.3467	Si II*	1.28±0.15
5796.8	1334.5	3.3467	C II	0.62±0.18
5824.8	1608.4	2.6208	Fe II	1.47±0.13
5973.0	2344.2	1.5481	Fe II	0.90±0.14
6052.4	1393.7	3.3467	Si IV	6.53±0.14
	2374.5	2.6208	Fe II	
	1670.7	1.5481	Al II	
6070.9	2382.8	1.5481	Fe II	1.45±0.14
6093.2	1402.7	3.3467	Si IV	1.85±0.15
6470.1				0.8±0.2
6256.1	1548.2	3.0383	C IV	3.57±0.15
	1550.8	3.0383	C IV	
6591.0	2586.6	1.5481	Fe II	1.15±0.15
6625.0	1526.7	3.3467	Si II	1.85±0.15
	2600.2	1.5481	Fe II	
6729.8	1548.2	3.3467	C IV	13.99±0.20
	1550.8	3.3467	C IV	
7124.9	2796.3	1.5481	Mg II	2.10±0.17
7144.6	2803.5	1.5481	Mg II	2.08±0.17
8489.0	2344.2	2.6208	Fe II	3.70±0.40
8594.4	2374.5	2.6195	Fe II	4.60±1.0
8625.7	2382.8	2.6208	Fe II	8.5±1.0
8818.1	2026.1	3.3467	Zn II	5.0±1.0
	2026.5	3.3467	Mg I	

Table 13—Continued

$\lambda_{\rm obs}$ [Å]	$\lambda_{\rm rest}$ [Å]	z	Feature	$\rm EW_{obs}$ [Å]

Table 14. GRB 050922C ($z = 2.1995$)

$\lambda_{\rm obs}$ [Å]	$\lambda_{\rm rest}$ [Å]	z	Feature	$\rm EW_{obs}$ [Å]
3630.0	1215.7	1.9904	Lyα	
3654.6	1215.7	2.0008	Lyα	
3740.0	1215.7	2.0768	Lyα	
3893.0	1215.7	2.1995	Lyα	
3975.5	1242.8	2.1995	NV	2.5±0.2
4004.1	1302.2	2.0768	O I	0.8±0.2
	1304.4	2.0768	Si II	
	1250.6	2.1995	S II	
4030.3	1260.4	2.1995	Si II	2.1±0.2
4042.5	1264.7	2.196	Si II*	1.6±0.2
4104.9	1334.5	2.0768	C II	1.0±0.2
4179.6	1302.2	2.1995	O I	7.0±0.3
	1304.4	2.1995	Si II	
	1393.7	1.9904	Si IV	
	1402.7	1.9904	Si IV	
4273.0	1334.5	2.1995	C II	4.6±0.2
4273.0	1335.7	2.1995	C II*	
4458.6	1393.7	2.1995	Si IV	1.5±0.1
4486.8	1402.7	2.1995	Si IV	1.4±0.1
4578.8	1533.4	1.9904	Si II*	0.8±0.1
4630.0	1548.2	1.9904	C IV	6.2±0.2
4661.1	1550.8	1.9904	C IV	
4630.0	1548.2	2.0008	C IV	
4661.1	1550.8	2.0008	C IV	
4769.2	1548.2	2.0768	C IV	1.3±0.1
	1550.8	2.0768	C IV	
4699.0	1526.7	2.0768	Si II	0.5±0.2
4882.7	1526.7	2.1995	Si II	2.0±0.1
4908.7	1533.4	2.1995	Si II*	0.9±0.1
4957.6	1548.2	2.1995	C IV	4.1±0.1
4957.6	1550.8	2.1995	C IV	
5146.5	1608.4	2.1995	Fe II	0.6±0.1
5346.9	1670.7	2.1995	Al II	2.7±0.1

Table 14—Continued

$\lambda_{\rm obs}$ [Å]	$\lambda_{\rm rest}$ [Å]	z	Feature	$\rm EW_{obs}$ [Å]
5896.5	2796.3	1.1083	Mg II	1.98±0.17
5909.7	2803.5	1.1083	Mg II	

Table 15. GRB 060115 ($z = 3.5328$)

$\lambda_{\rm obs}$ [Å]	$\lambda_{\rm rest}$ [Å]	z	Feature	$\rm EW_{obs}$ [Å]
5507.0	1215.7	3.5328	Lyα	
5634.3	1242.8	3.5328	NV	4±2
5713.1	1260.4	3.5328	Si II	8±3
5735.2	1264.7	3.5328	Si II*	5±2
5909.3	1302.2	3.5328	O I	11.5±1.8
	1304.4	3.5328	Si II	
6030.0				2.8±1.4
6051.0	1334.5	3.5328	C II	8.6±1.8
6918.5	1526.7	3.5328	Si II	6.3±1.6
7022.5	1548.8	3.5328	C IV	6.0±1.6
	1550.2	3.5328	C IV	
7572.8	1670.8	3.5328	Al II	8.1±1.5

Table 16. GRB 060124 ($z = 2.3000$)

λ_{obs} [Å]	λ_{rest} [Å]	z	Feature	$\mathrm{EW}_{\mathrm{obs}}$ [Å]
		LRIS/R300		
4011.7	1215.7	2.3000	Lyα	13.12 ± 2.44
4231.2				10.03 ± 1.70
4598.5	1393.8	2.3000	SiIV	4.73 ± 1.08
4846.6				5.73 ± 0.84
4862.6				2.43 ± 0.71
5108.8	1548.2	2.3000	CIV	9.68 ± 0.74
	1550.8	2.3000	CIV	
6873.6				2.56 ± 0.70

Table 17. GRB 060206 ($z = 4.0559$)

λ_{obs} [Å]	λ_{rest} [Å]	z	Feature	$\mathrm{EW}_{\mathrm{obs}}$ [Å]
6147.9	1215.7	4.0559	Lyα	
6370.8	1260.4	4.0559	Si II	11.99±0.09
6395.2	1264.7	4.0559	Si II*	
6421.5	2586.7	1.4822	Fe II	0.29±0.09
6453.7	2600.2	1.4822	Fe II	0.68±0.09
6589.0	1302.2	4.0559	O I	14.04±0.09
	1304.4	4.0559	Si II	
6746.0	1334.5	4.0559	C II	11.45±0.14

Table 18. GRB 060210 ($z = 3.9122$)

$\lambda_{\rm obs}$ [Å]	$\lambda_{\rm rest}$ [Å]	z	Feature	$\rm EW_{obs}$ [Å]
		GMOS/R400		
5963.5	2026.1	1.9253	ZnII	174.46 ± 1.59
	1215.7	3.9133	Lyα	
6088.3	1238.8	3.9133	NV	5.02 ± 0.53
	1239.9	3.9133	MgII	
	1240.4	3.9133	MgII	
6106.9	1242.8	3.9133	NV	4.93 ± 0.46
6154.4	1250.6	3.9133	SII	8.32 ± 0.49
	1253.8	3.9133	SII	
6196.5	1259.5	3.9133	SII	21.69 ± 0.42
	1260.4	3.9133	SiII	
	1260.5	3.9133	FeII	
	1260.7	3.9133	CI	
6214.0	1264.7	3.9133	SiII*	7.30 ± 0.29
	1265.0	3.9133	SiII*	
6280.0	1302.2	3.8186	OI	3.52 ± 0.36
	1304.4	3.8186	SiII	
	1276.5	3.9133	CI	
	1277.2	3.9133	CI	
	1280.1	3.9133	CI	
6407.3	1301.9	3.9133	PII	23.82 ± 0.41
	1302.2	3.9133	OI	
	1304.4	3.9133	SiII	
	1304.9	3.9133	OI*	
	1306.0	3.9133	OI**	
6432.6	1334.5	3.8186	CII	2.85 ± 0.24
	1309.3	3.9133	SiII*	
6561.3	1328.8	3.9133	CI	21.23 ± 0.40
	1334.5	3.9133	CII	
	1335.7	3.9133	CII*	

Table 18—Continued

$\lambda_{\rm obs}$ [Å]	$\lambda_{\rm rest}$ [Å]	z	Feature	$\mathrm{EW}_{\rm obs}$ [Å]
6536.1				1.27 ± 0.21
6759.6				1.31 ± 0.17
6848.5	2344.2	1.9253	FeII	14.99 ± 0.28
	1393.8	3.9133	SiIV	
6873.9				4.45 ± 0.19
6885.9	1400.4	3.9133	SnII	2.91 ± 0.11
6892.8	1402.8	3.9133	SiIV	9.74 ± 0.14
6895.1				2.24 ± 0.16
6946.7	2374.5	1.9253	FeII	1.58 ± 0.16
	1414.4	3.9133	GaII	
6970.1	1419.0	3.9133	CO	0.88 ± 0.15
7400.2				0.96 ± 0.14
7460.3	1548.2	3.8186	CIV	3.51 ± 0.13
7471.8	1550.8	3.8186	CIV	2.35 ± 0.13
7505.2	1526.7	3.9133	SiII	18.04 ± 0.19
7534.4	1532.5	3.9133	PII	5.17 ± 0.14
	1533.4	3.9133	SiII*	
7566.1	2586.7	1.9253	FeII	1.21 ± 0.13
7614.2	2600.2	1.9253	FeII	42.36 ± 0.24
	1544.3	3.9133	CO	
	1548.2	3.9133	CIV	
	1550.8	3.9133	CIV	
7677.5	1560.3	3.9133	CI	3.83 ± 0.16
7909.2	1608.5	3.9133	FeII	7.91 ± 0.22
	1611.2	3.9133	FeII	
	1612.8	3.9133	FeII*	
	1613.4	3.9133	CI	

Table 19. GRB 060502A ($z = 1.5025$)

$\lambda_{\rm obs}$ [Å]	$\lambda_{\rm rest}$ [Å]	z	Feature	$\mathrm{EW}_{\rm obs}$ [Å]
		GMOS/R400		
5688.2	2796.4	1.0323	MgII	5.11 ± 0.47
	2803.5	1.0323	MgII	
5727.5				3.53 ± 0.48
5860.6	2338.7	1.5026	FeII*	1.31 ± 0.43
5897.1				1.96 ± 0.40
5936.4	2374.5	1.5026	FeII	2.73 ± 0.30
5957.8	2381.5	1.5026	FeII*	2.82 ± 0.26
5970.9	2382.8	1.5026	FeII	6.01 ± 0.28
	2383.8	1.5026	FeII*	
6013.0	2396.2	1.5026	FeII*	12.57 ± 0.52
	2396.4	1.5026	FeII*	
	2400.0	1.5026	FeII*	
	2405.2	1.5026	FeII*	
	2405.6	1.5026	FeII*	
	2407.4	1.5026	FeII*	
	2411.3	1.5026	FeII*	
	2411.8	1.5026	FeII*	
	2414.1	1.5026	FeII*	
6090.6				1.13 ± 0.23
6445.6	2576.9	1.5026	MnII	0.83 ± 0.21
6470.2	2586.7	1.5026	FeII	2.08 ± 0.25
6504.7	2599.2	1.5026	FeII*	3.91 ± 0.23
	2600.2	1.5026	FeII	
6521.0	2606.5	1.5026	MnII	0.77 ± 0.22
	2607.9	1.5026	FeII*	
6535.6	2612.7	1.5026	FeII*	1.10 ± 0.25
6839.2				2.38 ± 0.33
6884.7	2740.4	1.5026	FeII*	7.74 ± 0.46
	2747.3	1.5026	FeII*	
	2747.9	1.5026	FeII*	

Table 19—Continued

$\lambda_{\rm obs}$ [Å]	$\lambda_{\rm rest}$ [Å]	z	Feature	$\rm EW_{obs}$ [Å]
	2750.2	1.5026	FeII*	
	2756.6	1.5026	FeII*	
6998.0	2796.4	1.5026	MgII	4.73 ± 0.18
7016.0	2803.5	1.5026	MgII	4.26 ± 0.21
7033.5				3.34 ± 0.24
7139.9	2853.0	1.5026	MgI	2.26 ± 0.20
7208.9				1.08 ± 0.30

Table 20. GRB 060512 ($z = 2.1$)

$\lambda_{\rm obs}$ [Å]	$\lambda_{\rm rest}$ [Å]	z	Feature	$\rm EW_{obs}$ [Å]
3750	1215.7	2.1	Lyα	-

Table 21. GRB 060526 ($z = 3.2213$)

$\lambda_{\rm obs}$ [Å]	$\lambda_{\rm rest}$ [Å]	z	Feature	$\rm EW_{obs}$ [Å]
5131.0	1215.7	3.2213	Lyα	
5248.0	1242.8	3.2213	NV	1.1±0.3
5319.8	1260.4	3.2213	Si II	6.0±0.3
5500.7	1302.2	3.2213	O I	7.5±0.4
	1304.4	3.2213	Si II	
5633.4	1334.4	3.2213	C II	7.5±0.4
6443.9	1526.7	3.2213	Si II	3.3±0.4
6539.0	1548.2	3.2213	C IV	1.9±0.4
	1550.8	3.2213	C IV	
6788.7	1608.4	3.2213	Fe II	1.9±0.4
7053.2	1670.7	3.2213	Al II	3.6±0.4

Table 22. GRB 060604

$\lambda_{\rm obs}$ [Å]	$\lambda_{\rm rest}$ [Å]	z	Feature	EW$_{\rm obs}$ [Å]
5217.0				13±4

Table 23. GRB 060607A ($z = 3.0749$)

$\lambda_{\rm obs}$ [Å]	$\lambda_{\rm rest}$ [Å]	z	Feature	$\mathrm{EW}_{\rm obs}$ [Å]
6308.8	1548.2	3.0746	CIV	1.13 ± 0.05
6319.4	1550.8	3.0746	CIV	0.83 ± 0.05

Table 24. GRB 060707 ($z = 3.4240$)

$\lambda_{\rm obs}$ [Å]	$\lambda_{\rm rest}$ [Å]	z	Feature	$\mathrm{EW}_{\rm obs}$ [Å]
5342.6	1215.7	3.4240	Lyα	
5538.8	1250.6	3.4240	S II	6.7±1.3
5724.4				4.5±1.2
5760.8	1302.2	3.4240	O I	9.2±1.1
5768.8	1304.4	3.4240	Si II	6.0±2.0
5902.1	1334.5	3.4240	C II	10.4±1.3
5909.0	1335.7	3.4240	C II*	
6755.7	1526.7	3.4240	Si II	10.2±1.4
6851.6	1548.2	3.4240	C IV	5.7±1.2
6858.3	1550.8	3.4240	C IV	
7391.4	1670.8	3.4240	Al II	9.4±1.6
8002.1	1808.0	3.4240	Si II	3.8±1.9

Table 25. GRB 060714 ($z = 2.7108$)

$\lambda_{\rm obs}$ [Å]	$\lambda_{\rm rest}$ [Å]	z	Feature	$\mathrm{EW}_{\rm obs}$ [Å]
4503.8	1215.7	2.7108	Lyα	
4640.2	1250.6	2.7108	S II	3.3±0.7
4651.6	1253.8	2.7108	S II	3.5±0.6
4676.5	1260.4	2.7108	Si II	7.2±0.6
4693.8	1264.7	2.7108	Si II*	3.7±0.6
4837.3	1302.2 1304.4	2.7108 2.7108	O I Si II	12.7±0.6
4859.7	1309.3	2.7108	Si II*	1.0±0.4
4954.3	1335.3	2.7108	C II	10.5±0.5
5171.4	1393.8	2.7108	Si IV	5.8±0.4
5205.1	1402.8	2.7108	Si IV	5.0±0.4
5665.5	1526.7	2.7108	Si II	6.8±0.5
5691.1	1533.4	2.7108	Si II*	2.2±0.4
5749.1	1549.1	2.7108	C IV	13.1±0.4
5969.9	1608.4	2.7108	Fe II	5.0±0.5
6200.3	1670.8	2.7108	Al II	7.6±0.5
6345.1	1709.6	2.7108	Ni II	0.7±0.3
6462.8	1741.6	2.7108	Ni II	1.0±0.3
6709.0	1808.0	2.7108	Si II	2.2±0.4
6880.9	1854.7	2.7108	Al III	9.1±0.5
6912.0	1862.8	2.7108	Al III	4.3±0.5
7516.9	2026.1 2026.5	2.7108 2.7108	Zn II Mg I	1.8±0.6
7652.9	2062.7	2.7108	Zn II	in telluric band
8227.8				3.1±0.7
8700.2	2344.2	2.7108	Fe II	8.0±1.1
8812.1	2374.5	2.7108	Fe II	6.8±1.0
8843.4	2382.8	2.7108	Fe II	9.6±1.0

Table 26. GRB 060729 ($z = 0.5428$)

$\lambda_{\rm obs}$ [Å]	$\lambda_{\rm rest}$ [Å]	z	Feature	EW$_{\rm obs}$ [Å]
4010.7	2600.2	0.5428	Fe II	0.7±0.2
4314.7	2796.3	0.5428	Mg II	2.80±0.06
4325.5	2803.5	0.5428	Mg II	
4402.1	2853.0	0.5428	Mg I	0.91±0.06
6070.1	3934.8	0.5428	Ca II (K)	1.16±0.04
6123.7	3969.6	0.5428	Ca II (H)	0.85±0.04

Table 27. GRB 060807

$\lambda_{\rm obs}$ [Å]	$\lambda_{\rm rest}$ [Å]	z	Feature	EW$_{\rm obs}$ [Å]
5200.0				0.6±0.3

Table 28. GRB 060904B ($z = 0.7029$)

$\lambda_{\rm obs}$ [Å]	$\lambda_{\rm rest}$ [Å]	z	Feature	EW$_{\rm obs}$ [Å]
4383.5	2576.9	0.7029	Mn II	0.6±0.3
4404.0	2586.7	0.7029	Fe II	1.6±0.3
4427.3	2600.2	0.7029	Fe II	3.1±0.3
4763.7	2796.3	0.7029	Mg II	7.9±0.2
4772.6	2803.5	0.7029	Mg II	
4858.4	2853.0	0.7029	Mg I	1.7±0.2
6352.6	3727.7	0.7029	[O II]	emission
6701.7	3934.8	0.7029	Ca II (K)	2.3±0.2
6760.6	3969.6	0.7029	Ca II (H)	1.8±0.2
8531.7	5008.2	0.7029	[O III]	emission

Table 29. GRB 060906 ($z = 3.6856$)

$\lambda_{\rm obs}$ [Å]	$\lambda_{\rm rest}$ [Å]	z	Feature	$\mathrm{EW}_{\rm obs}$ [Å]
5689.8	1215.7	3.6856	Lyα	
5904.0	1260.4	3.6856	Si II	4.0±1.0
6108.2	1302.2	3.6856	O I	5.5±1.1
	1304.4	3.6856	Si II	
6254.6	1334.5	3.6856	C II	6.1±0.9
6335.9	2796.3	1.2659	Mg II	3.7±0.7
6352.5	2803.5	1.2659	Mg II	
6529.2	1393.8	3.6856	Si IV	3.2±0.8
7153.6	1526.7	3.6856	Si II	2.2±0.9
7258.1	1548.2	3.6856	C IV	3.4±0.9
	1550.8	3.6856	C IV	

Table 30. GRB 060908 ($z = 1.8836$)

$\lambda_{\rm obs}$ [Å]	$\lambda_{\rm rest}$ [Å]	z	Feature	$\mathrm{EW}_{\rm obs}$ [Å]
4464.8	1548.2	1.8836	C IV	9.3±1.5
4471.5	1550.8	1.8836	C IV	

Table 31. GRB 060926 ($z = 3.2086$)

$\lambda_{\rm obs}$ [Å]	$\lambda_{\rm rest}$ [Å]	z	Feature	$\rm EW_{obs}$ [Å]
5116.2	1215.7	3.2086	Lyα	
5382.1	2796.3	0.9242	Mg II	4.8±1.8
5393.1	2803.5	0.9242	Mg II	
5614.3	1334.5	3.2086	C II	5.5±1.4
5625.1	1335.7	3.2086	C II*	
5863.7	1393.8	3.2086	Si IV	3.9±1.4
6426.2	1526.7	3.2086	Si II	4.0±1.1
6517.7	1548.2	3.2086	C IV	8.0±1.2
	1550.8	3.2086	C IV	
6637.5	2374.5	1.7954	Fe II	4.8±1.0
6660.6	2382.8	1.7954	Fe II	4.7±1.4
7232.3	2586.7	1.7954	Fe II	7.3±1.5
7267.9	2600.2	1.7954	Fe II	4.6±1.5
7816.2	2796.3	1.7954	Mg II	7.5±2.0
7837.1	2803.5	1.7954	Mg II	7.8±2.0

Table 32. GRB 060927 ($z = 5.4636$)

$\lambda_{\rm obs}$ [Å]	$\lambda_{\rm rest}$ [Å]	z	Feature	$\rm EW_{obs}$ [Å]
7865.	1215.7	5.4636	Lyα	
8146.7	1260.4	5.4636	Si II	9.0±4.0

Table 33. GRB 061007 ($z = 1.2622$)

λ_{obs} [Å]	λ_{rest} [Å]	z	Feature	$\mathrm{EW}_{\mathrm{obs}}$ [Å]
5302.8	2344.2	1.2622	Fe II	6.4±1.7
5370.4	2374.5	1.2622	Fe II	8.0±2.0
5389.5	2382.8	1.2622	Fe II	5.1±1.5
5777.2	2796.3	1.0660	Mg II	13.9±1.8
5788.2	2803.5	1.0660	Mg II	
5827.7	2576.9	1.2622	Mn II	2.8±1.3
5852.0	2586.7	1.2622	Fe II	7.3±1.3
5884.5	2600.2	1.2622	Fe II	5.9±1.4
6324.5	2796.3	1.2622	Mg II	5.8±1.1
6341.9	2803.5	1.2622	Mg II	6.4±1.1
8134.3	3934.8	1.0660	Ca II	3.5±1.1
8429.3	3726.0	1.2622	[O II]	emission
8440.3	3728.8	1.2622	[O II]	emission

Table 34. GRB 061021 ($z = 0.3463$)

λ_{obs} [Å]	λ_{rest} [Å]	z	Feature	$\mathrm{EW}_{\mathrm{obs}}$ [Å]
3767.9	2796.4	0.3463	Mg II	2.5 ± 0.7
	2803.5	0.3463	Mg II	

Table 35. GRB 061110A ($z = 0.7578$)

λ_{obs} [Å]	λ_{rest} [Å]	z	Feature	$\mathrm{EW}_{\mathrm{obs}}$ [Å]
4914.	2796.3	0.7578	Mg II	6.4±1.4
	2803.5	0.7578	Mg II	
6551.8	3727.7	0.7578	Hβ	emission
8719.7	4960.3	0.7578	[O III]	emission
8803.3	5008.2	0.7578	[O III]	emission

Table 36. GRB 061110B ($z = 3.4344$)

$\lambda_{\rm obs}$ [Å]	$\lambda_{\rm rest}$ [Å]	z	Feature	$\rm EW_{obs}$ [Å]
5350.7	1215.7	3.4344	Lyα	
5774.2	1302.2	3.4344	O I	4.7 ± 1.0
5785.8	1304.4	3.4344	Si II	6.9 ± 1.1
5919.3	1334.5	3.4344	C II	6.7 ± 1.4
	1335.7	3.4344	C II*	
6182.1	1393.8	3.4344	Si IV	6.6 ± 1.2
6221.4	1402.8	3.4344	Si IV	5.9 ± 1.3
6767.8	1526.7	3.4344	Si II	3.2 ± 0.8
6802.2	1533.4	3.4344	Si II*	3.5 ± 0.9
6862.5	1548.2	3.4344	C IV	9.6 ± 1.5
6875.3	1550.8	3.4344	C IV	
7409.6	1670.8	3.4344	Al II	4.1 ± 1.3

Table 37. GRB 061121 ($z = 1.3145$)

$\lambda_{\rm obs}$ [Å]	$\lambda_{\rm rest}$ [Å]	z	Feature	$\rm EW_{obs}$ [Å]
		LRISb/B600		
3534.1	1526.7	1.3145	SiII	4.74 ± 0.13
3549.0	1532.5	1.3145	PII	1.75 ± 0.13
	1533.4	1.3145	SiII*	
3587.2	1548.2	1.3145	CIV	10.20 ± 0.14
	1550.8	1.3145	CIV	
3609.2	1560.3	1.3145	CI	1.14 ± 0.10
3722.7	1608.5	1.3145	FeII	4.26 ± 0.08
3732.4	1611.2	1.3145	FeII	1.16 ± 0.09
	1612.8	1.3145	FeII*	
	1613.4	1.3145	CI	
3745.8	1618.5	1.3145	FeII*	0.33 ± 0.07
3753.0	1621.7	1.3145	FeII*	0.61 ± 0.07
3762.3				0.31 ± 0.07
3770.7	1629.2	1.3145	FeII*	0.49 ± 0.07
3785.3	1637.4	1.3145	FeII*	1.38 ± 0.11
	1634.4	1.3145	FeII*	
	1636.3	1.3145	FeII*	
3817.6				0.20 ± 0.07
3836.6	1656.9	1.3145	CI	0.57 ± 0.09
3867.7	1670.8	1.3145	AlII	5.42 ± 0.08
3939.0	1702.0	1.3145	FeII*	0.49 ± 0.05
3957.3	1709.6	1.3145	NiII	0.77 ± 0.07
4031.7	1741.6	1.3145	NiII	1.22 ± 0.08
4044.8	1747.8	1.3145	MgI	0.23 ± 0.06
4056.3	1751.9	1.3145	NiII	0.71 ± 0.08
4185.4	1807.3	1.3145	SI	2.82 ± 0.07
	1808.0	1.3145	SiII	
4205.6	1816.9	1.3145	SiII*	0.38 ± 0.06
	1817.5	1.3145	SiII*	

Table 37—Continued

$\lambda_{\rm obs}$ [Å]	$\lambda_{\rm rest}$ [Å]	z	Feature	$\mathrm{EW_{obs}}$ [Å]
4231.1	1827.9	1.3145	MgI	0.49 ± 0.05
4293.4	1854.7	1.3145	AlIII	4.68 ± 0.06
4312.1	1862.8	1.3145	AlIII	3.75 ± 0.06
4690.0	2026.1	1.3145	ZnII	2.43 ± 0.06
	2026.3	1.3145	CrII	
	2026.5	1.3145	MgI	
4759.7	2056.3	1.3145	CrII	1.70 ± 0.06
4774.0	2062.2	1.3145	CrII	2.31 ± 0.06
	2062.7	1.3145	ZnII	
4782.2	2066.2	1.3145	CrII	1.09 ± 0.06
5013.1	2166.2	1.3145	NiII*	0.68 ± 0.05
5020.8	2169.8	1.3145	NiII*	0.24 ± 0.05
5034.3	2175.4	1.3145	NiII*	0.31 ± 0.06
5131.1	2217.2	1.3145	NiII*	1.32 ± 0.05
5146.0	2223.6	1.3145	NiII*	0.53 ± 0.05
5152.8				0.32 ± 0.05
5207.7	2249.9	1.3145	FeII	1.44 ± 0.06
5215.7				0.64 ± 0.06
5233.1	2260.8	1.3145	FeII	1.76 ± 0.06
5277.3				0.38 ± 0.05
5331.5				0.20 ± 0.05
5361.8	2316.8	1.3145	NiII*	0.93 ± 0.05
5387.8	2328.1	1.3145	FeII*	0.92 ± 0.06
5400.1	2333.5	1.3145	FeII*	2.11 ± 0.07
5412.7	2338.7	1.3145	FeII*	1.16 ± 0.06
5426.7	2344.2	1.3145	FeII	6.53 ± 0.06
	2345.0	1.3145	FeII*	
5436.5	2349.0	1.3145	FeII*	1.80 ± 0.05
5452.6				0.20 ± 0.05
5463.3	2359.8	1.3145	FeII*	2.09 ± 0.06
5475.1	2365.6	1.3145	FeII*	1.34 ± 0.06
5483.7				0.51 ± 0.05
5497.3	2374.5	1.3145	FeII	6.01 ± 0.07

Table 37—Continued

$\lambda_{\rm obs}$ [Å]	$\lambda_{\rm rest}$ [Å]	z	Feature	EW$_{\rm obs}$ [Å]
5515.9	2381.5	1.3145	FeII*	8.53 ± 0.07
	2382.8	1.3145	FeII	
	2383.8	1.3145	FeII*	
5530.5	2389.4	1.3145	FeII*	1.62 ± 0.06
5546.8	2396.2	1.3145	FeII*	2.86 ± 0.06
	2396.4	1.3145	FeII*	
5555.1	2400.0	1.3145	FeII*	1.69 ± 0.06
5568.2	2405.3	1.3145	FeII*	2.45 ± 0.06
	2405.6	1.3145	FeII*	
5572.4	2407.4	1.3145	FeII*	1.46 ± 0.05
5582.0	2411.3	1.3145	FeII*	2.34 ± 0.08
	2411.8	1.3145	FeII*	
5587.8	2414.1	1.3145	FeII*	1.30 ± 0.06
5608.5				0.26 ± 0.06
		LRISr/R400		
5570.8	2405.2	1.3145	FeII*	2.41 ± 0.21
	2405.6	1.3145	FeII*	
	2407.4	1.3145	FeII*	
5583.1	2411.3	1.3145	FeII*	2.71 ± 0.21
	2411.8	1.3145	FeII*	
	2414.1	1.3145	FeII*	
5935.1				1.47 ± 0.09
5966.8	2576.9	1.3145	MnII	3.08 ± 0.09
5989.2	2586.7	1.3145	FeII	7.34 ± 0.09
6006.8	2594.5	1.3145	MnII	3.01 ± 0.08
6020.0	2599.2	1.3145	FeII*	8.80 ± 0.07
	2600.2	1.3145	FeII	
6035.8	2606.6	1.3145	MnII	3.49 ± 0.08
	2607.9	1.3145	FeII*	
6049.4	2612.7	1.3145	FeII*	3.61 ± 0.07
	2614.6	1.3145	FeII*	

Table 37—Continued

λ_{obs} [Å]	λ_{rest} [Å]	z	Feature	$\mathrm{EW}_{\mathrm{obs}}$ [Å]
6061.4	2618.4	1.3145	FeII*	1.13 ± 0.08
	2621.2	1.3145	FeII*	
	2622.5	1.3145	FeII*	
6083.6	2621.2	1.3145	FeII*	5.16 ± 0.13
	2622.5	1.3145	FeII*	
	2626.5	1.3145	FeII*	
	2629.1	1.3145	FeII*	
	2631.8	1.3145	FeII*	
	2632.1	1.3145	FeII*	
6284.7				0.88 ± 0.09
6315.2				0.84 ± 0.09
6343.0	2740.4	1.3145	FeII*	1.55 ± 0.08
6361.6	2747.3	1.3145	FeII*	4.45 ± 0.10
	2747.9	1.3145	FeII*	
	2750.2	1.3145	FeII*	
6380.3	2756.6	1.3145	FeII*	1.49 ± 0.09
6473.6	2796.4	1.3145	MgII	10.25 ± 0.09
6490.3	2803.5	1.3145	MgII	9.71 ± 0.07
6603.9	2853.0	1.3145	MgI	5.70 ± 0.09
6873.2	2967.8	1.3145	FeI	2.33 ± 0.10
6897.3				1.10 ± 0.11
7839.8	3384.7	1.3145	TiII	1.52 ± 0.15
8231.0				1.84 ± 0.11
9106.0	3934.8	1.3145	CaII	4.07 ± 0.19
9186.8	3969.6	1.3145	CaII	3.30 ± 0.16

Table 38. GRB 070110 ($z = 2.3521$)

λ_{obs} [Å]	λ_{rest} [Å]	z	Feature	$\mathrm{EW}_{\mathrm{obs}}$ [Å]
4067.7	1215.7	2.3521	Lyα	
4224.2	1260.4	2.3521	Si II	4.5 ± 0.4
4240.7	1264.7	2.3521	Si II*	2.4 ± 0.4
4368.6	1302.2	2.3521	O I	7.1 ± 0.4
	1304.4	2.3521	Si II	
4425.1	1548.2	1.856	C IV	8.2 ± 0.4
	1550.8	1.856	C IV	
4474.1	1334.5	2.3521	C II	3.8 ± 0.3
	1335.7	2.3521	C II*	
4672.1	1393.8	2.3521	Si IV	1.4 ± 0.3
4702.8	1402.8	2.3521	Si IV	1.4 ± 0.3
4773.7	1670.8	1.856	Al II	1.1 ± 0.3
5116.3	1526.7	2.3521	Si II	3.5 ± 0.3
5141.7	1533.4	2.3521	Si II*	1.2 ± 0.3
5193.5	1548.2	2.3521	C IV	3.1 ± 0.3
	1550.8	2.3521	C IV	
5391.1	1608.4	2.3521	Fe II	2.5 ± 0.3
5600.4	1670.8	2.3521	Al II	3.0 ± 0.3
5730.3	1709.6	2.3521	Ni II	1.2 ± 0.3
5838.9	1741.6	2.3521	Ni II	0.9 ± 0.3
6059.4	1808.0	2.3521	Si II	1.4 ± 0.3
6215.6	1854.7	2.3521	Al III	1.1 ± 0.3
6246.4	1862.8	2.3521	Al III	1.0 ± 0.3
6790.1	2026.1	2.3521	Zn II	2.0 ± 0.4
	2026.5	2.3521	Mg I	
7860.9	2344.2	2.3521	Fe II	2.9 ± 0.8
7959.6	2374.5	2.3521	Fe II	3.3 ± 0.6
7985.9	2382.8	2.3521	Fe II	7.1 ± 0.8
8670.6	2586.7	2.3521	Fe II	1.9 ± 0.9
8714.4	2600.2	2.3521	Fe II	6.8 ± 0.6

Table 39. GRB 070125 ($z = 1.5471$)

$\lambda_{\rm obs}$ [Å]	$\lambda_{\rm rest}$ [Å]	z	Feature	$\mathrm{EW}_{\rm obs}$ [Å]
3950.3	1548.2	1.5471	C IV	1.7 ± 0.3
	1550.8	1.5471	C IV	
7122.4	2796.3	1.5471	Mg II	0.5 ± 0.1
7140.8	2803.5	1.5471	Mg II	0.4 ± 0.1

Table 40. GRB 070306 ($z = 1.4965$)

$\lambda_{\rm obs}$ [Å]	$\lambda_{\rm rest}$ [Å]	z	Feature	$\mathrm{EW}_{\rm obs}$ [Å]
9306.3	3727.7	1.4965	[O II]	emission

Table 41. GRB 070318 ($z = 0.8397$)

$\lambda_{\rm obs}$ [Å]	$\lambda_{\rm rest}$ [Å]	z	Feature	$\mathrm{EW}_{\rm obs}$ [Å]
4313.1	2344.2	0.8397	Fe II	1.4 ± 0.3
4365.2	2374.5	0.8397	Fe II	0.8 ± 0.2
4381.7	2382.8	0.8397	Fe II	2.2 ± 0.3
4743.5	2576.9	0.8397	Mn II	6.7 ± 0.4
4758.1	2586.7	0.8397	Fe II	
4772.6	2594.5	0.8397	Mn II	
4783.6	2600.2	0.8397	Fe II	
4795.0	2606.5	0.8397	Mn II	
5145.4	2796.4	0.8397	Mg II	4.8 ± 0.3
5157.9	2803.5	0.8397	Mg II	
5247.8	2853.0	0.8397	Mg I	1.2 ± 0.2
6228.2	3384.7	0.8397	Ti II	1.0 ± 0.3
7238.4	3934.8	0.8397	Ca II	3.8 ± 0.4
7305.5	3969.6	0.8397	Ca II	1.8 ± 0.4

Table 42. GRB 070411 ($z = 2.9538$)

$\lambda_{\rm obs}$ [Å]	$\lambda_{\rm rest}$ [Å]	z	Feature	$\mathrm{EW}_{\rm obs}$ [Å]
4806.5	1215.7	2.9538	Lyα	
4983.9	1260.4	2.9538	Si II	1.1 ± 0.3
5156.9	1302.2	2.9538	O I	1.3 ± 0.3
	1304.4	2.9538	Si II	
5276.6	1334.5	2.9538	C II	2.1 ± 0.3
5280.6	1335.7	2.9538	C II*	0.7 ± 0.2
5509.3	1393.8	2.9538	Si IV	3.1 ± 0.4
5545.9	1402.8	2.9538	Si IV	2.6 ± 0.4
6033.8	1526.7	2.9538	Si II	1.7 ± 0.4
6120.5	1548.2	2.9538	C IV	10.1 ± 0.5
6131.8	1550.8	2.9538	C IV	
6358.8	1608.4	2.9538	Fe II	0.9 ± 0.3
6606.3	1670.8	2.9538	Al II	1.8 ± 0.3

Table 43. GRB 070419A ($z = 0.9705$)

λ_{obs} [Å]	λ_{rest} [Å]	z	Feature	$\mathrm{EW}_{\mathrm{obs}}$ [Å]
GMOS/R831				
7753.8	3934.8	0.9705	CaII	2.46 ± 0.31
7822.2	3969.6	0.9705	CaII	1.21 ± 0.29
8332.3	4227.9	0.9705	CaI	0.84 ± 0.18

Table 44. GRB 070506 ($z = 2.3090$)

λ_{obs} [Å]	λ_{rest} [Å]	z	Feature	$\mathrm{EW}_{\mathrm{obs}}$ [Å]
4017.1	1215.7	2.3090	Lyα	
4166.8	1260.4	2.3090	Si II	9.0±2.0
4314.5	1302.2	2.3090	O I	8.5±2.0
	1304.4	2.3090	Si II	
4641.3	1402.7	2.3090	Si IV	4.4±1.5
4758.7	1548.2	2.0709	C IV	7.5±1.4
	1550.8	2.0709	C IV	
5049.5	1526.7	2.3090	Si II	6.7±0.9
5085.2				6.4±0.9
5122.	1548.2	2.3090	C IV	6.4±1.0
	1550.8	2.3090	C IV	
5324.7	1608.4	2.3090	Fe II	4.4±0.7
5528.4	1670.7	2.3090	Al II	4.7±0.6
5694.2	1854.7	2.0709	Al III	3.1±0.5
5721.4	1862.7	2.0709	Al III	3.1±0.5
6140.1	1854.7	2.3090	Al III	2.6±0.5
6706.8	2026.1	2.3090	Zn II	2.8±0.5
	2026.5	2.3090	Mg I	
6824.8	2062.2	2.3090	Cr II	2.9±0.5
	2062.6	2.3090	Zn II	

Table 45. GRB 070611 ($z = 2.0394$)

$\lambda_{\rm obs}$ [Å]	$\lambda_{\rm rest}$ [Å]	z	Feature	$\mathrm{EW}_{\rm obs}$ [Å]
3694.8	1215.7	2.0394	Lyα	
4359.4	2796.3	0.5588	Mg II	2.5±1.0
4369.8	2803.5	0.5588	Mg II	2.5±1.0
4708.8	1548.2 1550.8	2.0394 2.0394	C IV C IV	2.9±1.0
5472.6	2382.8	1.2973	Fe II	2.2±0.7
6425.4	2796.3	1.2973	Mg II	3.9±0.7
6440.4	2803.5	1.2973	Mg II	3.2±0.7
8497.0	2796.3	2.0394	Mg II	2.8±1.2
8523.2	2803.5	2.0394	Mg II	3.6±0.9

Table 46. GRB 070721B ($z = 3.6298$)

$\lambda_{\rm obs}$ [Å]	$\lambda_{\rm rest}$ [Å]	z	Feature	$\mathrm{EW}_{\rm obs}$ [Å]
4970.0	1215.7	3.0939	Lyα	
5590.0	1215.7	3.6298	Lyα	
6028.1	1302.2 1304.4	3.6298 3.6298	O I Si II	6.5±1.9
6179.8	1334.5	3.6298	C II	5.0±2.0
6248.7	1526.7	3.0939	Si II	7.0±2.2
6337.3	1548.2	3.0939	C IV	19.0±3.0
6349.9	1550.8	3.0939	C IV	
6450.2	1393.8	3.6298	Si IV	6.0±1.9
6492.7	1402.8	3.6298	Si IV	7.0±2.2
6584.2	1608.5	3.0939	Fe II	9.0±1.9
6842.2	1670.8	3.0939	Al II	7.6±2.0
7066.2	1526.7	3.6298	Si II	5.8±1.9
7104.6	1533.4	3.6298	Si II*	5.9±1.8
7167.5	1548.2	3.6298	C IV	14.6±2.6
7180.8	1550.8	3.6298	C IV	

Table 47. GRB 070802 ($z = 2.4511$)

$\lambda_{\rm obs}$ [Å]	$\lambda_{\rm rest}$ [Å]	z	Feature	$\rm EW_{obs}$ [Å]
4200.0	1215.7	2.4541	Lyα	
4607.9	1334.5	2.4541	C II	16±6
5141.4	1670.7	2.0785	Al II	6.0±1.7
5273.9	1526.7	2.4541	Si II	10±2
5350.9	1548.2	2.4541	C IV	7.3±1.8
	1550.8	2.4541	C IV	
5390.7	1560.3	2.4541	C I	2.4±1.2
5556.4	1608.4	2.4541	Fe II	10.5±1.6
5724.5	1656.9	2.4541	C I	4.7±1.1
5771.2	1670.7	2.4541	Al II	14.3±1.2
6246.5	1808.8	2.4541	Si II	3.9±1.0
6404.9	1854.7	2.4541	Al III	2.4±1.0
7000.1	2026.1	2.4541	Zn II	4.2±1.0
	2026.5	2.4541	Mg I	
7104.1	2056.3	2.4541	Cr II	2.0±0.9
7124.8	2062.2	2.4541	Cr II	2.53±0.9
7126.3	2062.7	2.4541	Zn II	
7218.7	2344.2	2.0785	Fe II	3.4±1.0
7311.4	2374.5	2.0785	Fe II	4.5±1.0
7335.7	2382.8	2.0785	Fe II	4.9±1.0
7810.7	2260.8	2.4541	Fe II	6.6±1.0
8005.9	2600.2	2.0785	Fe II	4.7±1.1
8094.1	2344.2	2.4541	Fe II	16.5±2.0
8200.5	2374.5	2.4541	Fe II	12.7±1.5
8228.0	2382.8	2.4541	Fe II	18.8±1.5
8277.1	2396.4	2.4541	Fe II*	2.9±1.4
8308.7	2405.6	2.4541	Fe II**	2.8±1.4
8515.5	2586.7	2.2921	Fe II	2.3±0.6
8560.6	2600.2	2.2921	Fe II	2.2±0.6
8607.0	2796.3	2.0785	Mg II	11.3±0.6
8631.0	2803.5	2.0785	Mg II	11.5±0.6
8780.1	2853.0	2.0785	Mg I	2.7±1.1
8902.8	2576.9	2.4541	Mn II	5.0±1.2

Table 47—Continued

$\lambda_{\rm obs}$ [Å]	$\lambda_{\rm rest}$ [Å]	z	Feature	$\rm EW_{obs}$ [Å]
8934.4	2586.7	2.4541	Fe II	19.5±1.3
8979.5	2600.2	2.4541	Fe II	29.0±1.3
9208.6	2796.3	2.2921	Mg II	1.8±0.6
9226.5	2803.5	2.2921	Mg II	1.4±0.6

Table 48. GRB 071020 ($z = 2.1462$)

$\lambda_{\rm obs}$ [Å]	$\lambda_{\rm rest}$ [Å]	z	Feature	$\rm EW_{obs}$ [Å]
5254.7	1670.8	2.1462	Al II	6±2
7376.8	2344.2	2.1462	Fe II	5±2
7498.3	2382.8	2.1462	Fe II	6±2
8136.8	2586.7	2.1462	Fe II	7±2
8181.6	2600.2	2.1462	Fe II	11±2
8274.5				6±2
8797.7	2796.3	2.1462	Mg II	14±2
8820.9	2803.5	2.1462	Mg II	10±2

Table 49. GRB 071031 ($z = 2.6918$)

$\lambda_{\rm obs}$ [Å]	$\lambda_{\rm rest}$ [Å]	z	Feature	$\mathrm{EW}_{\rm obs}$ [Å]
4483.0	1215.7	2.6918	Lyα	
4652.0	1260.4	2.6918	Si II	2.65±0.15
4670.0	1264.7	2.6918	Si II*	2.00±0.15
4815.2	1302.2	2.6918	O I	4.91±0.11
	1304.4	2.6918	Si II	
4833.5	1309.3	2.6918	Si II*	1.45±0.13
4862.9	1317.2	2.6918	Ni II	0.46±0.15
4900.1	1854.7	1.6421	Al III	0.56±0.12
4928.5	1334.5	2.6918	C II	4.45±0.13
	1335.7	2.6918	C II*	
5056.8	1370.1	2.6918	Ni II	0.62±0.14
5145.1	1393.8	2.6918	Si IV	3.70±0.15
5178.9	1402.8	2.6918	Si IV	2.76±0.15
5224.5	1549.1	2.3726	C IV	1.40±0.14
5636.1	1526.7	2.6918	Si II	1.99±0.11
5661.1	1533.4	2.6918	Si II*	1.75±0.11
5717.1	1549.1	2.6918	C IV	8.05±0.16
5755.5	1559	2.6918	Fe II*****	1.22±0.12
5938.2	1608.4	2.6918	Fe II	3.25±0.16
5976.9	1618.5	2.6918	Fe II*	0.93±0.12
5987.0	1621.7	2.6918	Fe II*	
6015.9	1629.2	2.6918	Fe II**	0.94±0.12
6041.9	1636.3	2.6918	Fe II***	1.37±0.12
6168.3	1670.8	2.6918	Al II	2.33±0.11
6429.7	1741.6	2.6918	Ni II	0.59±0.12
6466.7	1751.9	2.6918	Ni II	0.42±0.12
6674.6	1808.0	2.6918	Si II	0.94±0.10
6848.3	1854.7	2.6918	Al III	0.96±0.12
7032.1	2382.8	1.9514	Fe II	1.48±0.12
7388.5	2796.3	1.6421	Mg II	1.83±0.13
7407.3	2803.5	1.6421	Mg II	1.42±0.15
7479.6	2026.1	2.6918	Zn II	0.31±0.15
	2026.5	2.6918	Mg I	

Table 49—Continued

$\lambda_{\rm obs}$ [Å]	$\lambda_{\rm rest}$ [Å]	z	Feature	$\rm EW_{obs}$ [Å]
7673.6	2600.2	1.9514	Fe II	0.40±0.20
7996.0	2166.2	2.6918	Ni II**	1.50±0.20
8252.9	2796.3	1.9514	Mg II	2.40±0.19
8275.0	2803.5	1.9514	Mg II	1.47±0.19
8553.0	2316.7	2.6918	Ni II**	0.90±0.20
8594.7	2328.1	2.6918	Fe II**	0.90±0.20
8614.1	2333.5	2.6918	Fe II*	2.70±0.18
8635.7	2338.7	2.6918	Fe II***	0.73±0.22
8655.8	2344.2	2.6918	Fe II	4.30±0.25
8672.1	2349.0	2.6918	Fe II**	2.60±0.25
8714.7	2359.8	2.6918	Fe II***	2.30±0.17
8733.5	2365.6	2.6918	Fe II*	1.68±0.17
8766.4	2374.5	2.6918	Fe II	2.43±0.35
8797.0	2382.8	2.6918	Fe II	4.47±0.20
8821.5	2389.4	2.6918	Fe II*	1.35±0.35
8846.5	2396.4	2.6918	Fe II*	1.77±0.35
8860.2	2400.0	2.6918	Fe II**	1.79±0.35
8883.5	2405.6	2.6918	Fe II**	3.96±0.35
8902.2	2411.3	2.6918	Fe II***	3.30±0.35
9549.1	2586.7	2.6918	Fe II	3.43±0.60
9596.5	2600.2	2.6918	Fe II	5.17±0.32

Table 50. GRB 071112C ($z = 0.8227$)

$\lambda_{\rm obs}$ [Å]	$\lambda_{\rm rest}$ [Å]	z	Feature	$\rm EW_{obs}$ [Å]
4273.4	2344.2	0.8227	Fe II	2.0±0.5
4328.7	2374.5	0.8227	Fe II	1.0±0.5
4345.0	2382.8	0.8227	Fe II	1.6±0.5
4715.9	2586.7	0.8227	Fe II	2.0±0.5
4741.0	2600.2	0.8227	Fe II	2.4±0.5
5096.4	2796.3	0.8227	Mg II	4.9±0.6
5110.1	2803.5	0.8227	Mg II	
6795.8	3727.7	0.8227	[O II]	emission
7051.2	3869.8	0.8227	[Ne III]	emission
7170.0	3934.8	0.8227	Ca II	2.4±0.5
7233.1	3969.6	0.8227	Ca II	2.8±0.8
9038.5	4960.3	0.8227	[O III]	emission
9127.7	5008.2	0.8227	[O III]	emission

Table 51. GRB 080210 ($z = 2.6419$)

$\lambda_{\rm obs}$ [Å]	$\lambda_{\rm rest}$ [Å]	z	Feature	$\mathrm{EW}_{\rm obs}$ [Å]
4406.6	1215.7	2.6419	Lyα	
4591.5	1260.4	2.6419	Si II	4.2±0.7
4609.3	1264.7	2.6419	Si II*	2.3±0.6
4652.8				1.4±0.4
4747.6	1302.2 1304.4	2.6419 2.6419	O I Si II	9.7±0.6
4768.8	1309.3	2.6419	Si II*	1.3±0.5
4862.5	1334.5	2.6419	C II	8.7±0.5
5076.3	1393.8	2.6419	Si IV	5.7±0.4
5109.4	1402.8	2.6419	Si IV	4.7±0.4
5354.3	1526.7	2.5084	Si II	1.0±0.3
5437.0	1549.1	2.5084	C IV	4.3±0.4
5559.2	1526.7	2.6419	Si II	5.1±0.3
5642.3	1548.2 1550.8	2.6419 2.6419	C IV C IV	12.7±0.4
5857.5	1608.4	2.6419	Fe II	3.7±0.3
6083.9	1670.8	2.6419	Al II	6.2±0.3
6582.7	1808.0	2.6419	Si II	2.1±0.3
6753.9	1854.7	2.6419	Al III	3.9±0.3
6782.0	1862.8	2.6419	Al III	2.4±0.3
7379.5	2026.1 2026.5	2.6419 2.6419	Zn II Mg I	2.3±0.4
8533.8	2344.2	2.6419	Fe II	6.3±0.4
8644.7	2374.5	2.6419	Fe II	1.8±0.5
8675.2	2382.8	2.6419	Fe II	6.8±0.5

Table 52. GRB 080310 ($z = 2.4274$)

$\lambda_{\rm obs}$ [Å]	$\lambda_{\rm rest}$ [Å]	z	Feature	$\rm EW_{obs}$ [Å]
		Kast/B830		
4167.8	1215.7	2.4293	Lyα	11.51 ± 0.54
4222.8				1.82 ± 0.46
4263.6				1.87 ± 0.45
		Kast/R600		
4562.6	1393.8	2.2810	SiIV	15.89 ± 1.21
	1334.3	2.4293	CII	
4756.5				1.73 ± 0.41
4778.0	1393.8	2.4293	SiIV	2.37 ± 0.36
4809.1				1.81 ± 0.37
5084.2	1548.2	2.2810	CIV	7.26 ± 0.37
	1550.8	2.2810	CIV	
5314.8	1548.2	2.4293	CIV	7.77 ± 0.31
	1550.8	2.4293	CIV	
5726.0	1670.8	2.4293	AlII	2.28 ± 0.25
6485.3				1.60 ± 0.25
6550.1				1.67 ± 0.25
6895.2				4.16 ± 0.27

Table 53. GRB 080319B ($z = 0.9382$)

$\lambda_{\rm obs}$ [Å]	$\lambda_{\rm rest}$ [Å]	z	Feature	$\rm EW_{obs}$ [Å]
4543.3	2344.2	0.9382	Fe II	1.4 ± 0.6
4798.6	2796.3	0.716	Mg II	3.0 ± 0.6
	2803.5	0.716	Mg II	
5013.5	2586.7	0.9382	Fe II	1.8 ± 0.5
5040.9	2600.2	0.9382	Fe II	1.4 ± 0.5
5419.6	2796.3	0.9382	Mg II	2.0 ± 0.5
5433.6	2803.5	0.9382	Mg II	1.7 ± 0.5

Table 54. GRB 080319C ($z = 1.9492$)

$\lambda_{\rm obs}$ [Å]	$\lambda_{\rm rest}$ [Å]	z	Feature	$\rm EW_{obs}$ [Å]
4502.5	1526.7	1.9492	Si II	3.9±1.7
4565.4	1548.2	1.9492	C IV	10.6±0.7
	1550.8	1.9492	C IV	
4743.9	1608.5	1.9492	Fe II	3.4±1.3
4926.7	1670.8	1.9492	Al II	5.7±0.9
5062.5	2796.4	0.8104	Mg II	4.0±0.8
5075.3	2803.5	0.8104	Mg II	3.7±0.8
5137.5	1741.6	1.9492	Ni II	3.0±0.6
5332.1	1808.0	1.9492	Si II	3.5±0.7
5470.3	1854.7	1.9492	Al III	4.3±0.6
5493.6	1862.8	1.9492	Al III	4.2±0.6
5976.4	2026.1	1.9492	Zn II	2.3±0.7
	2026.5	1.9492	Mg I	
6064.3	2056.3	1.9492	Cr II	1.9±0.6
6083.3	2062.2	1.9492	Cr II	2.3±0.6
	2062.7	1.9492	Zn II	
6634.0	2249.9	1.9492	Fe II	2.3±0.6

Table 55. GRB 080330 ($z = 1.5119$)

λ_{obs} [Å]	λ_{rest} [Å]	z	Feature	$\mathrm{EW}_{\mathrm{obs}}$ [Å]
3889.4	1548.2	1.5119	C IV	4.3±0.7
	1550.8	1.5119	C IV	
4028.8	1608.4	1.5119	Fe II	2.0±0.7
4198.2	1670.8	1.5119	Al II	2.0±0.7
5093.5	2026.1	1.5119	Zn II	4.3±0.4
	2026.5	1.5119	Mg I	
5190.3	2062.2	1.5119	Cr II	0.6±0.3
5190.3	2062.7	1.5119	Zn II	
5883.4	2344.2	1.5119	Fe II	1.4±0.5
5983.0	2382.8	1.5119	Fe II	2.2±0.5
6497.5	2586.7	1.5119	Fe II	11±2
6527.0	2600.2	1.5119	Fe II	
7031.1	2796.3	1.5119	Mg II	5.2±0.3
	2803.5	1.5119	Mg II	

Table 56. GRB 080411 ($z = 1.0301$)

$\lambda_{\rm obs}$ [Å]	$\lambda_{\rm rest}$ [Å]	z	Feature	$\rm EW_{obs}$ [Å]
3780.1	1862.8	1.0301	Al III	1.43±0.11
4112.2	2026.1	1.0301	Zn II	1.30±0.07
	2026.5	1.0301	Mg I	
4188.4	2062.2	1.0301	Cr II	1.12±0.08
4188.4	2062.7	1.0301	Zn II	
4398.0	2166.2	1.0301	Ni II**	0.62±0.06
4439.8				1.33±0.06
4500.8	2217.2	1.0301	Ni II**	0.61±0.06
4516.3	2223.0	1.0301	Ni II	0.20±0.06
4566.8	2249.9	1.0301	Fe II	0.69±0.06
4591.6	2260.8	1.0301	Fe II	0.68±0.06
4705.2	2316.7	1.0301	Ni II**	0.26±0.05
4734.8	2333.5	1.0301	Fe II*	0.91±0.05
	2338.7	1.0301	Fe II***	
4761.2	2344.7	1.0301	Fe II	2.87±0.06
	2349.0	1.0301	Fe II**	
4795.7	2359.8	1.0301	Fe II***	1.37±0.06
	2365.6	1.0301	Fe II**	
4822.2	2374.5	1.0301	Fe II	9.31±0.11
4836.3	2382.8	1.0301	Fe II	
4867.3	2396.4	1.0301	Fe II*	
	2400.0	1.0301	Fe II**	
4885.9	2405.6	1.0301	Fe II**	
	2411.3	1.0301	Fe II***	
5203.3				0.21±0.08
5231.0	2576.9	1.0301	Mn II	0.45±0.05
5252.1	2586.7	1.0301	Fe II	8.37±0.20
5277.7	2600.2	1.0301	Fe II	
5294.8	2607.9	1.0301	Fe II**	
5302.8	2612.7	1.0301	Fe II*	
5314.2	2614.6	1.0301	Fe II***	
	2618.4	1.0301	Fe II**	
	2622.5	1.0301	Fe II****	
5337.5				2.32±0.10

Table 56—Continued

$\lambda_{\rm obs}$ [Å]	$\lambda_{\rm rest}$ [Å]	z	Feature	EW$_{\rm obs}$ [Å]
	2626.5	1.0301	Fe II*	
	2629.1	1.0301	Fe II****	
	2631.9	1.0301	Fe II**	
5677.1	2796.3	1.0301	Mg II	6.43±0.15
5690.6	2805.3	1.0301	Mg II	
5791.5	2853.0	1.0301	Mg I	1.17±0.10
7984.6	3934.8	1.0301	Ca II (K)	2.19±0.30
8055.6	3969.6	1.0301	Ca II (H)	2.25±0.30

Table 57. GRB 080413A ($z = 2.4330$)

$\lambda_{\rm obs}$ [Å]	$\lambda_{\rm rest}$ [Å]	z	Feature	$\rm EW_{obs}$ [Å]
5241.9	1526.7	2.4330	SiII	1.9 ± 0.3
5314.6	1548.2	2.4330	CIV	2.8 ± 0.3
5323.3	1550.8	2.4330	CIV	2.5 ± 0.3

Table 58. GRB 080413B ($z = 1.1014$)

$\lambda_{\rm obs}$ [Å]	$\lambda_{\rm rest}$ [Å]	z	Feature	$\rm EW_{obs}$ [Å]
3374.5	1608.4	1.1014	Fe II	0.9±0.4
3508.7	1670.8	1.1014	Al II	4.9±1.0
3799.4	1808.0	1.1014	Si II	1.12±0.20
3896.7	1854.7	1.1014	Al III	0.76±0.20
3915.0	1862.8	1.1014	Al III	0.76±0.20
4258.2	2026.1	1.1014	Zn II	1.39±0.15
	2026.5	1.1014	Mg I	
4287.5				0.30±0.10
4322.5	2056.3	1.1014	Cr II	1.41±0.10
4334.1	2062.2	1.1014	Cr II	
	2062.7	1.1014	Zn II	
4659.9	2217.2	1.1014	Ni II**	0.29±0.08
4726.6	2249.9	1.1014	Fe II	0.49±0.08
4751.4	2260.8	1.1014	Fe II	0.72±0.08
4926.3	2344.2	1.1014	Fe II	4.56±0.08
4990.4	2374.5	1.1014	Fe II	3.04±0.15
5006.9	2382.8	1.1014	Fe II	5.08±0.15
5038.5	2396.4	1.1014	Fe II*	0.52±0.15
5057.1	2405.6	1.1014	Fe II**	0.45±0.15
5414.7	2576.9	1.1014	Mn II	15.84±0.30
5436.0	2586.7	1.1014	Fe II	
5463.3	2600.2	1.1014	Fe II	
5488.4	2612.7	1.1014	Fe II*	
5525.6	2626.5	1.1014	Fe II*	0.82±0.10
5877.0	2796.3	1.1014	Mg II	13.40±0.20
5889.0	2803.5	1.1014	Mg II	
5995.1	2853.0	1.1014	Mg I	2.18±0.10

Table 59. GRB 080520 ($z = 1.5457$)

$\lambda_{\rm obs}$ [Å]	$\lambda_{\rm rest}$ [Å]	z	Feature	$\rm EW_{obs}$ [Å]
7116.6	2796.3	1.5457	Mg II	6±3
7137.0	2803.5	1.5457	Mg II	8±3
7266.0	2853.0	1.5457	Mg I	6±3
9481.5	3727.1	1.5457	[O II]	emission
9494.4	3727.9	1.5457	[O II]	emission

Table 60. GRB 080603B ($z = 2.6892$)

$\lambda_{\rm obs}$ [Å]	$\lambda_{\rm rest}$ [Å]	z	Feature	$\rm EW_{obs}$ [Å]
4493.3	1215.7	2.6892	Lyα	
4668.0	1264.7	2.6892	Si II*	0.52±0.25
4712.5				1.51±0.20
4720.8				
4740.9				
4775.2				0.30±0.15
4807.5	1302.2	2.6892	O I	2.67±0.15
4815.0	1304.4	2.6892	Si II	
4831.5	1309.3	2.6892	Si II*	0.54±0.15
4925.8	1335.3	2.6892	C II	3.88±0.15
5141.3	1393.8	2.6892	Si IV	1.87±0.14
5174.5	1402.8	2.6892	Si IV	1.25±0.14
5628.6	1526.7	2.6892	Si II	0.56±0.14
5656.4	1533.4	2.6892	Si II*	0.58±0.14
5711.3	1548.2	2.6892	C IV	4.39±0.16
	1550.8	2.6892	C IV	
5912.4	2796.4	1.1156	Mg II	1.21±0.13
5930.4	2803.5	1.1156	Mg II	
	1608.4	2.6892	Fe II	
6040.0	2853.0	1.1156	Mg I	0.92±0.15
6160.8	1670.8	2.6892	Al II	1.55±0.13

Table 61. GRB 080604 ($z = 1.4171$)

λ_{obs} [Å]	λ_{rest} [Å]	z	Feature	$\mathrm{EW}_{\mathrm{obs}}$ [Å]
5665.8	2344.2	1.4171	Fe II	4.8±0.7
5739.4	2374.5	1.4171	Fe II	4.3±0.6
5759.4	2382.8	1.4171	Fe II	4.7±0.6
6252.4	2586.6	1.4171	Fe II	6.4±0.5
6285.0	2600.2	1.4171	Fe II	6.4±0.5
6758.4	2796.4	1.4171	Mg II	7.6±0.7
6777.4	2803.5	1.4171	Mg II	5.4±0.5
6896.	2853.0	1.4171	Mg I	in telluric band

Table 62. GRB 080605 ($z = 1.6403$)

$\lambda_{\rm obs}$ [Å]	$\lambda_{\rm rest}$ [Å]	z	Feature	$\rm EW_{obs}$ [Å]
3927.4				2.8±0.8
4030.4	1526.7	1.6403	Si II	5.2±0.6
4050.2	1533.4	1.6403	Si II*	2.8±0.6
4090.1	1548.2	1.6403	C IV	13.5±0.8
	1550.8	1.6403	C IV	
4121.5	1560.3	1.6403	C I	1.7±0.6
4151.5				1.3±0.5
4238.1				1.4±0.5
4247.6	1608.4	1.6403	Fe II	1.6±0.5
4375.2	1656.9	1.6403	C I	1.0±0.4
4411.0	1670.8	1.6403	Al II	6.1±0.5
4773.7	1808.0	1.6403	Si II	1.2±0.3
4897.0	1854.7	1.6403	Al III	5.6±0.3
4918.4	1862.8	1.6403	Al III	4.1±0.3
5351.2	2026.1	1.6403	Zn II	1.6±0.3
	2026.5	1.6403	Mg I	
5429.1	2056.4	1.6403	Cr II	1.0±0.3
5445.2	2062.2	1.6403	Cr II	1.0±0.3
	2062.7	1.6403	Zn II	
5973.1	2600.2	1.2987	Fe II	1.4±0.3
6189.2	2344.2	1.6403	Fe II	6.6±0.3
6269.3	2374.5	1.6403	Fe II	11.6±0.4
6290.5	2382.8	1.6403	Fe II	
6430.1	2796.4	1.2987	Mg II	1.77±0.2
6446.4	2803.5	1.2987	Mg II	1.27±0.2
6803.0	2576.9	1.6403	Mn II	1.35±0.2
6828.8	2586.7	1.6403	Fe II	5.6±0.3
6865.8	2600.2	1.6403	Fe II	in telluric band
7380.7	2796.4	1.6403	Mg II	22.6±0.6
7400.7	2803.5	1.6403	Mg II	
7531.4	2853.0	1.6403	Mg I	6.1±0.3

Table 63. GRB 080607 ($z = 3.0368$)

$\lambda_{\rm obs}$ [Å]	$\lambda_{\rm rest}$ [Å]	z	Feature	$\mathrm{EW}_{\rm obs}$ [Å]
		LRIS/R400		
5626.1	1393.8	3.0368	SiIV	10.78 ± 0.41
5663.2	1402.8	3.0368	SiIV	5.86 ± 0.28
5693.6				3.23 ± 0.32
5713.6	1414.4	3.0368	GaII	1.42 ± 0.21
5735.8	1419.0	3.0368	CO	5.40 ± 0.26
5753.4	1425.0	3.0368	SI	1.00 ± 0.17
5772.1	2344.2	1.4618	FeII	4.63 ± 0.19
5802.0	1433.9	3.0368	PbII	6.62 ± 0.29
5848.9	2374.5	1.4618	FeII	10.09 ± 0.20
	1447.4	3.0368	CO	
5868.1	2382.8	1.4618	FeII	9.45 ± 0.21
	1454.8	3.0368	NiII	
5899.3				6.09 ± 0.29
5924.2	1466.2	3.0368	CoII	1.88 ± 0.20
	1467.3	3.0368	NiII	
	1467.8	3.0368	NiII	
5943.1				1.53 ± 0.21
5975.2	1477.5	3.0368	CO	10.27 ± 0.24
6006.4				3.21 ± 0.20
6045.1	2586.7	1.3406	FeII	12.94 ± 0.29
6086.4	2600.2	1.3406	FeII	1.52 ± 0.13
6100.5	1509.6	3.0368	CO	8.03 ± 0.18
6132.1				7.78 ± 0.27
6163.0	1526.7	3.0368	SiII	7.85 ± 0.15
6189.4	1532.5	3.0368	PII	6.10 ± 0.15
	1533.4	3.0368	SiII*	
6220.6				1.43 ± 0.17
6252.0	1544.3	3.0368	CO	20.82 ± 0.25
	1548.2	3.0368	CIV	
	1550.8	3.0368	CIV	

Table 63—Continued

$\lambda_{\rm obs}$ [Å]	$\lambda_{\rm rest}$ [Å]	z	Feature	$\mathrm{EW}_{\rm obs}$ [Å]
6301.5	1560.3	3.0368	CI	8.76 ± 0.31
6325.3	1566.8	3.0368	FeII*	2.53 ± 0.14
6338.4	2576.9	1.4618	MnII	4.38 ± 0.14
6369.4	2586.7	1.4618	FeII	13.04 ± 0.25
	2594.5	1.4618	MnII	
	1574.6	3.0368	CoII	
6400.8	2600.2	1.4618	FeII	5.42 ± 0.13
6414.4	2606.5	1.4618	MnII	3.35 ± 0.12
	1589.2	3.0368	SiI	
6441.7	1595.8	3.0368	SiI	0.49 ± 0.12
6469.8	1602.5	3.0368	GeII	5.28 ± 0.14
6500.9	1608.5	3.0368	FeII	14.81 ± 0.19
	1611.2	3.0368	FeII	
	1612.8	3.0368	FeII*	
	1613.4	3.0368	CI	
6534.6	1618.5	3.0368	FeII*	2.74 ± 0.12
6545.7	2796.4	1.3406	MgII	6.88 ± 0.13
	1621.7	3.0368	FeII*	
6562.1	2803.5	1.3406	MgII	3.59 ± 0.13
6575.9	1629.2	3.0368	FeII*	2.17 ± 0.12
6616.6	1637.4	3.0368	FeII*	17.98 ± 0.26
	1631.1	3.0368	FeII*	
	1634.4	3.0368	FeII*	
	1636.3	3.0368	FeII*	
	1639.4	3.0368	FeII*	
6660.2				3.71 ± 0.13
6678.2	2853.0	1.3406	MgI	2.18 ± 0.10
6692.1	1656.9	3.0368	CI	8.21 ± 0.15
6713.3				1.45 ± 0.19
6744.1	1670.8	3.0368	AlII	9.25 ± 0.10
6758.9				2.25 ± 0.12
6807.3				1.62 ± 0.12
6834.8				1.62 ± 0.18

Table 63—Continued

λ_{obs} [Å]	λ_{rest} [Å]	z	Feature	$\mathrm{EW}_{\mathrm{obs}}$ [Å]
6849.2				0.71 ± 0.12
6871.8	1702.0	3.0368	FeII*	3.88 ± 0.11
6884.0	2796.4	1.4618	MgII	8.59 ± 0.11
	1703.4	3.0368	NiII	
	1707.1	3.0368	MgI	
6901.1	2803.5	1.4618	MgII	7.51 ± 0.11
	1707.1	3.0368	MgI	
	1709.6	3.0368	NiII	
6914.4				1.57 ± 0.12
6930.7				1.25 ± 0.13
6945.4				1.39 ± 0.14
6964.8				2.05 ± 0.13
6989.2				0.75 ± 0.12
7013.1	2853.0	1.4618	MgI	1.82 ± 0.15
7030.2	1741.6	3.0368	NiII	3.62 ± 0.10
7055.8	1747.8	3.0368	MgI	2.36 ± 0.12
7072.1	1751.9	3.0368	NiII	2.56 ± 0.12
7160.7	1772.3	3.0368	NiII	1.06 ± 0.12
	1774.0	3.0368	NiII	
7187.9	3073.9	1.3406	TiII	0.74 ± 0.12
7204.0	3073.9	1.3406	TiII	0.85 ± 0.13
	1783.3	3.0368	NiII	
7284.8	1804.5	3.0368	NiII	0.97 ± 0.14
7298.9	1807.3	3.0368	SI	5.72 ± 0.13
	1808.0	3.0368	SiII	
7334.4	1816.9	3.0368	SiII*	2.93 ± 0.17
	1817.5	3.0368	SiII*	
7378.6	1827.9	3.0368	MgI	1.64 ± 0.14
7486.0	1854.7	3.0368	AlIII	7.43 ± 0.14
7518.8	1862.8	3.0368	AlIII	6.13 ± 0.15
7568.6	3230.1	1.3406	TiII	0.63 ± 0.17
	3073.9	1.4618	TiII	
7637.5	3242.9	1.3406	TiII	25.95 ± 0.34

Table 63—Continued

$\lambda_{\rm obs}$ [Å]	$\lambda_{\rm rest}$ [Å]	z	Feature	$\rm EW_{obs}$ [Å]
	1892.0	3.0368	SiIII	
	1901.8	3.0368	FeII	
7776.5				1.01 ± 0.18
7982.5	3242.9	1.4618	TiII	1.74 ± 0.22
8122.6	2012.2	3.0368	CoII	1.20 ± 0.18
8180.1	2026.1	3.0368	ZnII	6.35 ± 0.18
	2026.3	3.0368	CrII	
	2026.5	3.0368	MgI	
8232.8				2.09 ± 0.23
8316.6	3384.7	1.4618	TiII	16.66 ± 0.70
	2056.3	3.0368	CrII	
	2062.2	3.0368	CrII	
	2062.7	3.0368	ZnII	
	2066.2	3.0368	CrII	
8398.3				5.94 ± 0.49
8434.2				2.56 ± 0.40
8443.2				1.15 ± 0.24
8480.9				2.10 ± 0.37
8513.3				1.93 ± 0.30
8606.0				5.68 ± 0.38
8749.4	2166.2	3.0368	NiII*	6.05 ± 0.53
	2169.8	3.0368	NiII*	
	2167.5	3.0368	FeI	
8780.5	2175.4	3.0368	NiII*	5.19 ± 0.64
8827.5				8.93 ± 0.77
8948.9	2217.2	3.0368	NiII*	4.32 ± 0.56
8979.8	2223.6	3.0368	NiII*	6.94 ± 0.60
9085.3	2249.9	3.0368	FeII	4.53 ± 0.37
9097.4				3.20 ± 0.42
9134.1	2260.8	3.0368	FeII	6.27 ± 0.53

Table 64. GRB 080707 ($z = 1.2322$)

λ_{obs} [Å]	λ_{rest} [Å]	z	Feature	$\mathrm{EW}_{\mathrm{obs}}$ [Å]
5236.7	2344.2	1.2322	Fe II	5.1±0.9
5300.4	2374.5	1.2322	Fe II	2.4±0.9
5320.4	2382.8	1.2322	Fe II	5.3±0.9
5779.2	2586.7	1.2322	Fe II	3.9±0.8
5799.2	2600.2	1.2322	Fe II	4.6±0.8
6241.6	2796.3	1.2322	Mg II	16.4±1.1
6257.3	2805.3	1.2322	Mg II	
6366.1	2853.0	1.2322	Mg I	4.9±0.8

Table 65. GRB 080710 ($z = 0.8454$)

$\lambda_{\rm obs}$ [Å]	$\lambda_{\rm rest}$ [Å]	z	Feature	$\rm EW_{obs}$ [Å]
GMOS/B600				
4326.5	2344.2	0.8454	FeII	0.77 ± 0.05
	2345.0	0.8454	FeII*	
4382.0	2374.5	0.8454	FeII	0.39 ± 0.04
4397.6	2381.5	0.8454	FeII*	1.05 ± 0.04
	2382.8	0.8454	FeII	
	2383.8	0.8454	FeII*	
4773.6	2586.7	0.8454	FeII	0.76 ± 0.03
4788.6	2594.5	0.8454	MnII	0.21 ± 0.04
4798.6	2599.2	0.8454	FeII*	1.32 ± 0.04
	2600.2	0.8454	FeII	
5160.5	2796.4	0.8454	MgII	2.23 ± 0.03
5173.8	2803.5	0.8454	MgII	1.95 ± 0.03
5264.9	2853.0	0.8454	MgI	0.67 ± 0.03
5895.2				0.58 ± 0.04
6281.2				0.47 ± 0.03

Table 66. GRB 080721 ($z = 2.5914$)

$\lambda_{\rm obs}$ [Å]	$\lambda_{\rm rest}$ [Å]	z	Feature	$\rm EW_{obs}$ [Å]
4358.0	1215.7	2.5914	Lyα	
4527.1	1260.4	2.5914	Si II	6.3±0.7
4680.5	1302.2	2.5914	O I	6.1±0.7
	1304.4	2.5914	Si II	
4796.5	1335.3	2.5914	C II	7.1±0.7
5005.7	1393.8	2.5914	Si IV	4.8±0.5
5038.9	1402.8	2.5914	Si IV	3.0±0.5
5482.9	1526.7	2.5914	Si II	6.0±0.4
5561.0	1548.2	2.5914	C IV	16.0±0.6
5571.4	1550.8	2.5914	C IV	
5776.3	1608.4	2.5914	Fe II	8.8±0.5
5787.9	1611.2	2.5914	Fe II	
6000.1	1670.8	2.5914	Al II	5.1±0.4
7271.6	2026.1	2.5914	Zn II	3.1±0.4
	2026.5	2.5914	Mg I	
7405.3	2062.2	2.5914	Cr II	2.53±0.9
	2062.7	2.5914	Zn II	

Table 67. GRB 080804

$\lambda_{\rm obs}$ [Å]	$\lambda_{\rm rest}$ [Å]	z	Feature	$\mathrm{EW_{obs}}$ [Å]
4648.5	1526.7	2.0446	SiII	4.10 ± 0.10
4961.3	1548.2	2.0446	CIV	2.37 ± 0.10
5323.3	1550.8	2.0446	CIV	1.90 ± 0.10

Table 68. GRB 080805 ($z = 1.5042$)

$\lambda_{\rm obs}$ [Å]	$\lambda_{\rm rest}$ [Å]	z	Feature	$\mathrm{EW_{obs}}$ [Å]
4184.0	1670.8	1.5042	Al II	15±4
6150.6	2796.3	1.197	Mg II	18.2±3.0
	2803.5	1.197	Mg II	
6479.8	2586.7	1.5042	Fe II	5.6±1.9
6511.8	2600.2	1.5042	Fe II	7.2±2.0
6999.8	2796.3	1.5042	Mg II	8.2±2.0
7019.4	2803.5	1.5042	Mg II	12.5±2.0
7146.0	2853.0	1.5042	Mg I	6.9±1.6

Table 69. GRB 080810 ($z = 3.3604$)

$\lambda_{\rm obs}$ [Å]	$\lambda_{\rm rest}$ [Å]	z	Feature	$\mathrm{EW_{obs}}$ [Å]
5047.6	1215.7	3.1585	Lyα	
5291.8	1215.7	3.3604	Lyα	
5551.7	1334.5	3.1585	C II	1.4±0.6
6012.8				1.8±0.6
6117.6	1402.7	3.3604	Si IV	1.7±0.6
6346.3	1526.7	3.1585	Si II	2.6±0.6
6438.3	1548.2	3.1585	C IV	1.7±0.6
	1550.8	3.1585	C IV	
6655.6	1526.7	3.3604	Si II	2.1±0.6
6754.4	1548.2	3.3604	C IV	13.6±0.9
	1550.8	3.3604	C IV	

Table 70. GRB 080905B ($z = 2.3739$)

$\lambda_{\rm obs}$ [Å]	$\lambda_{\rm rest}$ [Å]	z	Feature	$\rm EW_{obs}$ [Å]
4402.0	1302.2	2.3739	O I	9±2
	1304.4	2.3739	Si II	
5148.0	1526.7	2.3739	Si II	2.5±0.8
5227.2	1548.2	2.3739	C IV	5.6±0.7
	1550.8	2.3739	C IV	
5429.8	1608.4	2.3739	Fe II	2.7±0.7
5436.6	1611.2	2.3739	Fe II	
5635.6	1670.8	2.3739	Al II	3.4±0.6
6099.7	1808.0	2.3739	Si II	1.5±0.6
6256.3	1854.7	2.3739	Al III	2.7±0.6
6284.6	1862.8	2.3739	Al III	1.7±0.6
6777.7				1.2±0.5
6833.7	2026.1	2.3739	Zn II	2.0±0.6
	2026.5	2.3739	Mg I	
6876.9	2796.3	1.4588	Mg II	3.7±0.6
6896.2	2805.3	1.4588	Mg II	2.2±0.5
6959.7	2062.2	2.3739	Cr II	2.8±0.5
	2062.7	2.3739	Zn II	
7307.1	2166.2	2.3739	Ni II**	2.0±0.7
7815.8	2316.7	2.3739	Ni II**	2.8±0.7
7906.9	2344.2	2.3739	Fe II	5.1±1.0
8010.8	2374.5	2.3739	Fe II	5.3±0.6
8040.1	2382.8	2.3739	Fe II	4.3±0.7
8085.9	2396.4	2.3739	Fe II*	2.8±0.5
8117.5	2405.6	2.3739	Fe II**	2.1±0.6
8136.2	2411.3	2.3739	Fe II***	2.4±0.6
8696.2	2576.9	2.3739	Mn II	2.8±0.6
8727.1	2586.7	2.3739	Fe II	5.1±0.6
8770.7	2600.2	2.3739	Fe II	5.6±1.4
9442.5	2796.3	2.3739	Mg II	20±4
	2803.5	2.3739	Mg II	

Note. — The afterglow spectrum is blended with the spectrum of another object on the slit. Hence, the EWs in this table will be affected by this contaminating light.

Table 71. GRB 080916A ($z = 0.6887$)

$\lambda_{\rm obs}$ [Å]	$\lambda_{\rm rest}$ [Å]	z	Feature	$\rm EW_{obs}$ [Å]
4727.2	2796.3	0.6887	Mg II	8.2±1.4
	2803.5	0.6887	Mg II	
6295.6	3727.7	0.6887	[O II]	emission
8210.7	4862.7	0.6887	Hβ	emission
8456.8	5008.2	0.6887	[O III]	emission

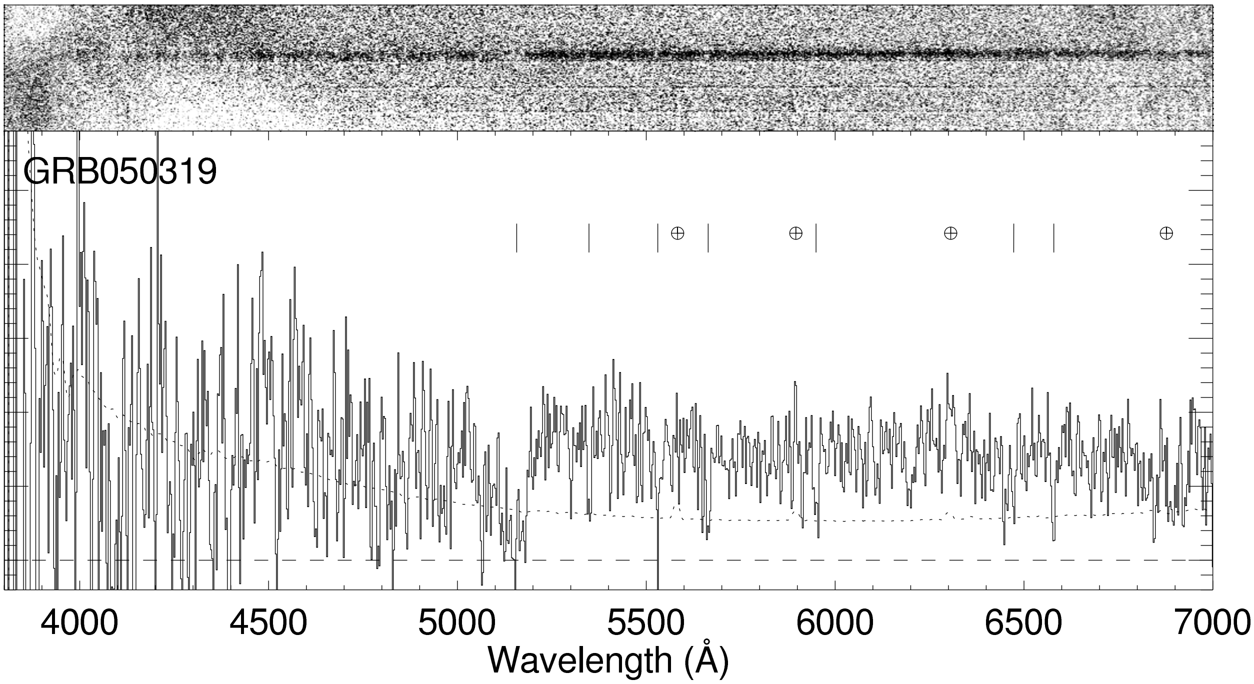

Fig. 14.— Shown are 1- and 2-dimensional spectra for GRBs 050319–080928. Lines from the GRB absorption systems are marked with vertical lines whereas unidentified lines or lines from intervening systems are marked with vertical dashed lines. Telluric features are marked with a telluric symbol. The error spectrum is plotted as a dotted line. When in the spectral range we also plot the position of the Lyman-limit as a vertical dashed line.

Table 72. GRB 080928 ($z = 1.6919$)

$\lambda_{\rm obs}$ [Å]	$\lambda_{\rm rest}$ [Å]	z	Feature	$\rm EW_{obs}$ [Å]
4133.8	2382.8	0.7359	Fe II	8.5±0.7
4172.8	1548.2	1.6919	C IV	5.7±0.7
	1550.8	1.6919	C IV	
4287.8				1.6±0.4
4327.8	1608.4	1.6919	Fe II	1.4±0.4
4490.8	2586.7	0.7359	Fe II	3.8±0.4
4513.9	2600.2	0.7359	Fe II	6.7±0.4
4857.7	2796.3	0.7359	Mg II	16.5±0.4
4865.3	2803.5	0.7359	Mg II	
4953.2	2853.0	0.7359	Mg I	4.0±0.3
5041.1				1.0±0.3
5092.6				1.0±0.3
5117.4				1.1±0.3
5709.2				0.7±0.3
5830.3	2166.2	1.6919	Ni II**	0.8±0.3
6310.4	2344.2	1.6919	Fe II	2.0±0.4
6392.7	2374.5	1.6919	Fe II	1.7±0.3
6415.6	2382.8	1.6919	Fe II	1.2±0.2
6828.8	3934.8	0.7359	Ca II	1.5±0.3
6893.4	3969.6	0.7359	Ca II	in telluric band
6938.0	2576.9	1.6919	Mn II	0.8±0.3
6964.5	2586.7	1.6919	Fe II	1.4±0.2
6999.2	2600.2	1.6919	Fe II	2.2±0.3
7526.6	2796.3	1.6919	Mg II	3.7±0.3
7547.5	2803.5	1.6919	Mg II	2.7±0.3

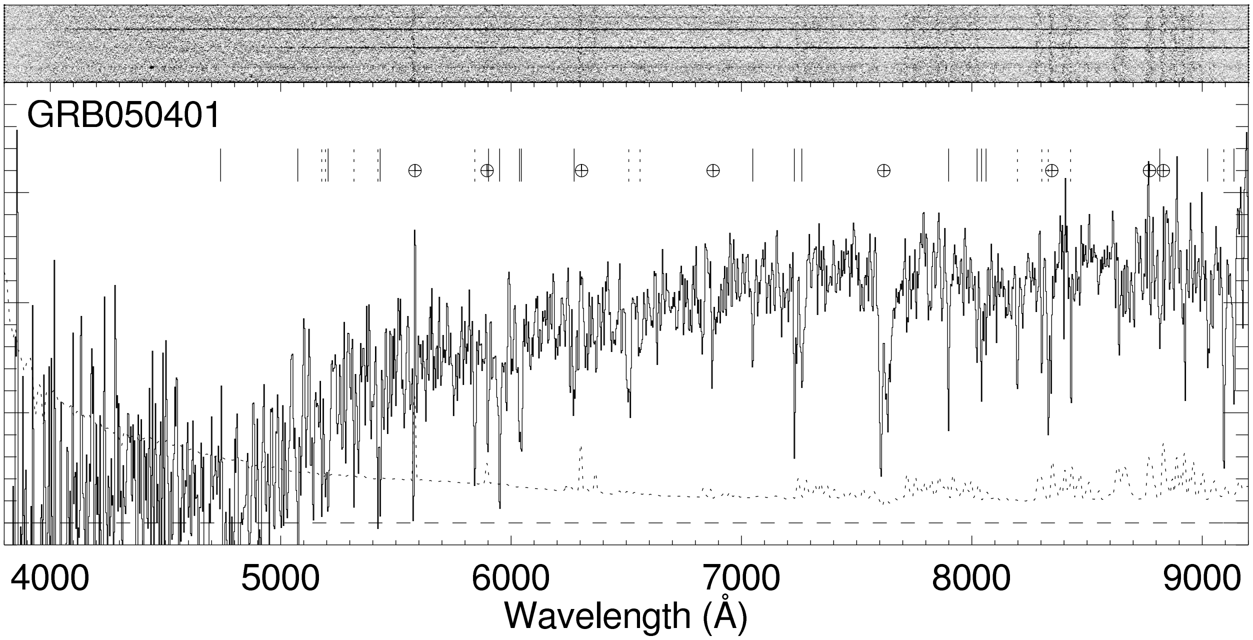
GRB050401
4000
5000
6000
7000
8000
9000
Wavelength (Å)

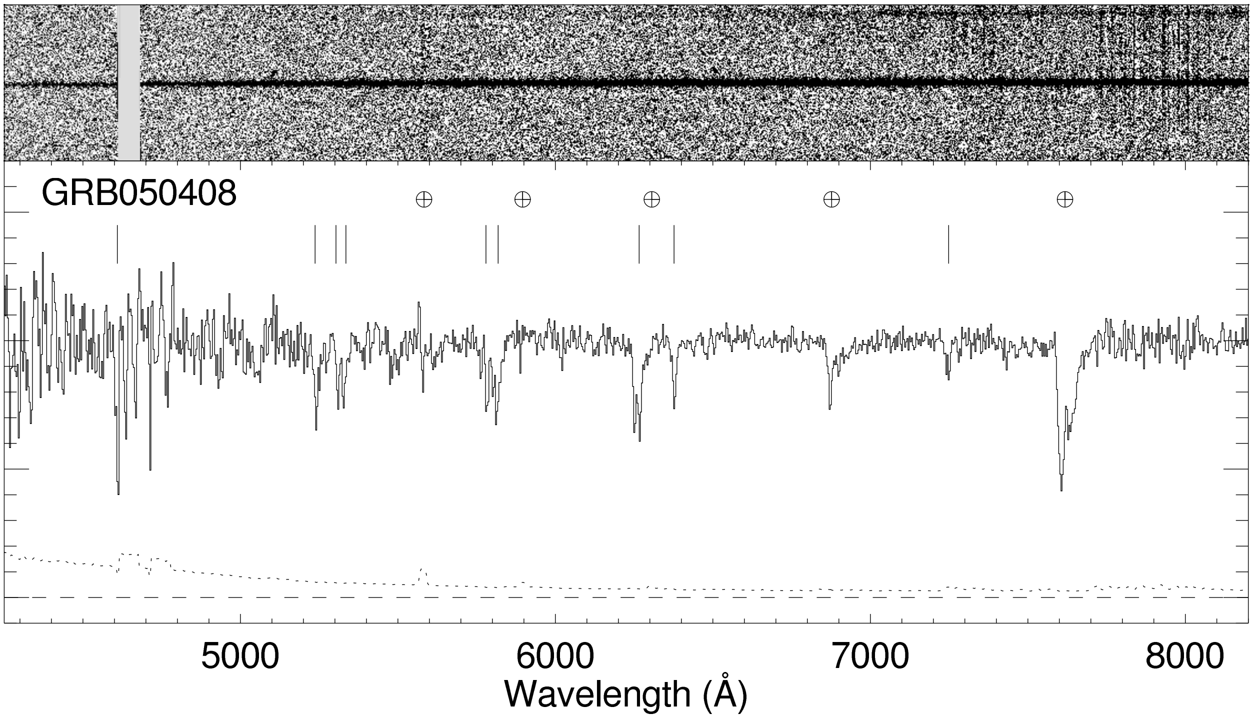
GRB050408
5000
6000
7000
8000
Wavelength (Å)

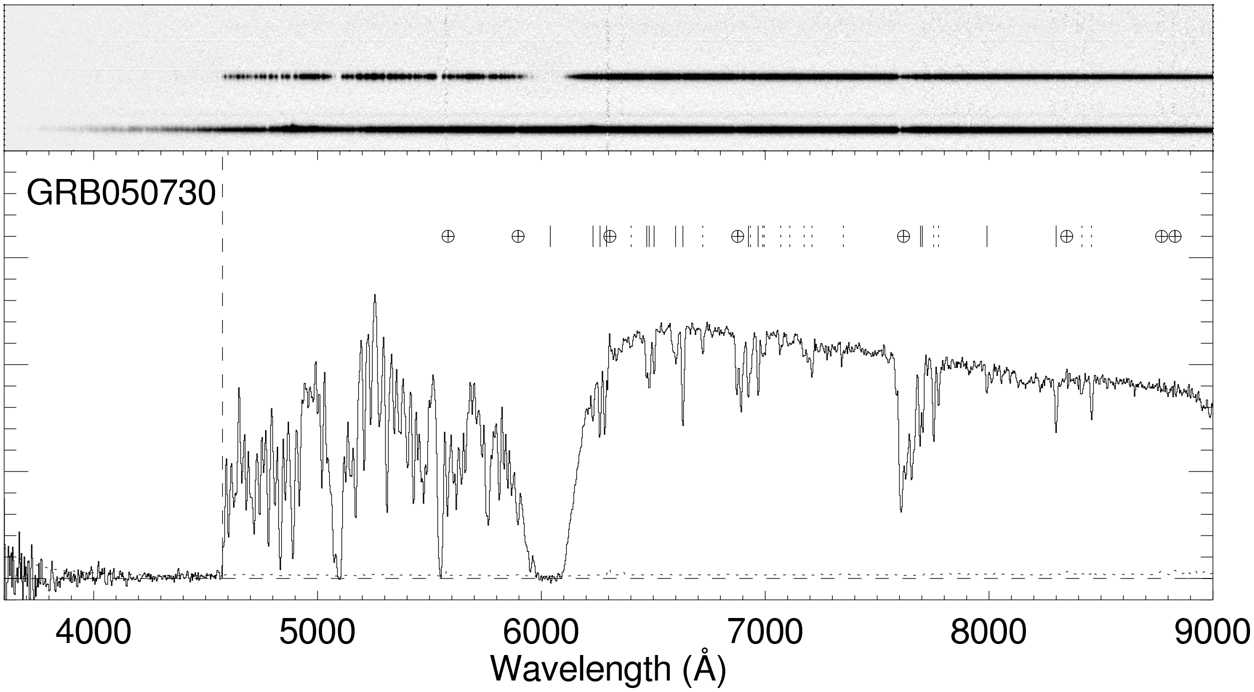
GRB050730
4000
5000
6000
7000
8000
9000
Wavelength (Å)

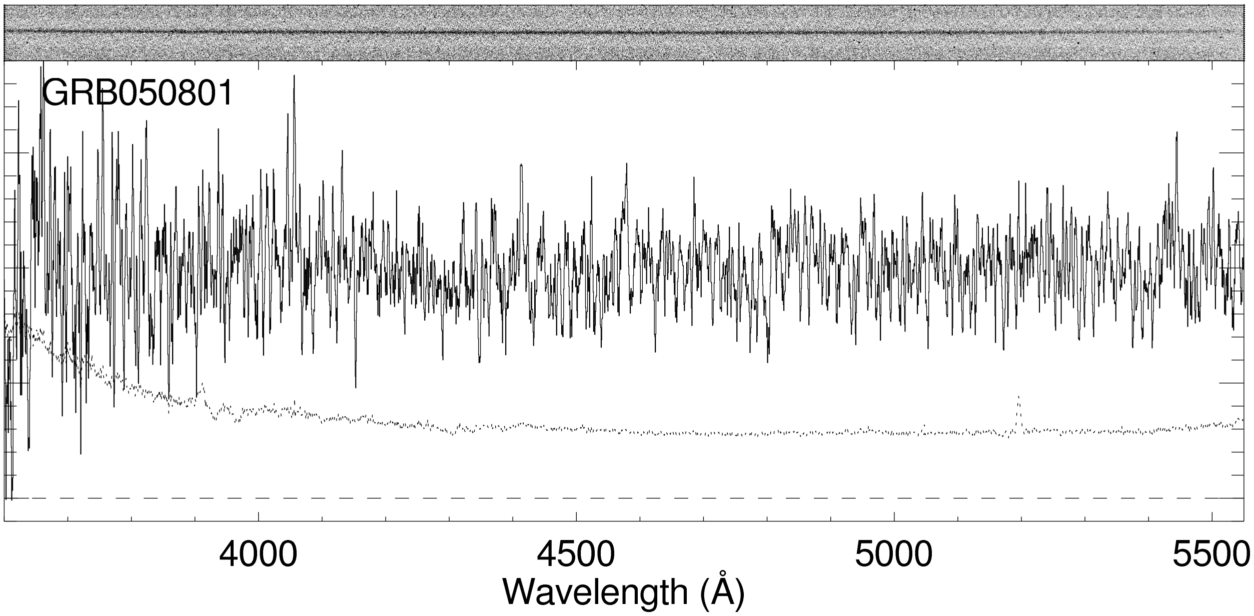
GRB050801
4000
4500
5000
5500
Wavelength (Å)

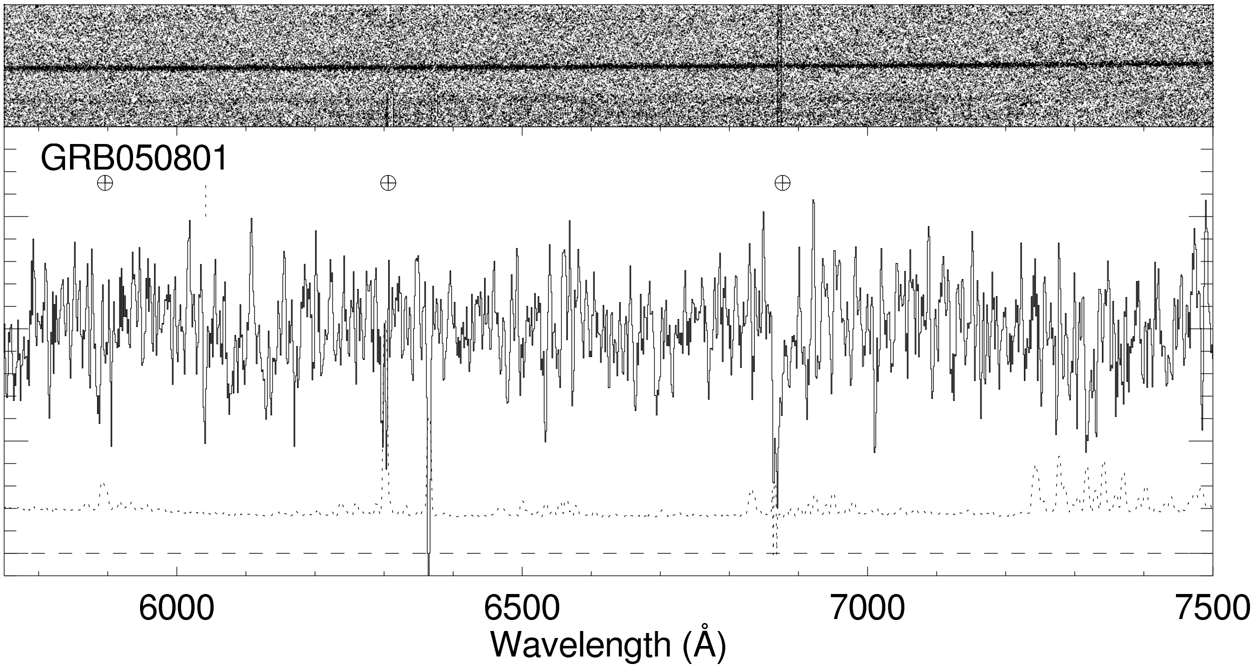
GRB050801
⊕
⊕
⊕
6000
6500
7000
7500
Wavelength (Å)

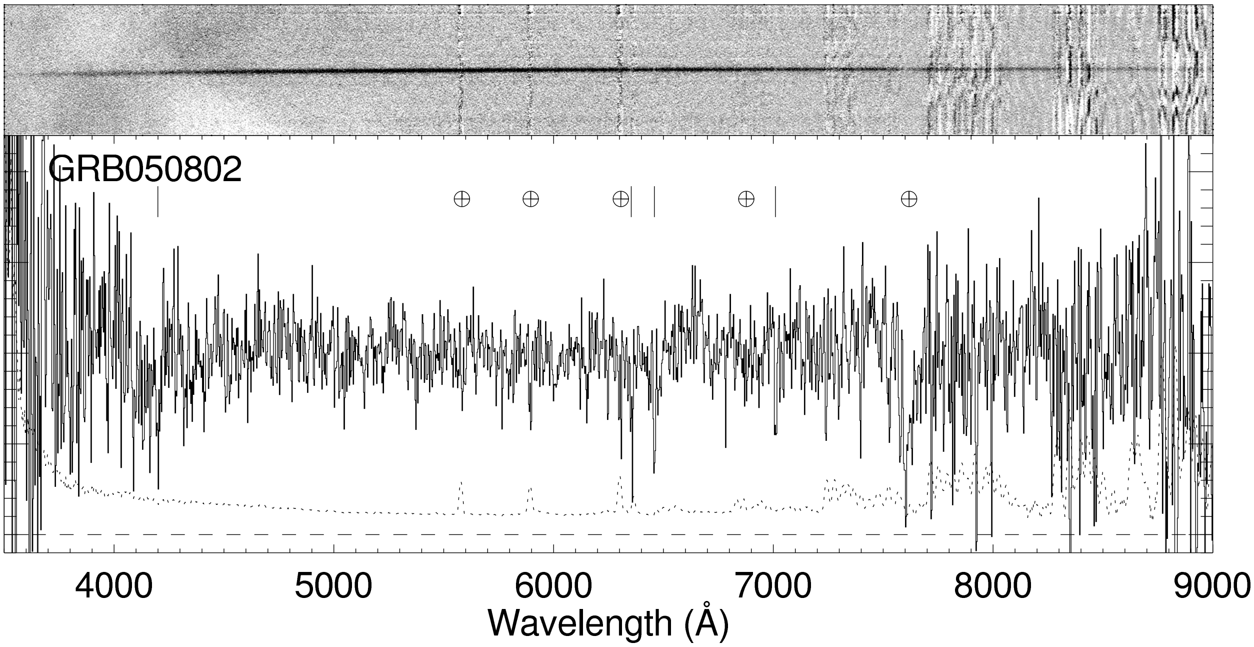
GRB050802
⊕
⊕
⊕
⊕
⊕
4000
5000
6000
7000
8000
9000
Wavelength (Å)

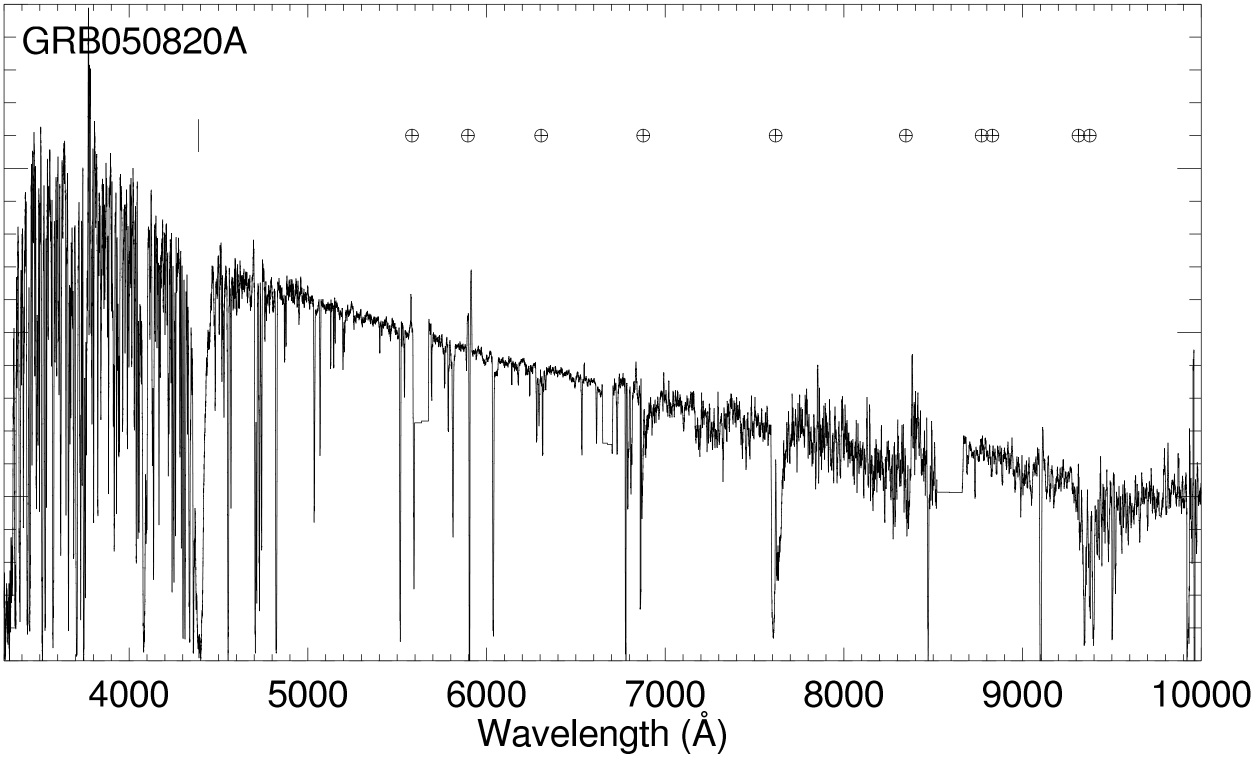
GRB050820A
4000
5000
6000
7000
8000
9000
10000
Wavelength (Å)

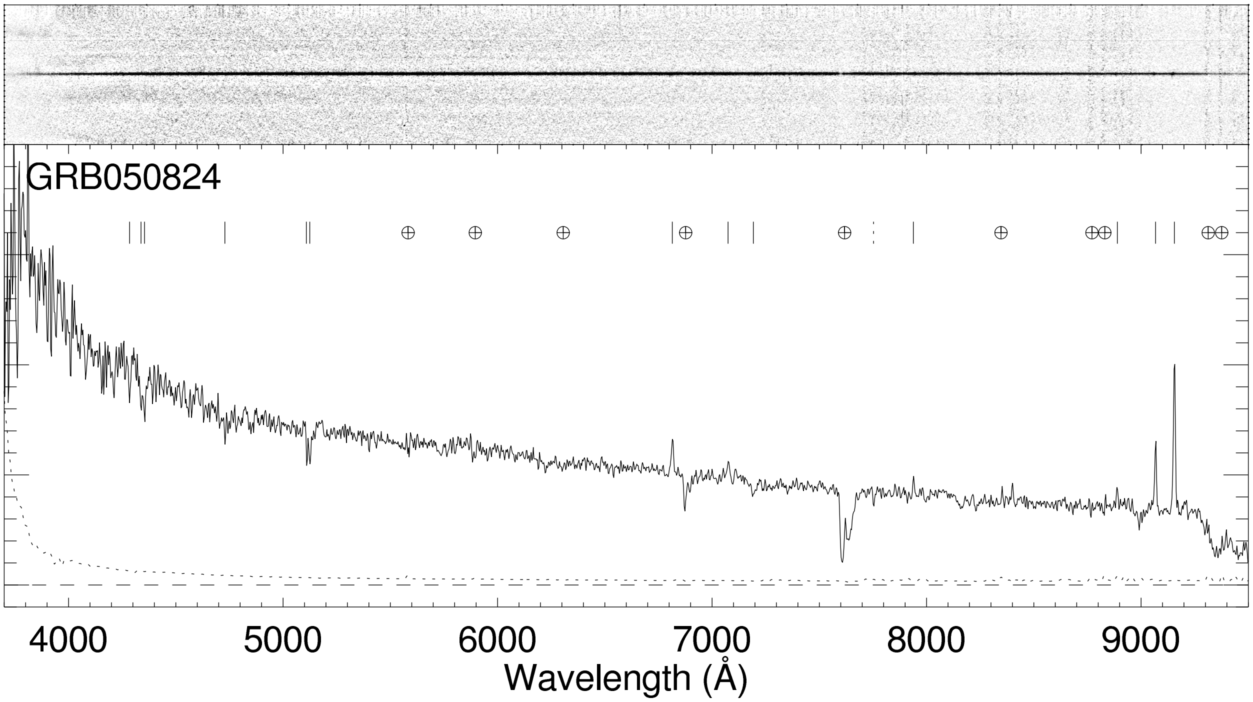
GRB050824
4000
5000
6000
7000
8000
9000
Wavelength (Å)

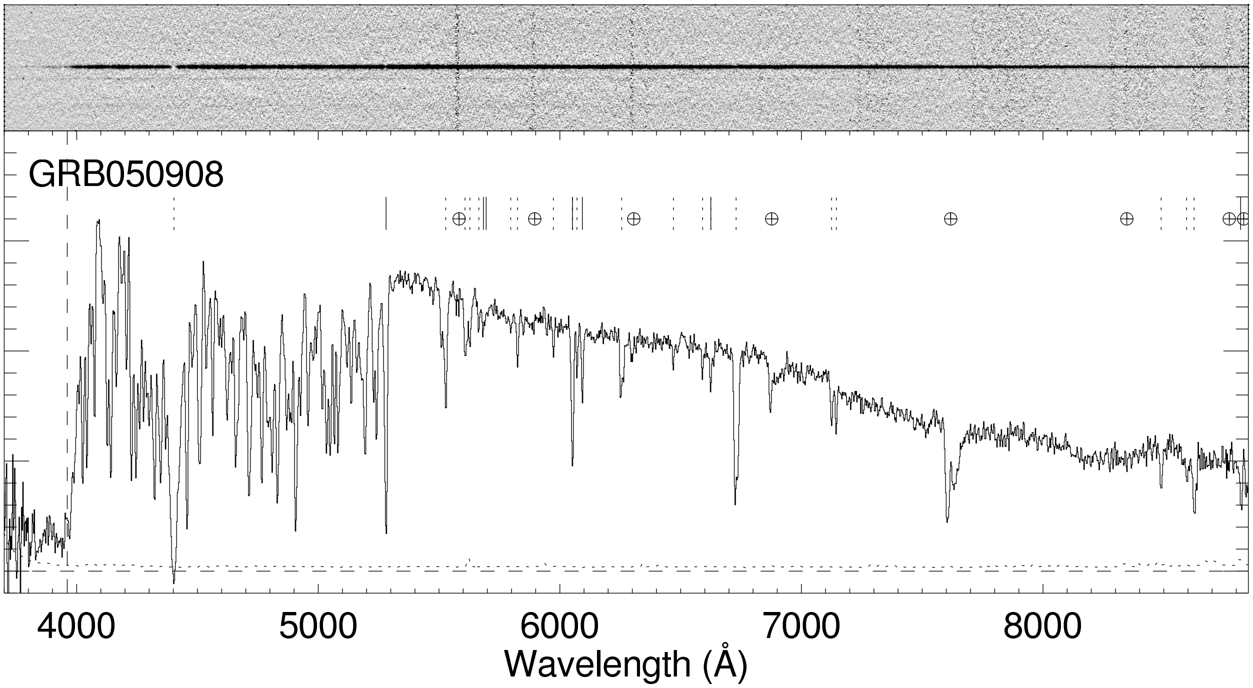
GRB050908
4000
5000
6000
7000
8000
Wavelength (Å)

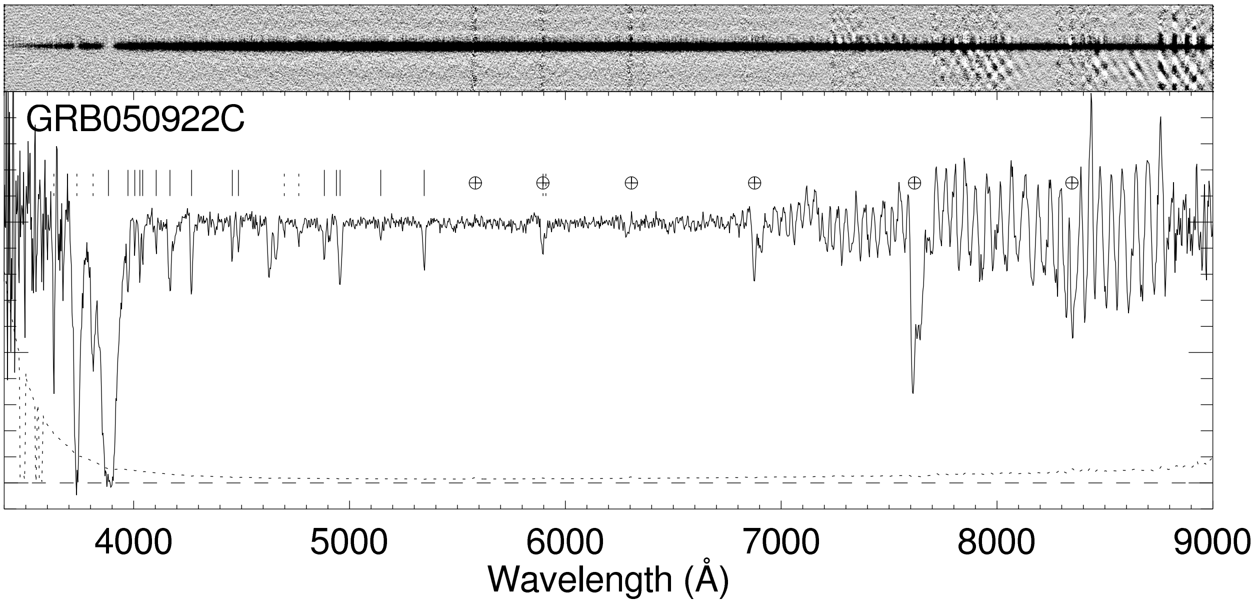
GRB050922C
4000
5000
6000
7000
8000
9000
Wavelength (Å)

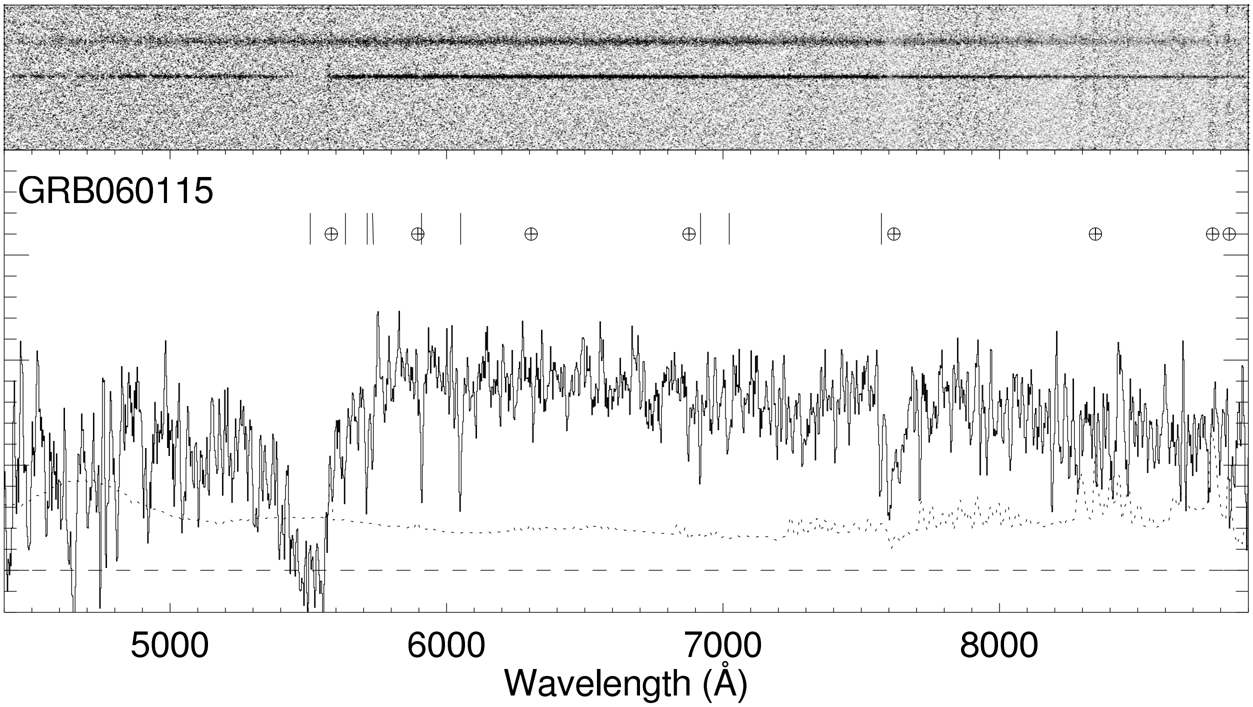
GRB060115
⊕
⊕
⊕
⊕
⊕
⊕
⊕⊕
5000
6000
7000
8000
Wavelength (Å)

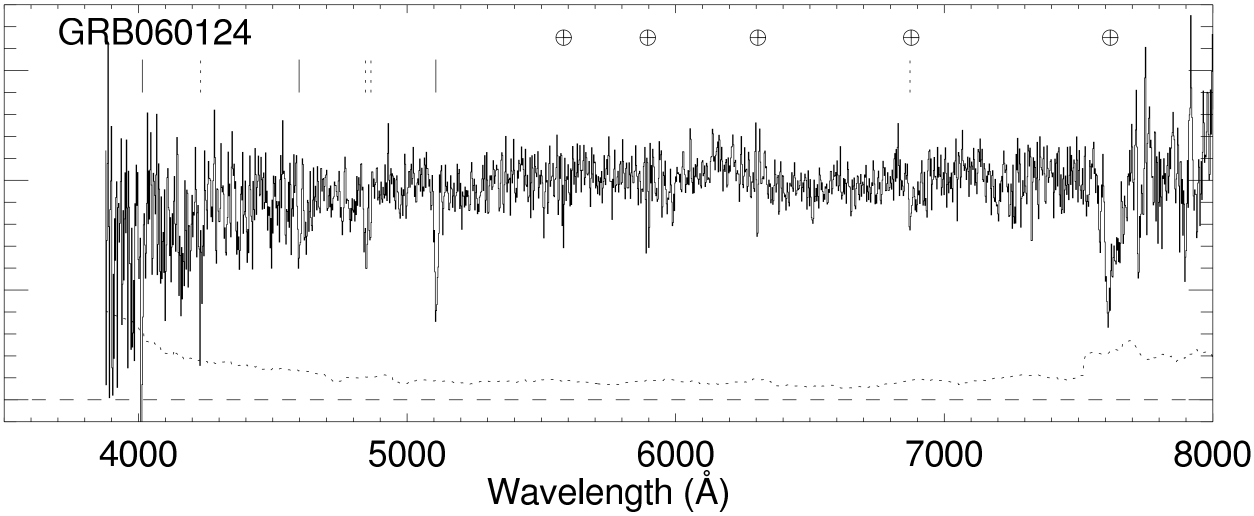
GRB060124
4000
5000
6000
7000
8000
Wavelength (Å)

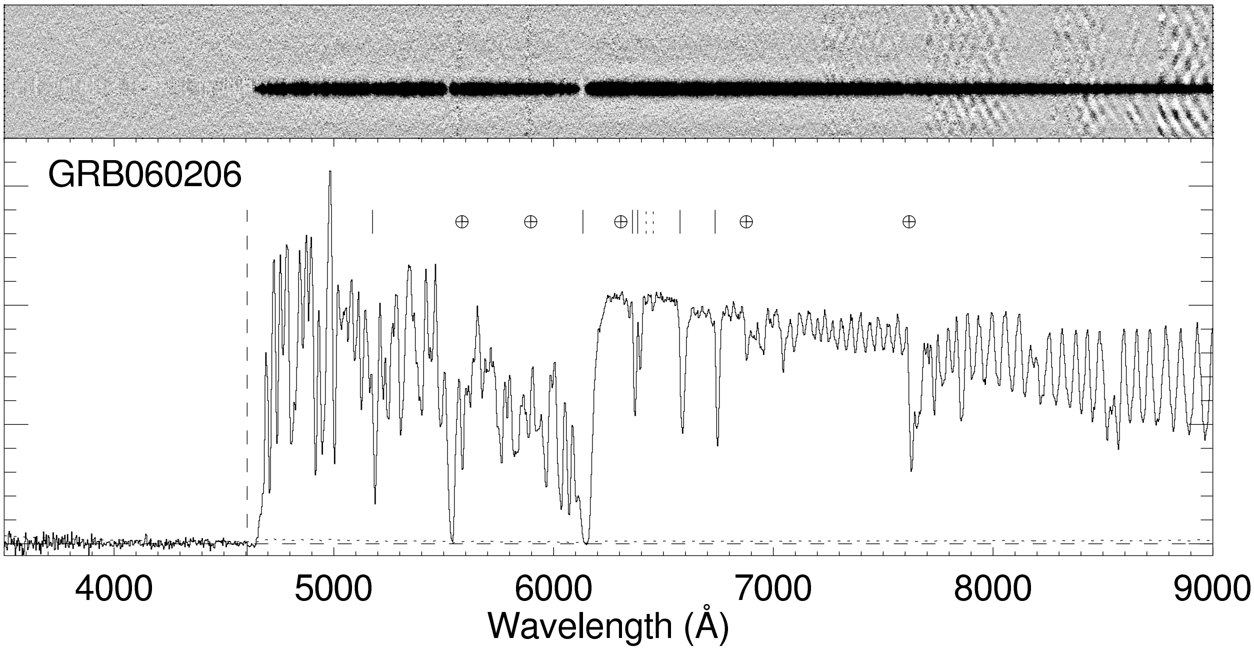
GRB060206
4000
5000
6000
7000
8000
9000
Wavelength (Å)

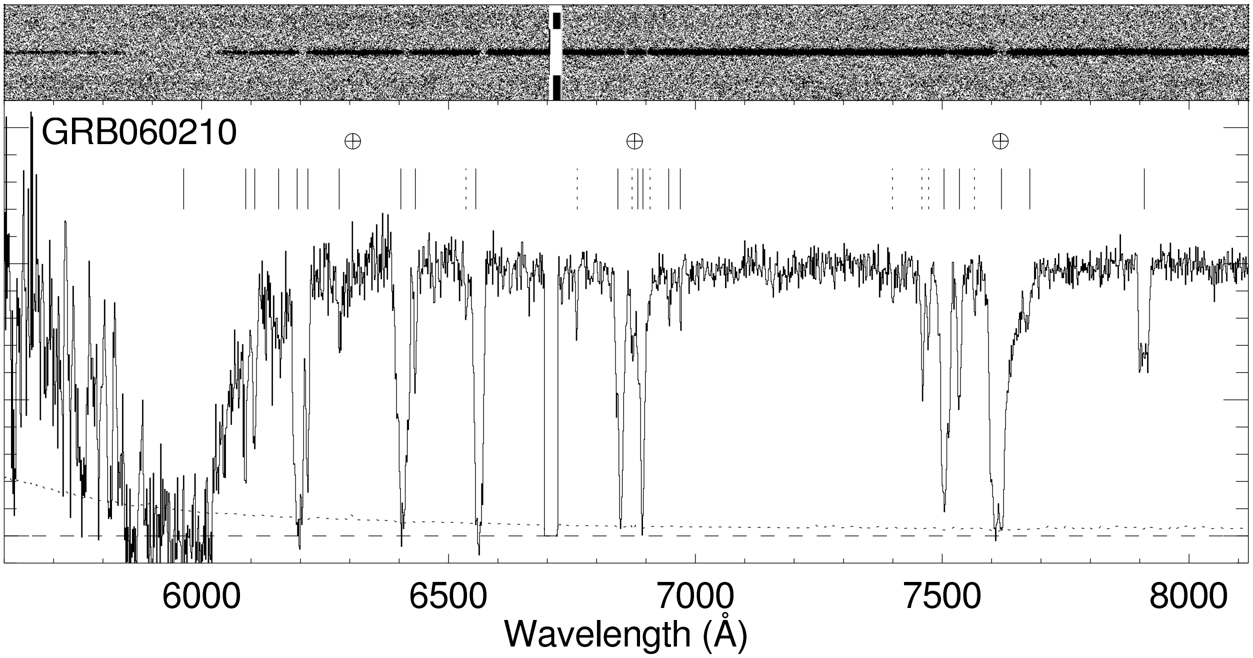
GRB060210
⊕
⊕
⊕
6000
6500
7000
7500
8000
Wavelength (Å)

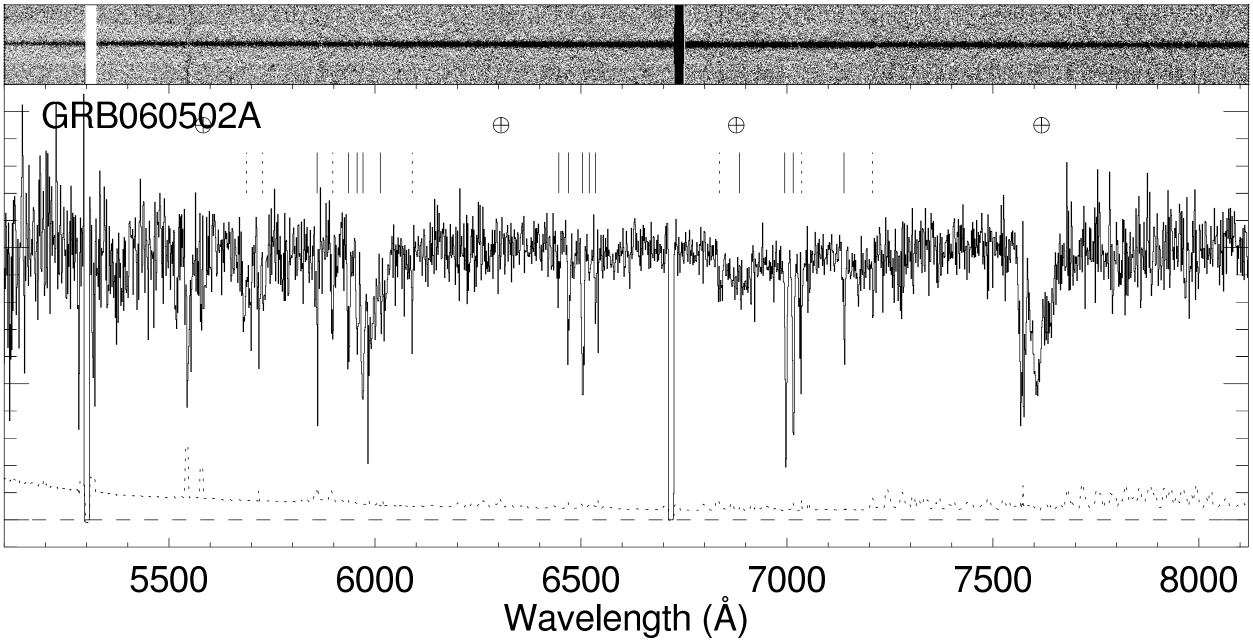
GRB060502A
⊕
⊕
⊕
⊕
5500
6000
6500
7000
7500
8000
Wavelength (Å)

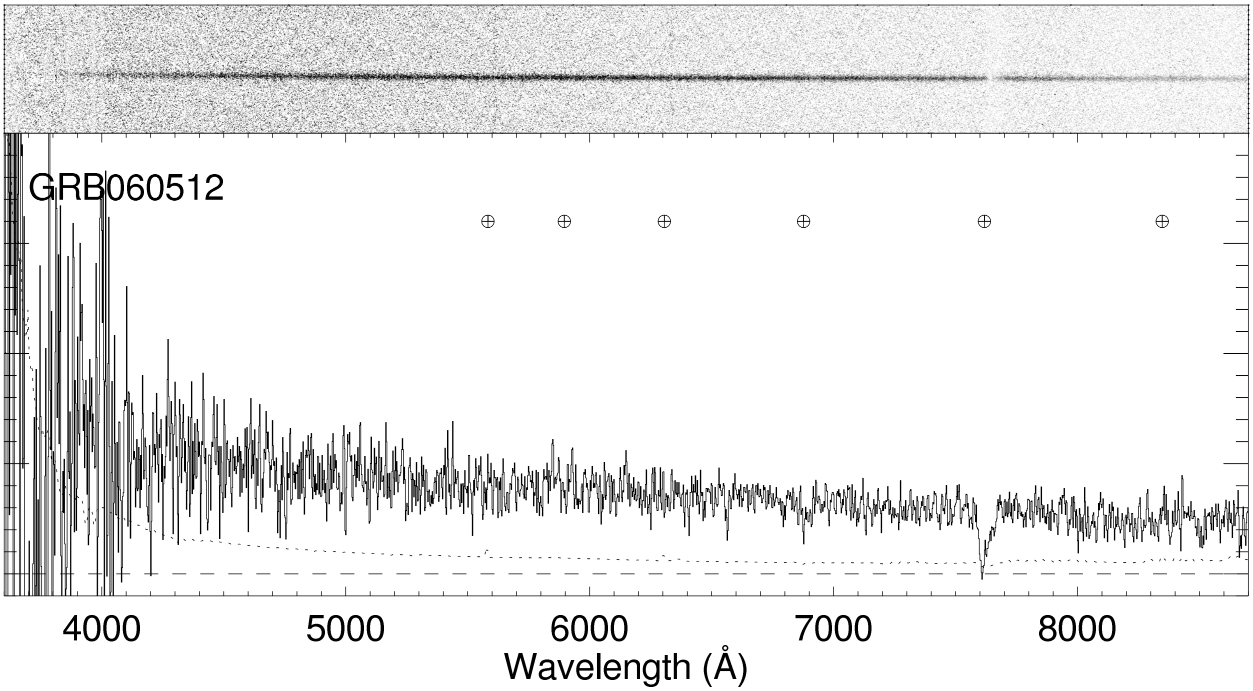
GRB060512
⊕
⊕
⊕
⊕
⊕
⊕
4000
5000
6000
7000
8000
Wavelength (Å)

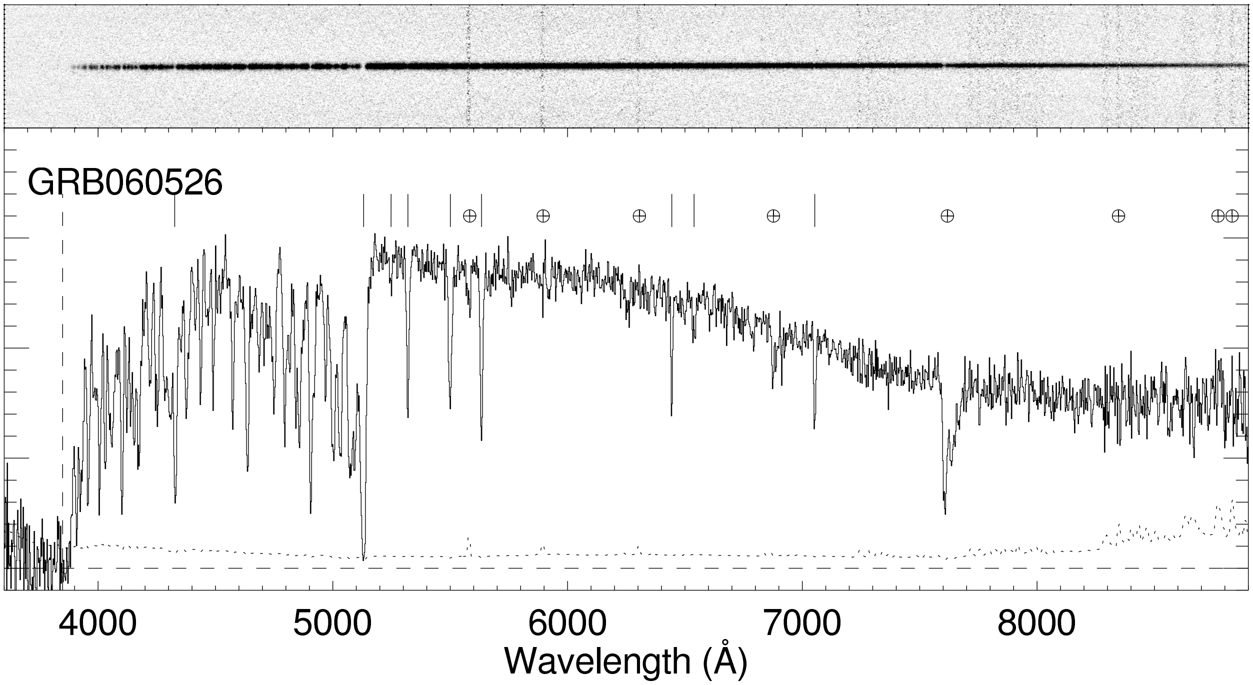
GRB060526
⊕
4000
5000
6000
7000
8000
Wavelength (Å)

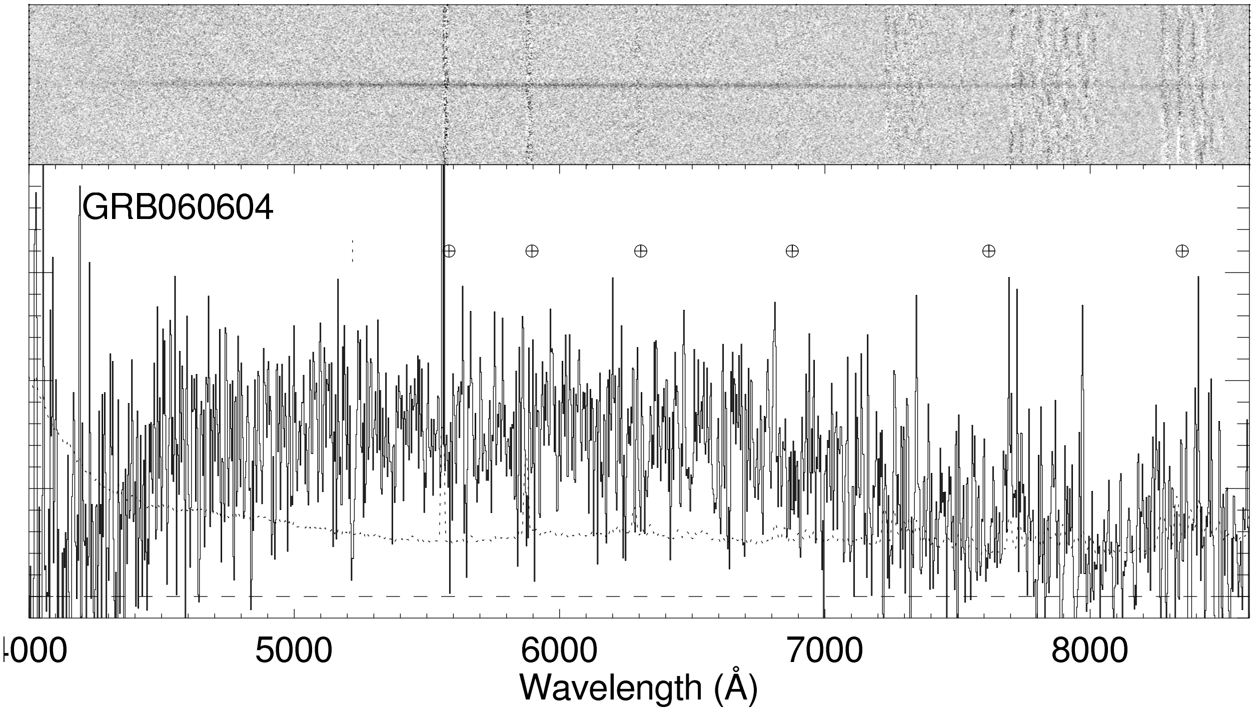
GRB060604
⊕
4000
5000
6000
7000
8000
Wavelength (Å)

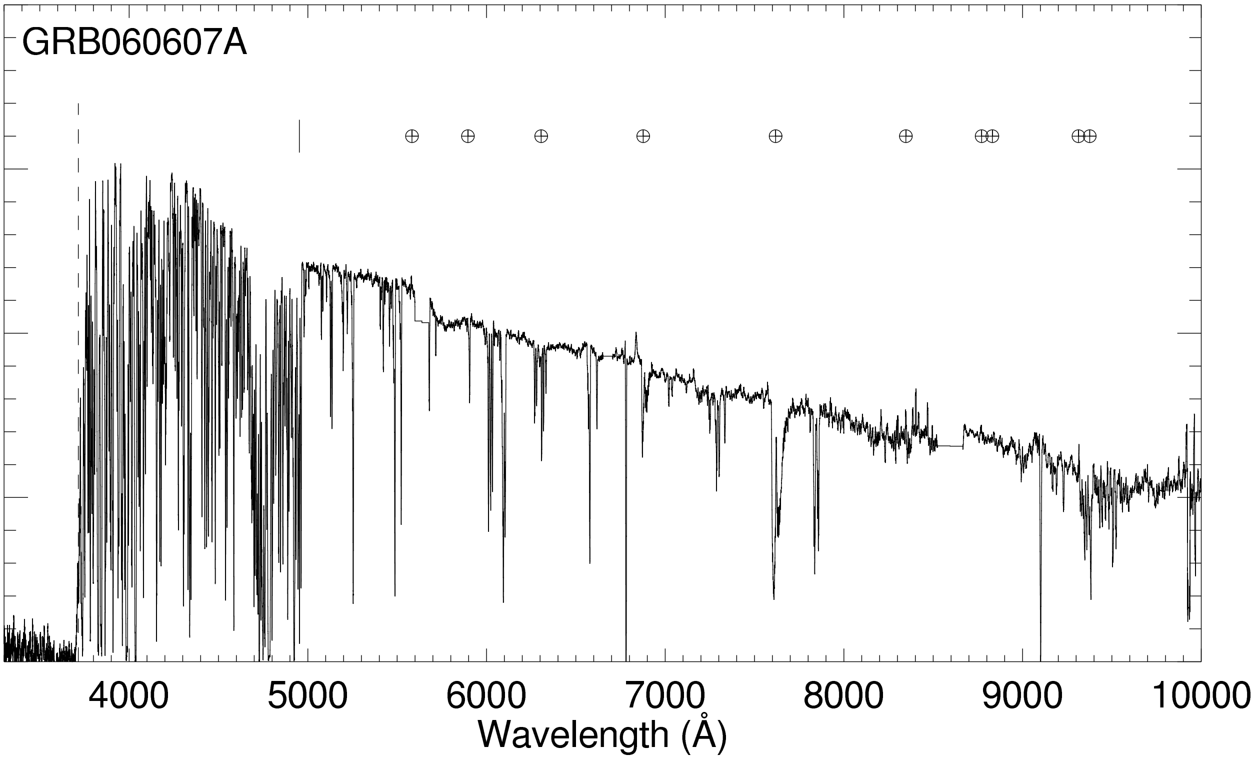
GRB060607A
⊕
4000
5000
6000
7000
8000
9000
10000
Wavelength (Å)

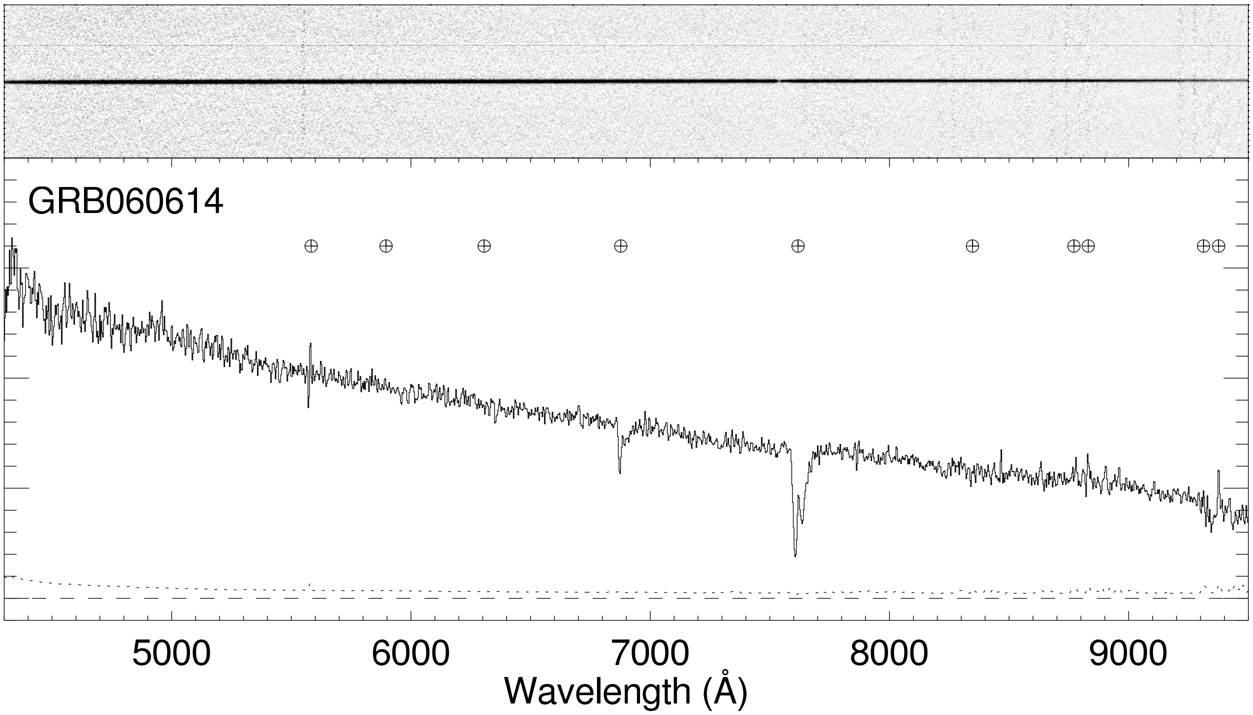
GRB060614
⊕
5000
6000
7000
8000
9000
Wavelength (Å)

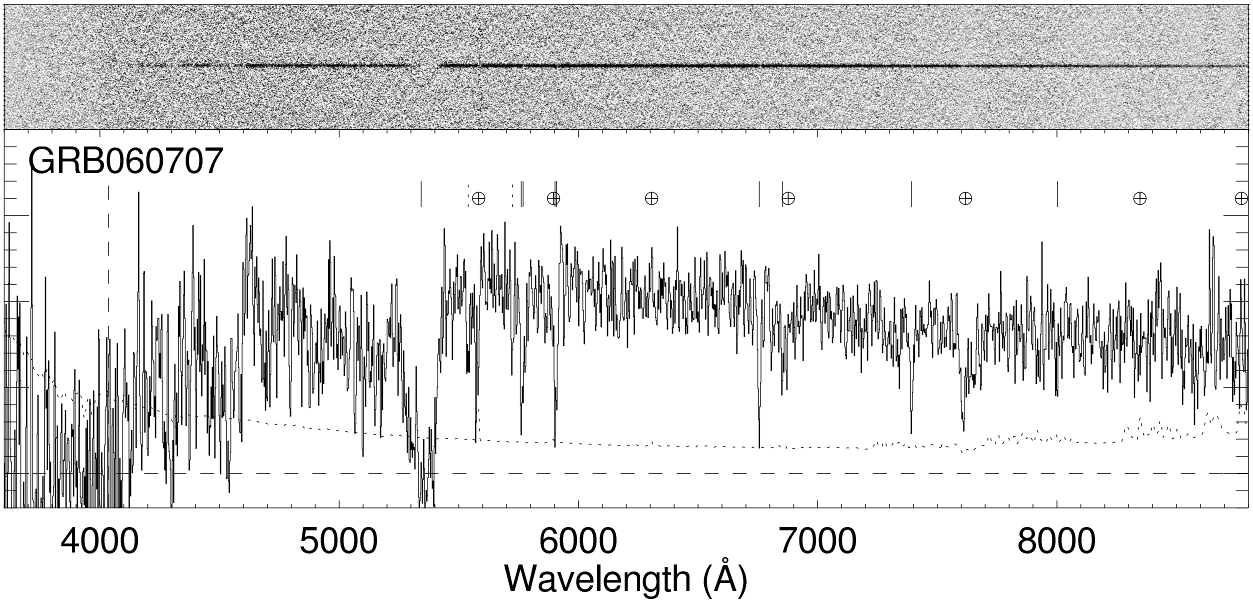
GRB060707
4000
5000
6000
7000
8000
Wavelength (Å)

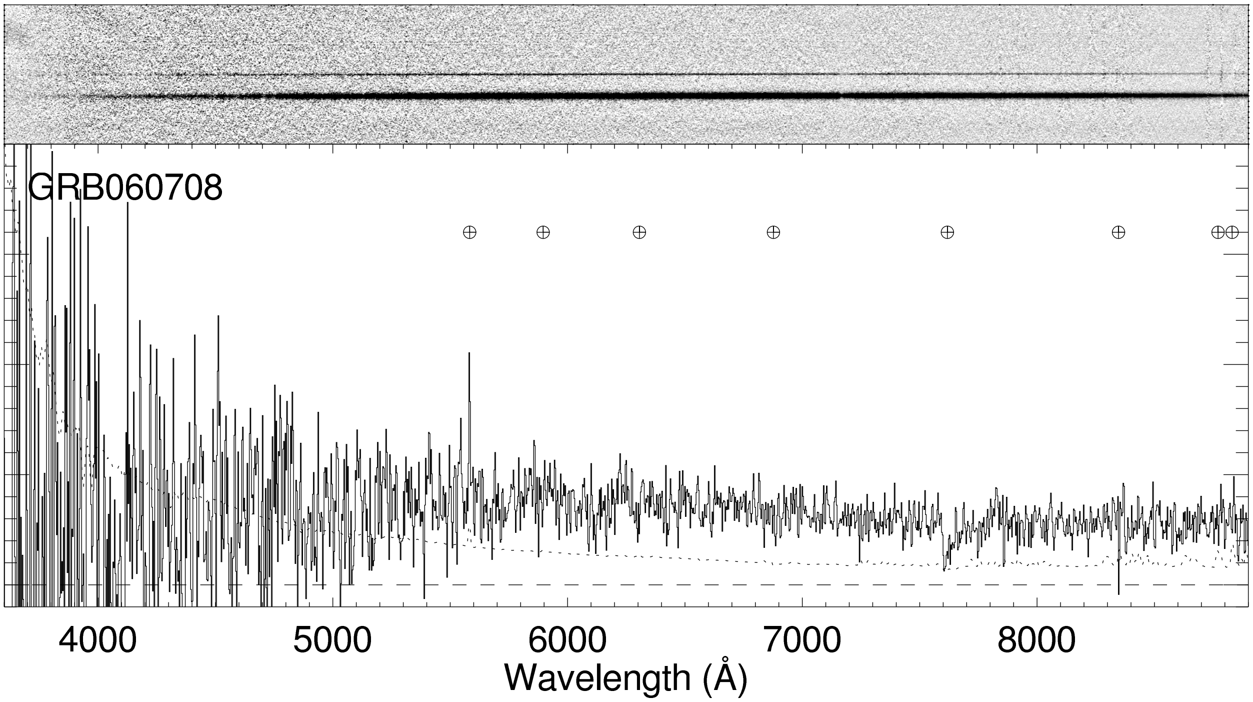
GRB060708
4000
5000
6000
7000
8000
Wavelength (Å)

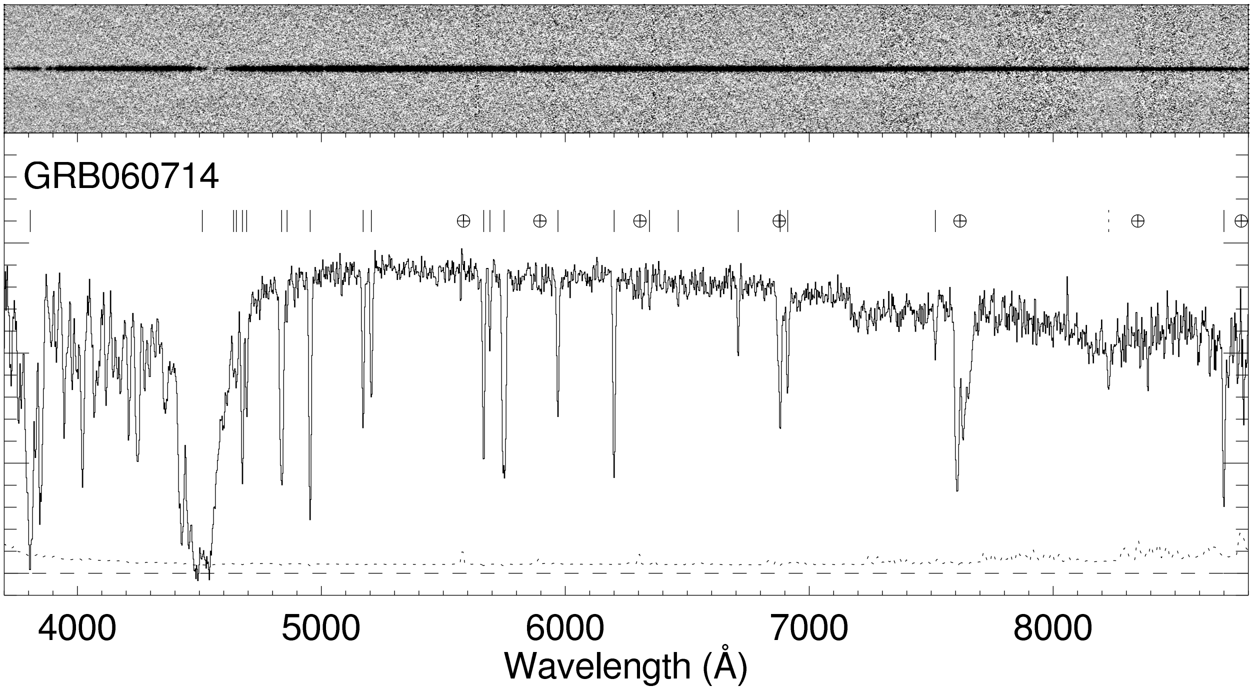
GRB060714
⊕
⊕
⊕
⊕
⊕
⊕
⊕
4000
5000
6000
7000
8000
Wavelength (Å)

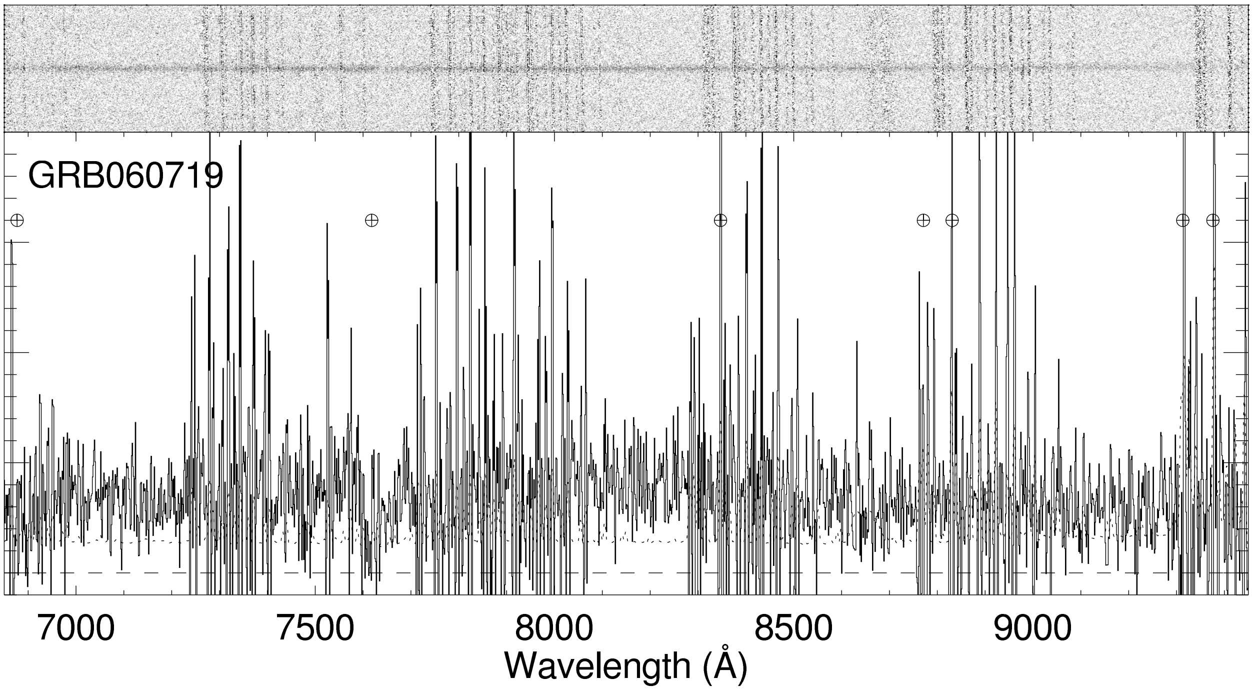
GRB060719
⊕
⊕
⊕
⊕
⊕
⊕
⊕
7000
7500
8000
8500
9000
Wavelength (Å)

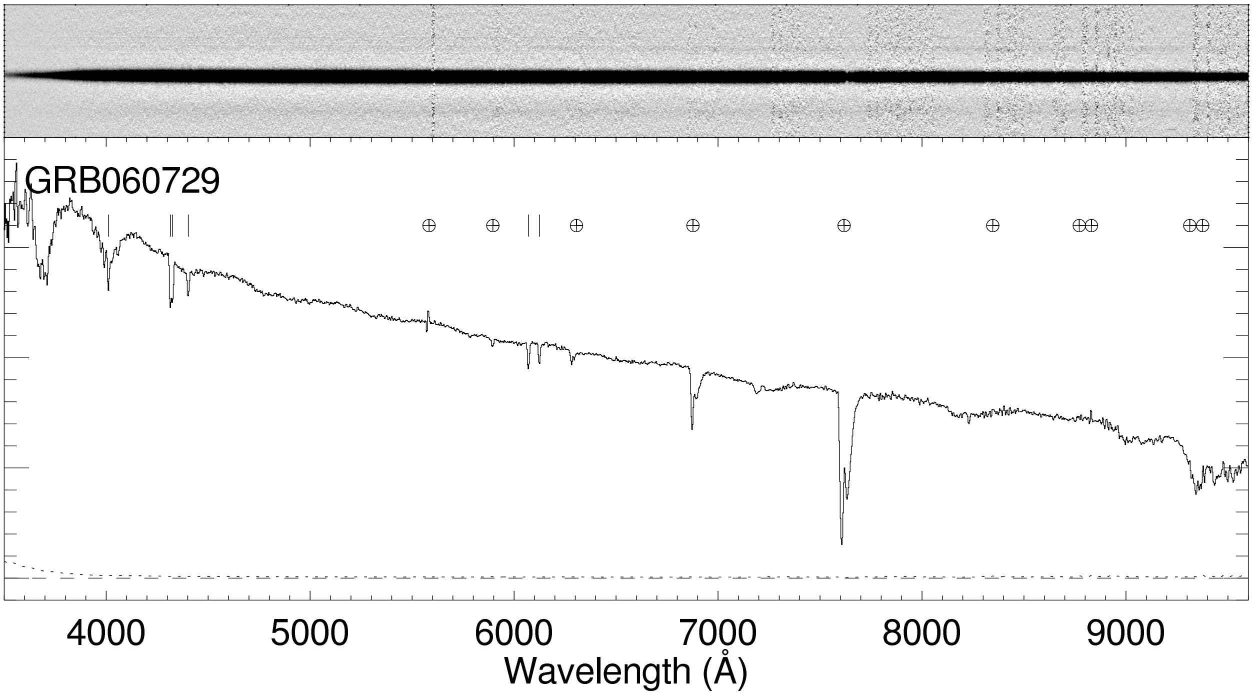
GRB060729
⊕
4000
5000
6000
7000
8000
9000
Wavelength (Å)

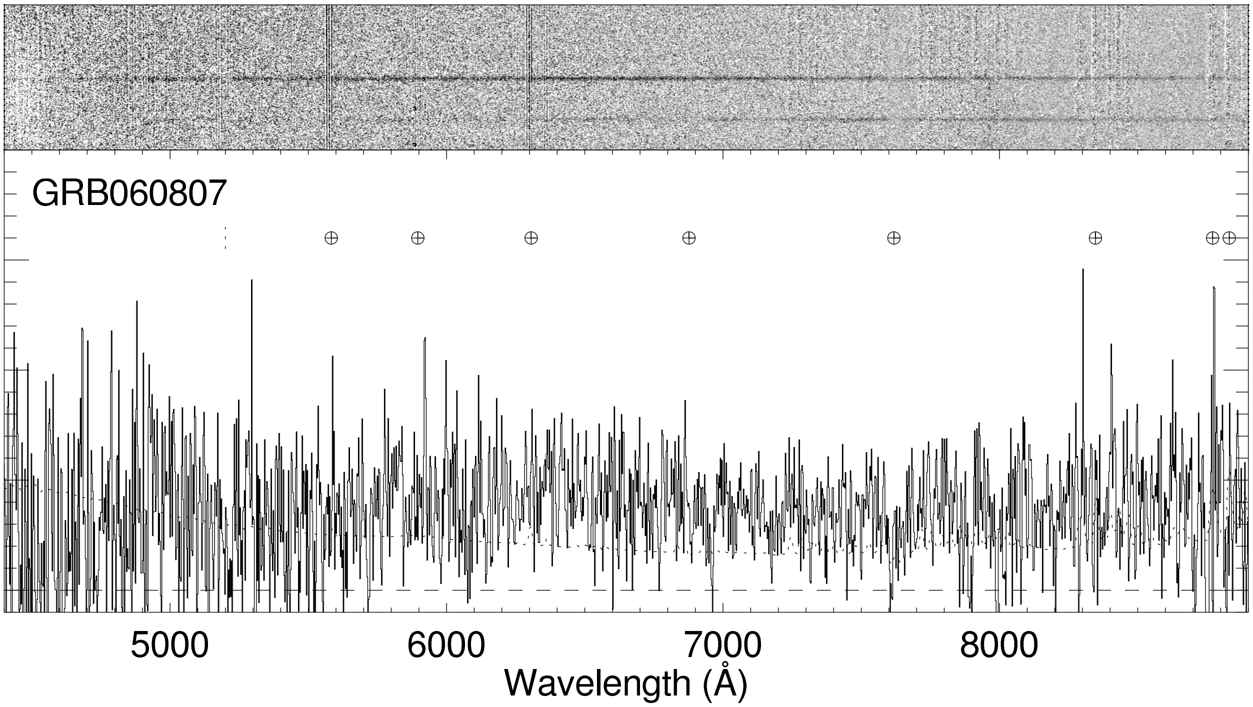
GRB060807
⊕
5000
6000
7000
8000
Wavelength (Å)

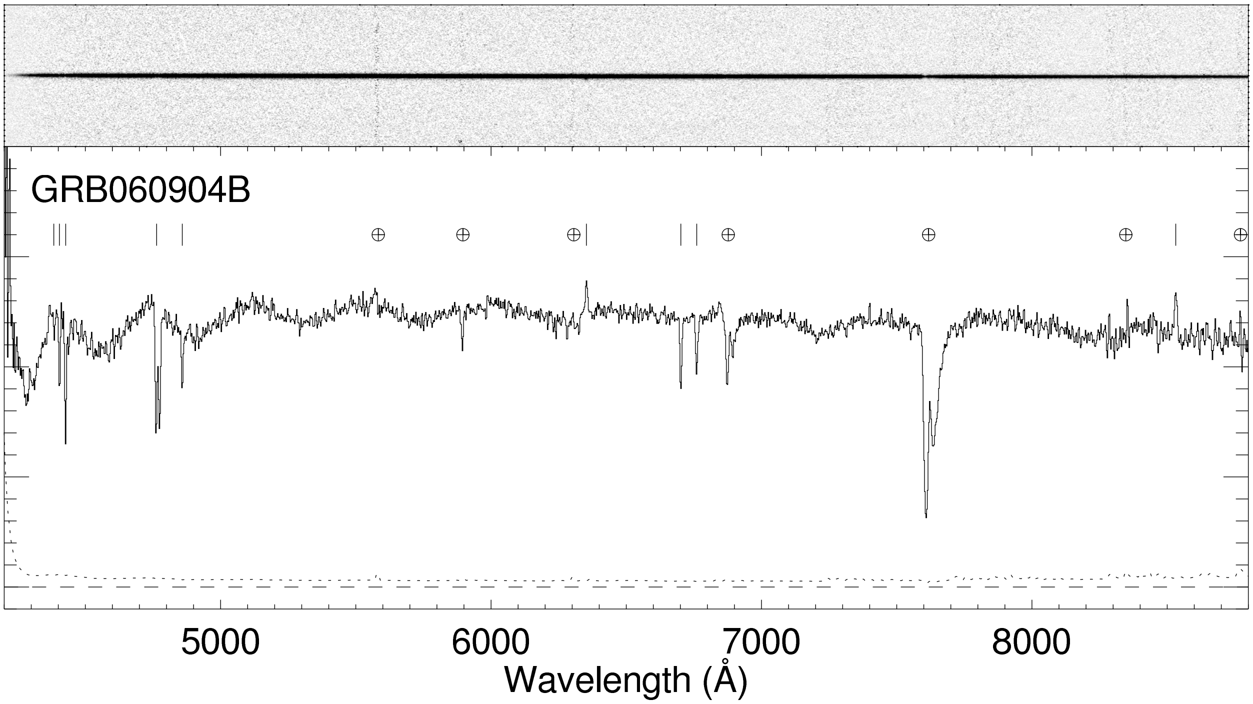
GRB060904B
5000
6000
7000
8000
Wavelength (Å)

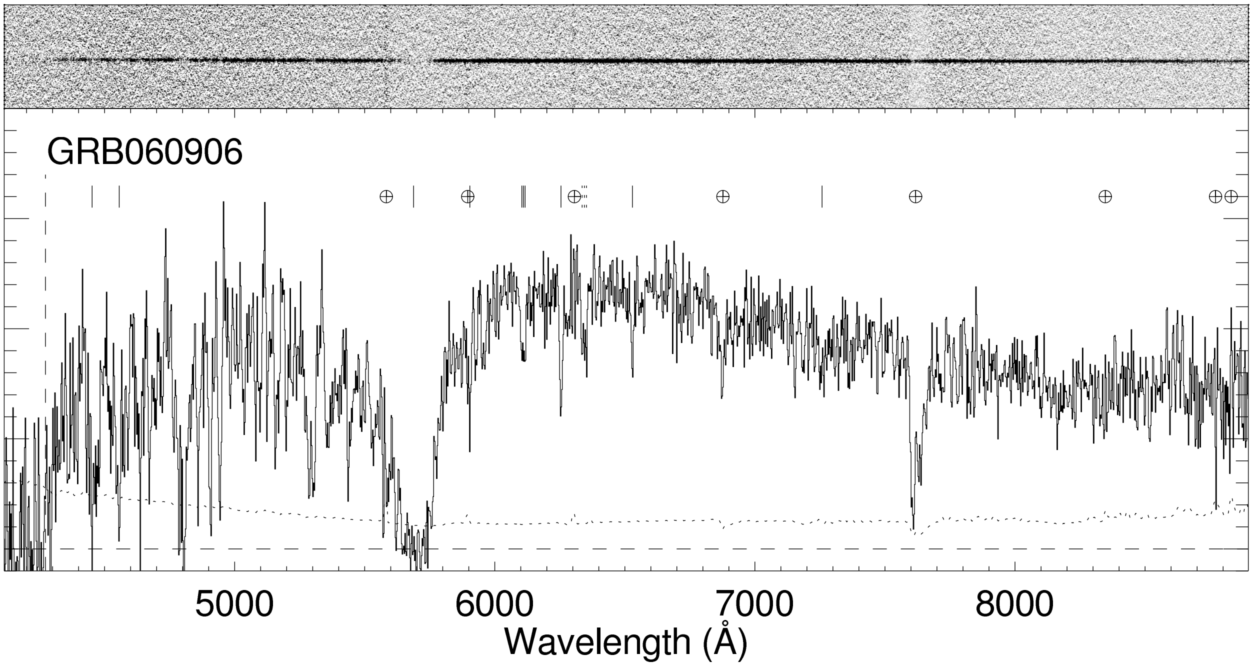
GRB060906
5000
6000
7000
8000
Wavelength (Å)

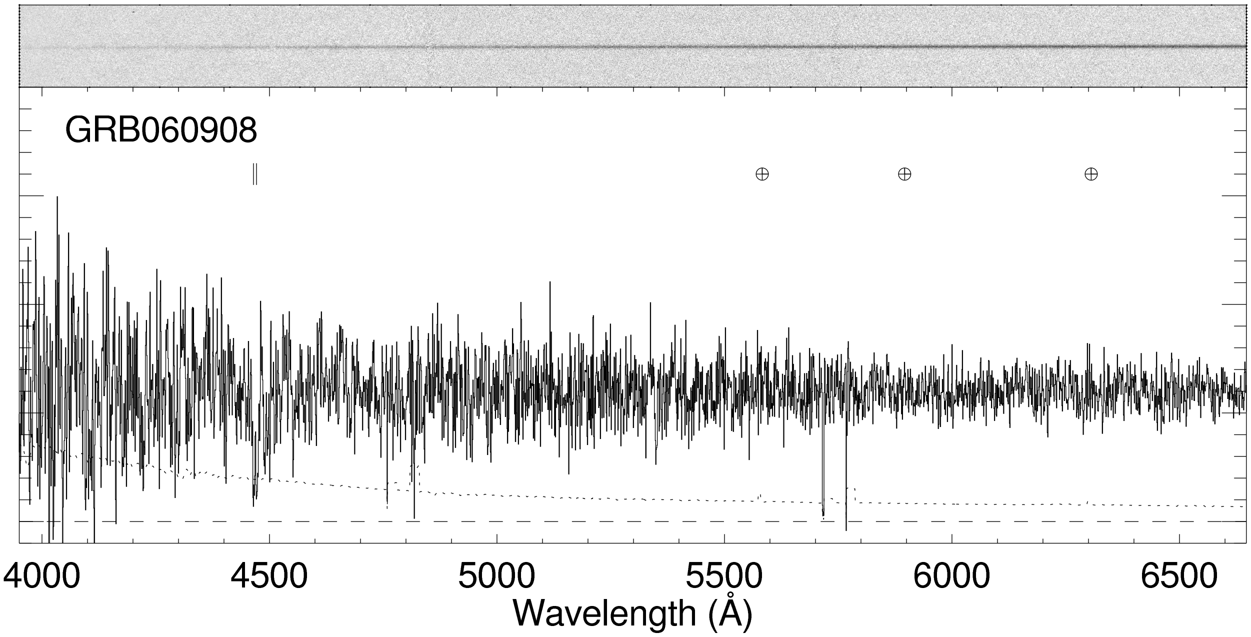
GRB060908
4000
4500
5000
5500
6000
6500
Wavelength (Å)

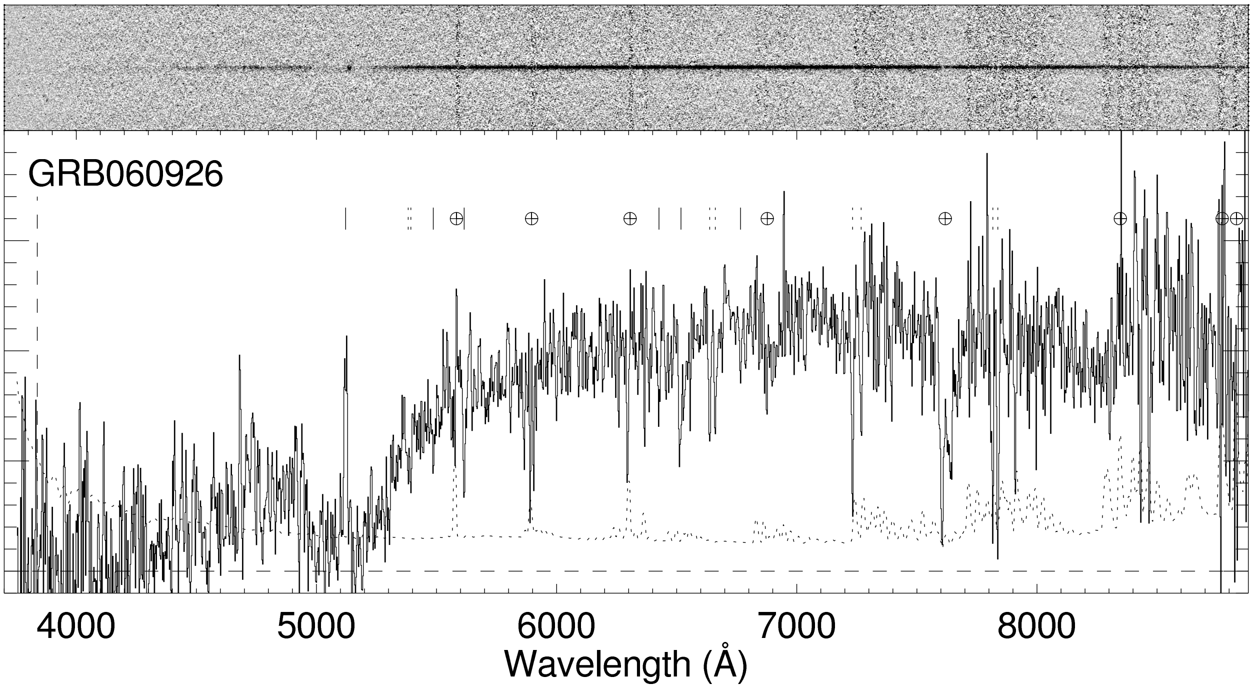
GRB060926
4000
5000
6000
7000
8000
Wavelength (Å)

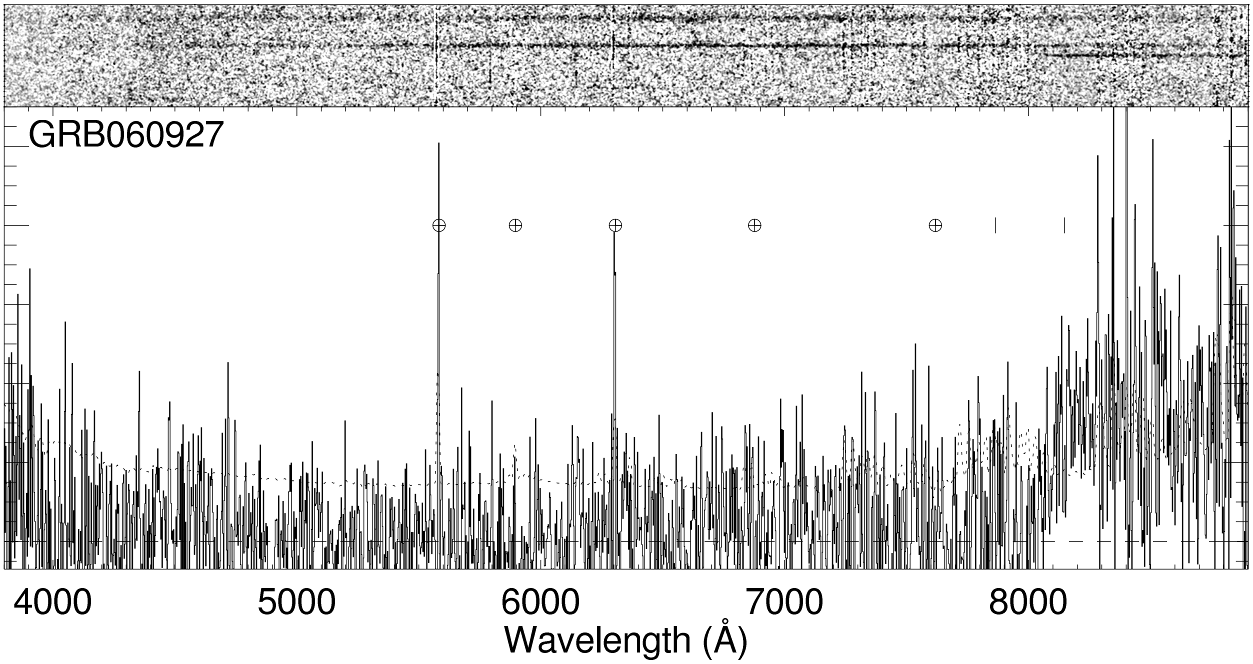
GRB060927
4000
5000
6000
7000
8000
Wavelength (Å)

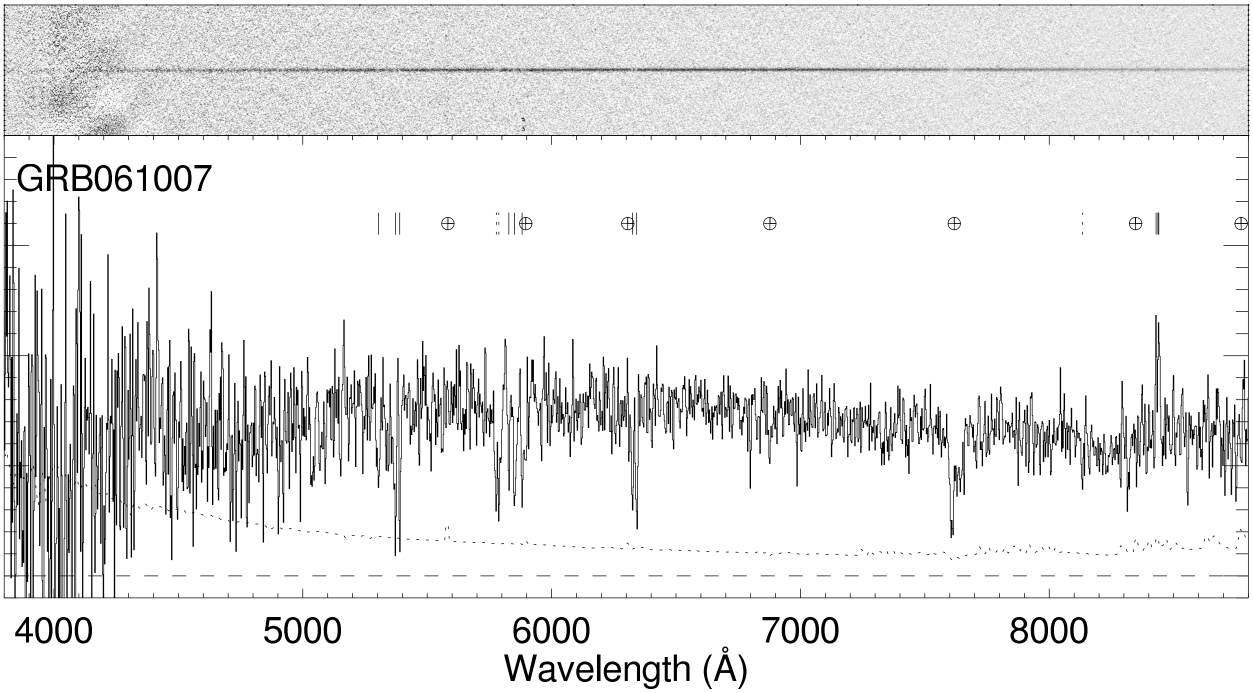
GRB061007
4000
5000
6000
7000
8000
Wavelength (Å)

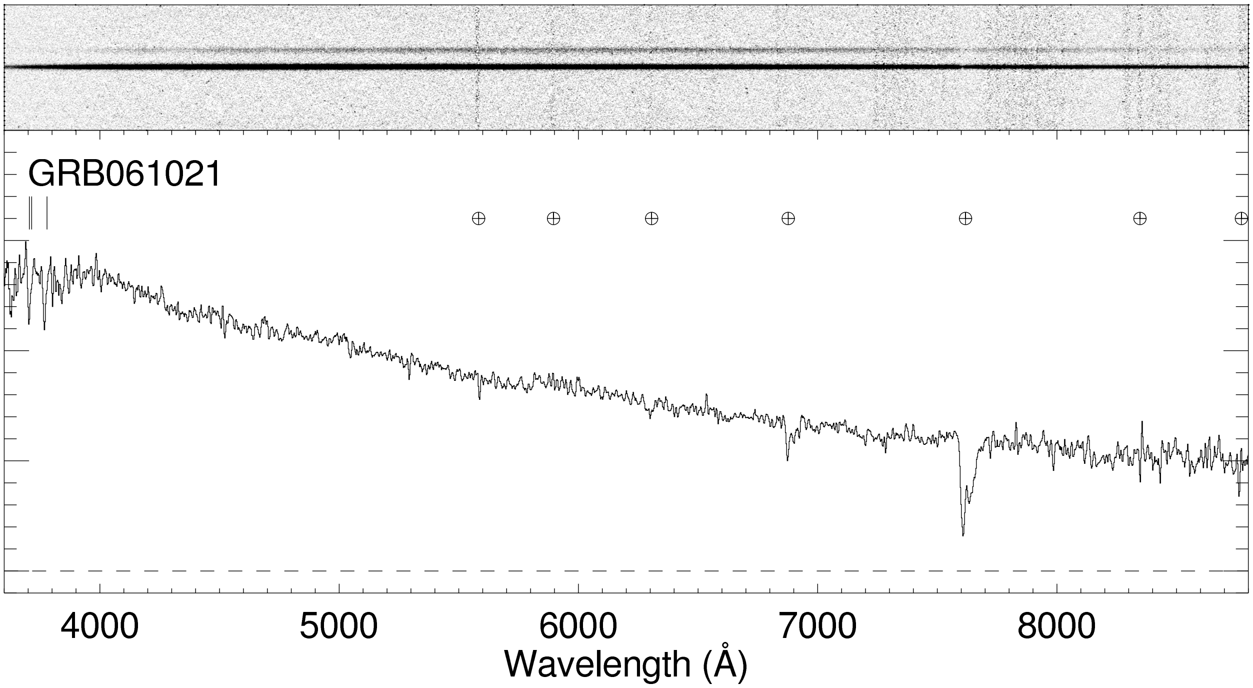
GRB061021
4000
5000
6000
7000
8000
Wavelength (Å)

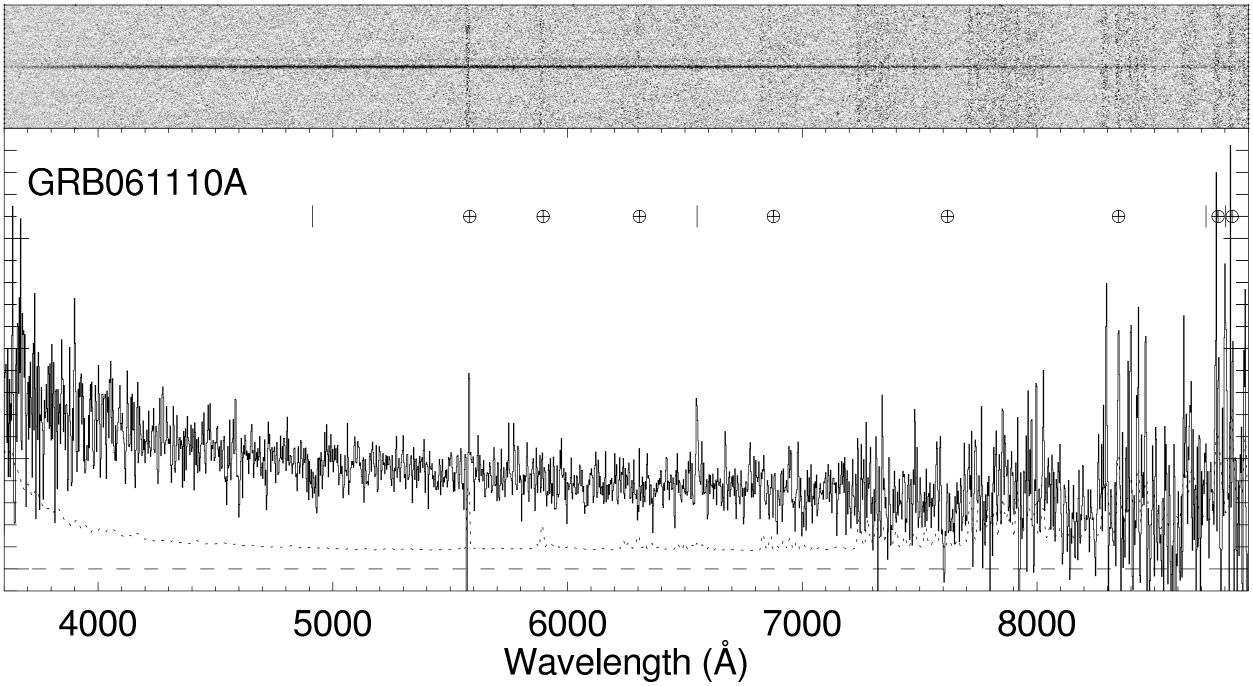
GRB061110A
4000
5000
6000
7000
8000
Wavelength (Å)

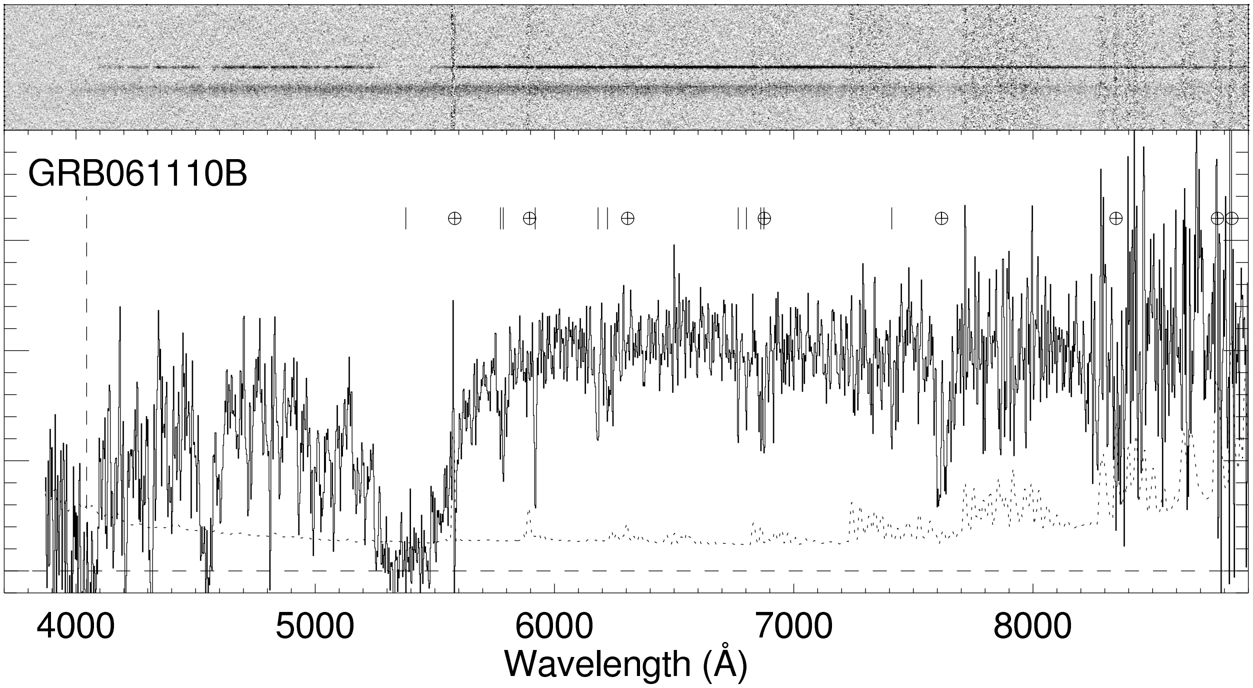
GRB061110B
4000
5000
6000
7000
8000
Wavelength (Å)

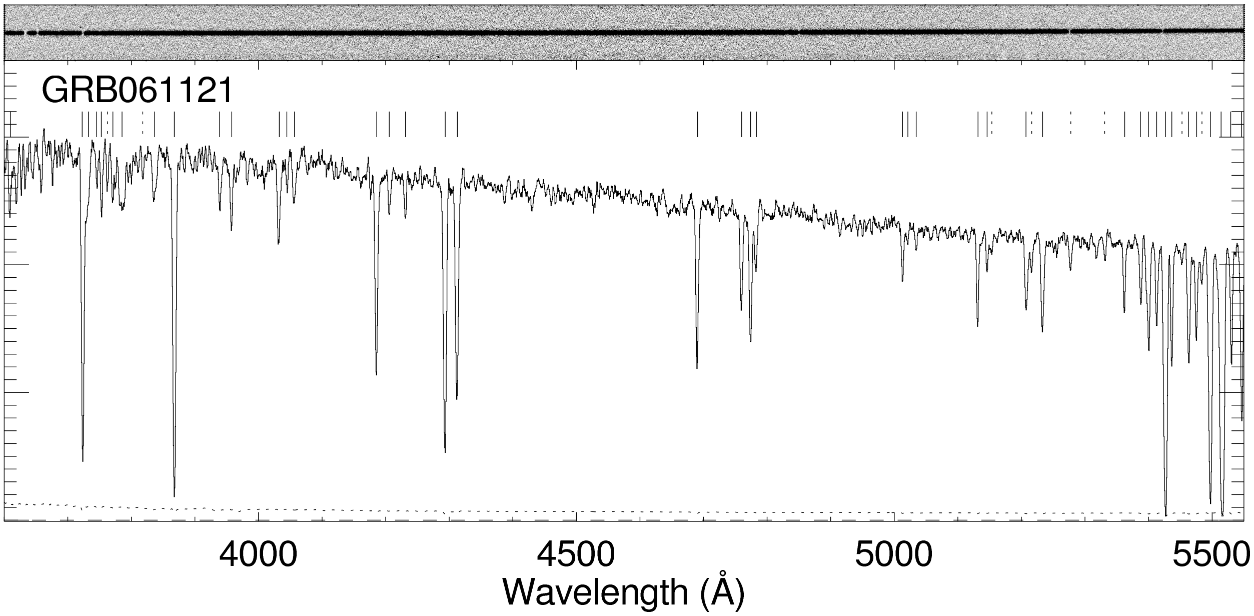
GRB061121
4000
4500
5000
5500
Wavelength (Å)

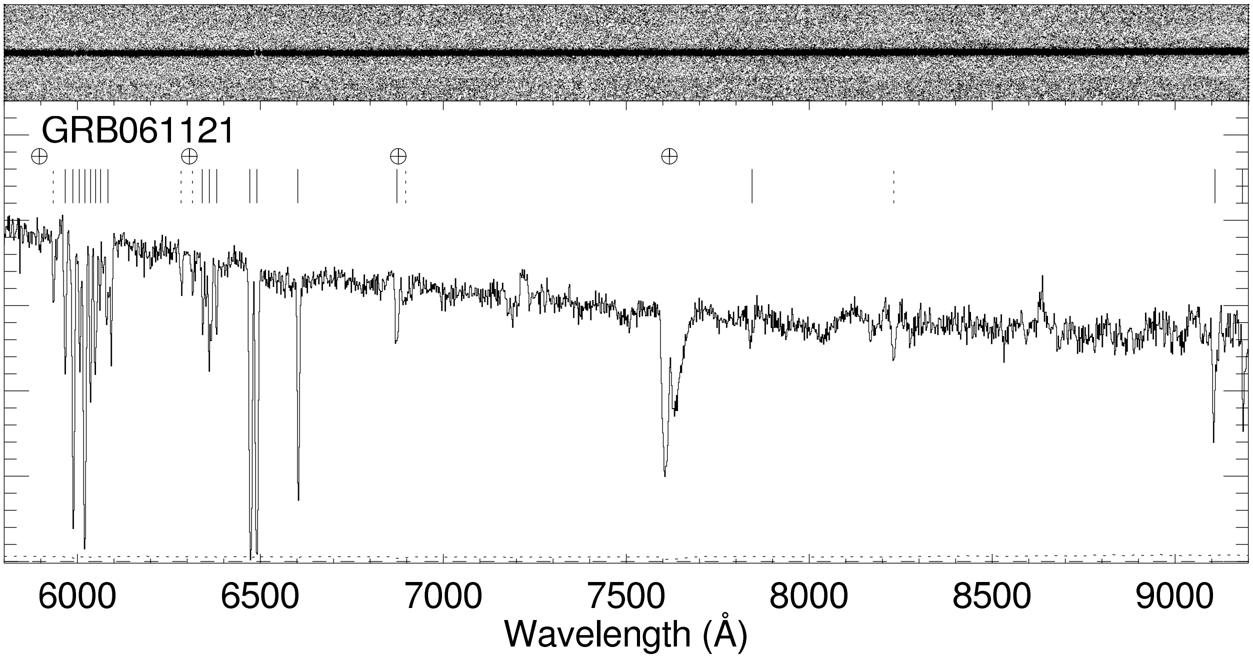
GRB061121
6000
6500
7000
7500
8000
8500
9000
Wavelength (Å)

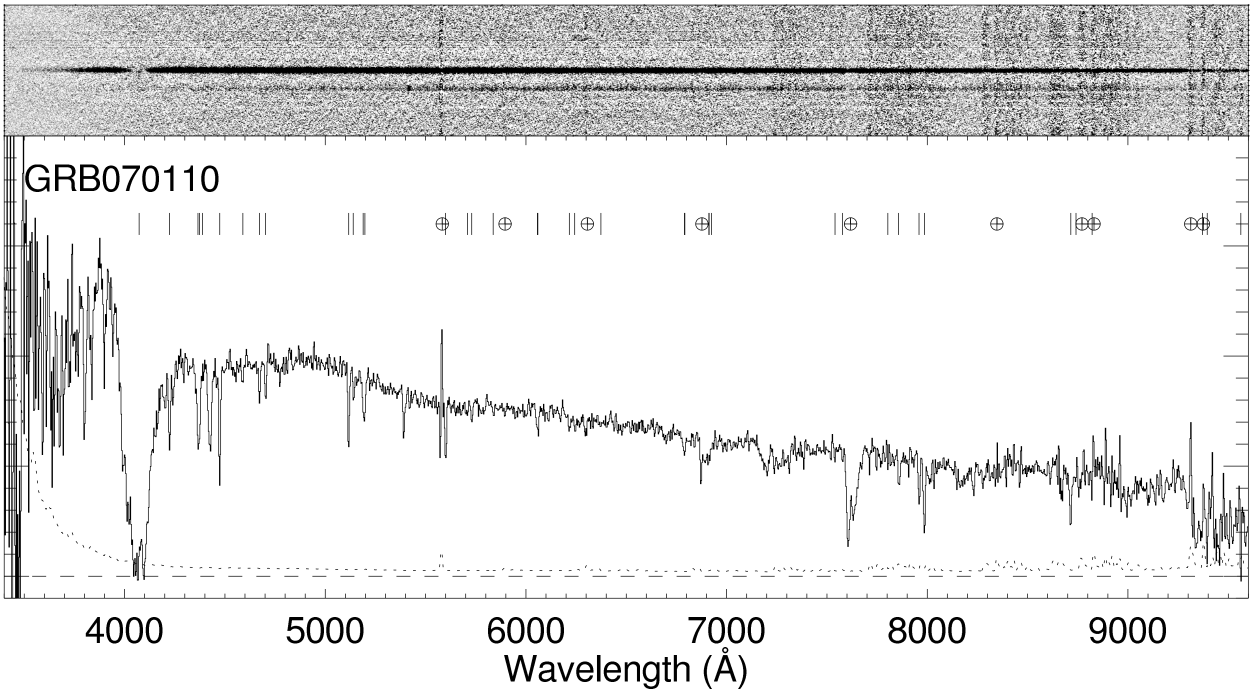
GRB070110
4000
5000
6000
7000
8000
9000
Wavelength (Å)

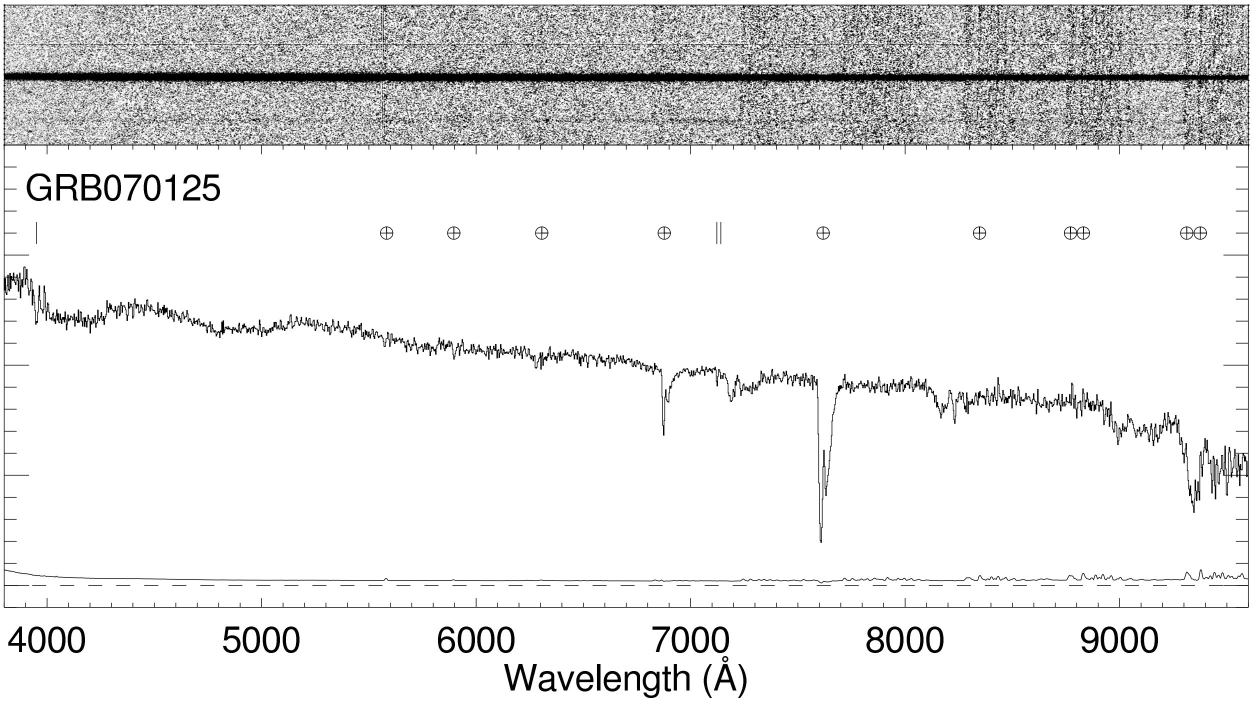
GRB070125
⊕ ⊕ ⊕ ⊕ ⊕ ⊕ ⊕⊕ ⊕⊕
4000
5000
6000
7000
8000
9000
Wavelength (Å)

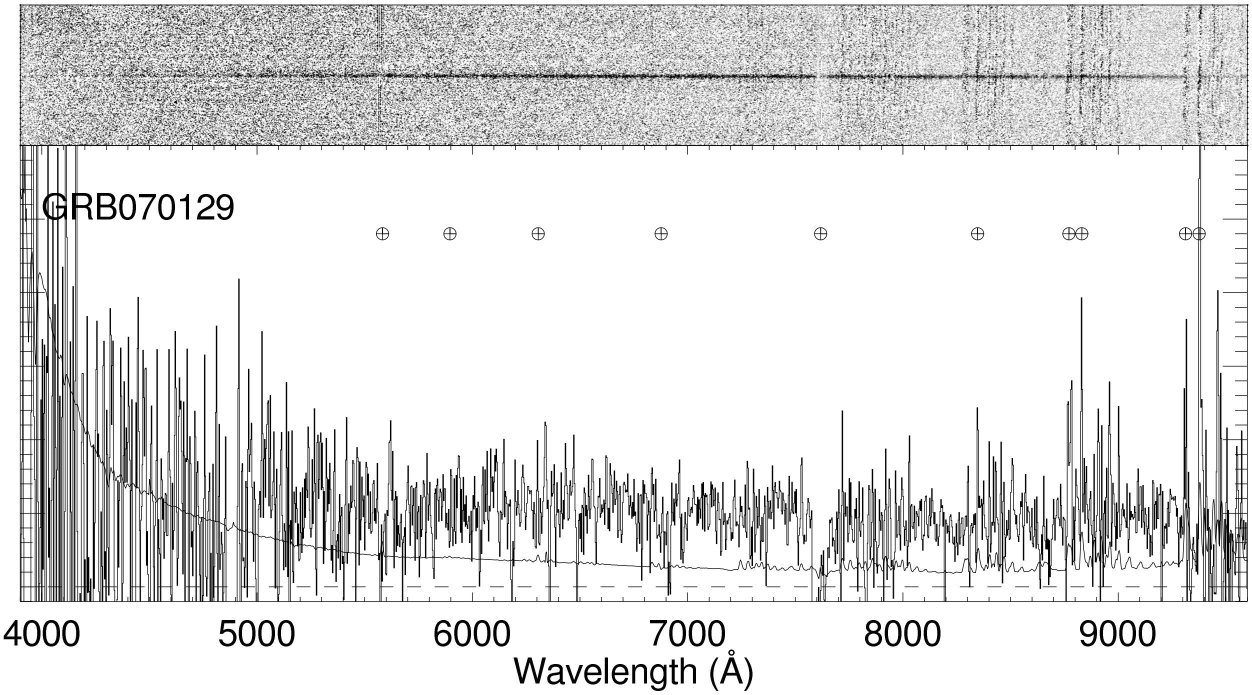
GRB070129
⊕ ⊕ ⊕ ⊕ ⊕ ⊕ ⊕⊕ ⊕⊕
4000
5000
6000
7000
8000
9000
Wavelength (Å)

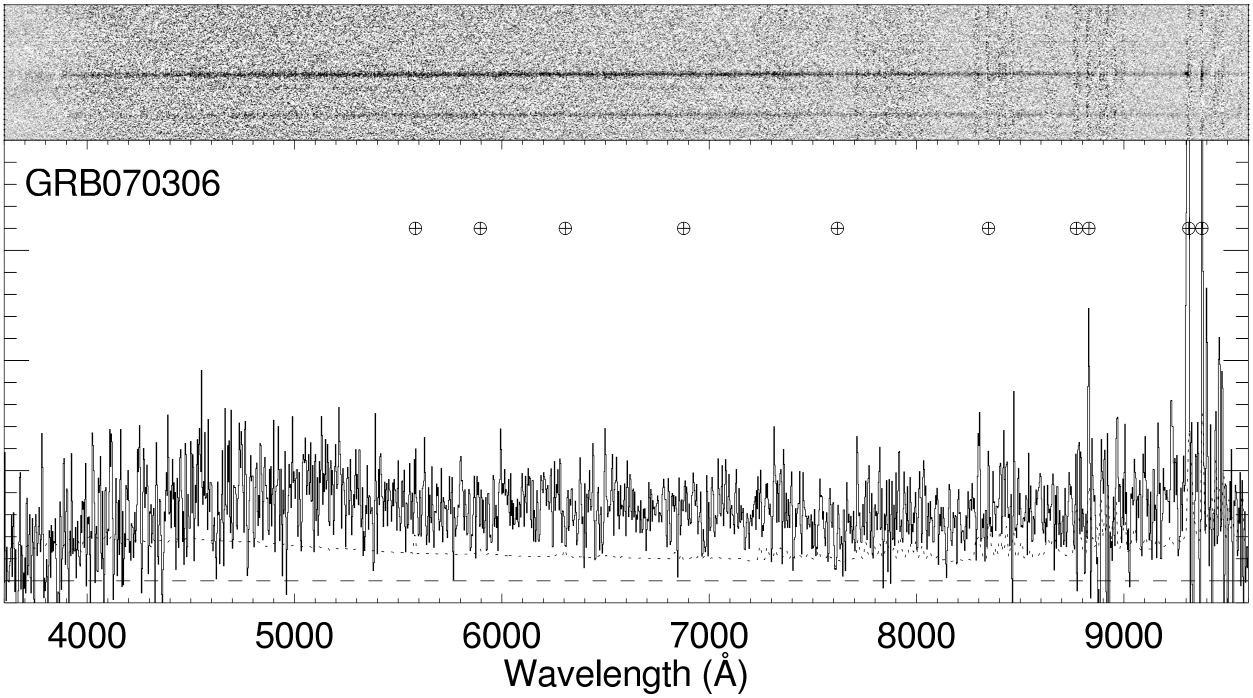
GRB070306
4000
5000
6000
7000
8000
9000
Wavelength (Å)

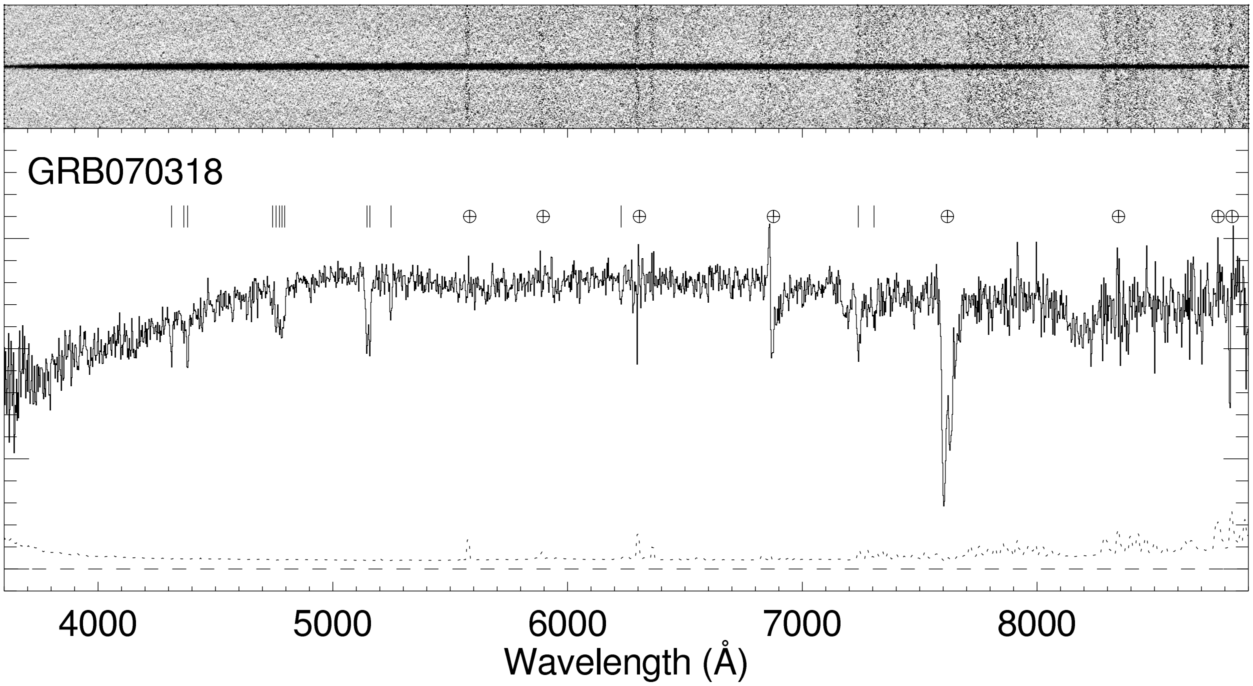
GRB070318
4000
5000
6000
7000
8000
Wavelength (Å)

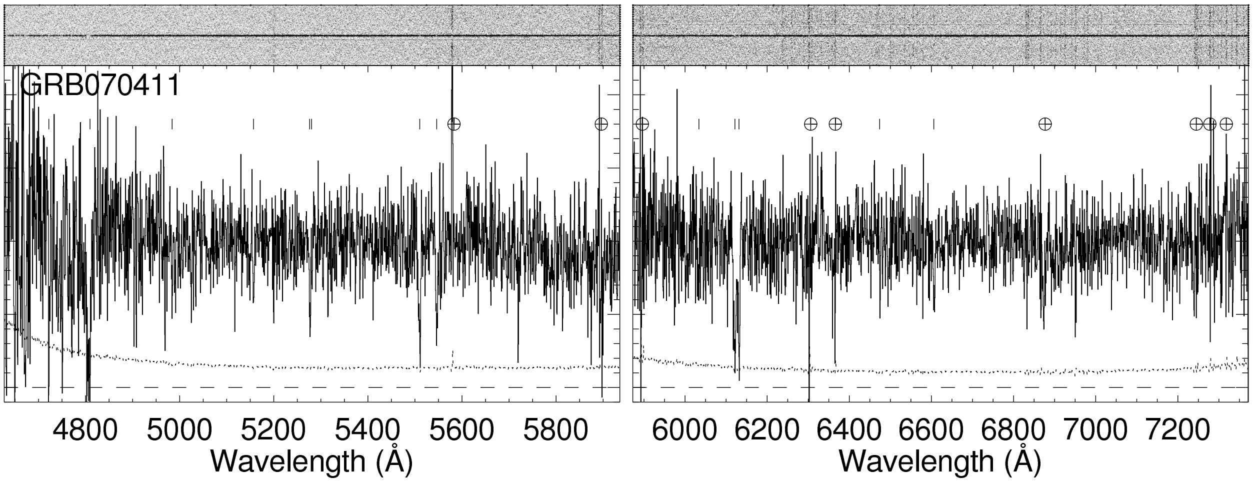
GRB070411
4800
5000
5200
5400
5600
5800
Wavelength (Å)
6000
6200
6400
6600
6800
7000
7200
Wavelength (Å)

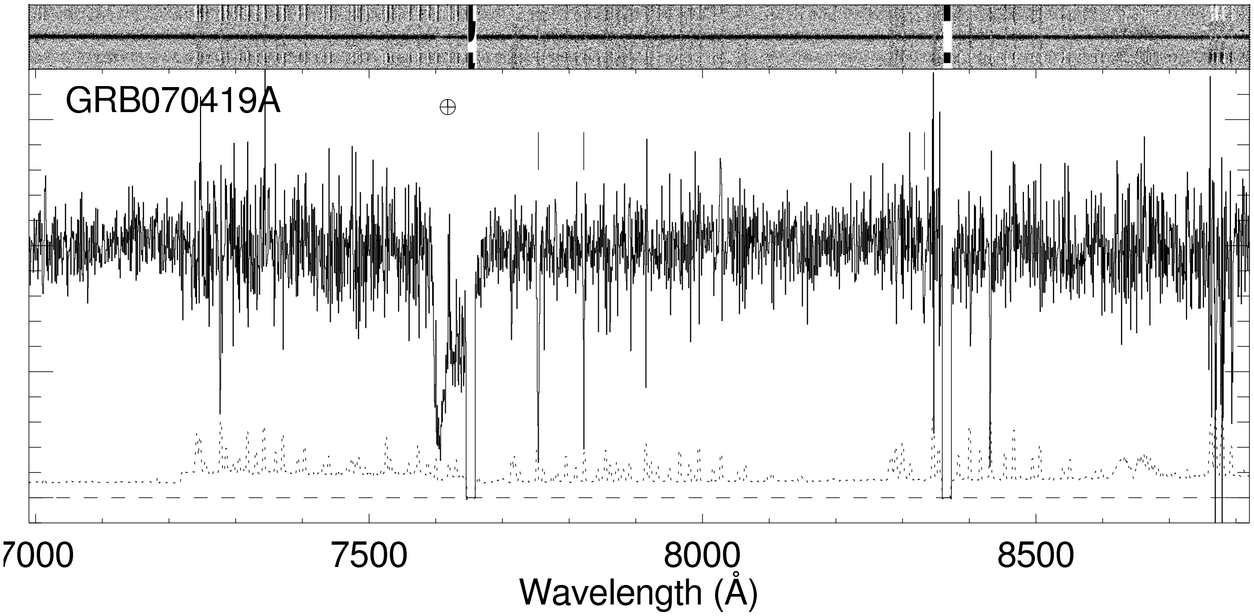
GRB070419A
⊕
7000
7500
8000
8500
Wavelength (Å)

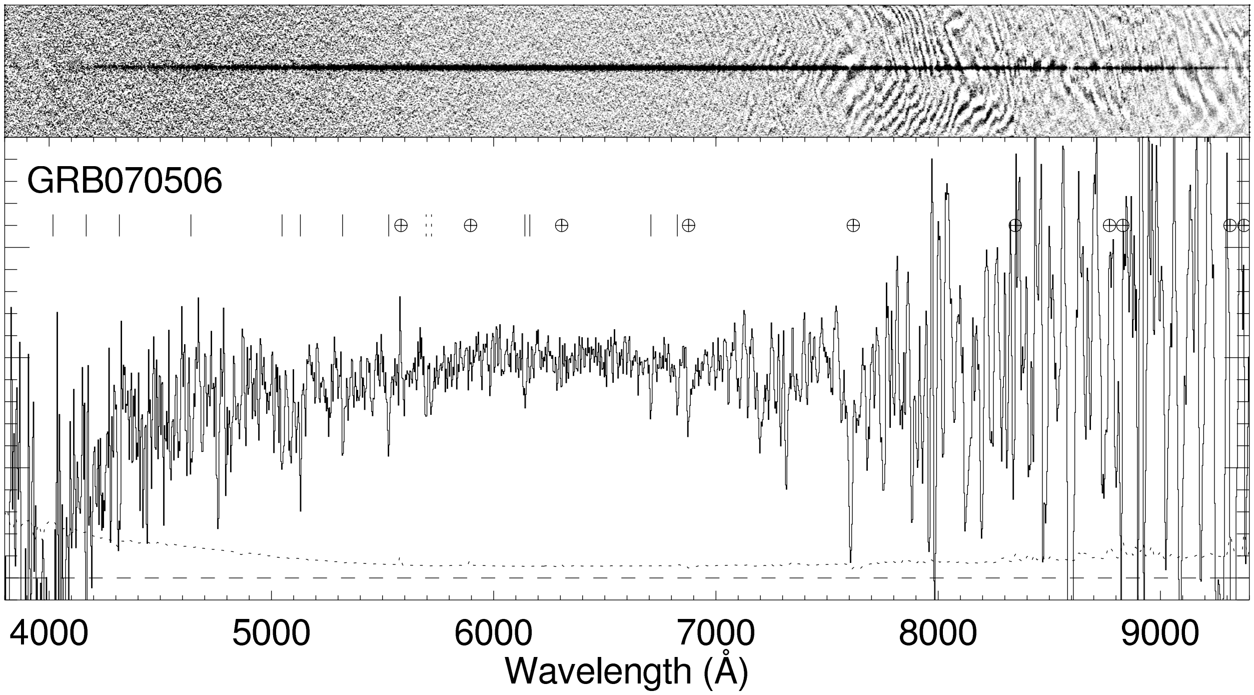
GRB070506
⊕
4000
5000
6000
7000
8000
9000
Wavelength (Å)

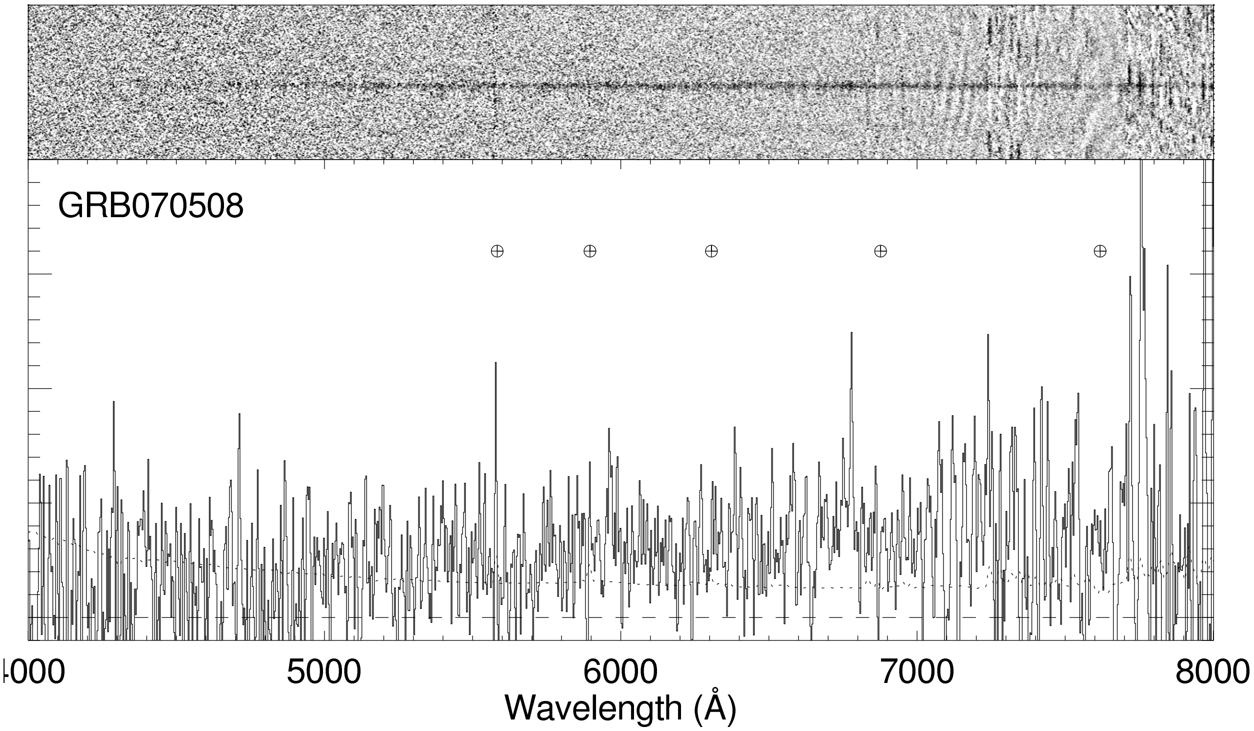
GRB070508
000
5000
6000
7000
8000
Wavelength (Å)

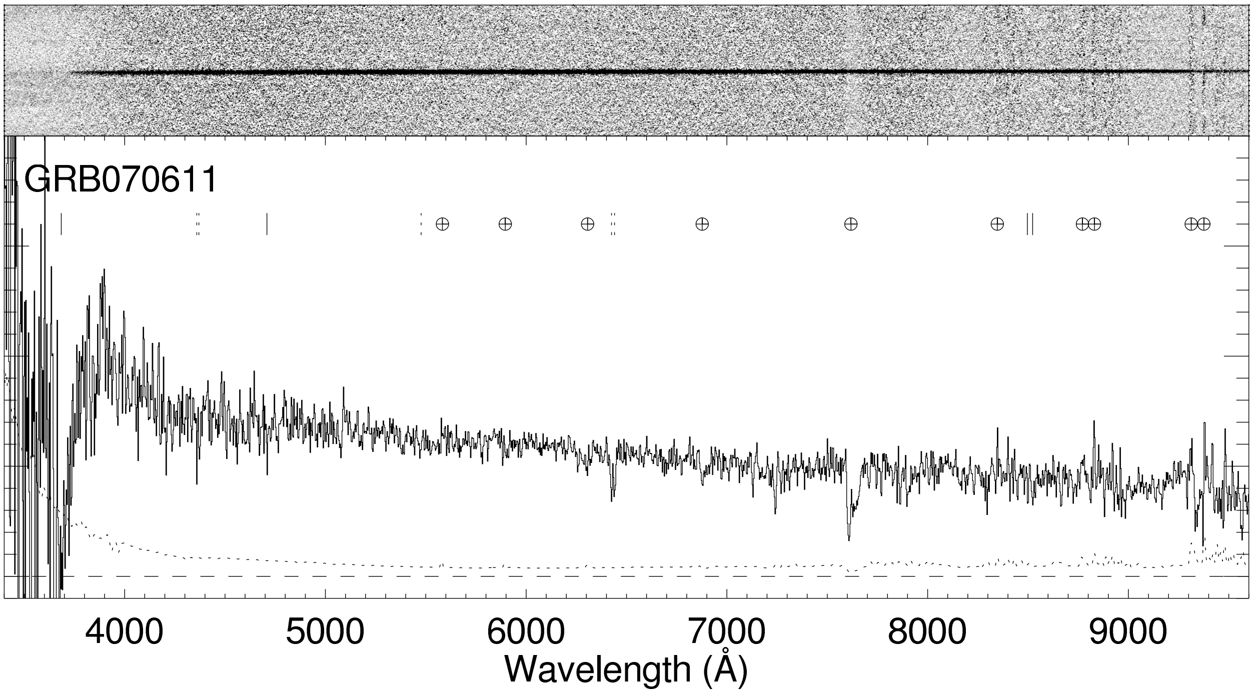
GRB070611
4000
5000
6000
7000
8000
9000
Wavelength (Å)

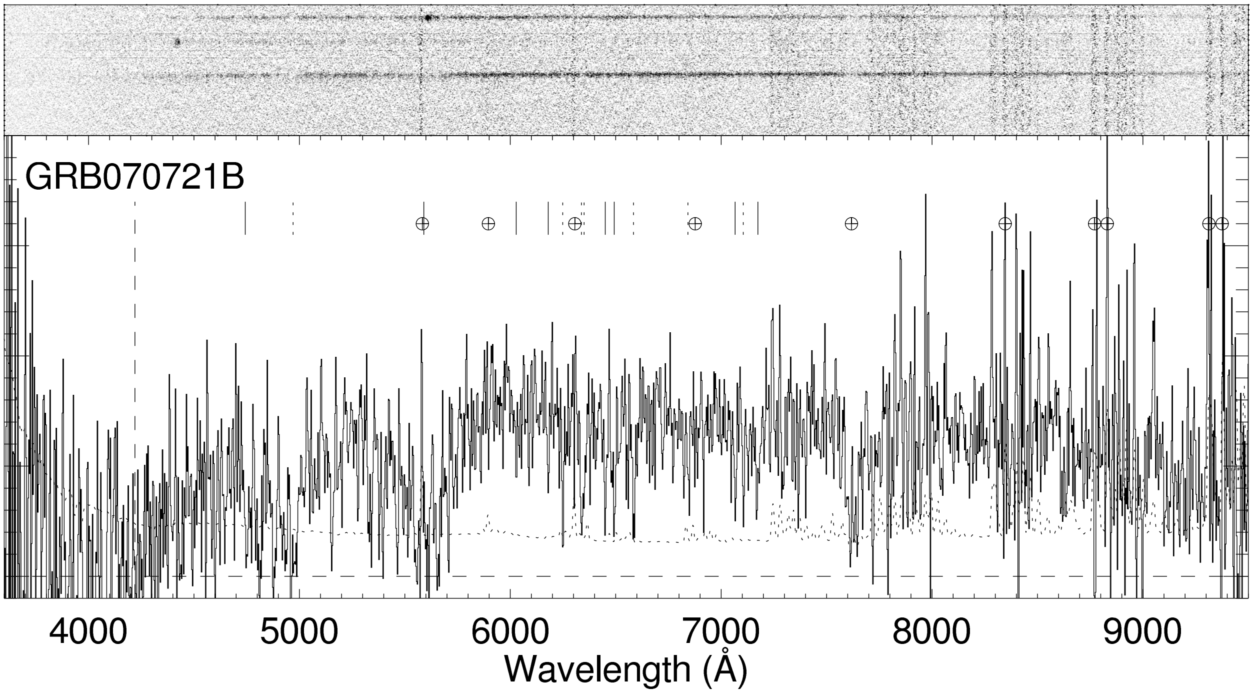
GRB070721B
⊕
4000
5000
6000
7000
8000
9000
Wavelength (Å)

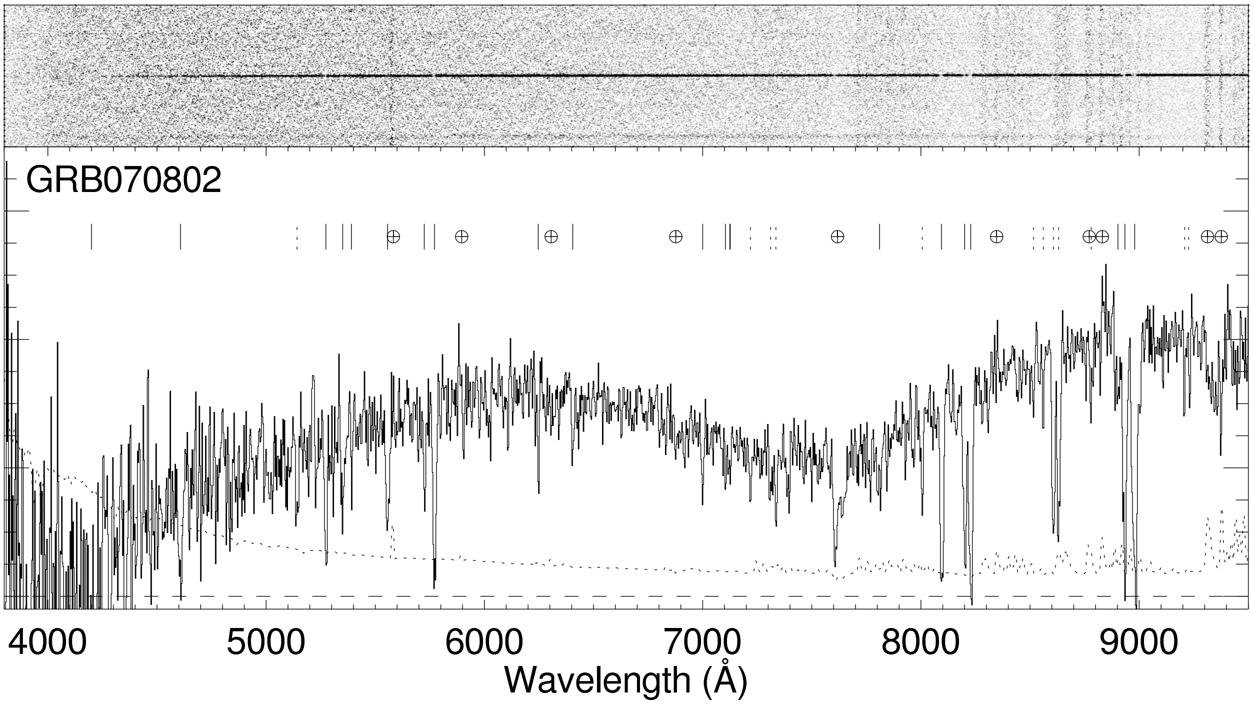
GRB070802
⊕
4000
5000
6000
7000
8000
9000
Wavelength (Å)

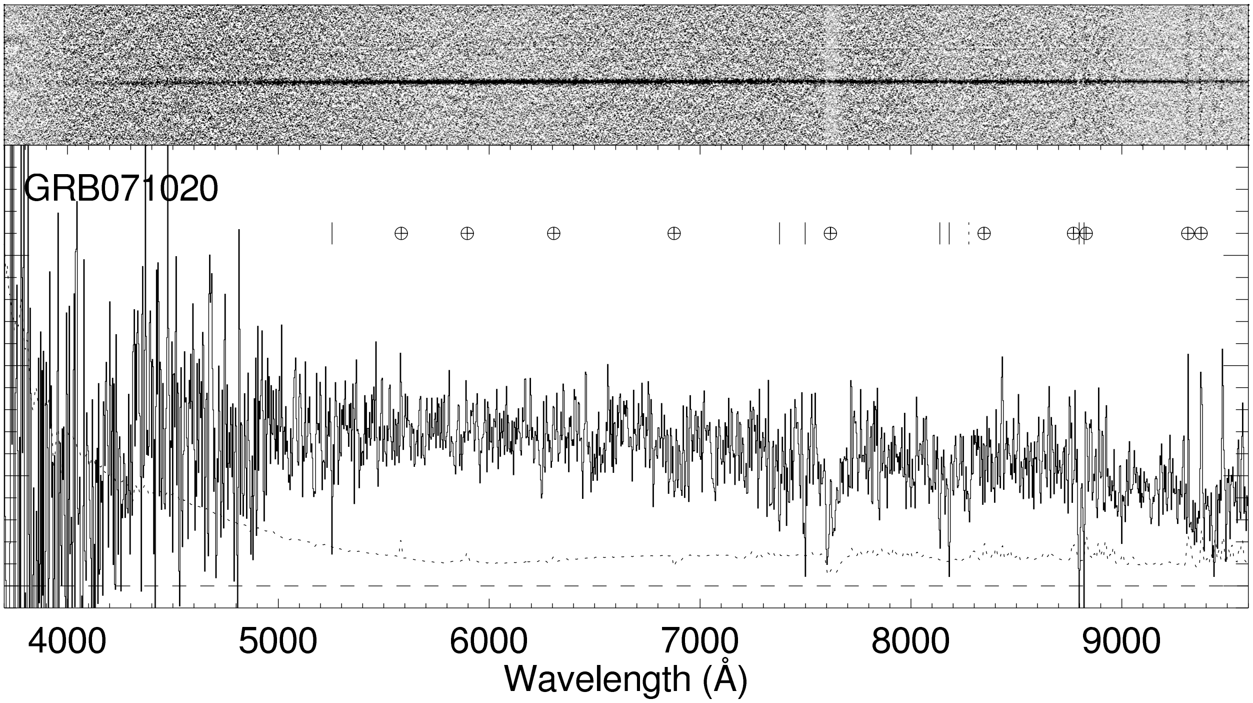
GRB071020
4000
5000
6000
7000
8000
9000
Wavelength (Å)

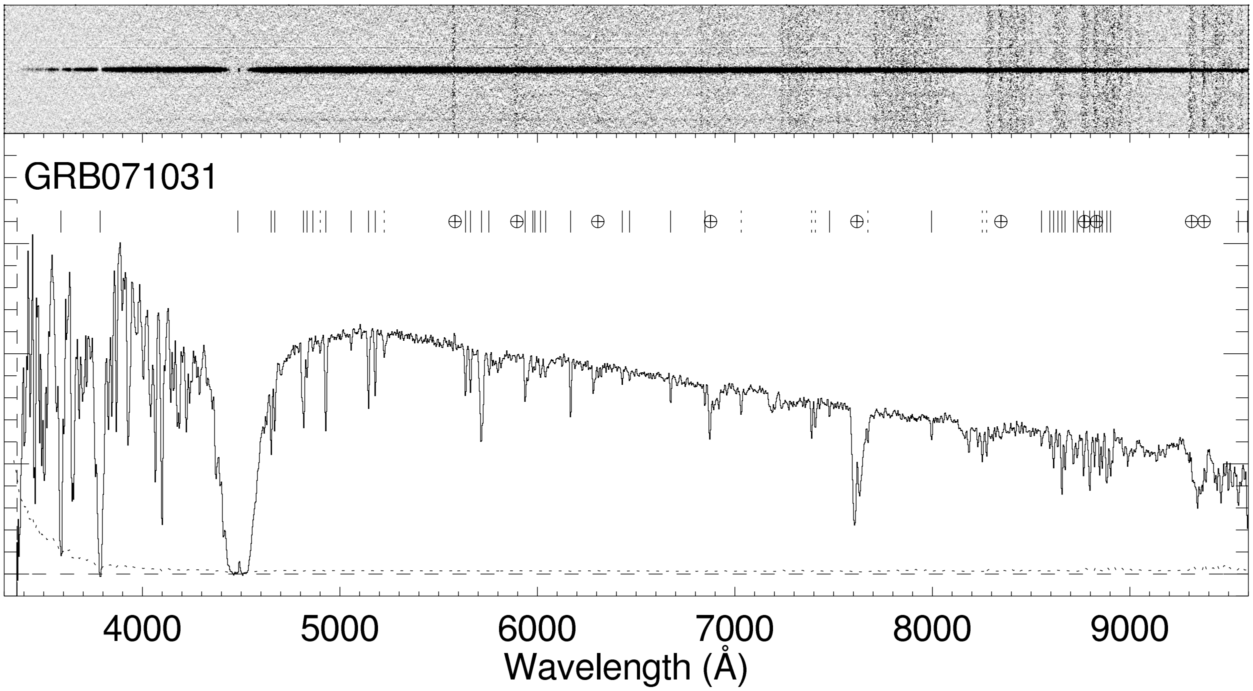
GRB071031
4000
5000
6000
7000
8000
9000
Wavelength (Å)

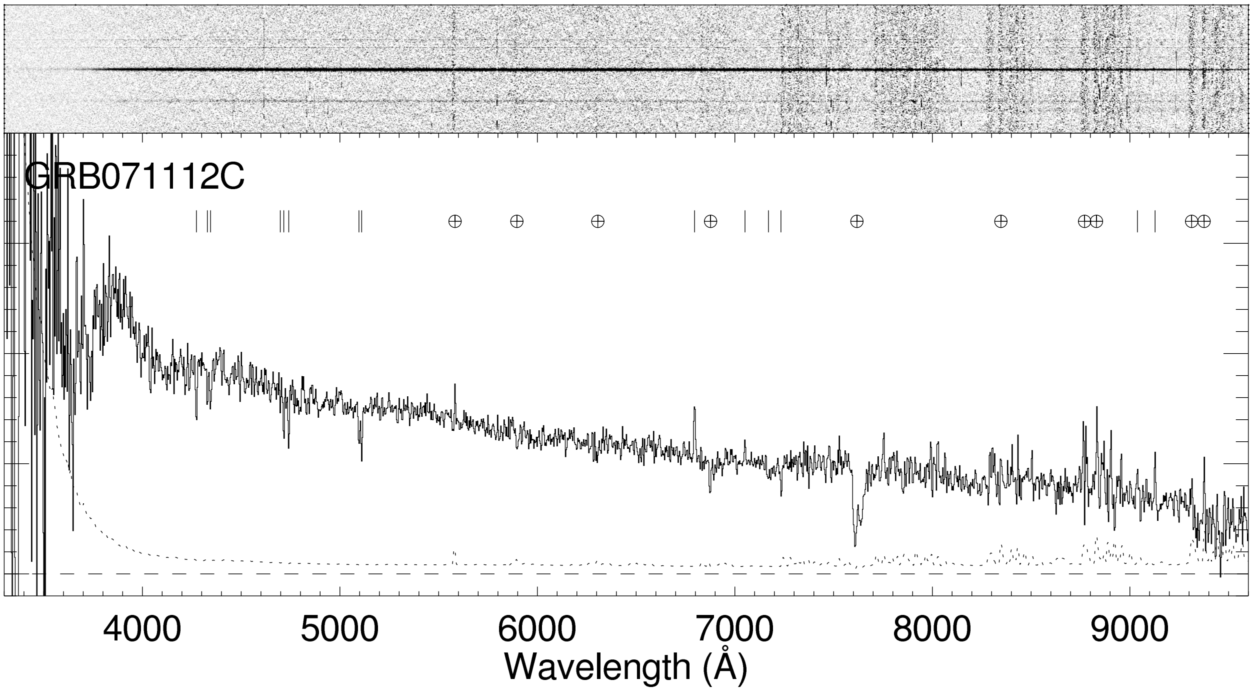
GRB071112C
4000
5000
6000
7000
8000
9000
Wavelength (Å)

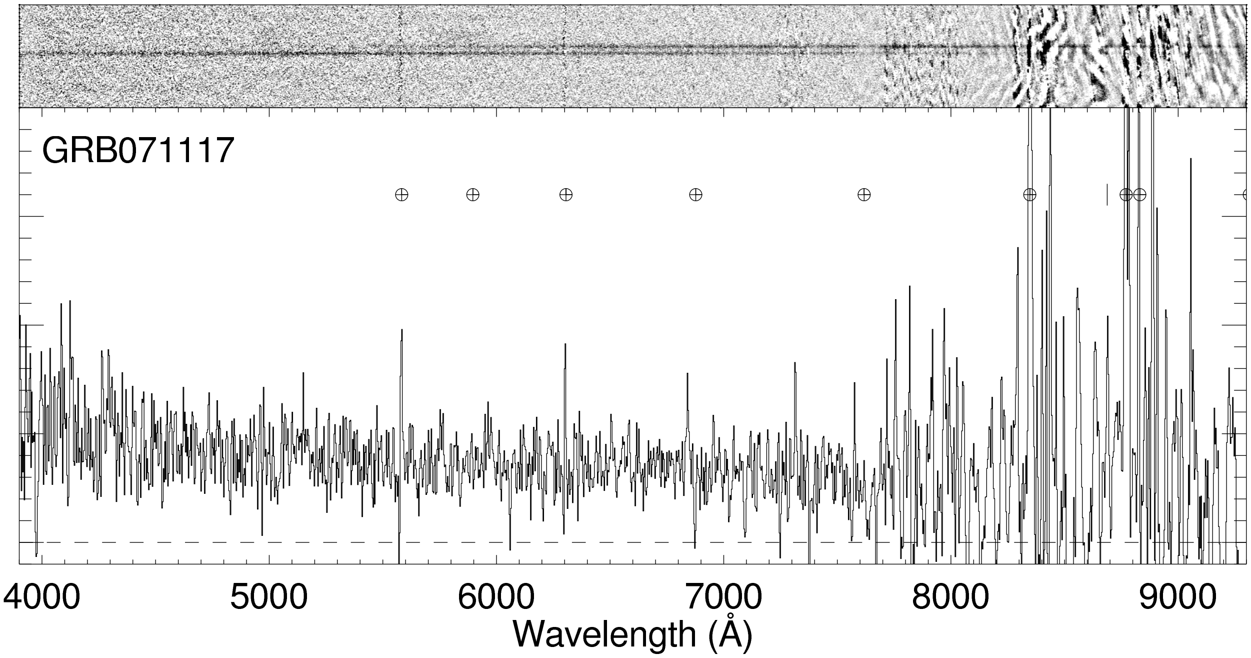
GRB071117
4000
5000
6000
7000
8000
9000
Wavelength (Å)

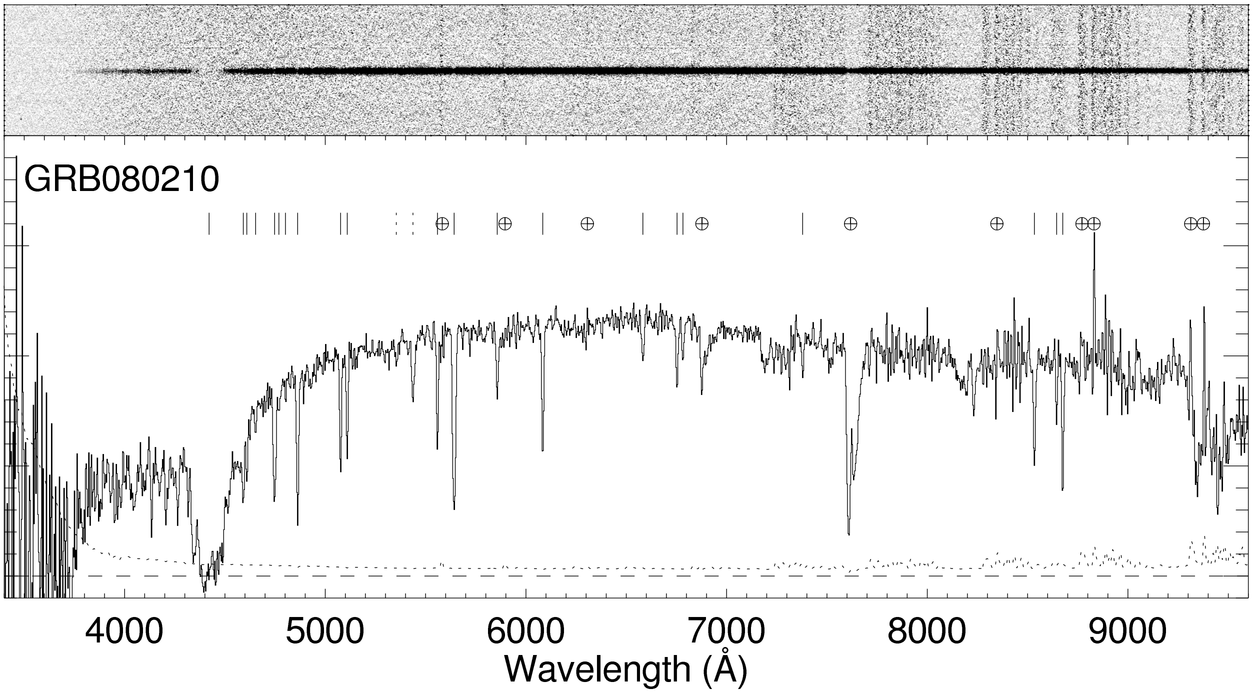
GRB080210
⊕
4000
5000
6000
7000
8000
9000
Wavelength (Å)

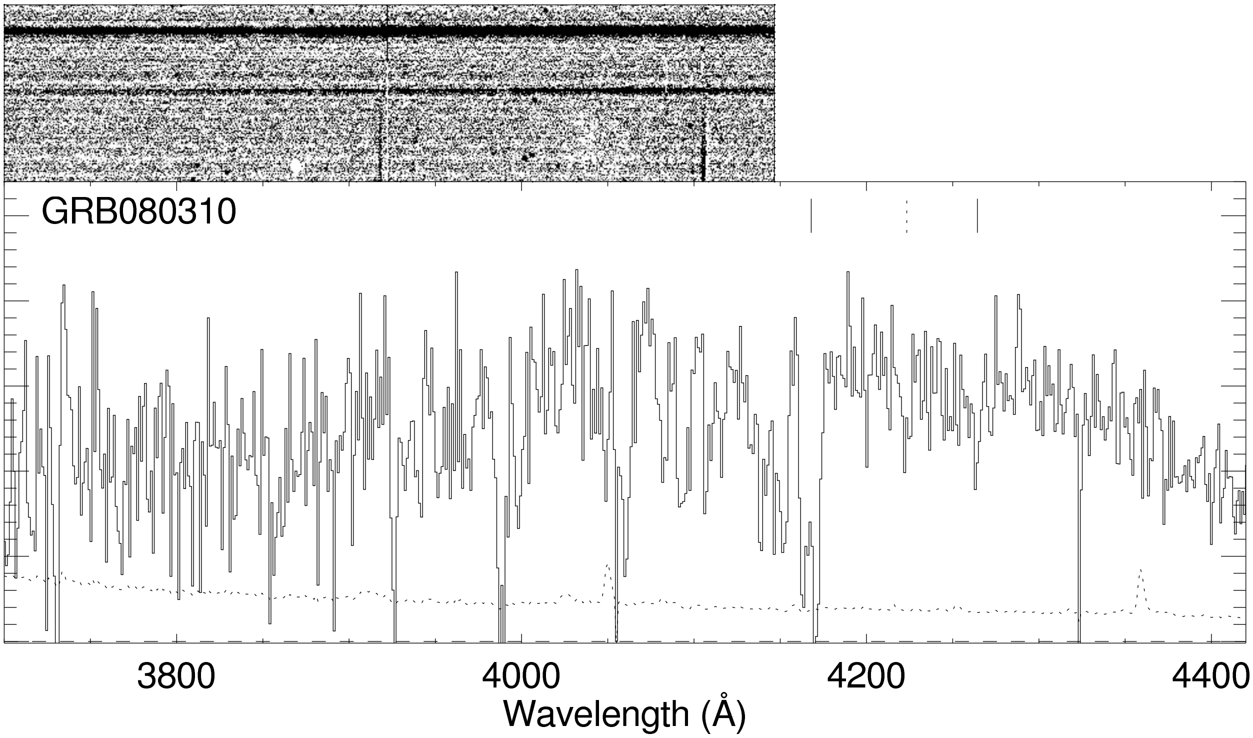
GRB080310
3800
4000
4200
4400
Wavelength (Å)

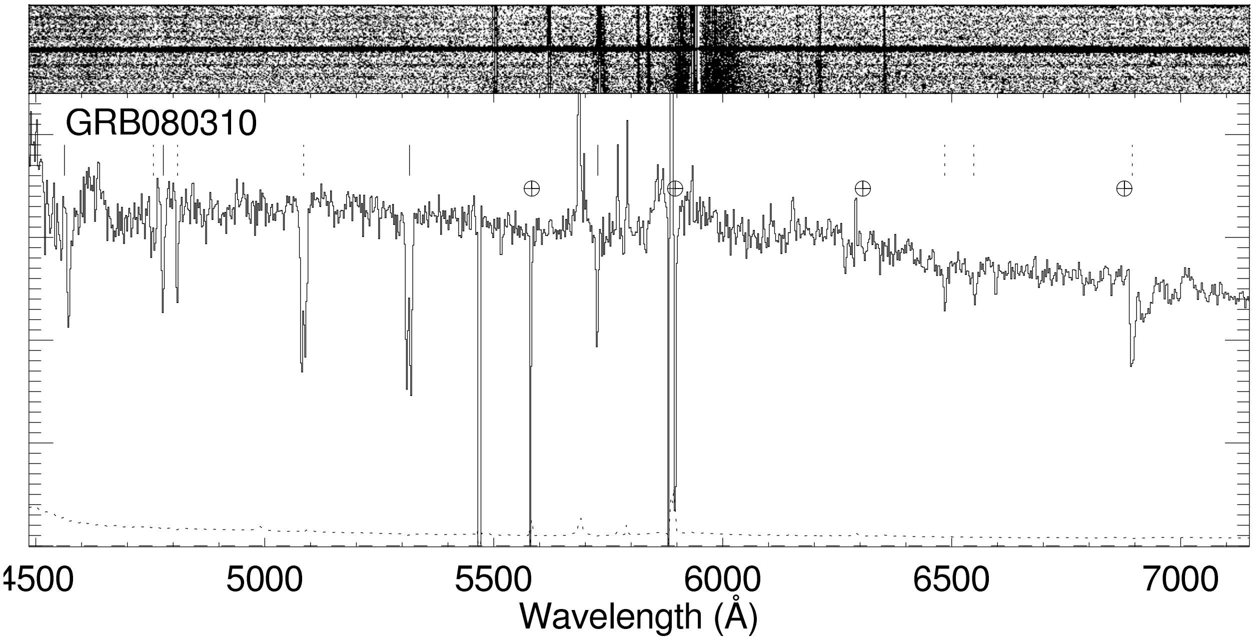
GRB080310
⊕
⊕
⊕
⊕
4500
5000
5500
6000
6500
7000
Wavelength (Å)

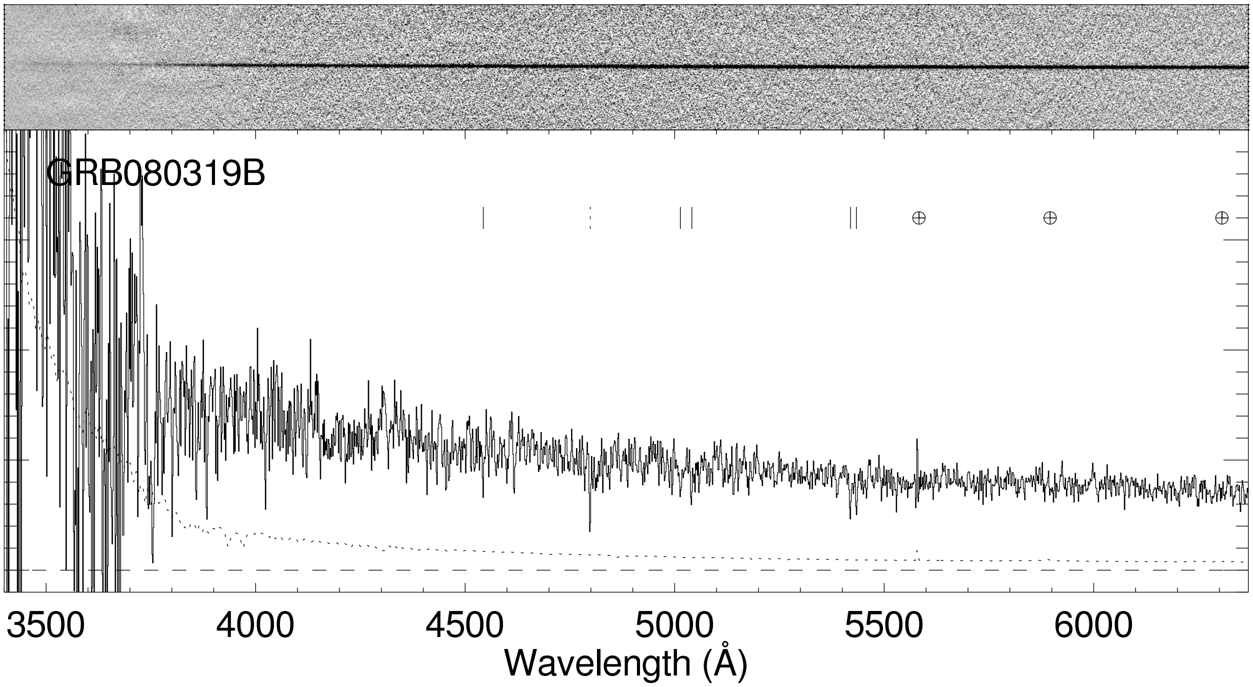
GRB080319B
⊕
⊕
⊕
3500
4000
4500
5000
5500
6000
Wavelength (Å)

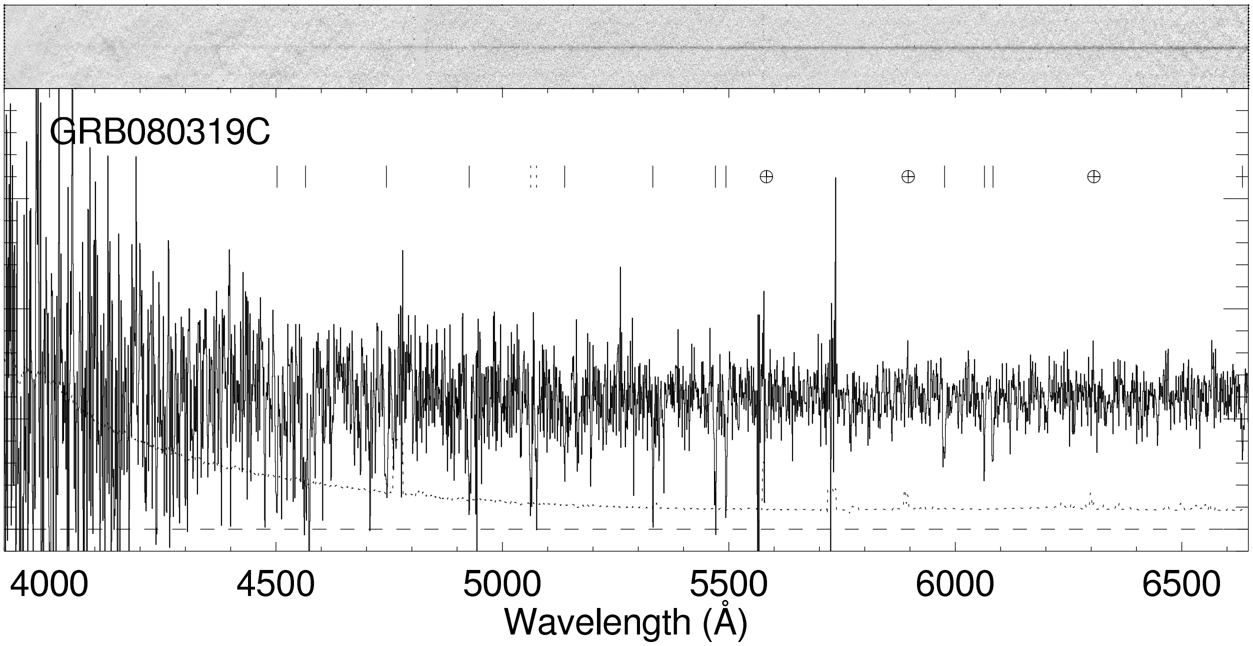
GRB080319C
4000
4500
5000
5500
6000
6500
Wavelength (Å)

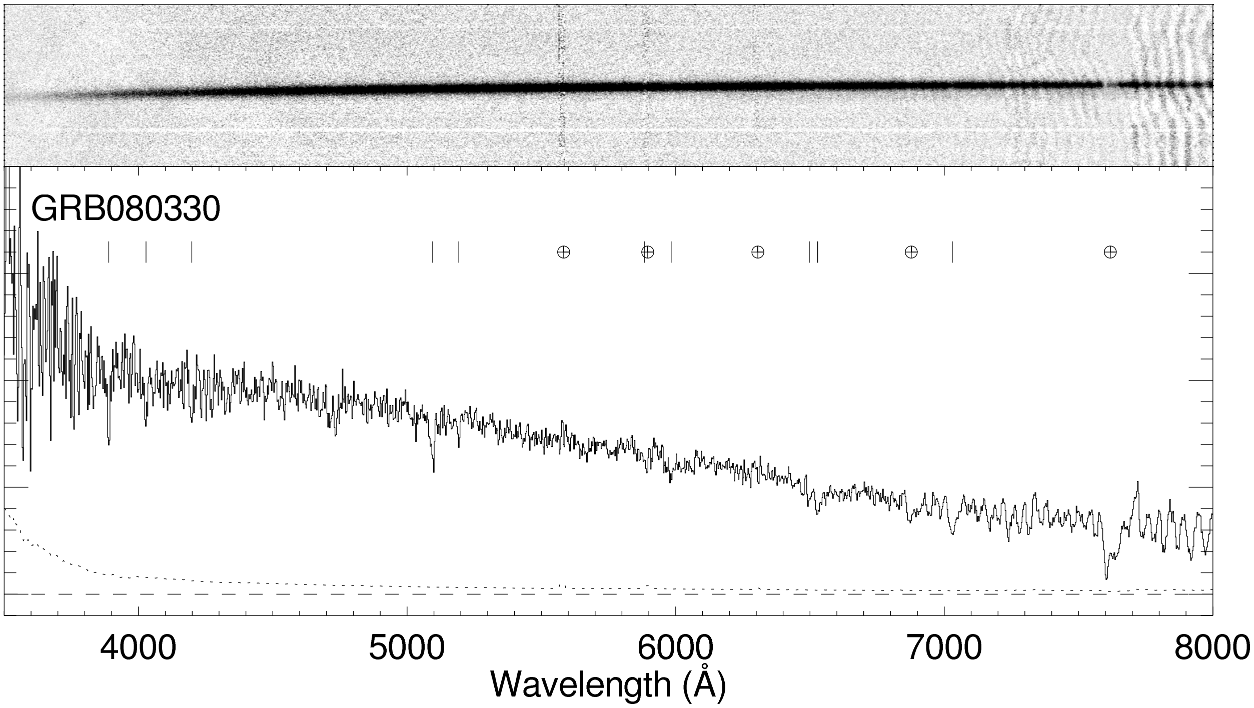
GRB080330
4000
5000
6000
7000
8000
Wavelength (Å)

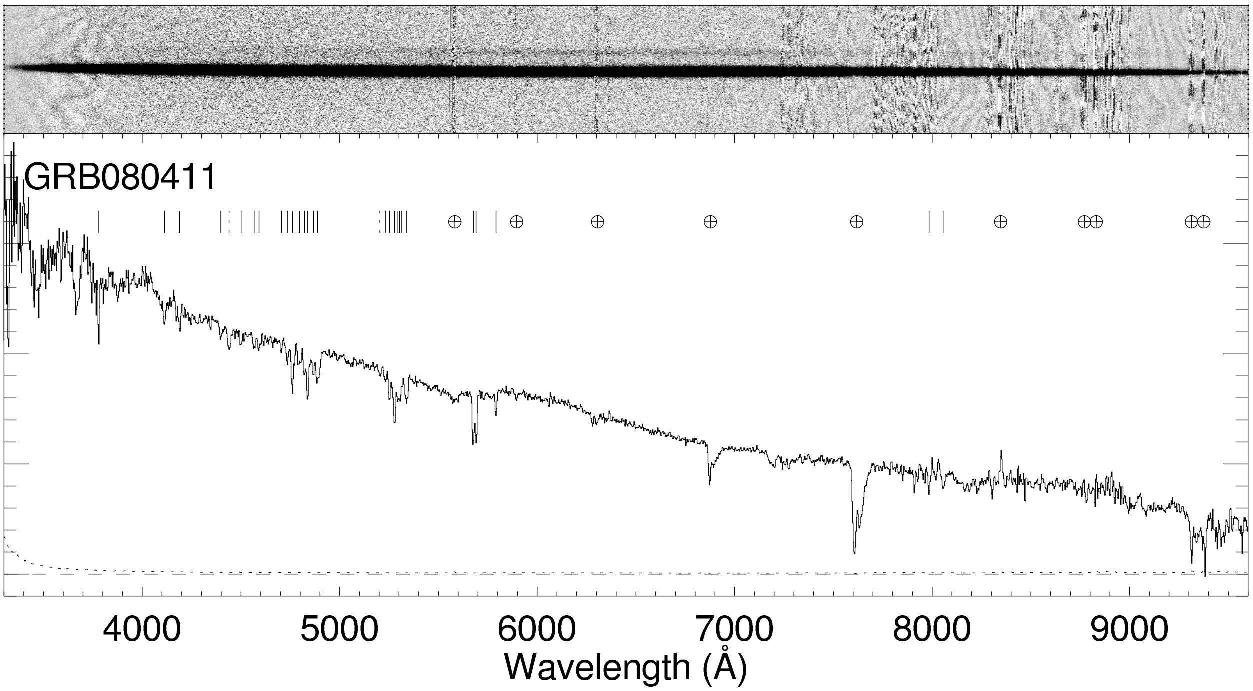
GRB080411
⊕ ⊕ ⊕ ⊕ ⊕ ⊕ ⊕⊕ ⊕⊕
4000
5000
6000
7000
8000
9000
Wavelength (Å)

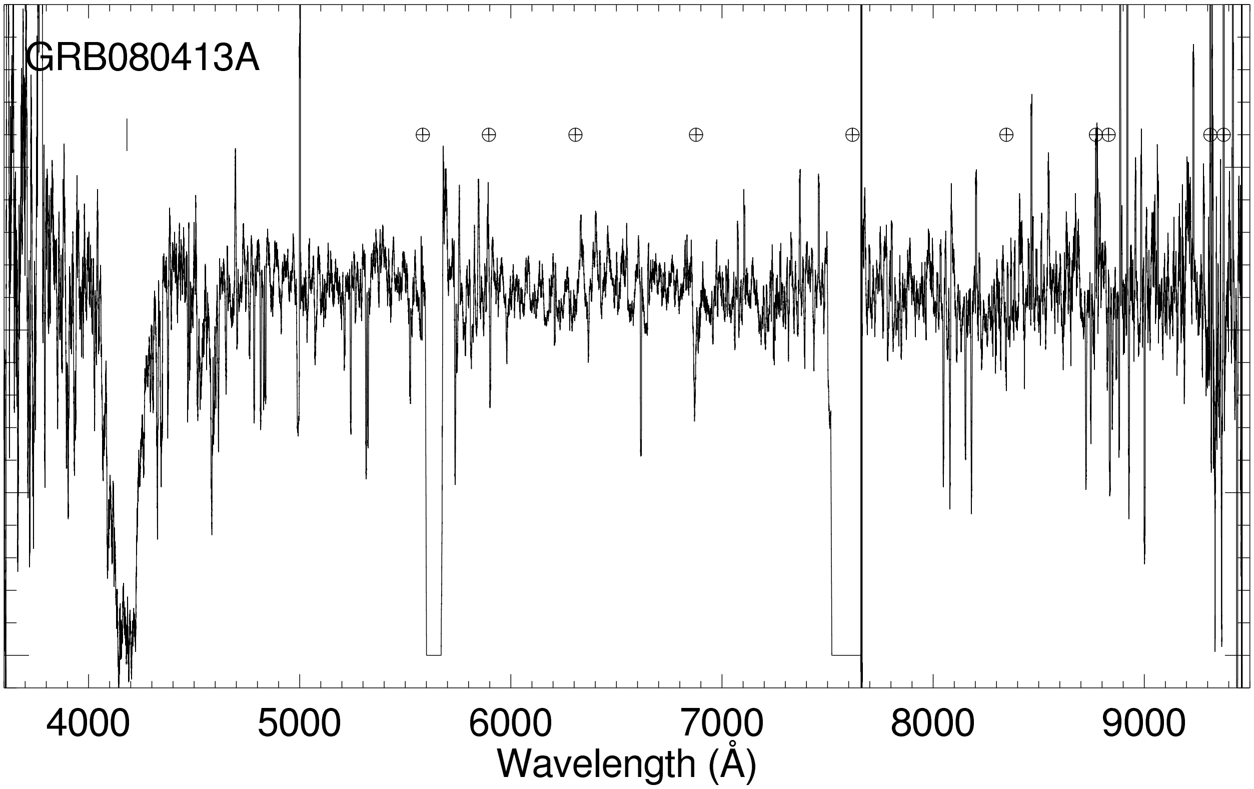
GRB080413A
⊕ ⊕ ⊕ ⊕ ⊕ ⊕ ⊕⊕ ⊕⊕
4000
5000
6000
7000
8000
9000
Wavelength (Å)

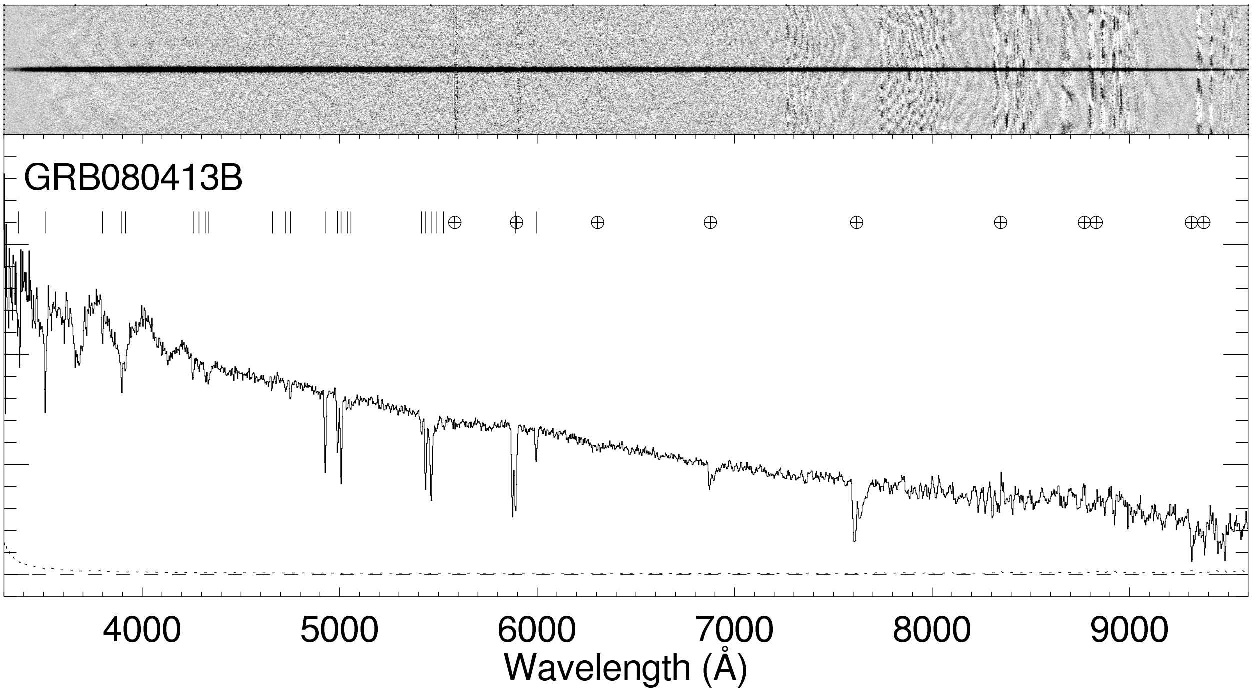
GRB080413B
4000
5000
6000
7000
8000
9000
Wavelength (Å)

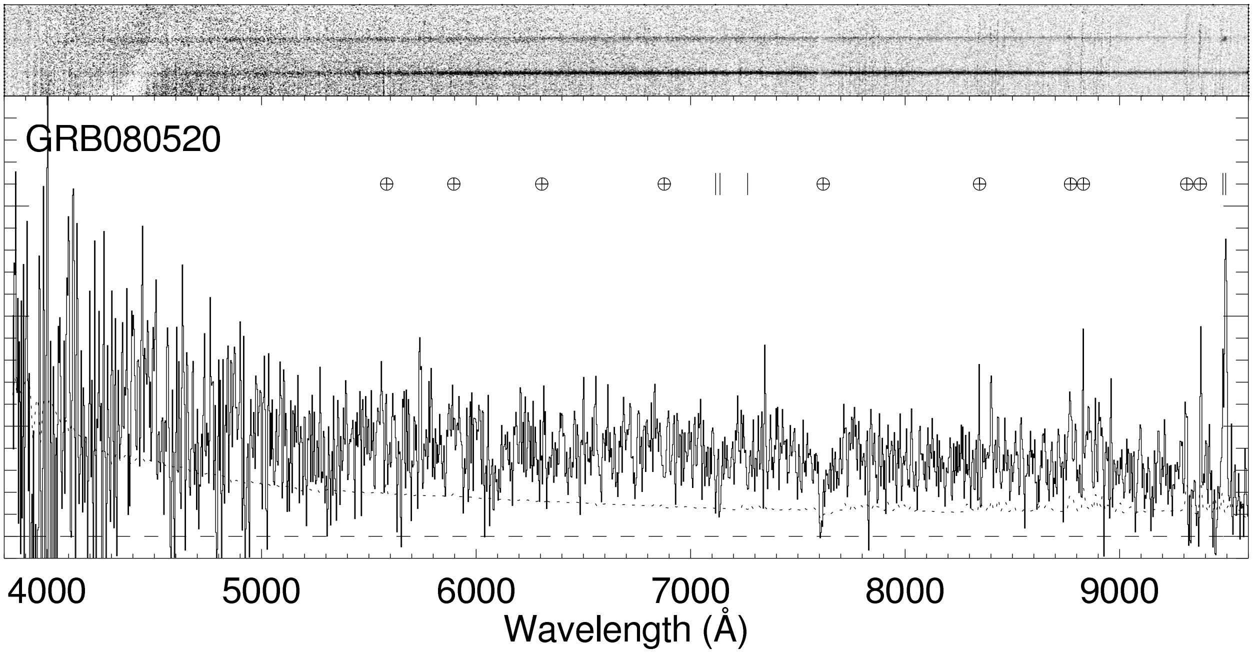
GRB080520
4000
5000
6000
7000
8000
9000
Wavelength (Å)

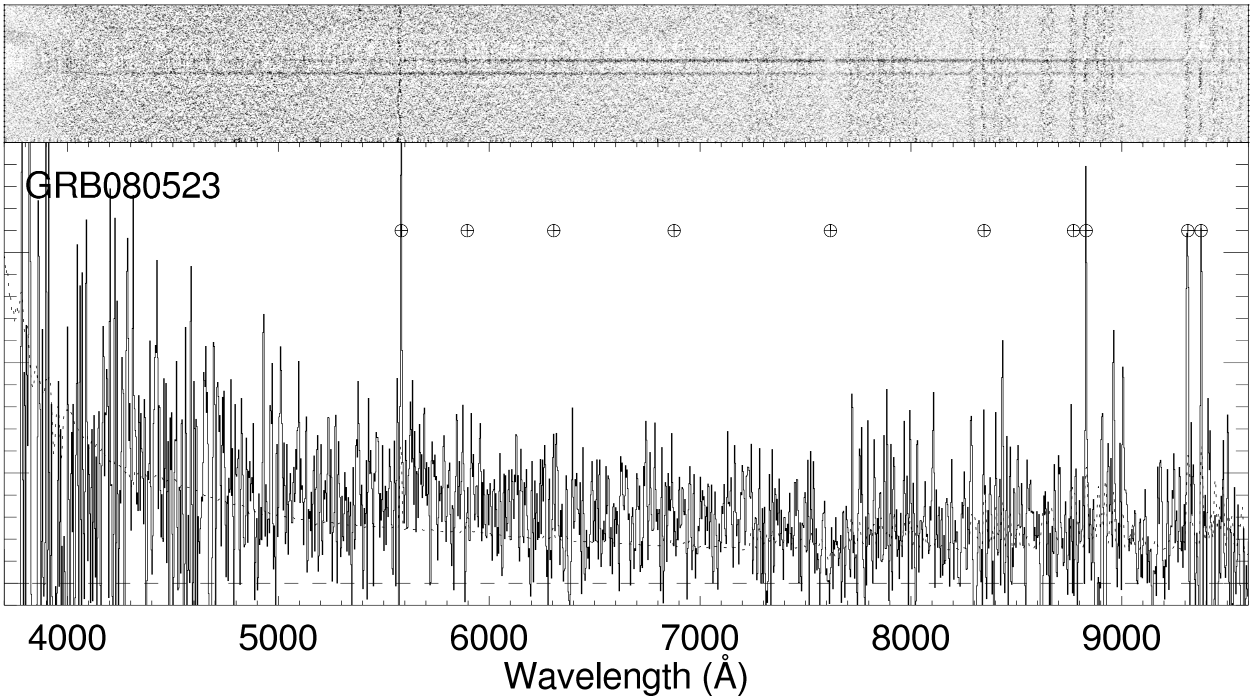
GRB080523
4000
5000
6000
7000
8000
9000
Wavelength (Å)

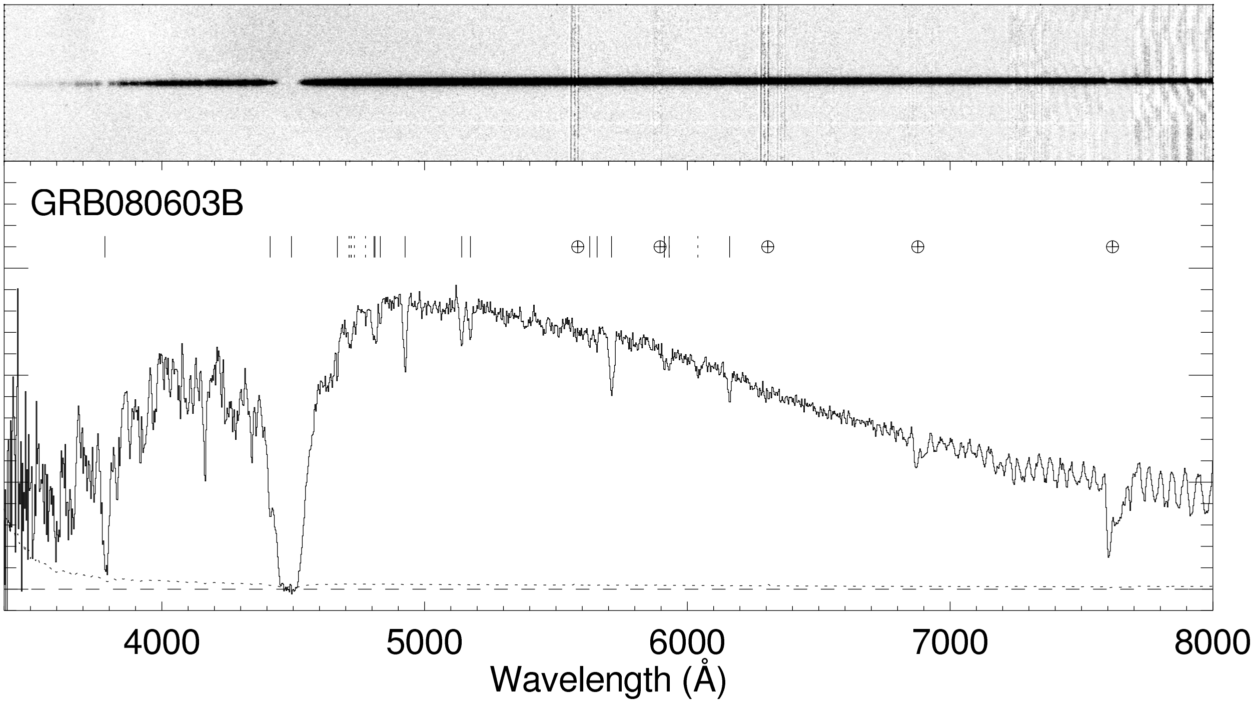
GRB080603B
⊕
4000
5000
6000
7000
8000
Wavelength (Å)

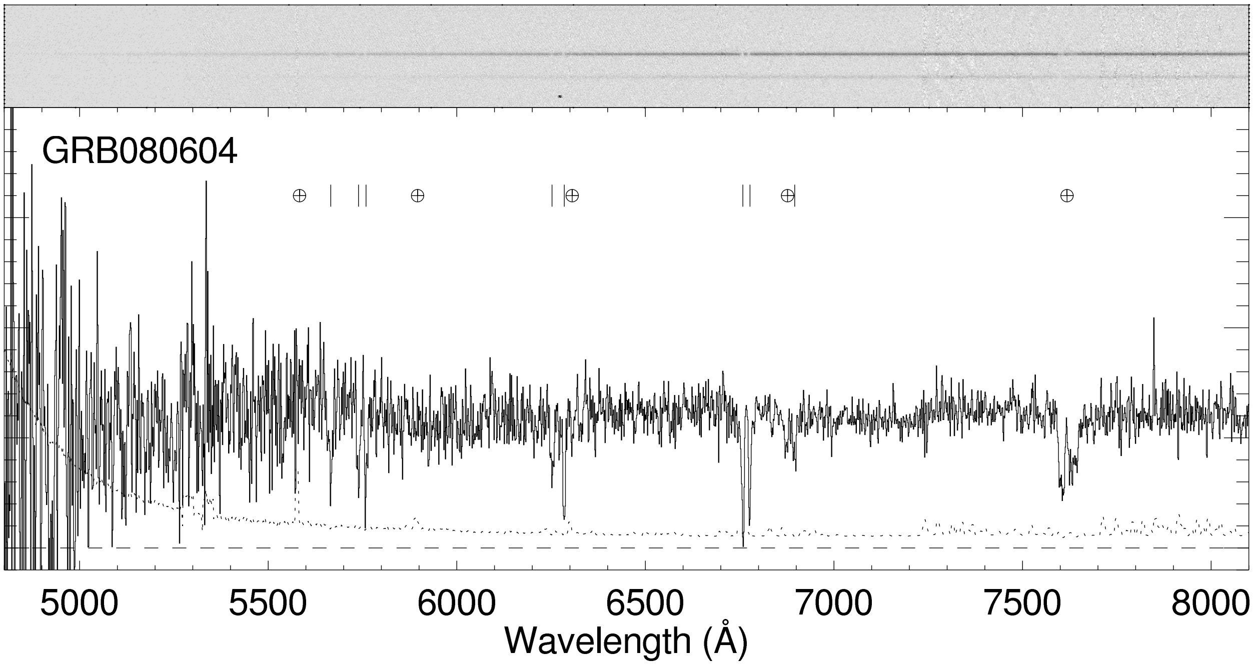
GRB080604
⊕
5000
5500
6000
6500
7000
7500
8000
Wavelength (Å)

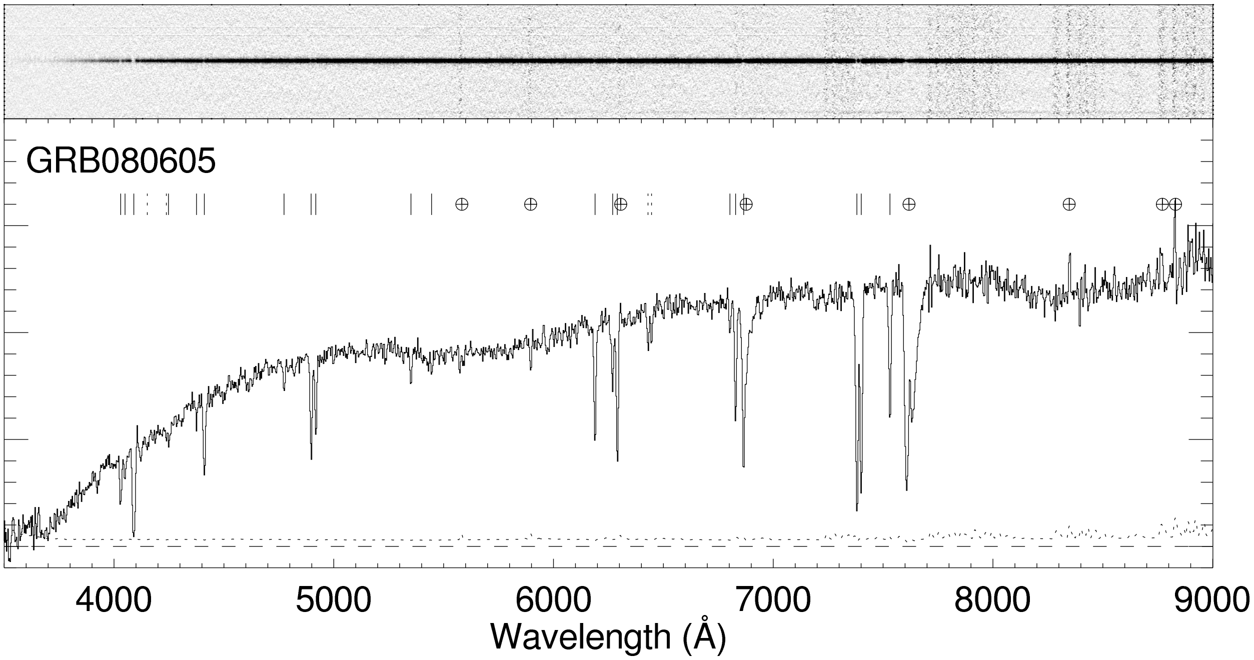
GRB080605
4000
5000
6000
7000
8000
9000
Wavelength (Å)

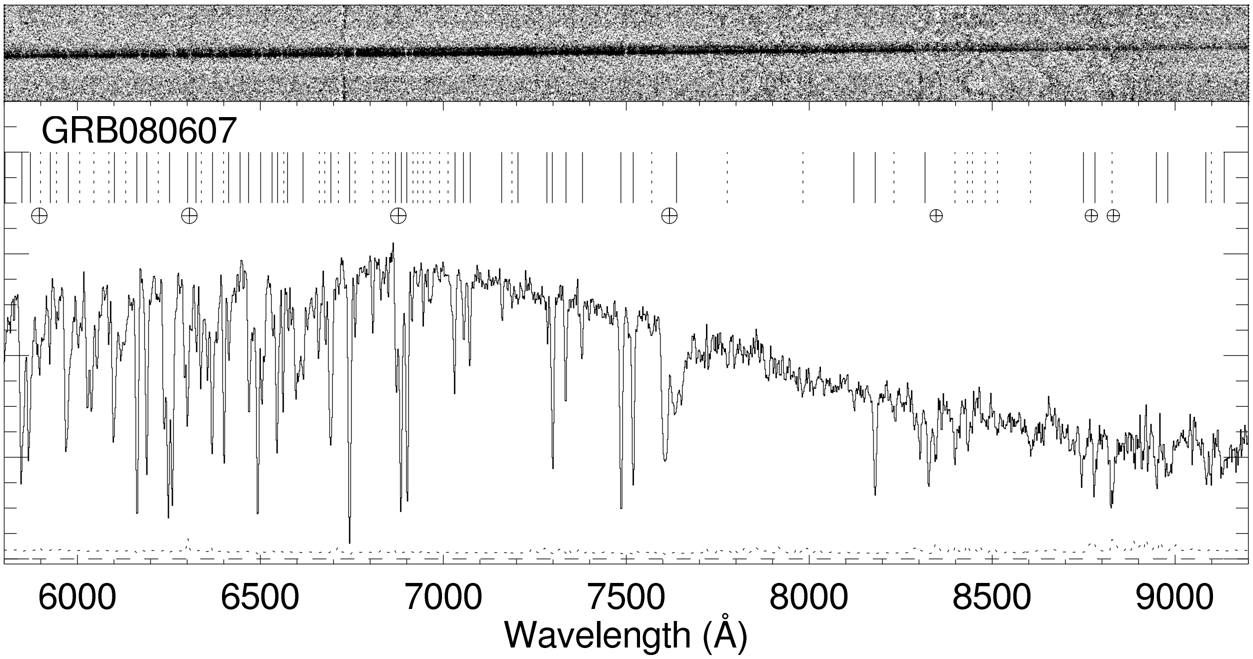
GRB080607
6000
6500
7000
7500
8000
8500
9000
Wavelength (Å)

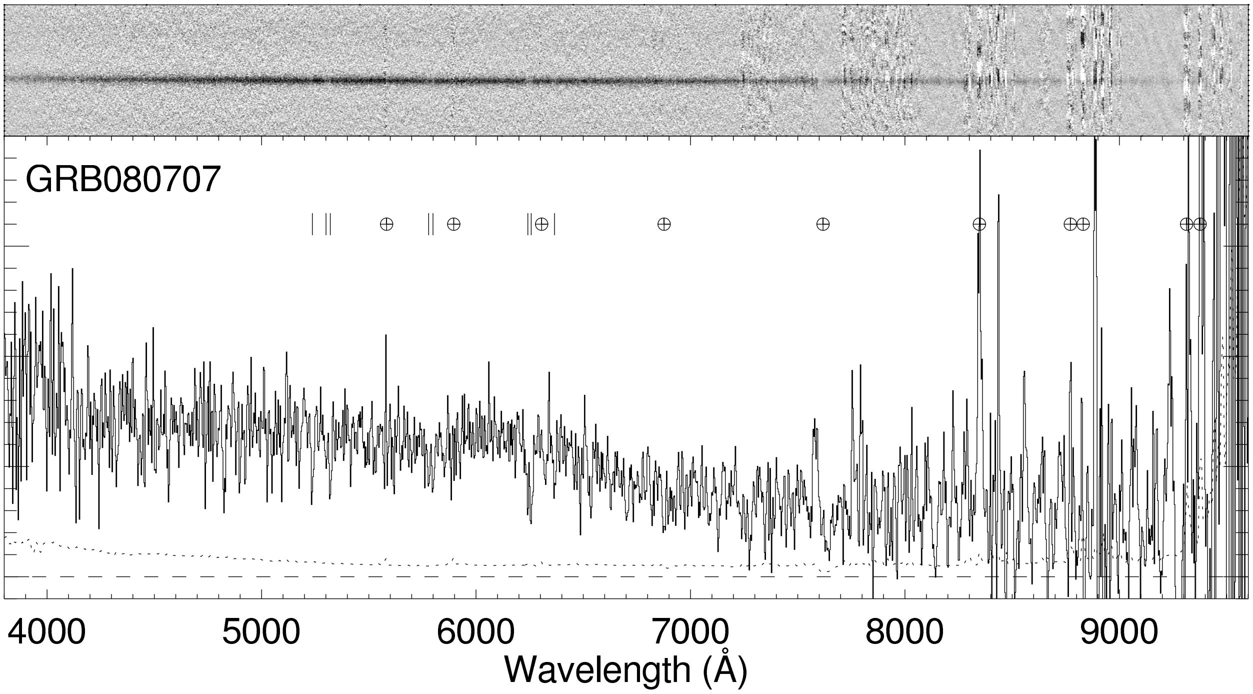
GRB080707
4000
5000
6000
7000
8000
9000
Wavelength (Å)

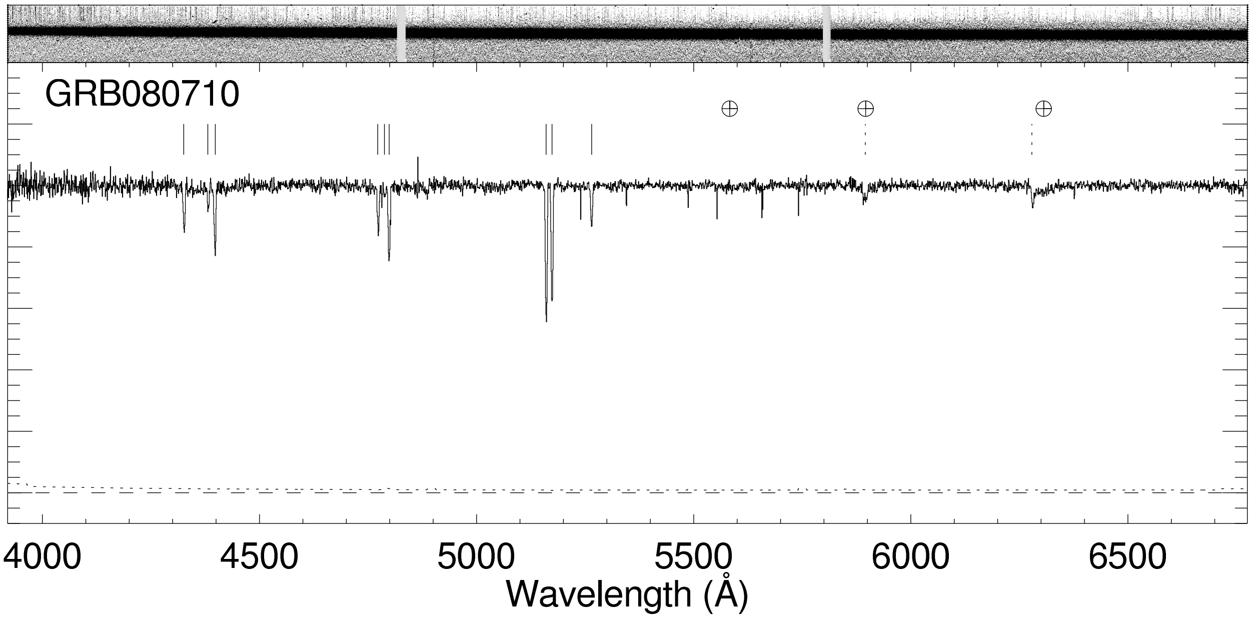
GRB080710
4000
4500
5000
5500
6000
6500
Wavelength (Å)

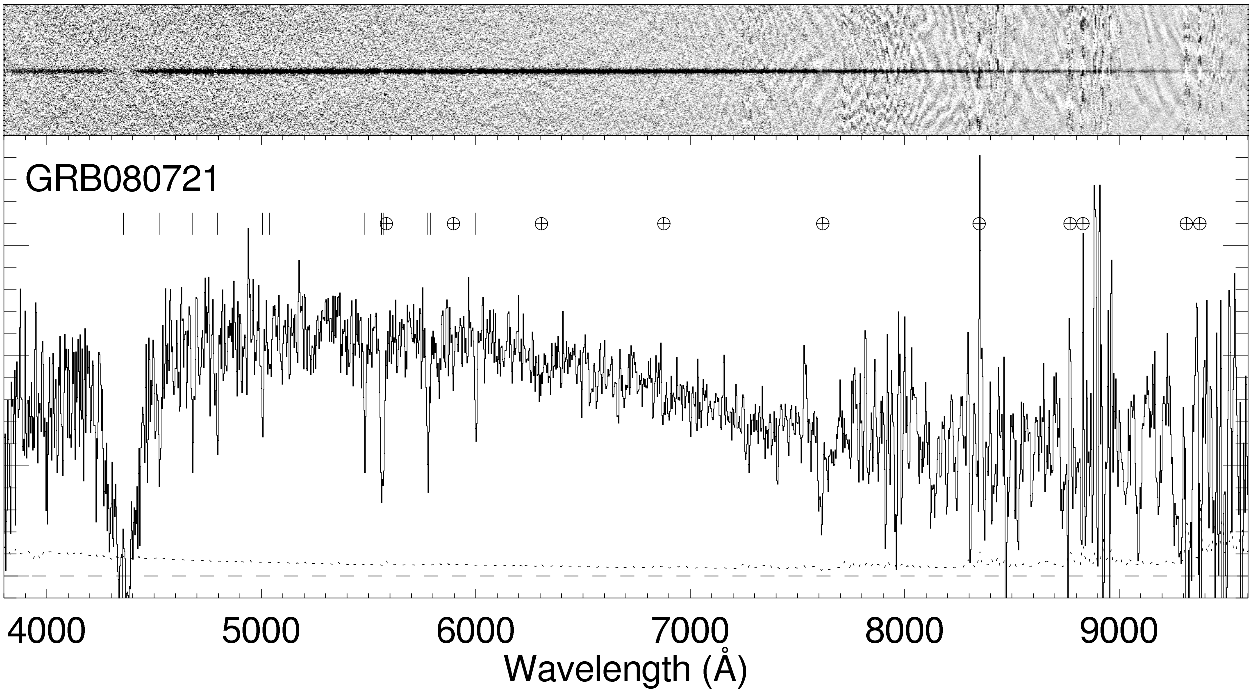
GRB080721
4000
5000
6000
7000
8000
9000
Wavelength (Å)

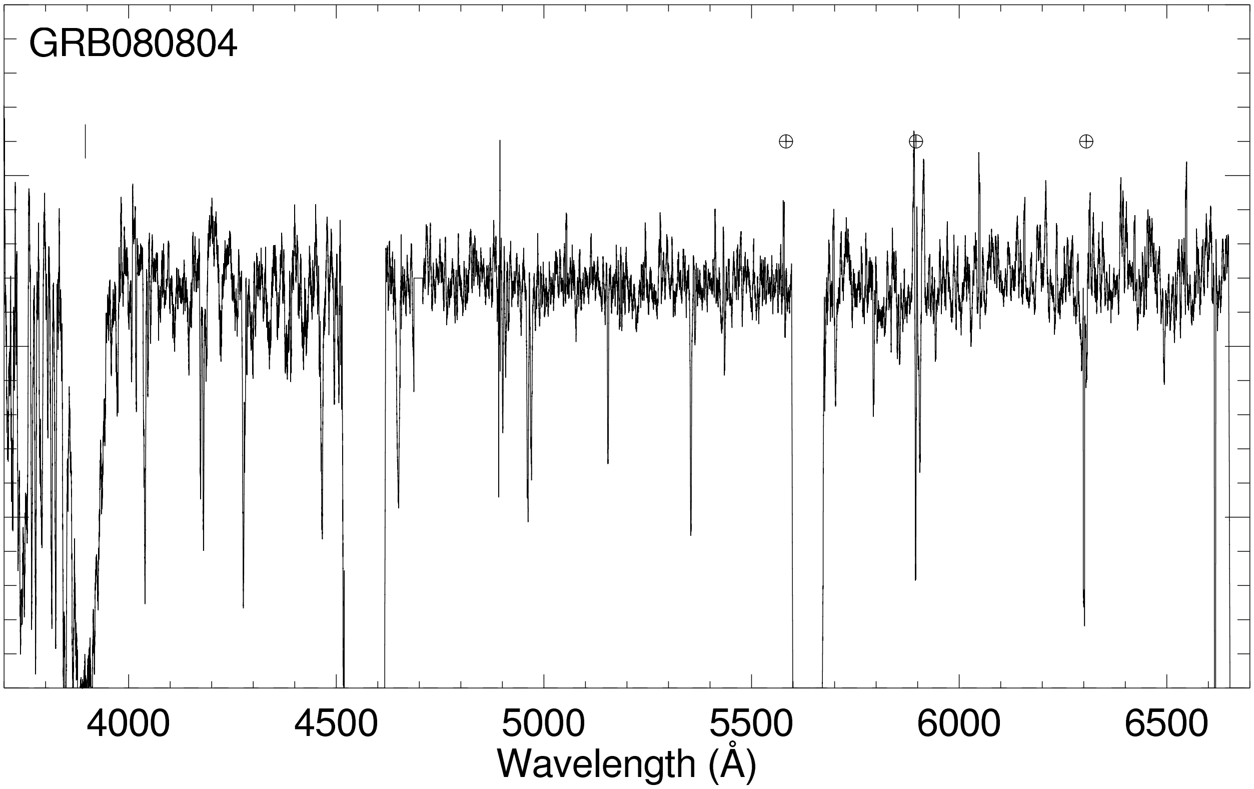
GRB080804
4000
4500
5000
5500
6000
6500
Wavelength (Å)

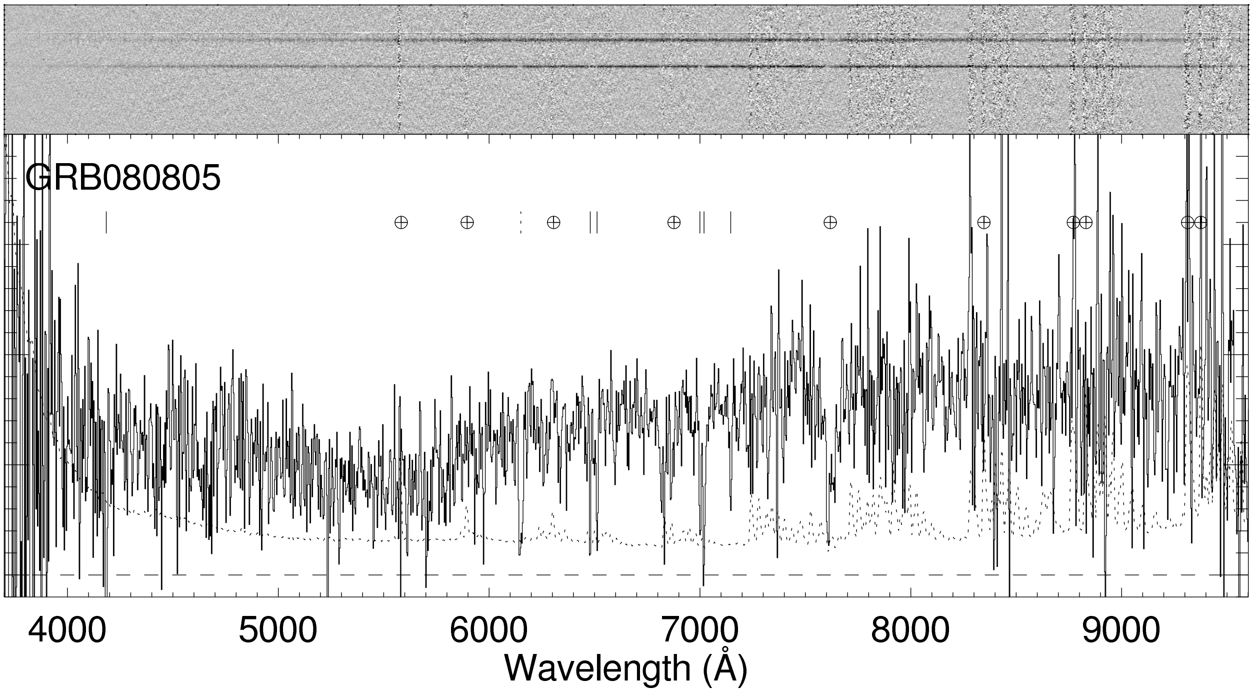
GRB080805
⊕
4000
5000
6000
7000
8000
9000
Wavelength (Å)

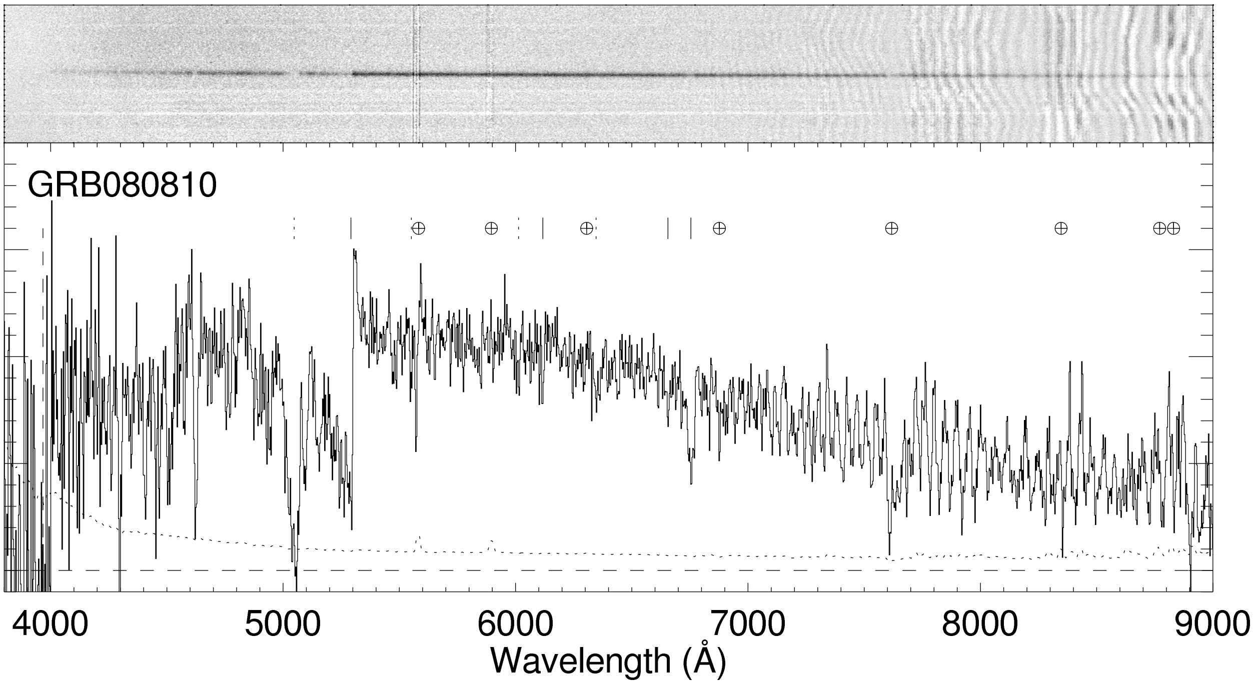
GRB080810
⊕
4000
5000
6000
7000
8000
9000
Wavelength (Å)

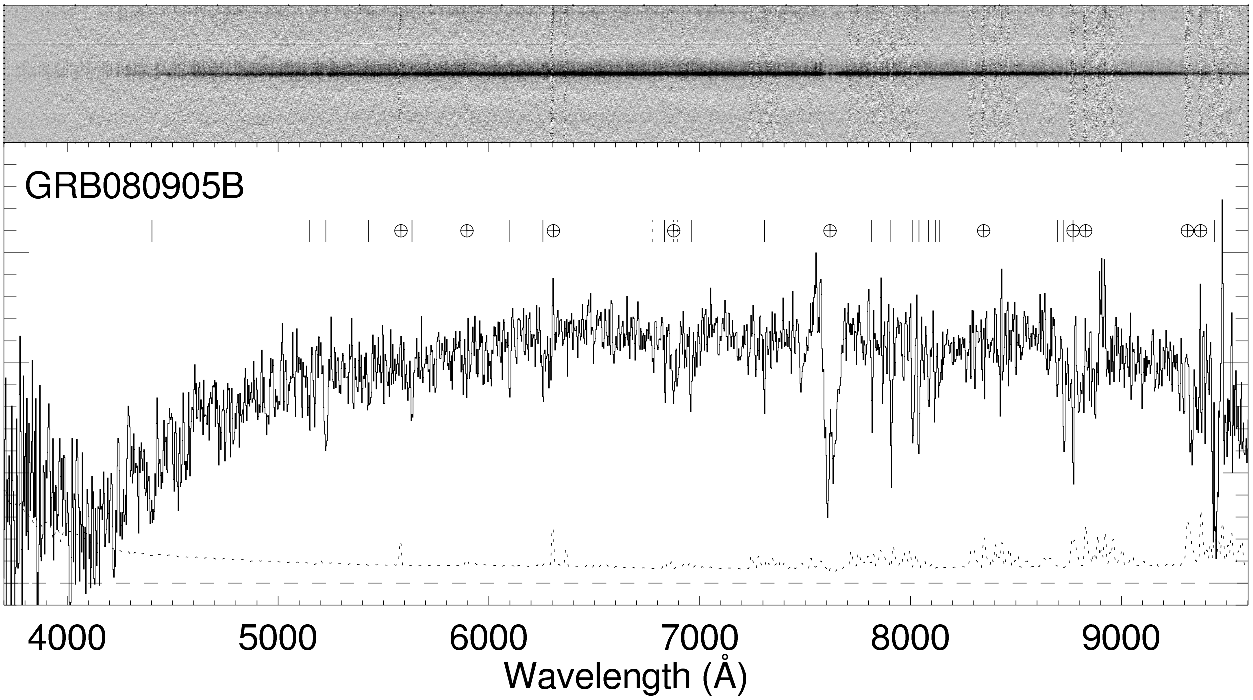
GRB080905B
4000
5000
6000
7000
8000
9000
Wavelength (Å)

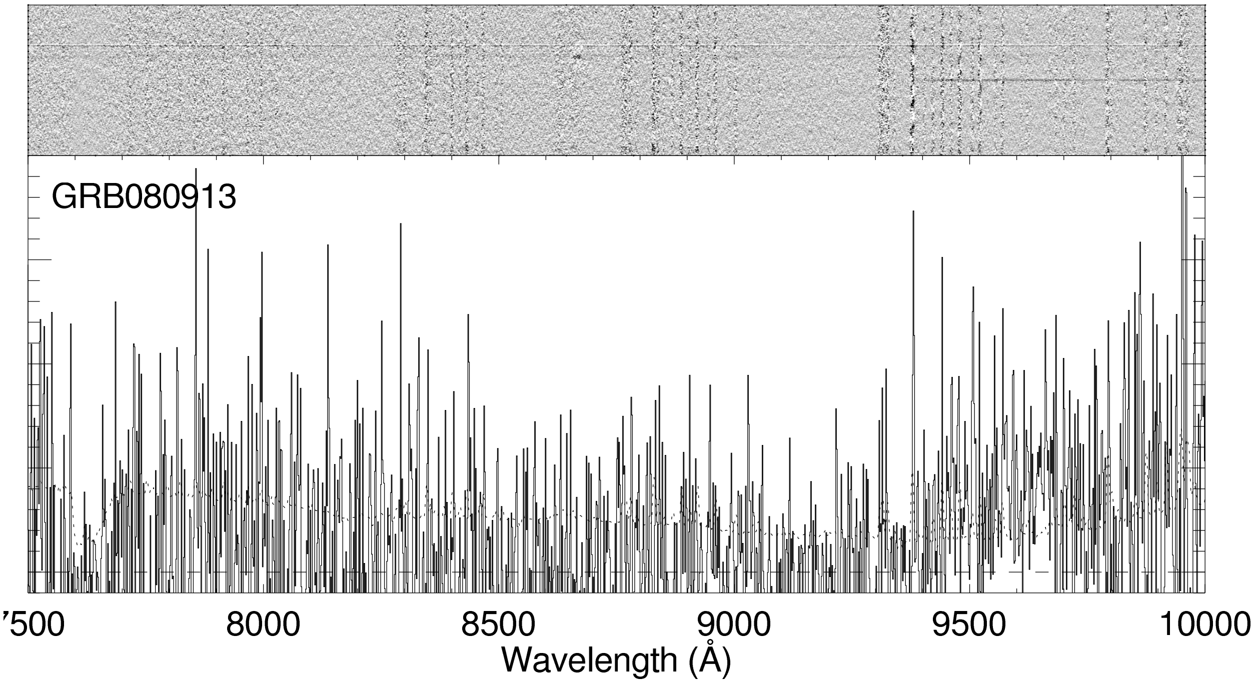
GRB080913
'500
8000
8500
9000
9500
10000
Wavelength (Å)

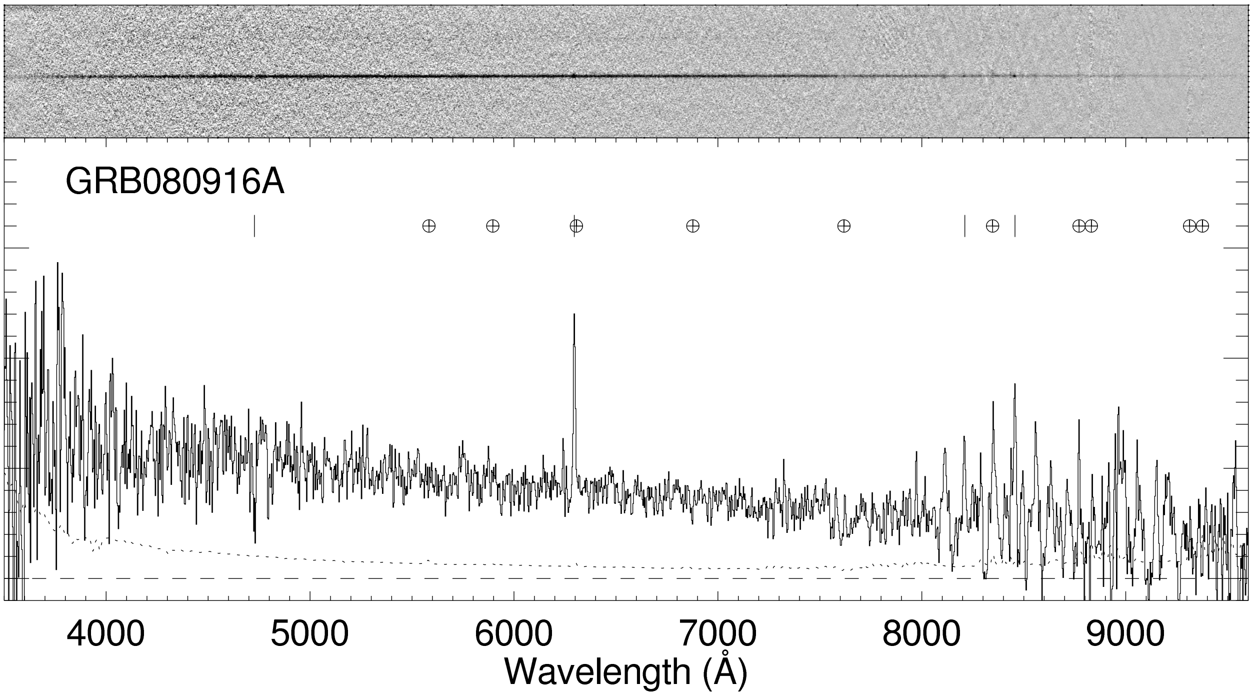
GRB080916A
⊕
4000
5000
6000
7000
8000
9000
Wavelength (Å)

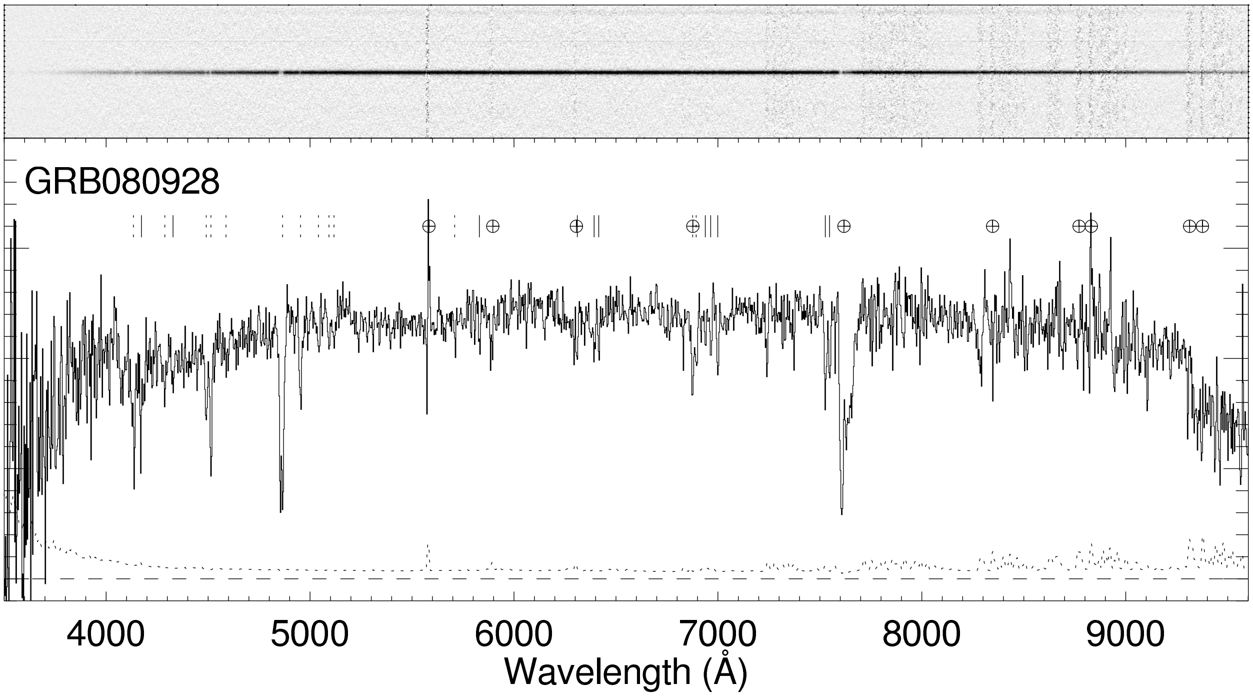
GRB080928
⊕
4000
5000
6000
7000
8000
9000
Wavelength (Å)

Table 73. The statistical sample. The z classes are a: afterglow spectrum; h: host galaxy emission, p: photometric redshift from afterglow imaging. For bursts where the optical afterglow is not detected we provide the excess X-ray absorption and the corresponding redshift limit when approriate (see maintext). We also provide references for redshift measurements.

GRB	z	z class	N_X [10^{21} cm^{-2}]	β_{OX}	Ref
080928	1.69	a	—	1.00	Vreeswijk et al. (2008e)
080916B	—	—	0	< 0.90	—
080916A	0.69	ah	—	0.69	Fynbo et al. (2008f)
080913	6.70	a	—	< 0.48	Greiner et al. (2009)
080905B	2.37	a	—	0.64	Vreeswijk et al. (2008d)
080810	3.35	a	—	0.96	de Ugarte Postigo et al. (2008)
080805	1.51	a	—	0.40	Jakobsson et al. (2008e)
080804	2.20	a	—	0.78	Thöne et al. (2008d)
080727A	—	—	0	< 0.76	—
080721	2.59	a	—	0.60	Jakobsson et al. (2008d)
080710	0.85	a	—	1.04	Perley et al. (2008)
080707	1.23	a	—	0.83	Fynbo et al. (2008d)
080703	< 5.5	a	—	0.42	Ward & Ziaeepour (2008)
080613B	—	—	0	< 0.79	—
080607	3.04	a	—	0.24	Prochaska et al. (2009)
080605	1.64	a	—	0.38	Jakobsson et al. (2008c)
080604	1.42	a	—	0.90	Wiersema et al. (2008b)
080603B	2.69	a	—	0.92	Fynbo et al. (2008c)
080602	—	—	1.0	< 0.28	—
080523	< 3.0	a	—	0.71	Fynbo et al. (2008b)
080520	1.55	ah	—	0.77	Jakobsson et al. (2008b)
080430	0.77	a	—	0.77	Cucchiara & Fox (2008)
080413B	1.10	a	—	0.89	Vreeswijk et al. (2008c)
080330	1.51	a	—	0.99	Guidorzi et al. (2009)
080325	—	—	1.5	< 0.79	—
080320	< 6.4	a	—	< 0.15	Tanvir et al. (2008b)
080319C	1.95	a	—	0.31	Wiersema et al. (2008a)
080319B	0.94	a	—	0.67	Vreeswijk et al. (2008b)
080319A	< 4.2	h	—	0.49	Perley et al. (2009)
080310	2.43	a	—	0.88	Fox et al. (2008)
080307	< 6.1	a	—	0.40	Xin et al. (2008)
080212	< 3.5	a	—	0.66	Kuepcue Yoldas et al. (2008)
080210	2.64	a	—	0.74	Jakobsson et al. (2008a)

Table 73—Continued

GRB	z	z class	N_X [10^{21} cm^{-2}]	β_{OX}	Ref
080207	< 3.5 (XRT)	—	6.1	< 0.43	—
080205	< 5.5	a	—	0.79	Oates & Markwardt (2008)
071122	1.14	a	—	0.83	Cucchiara et al. (2007a)
071117	1.33	h	—	0.58	Jakobsson et al. (2007e)
071112C	0.82	ah	—	0.72	Jakobsson et al. (2007d)
071031	2.69	a	—	0.97	Ledoux et al. (2008)
071025	5.2	ap	—	0.50	This work
071021	< 5.6	a	—	—	Piranomonte et al. (2007)
071020	2.15	a	—	0.56	Jakobsson et al. (2007c)
070808	< 3.5 (XRT)	—	6.5	< 0.48	—
070802	2.45	a	—	0.49	Elíasdóttir et al. (2009)
070721B	3.63	a	—	0.72	Malesani et al. (2007)
070621	< 3.5 (XRT)	—	3.2	< 0.53	—
070611	2.04	a	—	0.73	Thöne et al. (2007a)
070521	1.35	h	—	< -0.06	Perley et al. (2009)
070520B	—	—	0.6	< 0.88	—
070518	< 2.0	a	—	0.81	Cucchiara et al. (2007c)
070506	2.31	a	—	0.93	Thöne et al. (2007b)
070419B	< 5.9	a	—	0.25	de Ugarte Postigo et al. (2007)
070419A	0.97	a	—	0.94	Cenko et al. (2007)
070412	—	—	0.7	< 0.17	—
070330	< 5.5	a	—	0.68	Kuin et al. (2007)
070328	—	—	1.8	< 0.31	—
070318	0.84	a	—	0.78	Jaunsen et al. (2007a)
070306	1.50	h	—	< 0.23	Jaunsen et al. (2008)
070224	< 6.1	a	—	0.92	Thöne et al. (2007c)
070223	< 6.1	a	—	—	Rol et al. (2007b)
070219	< 3.5 (XRT)	—	2.2	< 0.38	—
070208	1.17	ah	—	0.68	Cucchiara et al. (2007b)
070129	< 3.4	a	—	0.62	This work
070110	2.35	ah	—	0.77	Jaunsen et al. (2007b)
070103	< 3.5 (XRT)	—	2.1	< 0.48	—
061222A	2.09	h	—	< 0.22	Perley et al. (2009)

Table 73—Continued

GRB	z	z class	N_X [10^{21} cm^{-2}]	β_{OX}	Ref
061121	1.31	a	—	0.64	Bloom et al. (2006b)
061110B	3.44	a	—	0.55	Fynbo et al. (2006a)
061110A	0.76	ah	—	0.99	Fynbo et al. (2007)
061102	—	—	0	< 0.91	—
061021	0.35	a	—	0.75	This work
061007	1.26	ah	—	0.79	Jakobsson et al. (2006d)
061004	—	—	0	< 0.47	—
061002	—	—	0.6	< 0.93	—
060929	—	—	0.4	< 0.67	—
060927	5.47	a	—	0.55	Ruiz-Velasco et al. (2007)
060923C	< 11.0	a	—	< 0.31	Fox (2006)
060923B	—	—	1.9	< 0.68	—
060923A	< 2.8	h	—	< 0.11	Tanvir et al. (2008a)
060919	< 3.5 (XRT)	—	5.5	< 1.02	—
060912A	0.94	h	—	0.62	Levan et al. (2007)
060908	1.88	a	—	0.38	This work
060904A	—	—	0	< 0.52	—
060814	0.84	h	—	< -0.06	Thöne et al. (2007d)
060807	< 3.4	a	—	0.54	This work
060805A	—	—	0.1	< 1.07	—
060729	0.54	a	—	0.80	Thöne et al. (2006a)
060719	< 4.6	a	—	< -0.13	This work
060714	2.71	ah	—	0.77	Jakobsson et al. (2006b)
060712	—	—	1.1	< 0.96	—
060708	1.92	p	—	1.04	Oates et al. (2009)
060707	3.43	a	—	0.73	Jakobsson et al. (2006b)
060614	0.13	h	—	0.79	Della Valle et al. (2006)
060607A	3.08	a	—	0.53	Fox et al. (2008)
060605	3.78	a	—	1.00	Savaglio et al. (2006)
060604	< 2.8	a	—	0.75	Blustin & Page (2006)
060526	3.21	a	—	1.03	Jakobsson et al. (2006b)
060522	5.11	a	—	0.74	Cenko et al. (2006)
060512	2.1	a	—	0.98	This work

Table 73—Continued

GRB	z	z class	N_X [10^{21} cm^{-2}]	β_{OX}	Ref
060502A	1.51	a	—	0.65	Cucchiara et al. (2006b)
060428B	< 5.5	a	—	1.00	de Pasquale & Campana (2006)
060427	—	—	0.7	< 0.81	—
060323	< 4.4	a	—	0.76	(Marshall & Vetere2006)
060319	1.15	h	—	< 0.41	D. Perley (private comm.)
060306	< 3.5 (XRT)	—	3.2	< 0.54	—
060219	< 3.5 (XRT)	—	2.6	< 0.54	—
060218	0.03	h	—	—	Sollerman et al. (2006)
060210	3.91	a	—	0.37	Cucchiara et al. (2006a)
060206	4.05	a	—	0.95	Fynbo et al. (2006b)
060204B	< 4.8	a	—	0.47	Fynbo et al. (2006d)
060202	0.78	h	—	< 0.20	Butler (2007)
060124	2.30	a	—	0.80	Mirabal & Halpern (2006)
060115	3.53	a	—	0.78	Piranomonte et al. (2006a)
060111A	< 5.5	a	—	0.70	Blustin et al. (2006)
060108	< 3.2	a	—	0.51	Oates et al. (2006)
051117B	—	—	0.6	< 1.06	—
051016B	0.94	h	—	0.63	Soderberg et al. (2005)
051006	< 3.5 (XRT)	—	5.1	< 1.30	—
051001	—	—	0.9	< 0.56	—
050922C	2.20	a	—	0.99	Jakobsson et al. (2006b)
050922B	—	—	1.1	< 0.58	—
050915A	< 15.0	a	—	< 0.44	Bloom (2005)
050908	3.34	a	—	1.14	Fugazza et al. (2005)
050904	6.30	a	—	< 0.41	Kawai et al. (2006)
050824	0.83	ah	—	0.91	Sollerman et al. (2007)
050822	—	—	0.6	—	—
050820A	2.61	a	—	0.77	Fox et al. (2008)
050819	—	—	0	< 0.90	—
050814	5.3	p	—	0.51	Jakobsson et al. (2006a)
050803	—	—	1.2	< -0.15	—
050802	1.71	a	—	0.51	Fynbo et al. (2005)
050801	1.38	p	—	0.95	Oates et al. (2009)

REFERENCES

Akerman, C. J., Ellison, S. L., Pettini, M., & Steidel, C. C. 2005, A&A, 440, 499

Aoki, K., Totani, T., Hattori, T., et al. 2008, PASJ, 61, 387

Berger, E., Kulkarni, S. R., Fox, D. B., et al. 2005, ApJ, 634, 501

Berger, E., Penprase, B. E., Cenko, S. B., Kulkarni, S. R., Fox, D. B., Steidel, C. C., & Reddy, N. A. 2006, ApJ, 642, 979

Berger, E., Fox, D. B., Kulkarni, S. R., Frail, D. A., & Djorgovski, S. G. 2007, ApJ, 660, 504

Bloom, J. S., Kulkarni, S. R., Djorgovski, S. G. 2002, AJ, 123, 1111

Bloom, J. S. 2003, AJ, 125, 2865

Bloom, J. S. 2005, GCN 3990

Bloom, J. S., Foley, R. J., Koceveki, D., & Perley, D. 2006a, GCN 5217

Bloom, J. S., Perley, D. A., & Chen, H.-W. 2006b, GCN 5826

Bloom, J. S., Perley, D. A., Li, W., et al. 2009 ApJ, 691, 723

Blustin, A. J., Zane, S., Rosen, S. R. 2006, GCN 4482

Blustin, A. J., & Page, M. J. 2006, GCN 5219

Butler, N., 2006, GCN 5435

Butler, N. R. 2007, ApJ, 656, 1001

Campana, S., Mangano, V., Blustin, A. J., et al. 2006, Nature, 442, 1008

Castro-Tirado, A., Amado, P., Negueruela, I., et al. 2006, GCN 5218

Cenko, S. B., & Fox, D. B. 2006, GCN 5975

Cenko, S. B., Fox, D. B., Rich, J., Schmidt, B., Christiansen, J., & Berger, E. 2005, GCN 3357

Cenko, S. B., Berger, E., Djorgovski, S. G., Mahabal, A. A., & Fox, D. B. 2006, GCN 5155

Cenko, S. B., Gezari, S., Small, T., Fox, D. B., & Chornock, R. 2007, GCN 6322

Cenko, S. B., Fox, D. B., Penprase, B. E., et al. 2008, ApJ, 677, 441

Chen, H.-W., Prochaska, J. X., Bloom, J. S., & Thompson, I. B. 2005, ApJ, 634, L25

Chen, H.-W., Prochaska, J. X., & Gnedin, N. Y. 2007a, ApJ, 667, L125

Chen, H.-W., Prochaska, J. X., Ramirez-Ruiz, E., Bloom, J.S., Dessauges-Zavadsky, M. & Fole, R.J. 2007b, ApJ, 663, 420

Chen, H.-W., Perley, D. A., Pollack, L. K., et al. 2009, ApJ, 691, 152

Christensen, L., Hjorth, J., Gorosabel, J. 2004 A&A, 425, 913

Costa, E., et al., 1997, Nature 387, 783

Coward, D. M., 2009, MNRAS, 393, L65

Cucchiara, A., Fox, D. B., Penprase, B. E., et al. 2006a, NCimB, 121, 1455

Cucchiara, A., Price, P. A., Fox, Cenko, S. B., & Schmidt, B. P. 2006b, GCN 5052

Cucchiara, A., Fox, D. B., & Cenko, S. B. 2007a, GCN 7124

Cucchiara, A., Fox, D. B., Cenko, S. B., & Price, P. A. 2007b, GCN 6083

Cucchiara, A., Marshall, F. E., & Guidorzi, C. 2007c, GCN 6419

Cucchiara, A., & Fox, D. B. 2008, GCN 7654

Curran, P. A., van der Horst, A. J., Beardmore, A. P, et al. 2007, A&A, 467, 1049

Cucchiara, A., Jones, T., Charlton, J. C., et al. 2009, ApJ, 697, 345

D'Elia, M., Melandri, A., Fiore, F., et al. 2005, GCN 3746

D'Elia, M., Guetta, D., Antonelli, L. A., et al. 2007, A&A, 467, 629

D'Elia, M., Fiore, F., Perna, R., et al. 2009a, ApJ, 694, 332

D'Elia, M., Fiore, F., Perna, R., et al. 2009b, A&A, 503, 437

Della Valle, M., Chincarini, G., Panagia, N., et al. 2006, Nat, 444, 1050

De Pasquale, M. & Cummings, J. 2006, GCN 5130

de Pasquale, M., & Campana, S. 2006, GCN 5035

Dessauges-Zavadsky, M., Chen, H.W., Prochaska, J. X., Bloom, J. S., & Barth, A. J. 2006, ApJ, 648, L89

Elíasdóttir, Á., Fynbo, J. P. U., Hjorth, J., et al. 2009, ApJ, 697, 1725

Ellison, S. L., Yan, L., Hook, I. M, et al. 2001, A&A, 379, 393

Ellison, S. L., York, B. A., Pettini, M., & Kanekar, N. 2008, MNRAS, 388, 1349

Evans, P., Beardmore, A. P., Page, K. L., et al. 2009, MNRAS, 397, 1177

Fiore, F., Guetta, D., Piranomonte, S., D'Elia, V., & Antonelli, L. A. 2007, A&A, 470, 515

Foley, R. J., Chen, H.-W., Bloom, J., & Prochaska, J. X. 2005, GCN 3483

Foley, R. J., Perley, D. A., Pooley, D., et al. 2007, ApJ, 645, 450

Fox, D. B. 2006, GCN 5607

Fox, A. J., Ledoux, C., Vreeswijk, P. M., Smette, A., & Jaunsen, A. O. 2008, A&A, 491, 189

Fruchter, A. S., Krolik, J. H., Rhoads, J. E. 2001, ApJ, 563, 597

Fruchter, A. S., Levan, A., Strolger, L., et al. 2006 Nature, 441, 463

Fugazza, D., et al. 2005, GCN 3948

Fugazza, D., et al. 2006, GCN 5513

Fynbo, J. P. U., Jensen, B. L., Gorosabel, J. U. et al. 2001, A&A, 369, 373

Fynbo, J. P. U., et al. 2005, GCN 3749

Fynbo, J. P. U., Malesani, D., Thöne, C. C., Vreeswijk, P. M., Hjorth, J., & Henriksen, C. 2006a, GCN 5809

Fynbo, J. P. U., et al. 2006b, A&A, 451, L47

Fynbo, J. P. U., et al. 2006c, Nat, 444, 1047

Fynbo, J. P. U., Gorosabel, J., Jensen, B. L., & Naeraenen, J. 2006d, GCN 4677

Fynbo, J. P. U., Thöne, C. C., Malesani, D., Hjorth, J., Vreeswijk, P. M., & Jakobsson, P. 2007, GCN 6759

Fynbo, J. P. U., Prochaska, J. X., Sommer-Larsen, J., Dessauges-Zavadsky, M., & Møller, P. 2008a, ApJ, 683, 321

Fynbo, J. P. U., Malesani, D., Jakobsson, P., Milvang-Jensen, B., & Hjorth, J. 2008a, GCN 7770

Fynbo, J. P. U., Quirion, P. O., Xu, D., et al. 2008c, GCN 7797

Fynbo, J. P. U., Malesani, D, & Milvang-Jensen, B., et al. 2008d, GCN 7949

Fynbo, J. P. U., Greiner, J., Kruehler, T., Rossi, A., Vreeswijk, P. M., & Malesani, D. 2008e, GCN 8225

Fynbo, J. P. U., Malesani, D., Hjorth, J., Sollerman, J., & Thöne, C. C. 2008f, GCN 8254

Gal-Yam, A., et al., 2006, Nat, 444, 1053

Gehrels, N., Chincarini, G., Giommi, P., et al. 2004, ApJ, 611, 1005

Gnedin, N., Kravtsov, A. V., & Chen, H.-W. 2008, ApJ, 672, 765

Greiner, J., Kruehler, T., Fynbo, J. P. U., et al. 2009, ApJ, 693, 1610

Groot, P., Galama, T. J., van Paradijs, J., et al. 1998, ApJ, 493, L27

Grupe, D., Nousek, J. A., vanden Berk, D. E., et al. 2007, ApJ, 133, 1216

Guetta, D., & Piran, T. 2007, JCAP, 7, 3

Guidorzi, C., Clemens, C., Kobayashi, S., et al., 2009, A&A, 499, 439

Hao, H., Stanek, K. Z., Dobrzycki, A., et al. 2007, ApJ, 659, L99

Hattori, T., Aoki, K., & Kawai, N. 2007, GCN 6444

Hirschi, R., Meynet, G., & Maeder, A. 2005, A&A, 443, 581

Hjorth, J., Sollerman, J., Møller, P., et al. 2003, Nature, 423, 847

Hogg, D. W., & Fruchter, A. S. 1999, ApJ, 520, 54

Jakobsson, P., et al. 2004, ApJ, 617, L21

Jakobsson, P., Björnsson, G., Fynbo, J. P. U., et al. 2005, MNRAS, 362, 245 ApJ, 617, L21

Jakobsson, P., Levan, A. J., Fynbo, J. P. U., et al. 2006a, A&A, 447, 897

Jakobsson, P., et al. 2006b, A&A, 460, L13

Jakobsson, P., et al. 2006c, GCN 5319

Jakobsson, P., Fynbo, J. P. U., Tanvir, N., & Rol, E. 2006d, GCN 5716

Jakobsson, P., Malesani, D., Thöne, C. C., Fynbo, J. P. U., Hjorth, J., Jaunsen, A. O., Andersen, M. I., & Vreeswijk, P. M. 2007a, GCN 6283

Jakobsson, P., Fynbo, J. P. U., Andersen, M. I., et al. 2007b, GCN 6398

Jakobsson, P., Vreeswijk, P. M., Hjorth, J., Malesani, D., Fynbo, J. P. U., & Thöne, C. C. 2007c, GCN 6952

Jakobsson, P., Fynbo, J. P. U., Vreeswijk, P. M., Malesani, D., & Sollerman, J. 2007d, GCN 7076

Jakobsson, P., Fynbo, J. P. U., Malesani, et al. 2007e, GCN 7117

Jakobsson, P., Vreeswijk, P. M., Malesani, D., Jaunsen, A. O., Fynbo, J. P. U., Hjorth, J., & Tanvir, N. R. 2008a, GCN 7286

Jakobsson, P., Fynbo, J. P. U., Malesani, D., Hjorth, J., & Milvang-Jensen, B. 2008b, GCN 7757

Jakobsson, P., Vreeswijk, P. M., Xu, D., & Thöne 2008c, GCN 7832

Jakobsson, P., Malesani, D., Vreeswijk, P. M., et al. 2008d, GCN 7998

Jakobsson, P., Vreeswijk, P. M., de Ugarte Postigo, A., et al. 2008e, GCN 8062

Jaunsen, A. O., Fynbo, J. P. U., Andersen, M. I., & Vreeswijk, P. M. 2007a, GCN 6216

Jaunsen, A. O., Malesani, D., Fynbo, J. P. U., Sollerman, J., & Vreeswijk, P. M. 2007b, GCN 6010

Jaunsen, A. O., Rol, E., Watson, D. J., et al. 2008, ApJ, 681, 453

Jensen, B. L., Fynbo, J. P. U., Gorosabel, J., et al. 2001, A&A, 370, 909

Kaper, L., D'Odorico, S., Hammer, F., et al. 2009, In "Science with the VLT in the ELT Era", p. 319

Kawai, N., Kosugi, G., Aoki, K., et al. 2006, Nature, 440, 184

Kistler, M. D., Yuksel, H., Beacom, J. F., & Stanek, K. Z. 2008, ApJ, 673, L119

Kouveliotou, C., Meegan, C. A., Fishman, G. J., et al. 1993, ApJ, 413, L101

Krühler, T., Küpcü Yoldaş A.; Greiner, J., et al. 2008, ApJ, 685, 376

Krumholz, M. R., Ellison, S. L., Prochaska, J. X., & Tumlinson, J. 2009, ApJ, 701, L12

Kuepcue Yoldas, A., Yoldas, A., Greiner, J., Kruehler, T., & Rossi, A. 2008, GCN 7303

Kuin, N. P. M., Grupe, D., & Brown, P. 2007, GCN 6238

Lazzati, D., Covino, S., & Ghisellini, G. 2002, MNRAS, 330, 583

Ledoux, C., Vreeswijk, P., Ellison, S., et al., 2005, GCN 3860

Ledoux, C., Vreeswijk, P., Smette, A., et al., 2006a, GCN 5237

Ledoux, C., Petitjean, P., Fynbo, J. P. U., Møller, P., & Srianand, R 2006b, A&A, 457, 71

Ledoux, C., Jakobsson, P., Jaunsen, A. O., Thöne, C. C., Vreeswijk, P. M., Malesani, D., Fynbo, J. P. U., & Hjorth, J. 2007, GCN 7023

Ledoux, C., et al. 2009, A&A, in press (arXiv:0907.1057)

Levan, A. J., Fruchter, A. S., Rhoads, J., et al. 2006, ApJ, 647, 471

Levan, A. J., Jakobsson, P., Hurkett, C., et al. 2007, MNRAS, 378, 1439

Malesani, D., Jakobsson, P., Fynbo, J. P. U., Stritzinger, M., & Covino, S. 2006, GCN 5350

Malesani, D., Jakobsson, P., Fynbo, J. P. U., Hjorth, J., & Vreeswijk, P. M. 2007, GCN 6651

Malesani, D., Fynbo, J. P. U., Jakobsson, P., Vreeswijk, P. M., & Niemi, S.-M. 2008, GCN 7544

Marshall, F. E., Godet, O., & Oates, S. R. 2008, GCN 7664

Marshall, F., & Vetere, L. 2006, GCN 4917

Mirabal, N., & Halpern, J. P. 2006, GCN 4591

Morgan, A. N., Vanden Berk, D. E., Brown, P., & Evans, P. A. 2006, GCN 7661

Møller, P., Fynbo, J. P. U., Hjorth, J. et al. 2002, A&AL, 396, L21

Noll, S., Mehlert, D., Appenzeller, I., et al. 2004, A&A, 418, 885

Noterdaeme, P., et al. 2009, A&A, A&A, in press (arxiv:908:1574)

Nysewander, M., Fruchter, A. S., & Peer, A. 2009, ApJ, 701, 824

Oates, S. R., & Markwardt, C. B. 2008, GCN 7253

Oates, S. R., Mundell, C. G., Piranomonte, S., et al. 2006, MNRAS, 372, 327

Oates, S. R., Page, M. J., Schady, P., et al. 2009, MNRAS, 395, 490

Oke, J. B., Cohen, J. G., Carr, M., et al. 1995, PASP, 107, 375

Page, K. L., Willingale, R., Bissaldi, E., et al. 2009, MNRAS, in press (arXiv:0907.4578)

van Paradijs J., Groot P.J., Galama T., et al., 1997, Nature 386, 686

Pedersen, K., Hurley, K., Hjorth, J., et al. 2006, ApJ, 636, 381

Perley, Chornock, R., & Bloom, J. S. 2008, GCN 7962

Perley, D. A., Cenko, S. B., Bloom, J. S., et al. 2009, AJ, submitted (arXiv:0905.0001)

Piranomonte, S., et al. 2006a, GCN 4520

Piranomonte, S., et al. 2006b, GCN 5626

Piranomonte, S., Ward, P. A., Fiore, F., et al. 2008, A&A, 492, 775

Piranomonte, S., D'Avanzo, P., Malesani, D., et al. 2007, GCN 6985

Pontzen, A., Deason, A., Governato, F., et al. 2009, MNRAS, submitted (arXiv:0909.1321)

Poole, T., Moretti, A., Holland, S. T., Chester, M., Angelini, L., & Gehrels, N. 2005, GCN 3698

Prochaska, J. X., Foley, R., Tran, H., Bloom, J. S., & Chen, H.-W. 2006a, GCN 4593

Prochaska, J. X., Chen, H.-W., & Bloom, J. S. 2006b, ApJ, 648, 95

Prochaska, J. X., Chen, H.-W., Dessauges-Zavadsky, M., & Bloom, J. S. 2007a, ApJ, 666, 267

Prochaska, J. X., Chen, H.-W., Bloom, J. S., et al. 2007b, ApJS, 168, 231

Prochaska, J. X., Dessauges-Zavadsky, M., Ramirez-Ruiz, E., & Chen, H.-W. 2008a, ApJ, 685, 344

Prochaska, J. X., Chen, H.-W., Wolfe, A. M., Dessauges-Zavadsky, M., & Bloom, J. S. 2008b, ApJ, 672, 59

Prochaska, J.X. Murphy, M., Malec, A., & Miller, S. 2008c, GCN 7388

Prochaska, J. X., Sheffer, Y., Perley, D. A., et al. 2009, ApJ, 691, L27

Prochter, G. E., Prochaska, J. X., Chen, H.-W., et al. 2006, ApJ, 648, L93

Racusin, J. L., Karpov, S. V., Sokolowski, M., et al. 2008, Nature, 455, 183

Rao, S. M., & Turnshek, D. A. 2000, ApJS, 130, 1

Reddy, N. & Steidel, C. C. 2008, ApJ, 692, 778

Rol, E., Jakobsson, P., Tanvir, N. R., & Levan, A. 2006, GCN 5555

Rol, E., Osborne, J. P., Page, K. L., et al. 2007a, MNRAS, 374, 1078

Rol, E.; Tanvir, N.; Mirabal, N., et al. 2007b, GCN 6221

Romano, P., Campana, S., Chincarini, G, et al. 2006, A&A, 456, 917

Ruiz-Velasco, A. E., et al. 2007, ApJ, 669, 1

Rykoff, E. S., Yuan, F., Schaefer, B. E., et al. 2007, GCN 6992

Salvaterra, R., Della Valle, M., Campana, S., et al. 2009, Nature, in press (arXiv:0906.1578)

Savaglio, S., Fiore, F., Israel, G. et al. 2002, GCN 1633

Savaglio, S., Fall, S. M., & Fiore, F. 2003, ApJ, 585, 638

Savaglio, S., Glazebrook, K., Abraham, R. G., et al. 2004, ApJ, 602, 51

Savaglio, S., 2006, NJPh, 8, 195

Savaglio, S., Palazzi, E., Ferrero, P., & Klose, S. 2006, GCN 6166

Schady, P., Mason, K. O., Osborne, J. P., et al. 2006, ApJ, 643, 276

Schady, P., & Moretti, A. 2006, GCN 5296

Schady, P., Mason, K. O., Page, M. J., et al. 2007a, MNRAS, 377, 273

Schady, P., De Pasquale, M., Cummings, J., et al. 2007b, MNRAS, 380, 1041

Sheffer, Y., Prochaska, J. X., Draine, B. T., Perley, D. A., & Bloom, J. S. 2009, ApJ, 701, L63

Schlegel, D. J., Finkbeiner, D. P., & Davis, M. 1998, ApJ, 500, 525

Schaye, J. 2001, ApJ, 562, L95

Shapley, A., Steidel, C. C., Pettini, M., & Adelberger, K. L. 2003, ApJ, 588, 65

Soderberg, A. M., Berger, E., Ofek, E. 2005, GCN 4186

Soderberg, A. M., Nakar, E., Cenko, S. B., et al. 2007, ApJ, 661, 982

Sollerman, J., Jaunsen, A. O., Fynbo, J. P. U., et al. 2006, A&A, 454, 503

Sollerman, J., et al. 2007, A&A, 466, 839

Stanek, K. Z., Matheson, T., Garnavich, P. M., et al. 2003, ApJ, 591, L17.

Starling, R. L. C., Vreeswijk, P. M., Ellison, S. L., et al. 2005, A&A, 442, L21

Starling, R., Thöne, C. C., Fynbo, J. P. U., Vreeswijk, P. M., & Hjorth, J. 2006a, GCN 5131

Starling, R., D'Elia, V., Piranomonte, S., et al. 2006b, GCN 5149

Starling, R. L. C., Rol, E., van der Horst, A. J., et al. 2009, MNRAS, in press (arXiv:0812.2490)

Sudilovsky, V., Savaglio, S., Vreeswijk, P., et al. 2007, ApJ, 669, 741

Tanvir, N. R., Levan, A. J., Rol, E., et al. 2008a, MNRAS, 388, 1743

Tanvir, N. R., Rol, E., & Stephens, A. 2008b, GCN 7488

Tanvir, N. R., Fox, D. B., Levan, A. J., et al. 2009, Nature, in press (arXiv:0906.1577)

Tejos, N., Lopez, S., Prochaska, J. X., Chen, H.-W., & Dessauges-Zavadsky, M. 2007, ApJ, 671, 622

Thöne, C. C., et al. 2006a, GCN 5373

Thöne, C. C., Fynbo, J. P. U., & Jakobsson, P. 2006b, GCN 5747

Thöne, C. C., Fynbo, J. P. U., Jakobsson, P., Vreeswijk, P. M., & Hjorth, J. 2006c, GCN 5812

Thöne, C. C., Jakobsson, P., Fynbo, J. P. U., Malesani, D., Hjorth, J., & Vreeswijk, P. M. 2007b, GCN 6499

Thöne, C. C., Jaunsen, A. O., Fynbo, J. P. U., Jakobsson, P., & Vreeswijk, P. M. 2007a, GCN 6379

Thöne, C. C., Kann, D. A., Augusteijn, T., & Reyle-Laffont, C. 2007c, GCN 6154

Thöne, C. C., Perley, D. A., & Bloom, J. S. 2007d, GCN 6663

Thöne, C. C., Wiersema, K., Ledoux, C., et al. 2008a, A&A, 489, 37

Thöne, C. C., De Cia, A., Malesani, D., & Vreeswijk, P. M. 2008b, GCN 7587

Thöne, C. C., Malesani, D., Vreeswijk, P. M., et al. 2008c, GCN 7602

Thöne, C. C., de Ugarte Postigo, A., Vreeswijk, P. M., Malesani, D., Jakobsson, P., et al. 2008d, GCN 8058

Thöne, C. C., Kann, D. A., Johannesson, G., et al. 2008e, A&A, submitted (arXiv:0806.1182)

de Ugarte Postigo, A., Jelinek, M., Tristram, P., Bond, I., Yock, P., Hearnshaw, J., & Castro-Tirado, A. J. 2007, GCN 6321

de Ugarte Postigo, A., Thöne, C. C., Fynbo, J. P. U., Jaunsen, A. O., & Ledoux, C. 2008, GCN 8089

Vergani, S. D., Petitjean, P., Ledoux, C., et al. 2009, /aap, 503, 771

Vreeswijk, P. M., Møller, P., & Fynbo, J. P. U. 2003, A&AL, 409, L5

Vreeswijk, P. M., Ellison, S., Ledoux, C., et al. 2004, A&A, 419, 927

Vreeswijk, P. M., Ledoux, C., Smette, A., et al. 2007, A&A, 468, 83

Vreeswijk, P. M., Jakobsson, P., Jaunsen, A. O., & Ledoux, C. 2008a, GCN 7391

Vreeswijk, Smette, A., Malesani, D., et al. 2008b, GCN 7444

Vreeswijk, Thöne, C. C., Malesani, D., et al. 2008c, GCN 7601

Vreeswijk, Fynbo, J. P. U., Malesani, D., Hjorth, J., & de Ugarte Postigo, A. 2008d, GCN 8191

Vreeswijk, P. M., Malesani, D., Fynbo, J. P. U., et al. 2008e, GCN 8301

Ward, P., & Ziaeepour, H. 2008, GCN 7941

Watson, D., et al. 2006, ApJ, 652, 1011

Weymann, R. J., Carswell, R. F., & Smith, M. G. 1981, ARA&A, 19, 41

Wiersema, K., Tanvir, N. R., Vreswijk, P. et al. 2008a, GCN 7517

Wiersema, K., Graham, J., Tanvir, N. R., et al. 2008b, GCN 7818

Wijers, R. A. M. J, Bloom, J. S., Bagla, J. S., & Natarajan, P. 1998, MNRAS, 294, L13

Williams, G. G., & Milne, P. A. 2007, GCN 6995

Wolfe, A. M., Gawaiser, E., & Prochaska, J. X. 2005, ARA&A, 43, 861

Woosley, S. E., & Heger, A. 2006, ApJ, 637, 914

Woosley, S., & Bloom, J. S. 2006, ARA&A, 44, 507

Woźniak, P. R., Vestrand, W. T., Panaitescu, A. D., et al. 2009, ApJ, 691, 495

Zheng, W., Deng, J., & Wang, J. 2009, RAA, in press

Xin, L. P., Meng, X. M., Zhai, M., et al. 2008, GCN 7371

This preprint was prepared with the AAS LaTeX macros v5.2.

Table 73—Continued

GRB	z	z class	N_X [10^{21} cm^{-2}]	β_{OX}	Ref
050730	3.97	a	—	0.79	D'Elia et al. (2005)
050726	< 5.5	a	—	< 0.89	Poole et al. (2005)
050716	< 11.0	a	—	< 0.28	Rol et al. (2007a)
050714B	< 3.5 (XRT)	—	2.2	< 0.48	—
050525A	0.61	ah	—	0.92	Foley et al. (2005)
050505	4.28	a	—	0.53	Berger et al. (2006)
050502B	< 6.4	a	—	< 0.58	Cenko et al. (2005)
050416A	0.65	h	—	0.70	Soderberg et al. (2007)
050412	—	—	0	< 0.60	—
050406	2.7	p	—	1.02	Schady et al. (2006)
050401	2.90	a	—	0.36	Watson et al. (2006)
050319	3.24	a	—	0.90	Jakobsson et al. (2006b)
050318	1.44	a	—	0.75	Berger et al. (2005)
050315	1.95	a	—	0.63	Berger et al. (2005)

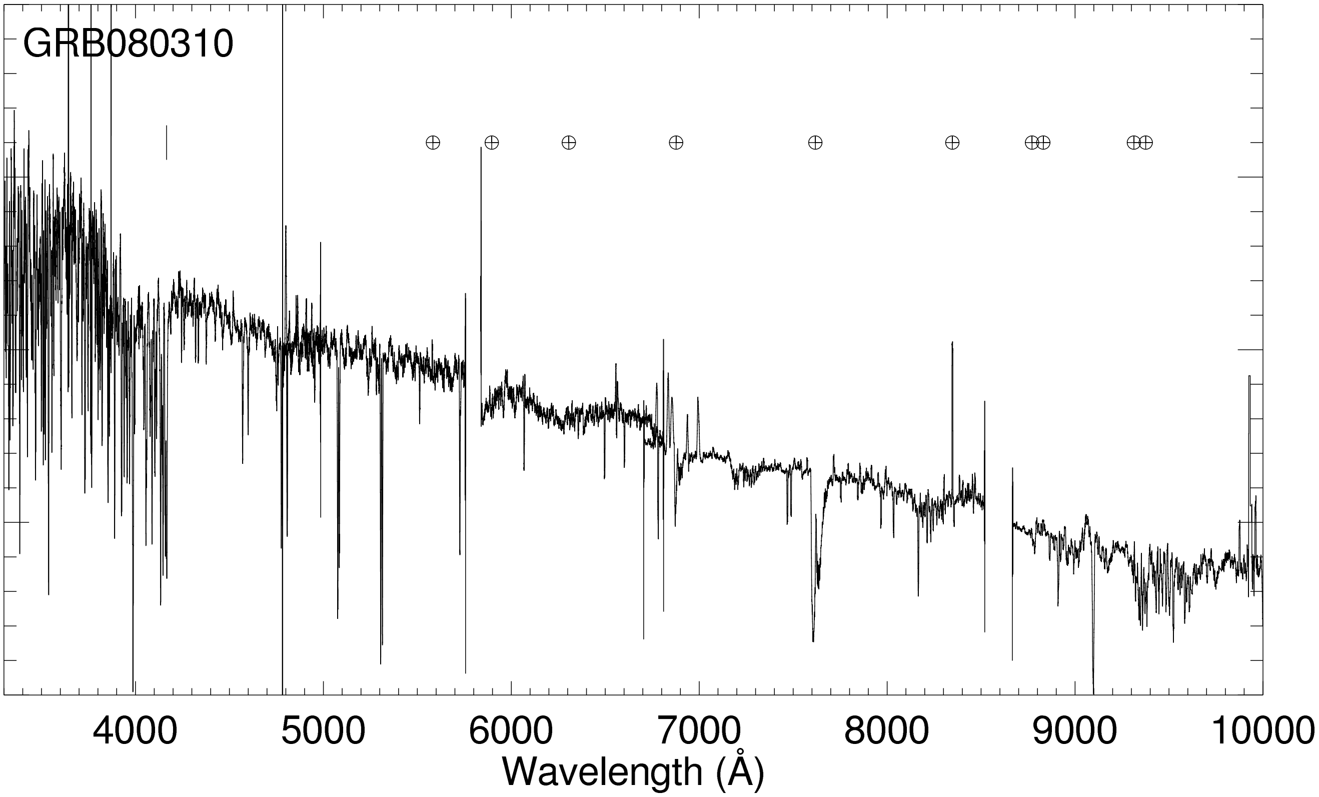
GRB080310
⊕ ⊕ ⊕ ⊕ ⊕ ⊕ ⊕⊕ ⊕⊕
4000
5000
6000
7000
8000
9000
10000
Wavelength (Å)

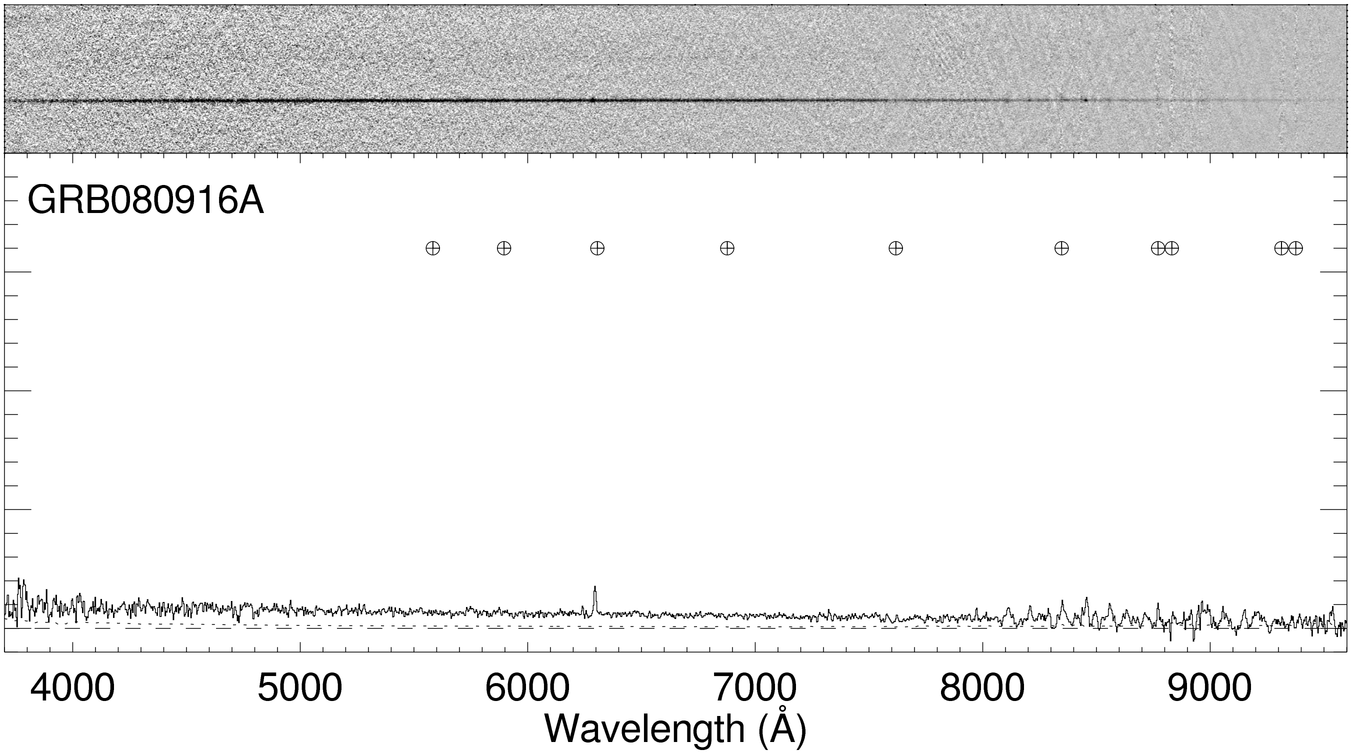
GRB080916A
⊕ ⊕ ⊕ ⊕ ⊕ ⊕ ⊕⊕ ⊕⊕
4000
5000
6000
7000
8000
9000
Wavelength (Å)